University of Stavanger

Faculty of Science and Technology

MASTER'S THESIS

Study programme / Specialization: MSc in Petroleum Engineering / Reservoir Engineering	Spring semester, 2018 Open
Author: Vladislav Stanislavskiy	…….. (Author's signature)
Programme coordinator / Supervisor: Dr. Dmitry Shogin	
Title of master's thesis: **Investigating the impact of solvent salinity on the viscometric functions of IOR polymers**	
Credits (ECTS): 30	
Key words: Rheology / Rheometry Polymers Flow behaviour / Fluid dynamics Constitutive equations Newtonian / Non- Newtonian fluid models Viscometric functions Salinity effect	Pages: 120 + enclosure: 20 Stavanger, 15.06.2018

Acknowledgements

First of all, I would like to express my sincere gratitude to my supervisor Dr. Dmitry Shogin for his guidance and very helpful discussions during the entire work, as well as arranging complementary courses without which this work would not be able to be carried out.

I am thankful to Professor Kim Andre Vorland for the instructions and training provided for the laboratory disciplines which were inalienable part of the experimental studies, as well as all the advice given that helped to get the best performance during whole experimental work.

I would also like to thank Eystein Opsahl for providing with many working materials, which gave an opportunity to conduct plenty of experiments in order to achieve the best results.

I am also thankful to the National IOR Centre of Norway and the University of Stavanger for giving a chance to be a part of a great team and enjoy the time during the entire stay in Stavanger.

And finally, I am grateful to my family and friends for their support and encouragement during the entire master's degree.

Vladislav Stanislavskiy, 2018

Abstract

One of the promising methods of enhanced oil recovery (EOR) is injection of polymers dissolved in low salinity water. This leads to a dramatic increase in the sweep efficiency due to increased apparent viscosity. It is well known that locally charged EOR polymers interact with salt ions in the solvent, which leads to a drop in the apparent viscosity i.e. the polymer solutions lose their desired property. The main focus of this work is to study the effect of salinity by a numerical analysis of rheological measurements conducted for several EOR polymers typically used in oil recovery operations. In particular, an important research question resolved in this thesis is how the functional form of the dependency of non-Newtonian viscosity on the local shear rate is changed with salt concentration in different brine solutions.

Taking into consideration that polymer solutions are non-Newtonian fluids and do not obey the laws of classical fluid dynamics, in order to describe the behaviour of these fluids in complex flows (like those in porous media), advanced fluid models need to be used. In this thesis the best possible prediction of the non-Newtonian viscosities of the considered polymeric solutions were suggested by testing several differential tensor non-Newtonian fluid models. The major non-Newtonian fluid models, that were juxtaposed with the data obtained throughout the experimental work, were FENE-P dumbbell model, Linear and Exponential Phan-Thien-Tanner models.

However, at the present time, salinity is not accounted for in these models. Thus, the major focus of the thesis is to give a hint on what kind of behaviour must be predicted by the future non-Newtonian fluid models that should take into account relation of the scalar parameters in the models and salinity of the solvents, as well as considering polymer concentration in the solutions and polymer molecular weight.

Nomenclature

Abbreviations:

CMC	Carboxylmethyl cellulose
EHEC	Ethylhydroxyethyl cellulose
EOR	Enhanced oil recovery
FENE	Finitely extensible non-linear elastic
FENE-P	Finitely extensible non-linear elastic with Peterlin closure
GNF	Generalized Newtonian Model
HEC	Hydroxyethyl cellulose
HPAM	Hydrolyzed polyacrylamide
IOR	Improved oil recovery
n·k (e.g. 5k)	$n \cdot 10^3$ (e.g. 5000)
PAM	Polyacrylamide
ppm	Parts per million
PS	Polystyrene
PTT	Phan-Thien & Tanner
RPM	Rounds per minute
VHM	Very high molecules
VLM	Very low molecules

Variables:

$\underline{\underline{\dot{\gamma}}}$	Rate of deformation tensor
$\dot{\gamma}_{xy}^{G}$	Solid element shear rate
$\dot{\gamma}_{xy}^{\eta}$	Liquid element shear rate
$\underline{\underline{\tau}}$	Stress tensor
F^c	Connector force,
G_i	Rigidity modulus spectra
$\langle Q \rangle$	Average value of connector vector
Q_o	Upper limit of the spring extension
$\vec{V}$	Vector velocity

a_x	Acceleration in x-direction
$\vec{f}$	Body force per unit mass
f_x	x-component of body force
f_y	y-component of body force
f_z	z-component of body force
$\vec{\imath}$	Unit vector along x-axes
$\vec{\jmath}$	Unit vector along y-axes
$\vec{k}$	Unit vector along z-axes
$\vec{n}$	Unit vector
t_p	Time scale
$\dot{\gamma}$	Shear rate
γ_{xy}^{G}	Elastic strain
γ_{xy}^{η}	Viscous strain
η_∞	Infinite shear rate viscosity
η_a	Apparent viscosity
η_o	Viscosity of pure solvent
η_o	Zero shear rate viscosity
η_r	Relative viscosity
η_s	Viscosity of solvent
η_{sp}	Specific viscosity
λ_i	Relaxation time
ρ_1	Fluid density at initial time
ρ_2	Fluid density at point 2
$\tau^{[p]}$	Polymer stress
$\tau^{[s]}$	Newtonian stress due to the solvent
τ^*	Critical shear stress at the transition from Newtonian plateau
τ_o	Yield stress
τ_{xx}	Normal stress x-direction
τ_{xy}^{G}	Solid element stress
τ_{xy}^{η}	Liquid element stress
τ_{yx}	y-component shear stress in x-direction
τ_{yy}	Normal stress in y-direction

τ_{zx}	z-component shear stress in x-direction
τ_{zz}	Normal stress in z-direction
$[\eta]$	Intrinsic viscosity
∇	Vector operator
$\nabla \underline{u}$	Velocity gradient tensor
$\nabla \cdot \vec{V}$	Velocity divergence
A	Cross-sectional area
a	Width of the transition region between zero shear viscosity and the Power Law region
*d*S	Infinitesimal surface element
*d*V	Finite control volume
F	Shear force
h	Distance
N1	1st normal stress difference
N2	2nd normal stress difference
p	Local fluid pressure
Q	Volumetric flow rate
r	Inner tube radius
R	Tube radius
S	Control surface
S	Entropy
T	Absolute temperature
t_1	Initial time
t_2	Time at point 2
V	Velocity
V	Volume
V_{max}	Maximum velocity
V_{min}	Minimum velocity
De	Deborah Number
H	Spring constant
K	Time constant
Q	Connector vector between the beads

We	Weissenberg number
$d\vec{S}$	Vector elemental surface area
dE	Change in energy of the system
dS	Change in the entropy
$d\rho/dt$	Substantial derivative
m	Consistency index
n	Power Law or flow index
u	Velocity component
v	Velocity component
w	Velocity component
ΔV	Control volume
Δt	Time increment
γ	Shear
δQ	Heat exchange with the system
δQ	Heat transfer
δV	Infinitesimal fluid element (volume)
δW	Work done by the system
δm	Infinitesimal fluid element (mass)
ε	Elasticity of the fluid
η	Shear viscosity
λ	Bulk viscosity coefficient
μ	Molecular viscosity coefficient
ν	Kinetic viscosity
ξ	Free parameter
ρ	Density
τ	Shear stress
ω	Angular velocity

Table of Contents

List of figures

List of tables

1. Introduction

The production history of any petroleum reservoir can be divided into various phases. Firstly, it is the phase when oil is flowing freely from a reservoir to the production well due to pressure change, and in the overwhelming majority cases it is the shortest one. Usually, energy must be supplied to the porous medium in the early life of a reservoir that contains the crude oil in order to maintain a flow to the producing wells. This energy is brought into the reservoir by injection of water and gas. This secondary method will give 30 to 40 percent recovery of the original oil in place, while the rest will be left in the earth. To recover some of the residual oil as well, tertiary methods have been developed which are still the subject of research. One of these methods called polymer flooding is based on adapting the viscosity of the displacing phase to that of the crude oil, which is carried out by adding water-soluble polymer to the floodwater [1]. The major goal of the water-soluble polymers is to improve the rheological properties of the displacing fluid. Because the amount of oil produced from the reservoir increases with the microscopic sweep of the reservoir as well as the displacement efficiency of the oil [2]. And, actually, use of water-soluble polymers increases the water-oil mobility ratio and, therefore, leads to enhanced oil recovery [2, 3]. However, urgent necessity arises over the control for the dynamics of displacement, liquid motion and sweep efficiencies that affect the oil recovery factor [4].

What it comes to liquid motion, it has attracted many generations of scientists and engineers. Many years of investigation and research have been dedicated to the study of fluids with low molecular weight, which, in turn, well described by the Navier-Stokes equations. However, many challenging problems still remain both in theory and applications. But even more challenges arise with polymeric liquids because their motion cannot be described by Navier-Stokes equations at all. Thus, understanding of polymer fluid dynamics is very important [5] as well as knowing the parameters that affect their rheological properties, which are showcased in this work.

2. Rheology and rheometry

2.1 Rheology

Rheology is known as a branch of physics and physical chemistry as far as the most significant parameters come from those fields and the field of mechanics i.e. forces, deflections and velocities. The origin of the term "*Rheology*" comes from the Greek language, where "*rhein*" means "*to flow*". So, one can literally state that rheology is a science of flow. Besides flow behaviour of liquids, rheological measurements are also known to reveal deformation behaviour of solids [6].

Let's take a closer look to flowing behaviour of liquids. One can muse upon the difference between flow and a simple movement in liquids. The answer is simple, the deformation occurs in the elements of a liquid while it is flowing as well as movement of adjacent points is present which is *relative* to one another. Flow is divided into two major forms: *shear* flow and *extensional* flow. The former flow imposes its elements to flow *over* or *past* each other, while in the latter one, they move *towards* or *away from* each other [7]. The figure below shows a clear representation of particles movement in two flows:

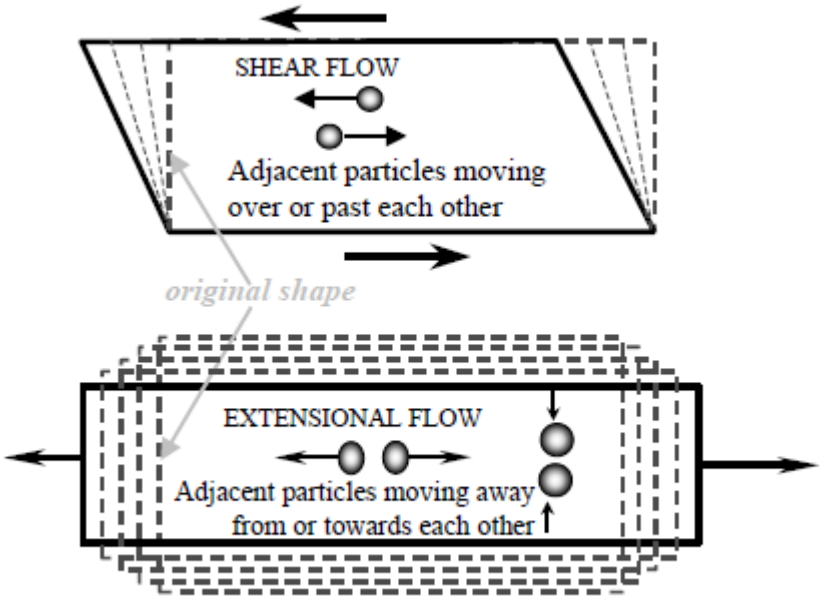

Figure 2. 1: Particle motion in shear and extensional flows [7].

Viscosity is a parameter that limits any kind of flow, which means that if one pours out a bucket of non-viscous fluid (e.g. water) it will flow much faster comparing to a bucket of viscous fluids (e.g. oils or polymers). The second important parameter is velocity which incurs fluids to flow. Rise in viscosity leads to an increase in the resulting force, for a constant velocity, whereas increasing viscosity reduces the needed velocity for a given force [7].

Measuring deformation, rheological behaviour and flow behaviour have been of a great importance for rheologists and an overview of the most important kinds of rheological behaviour is illustrated in the table 1.1:

Table 2. 1: Overview on different kinds of rheological behaviour [6].

Liquids		Solids	
(ideal-) viscous flow behavior Newton's law	viscoelastic flow behavior Maxwell's law	viscoelastic deformation behavior Kelvin/Voigt's law	(ideal-) elastic deformation behavior Hooke's law
flow/viscosity curves	creep tests, relaxation tests, oscillatory tests		

2.2 Rheometry

Technology that is used to identify and interpret rheological data is called rheometry [6]. There are two major instruments to measure the rheological data i.e. rheometers and viscometers. The former one has no measurement limitations and is used to measure the viscoelastic properties of fluids as well as solids and semi-solids. Whereas the latter instruments are restricted in their use and therefore in measuring the viscous flow behaviour. Figure 2.2 illustrates usage of various types of flow models [8]:

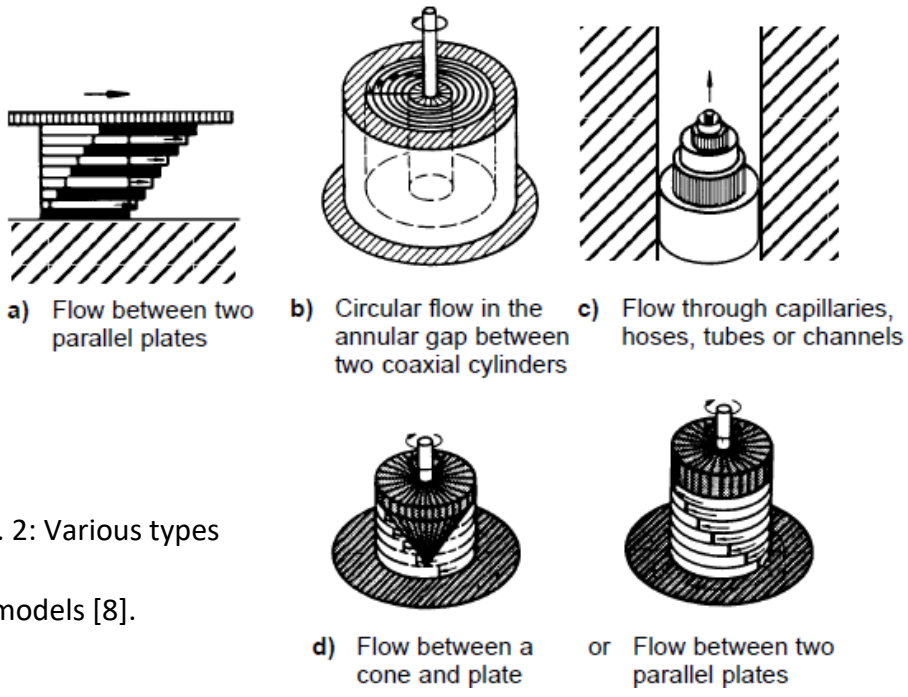

Figure 2. 2: Various types of flow models [8].

2.2.1 Flow between two parallel flat plates

This flow is produced by moving one plate (basically the upper plate) while the second plate remains stationary. This sort of movement forms layers of laminar flow. The pattern remains the same or similar when the upper plate is acting as a stationary one [8].

2.2.2 Flow in the annular gap between two concentric cylinders

In this model one of the two coaxial cylinders is supposed to be stationary while the second cylinder can rotate, displacing concentric layers located one inside another [8].

2.2.3 Flow through pipes, capillaries and tubes

This model is characterized by a pressure difference in the inlet and the outlet which forces a Newtonian liquid to flow with the parabolic rate of distribution throughout the whole diameter [8].

2.2.4 Flow between a cone and a plate or between parallel plates of rotational rheometers

Resembling the first and the second flow models, in the cone-and-plate sensor systems, one of the two is stationary (basically a plate) and the second one rotates. Rotational rheometers are the best representatives of such type of flow model [8].

3. Definition of terms

There are primary rheological parameters that are determined by utilizing two-plate-model, where the bottom plate being stationary and the upper plate is driven by the controlled velocity *V* and then finally measuring the resulting shear force *F*. Figure 3.1 gives an example of fundamental rheological parameters. The sample is sheared in the area between the two plates distance *h* and there are following shear conditions that are assumed to originate [6]:

- There are no wall-slip effects, and adhesion occurs to the both plates
- The sample can be imagined in the form of layers, i.e. there are no whirls in the flow, meaning that the flow showing an absolute laminar flow condition. Figure 3.2 gives an example of the laminar flow [6].

The further calculation of the rheological parameters is considered to be accurate only by meeting both of the conditions [6].

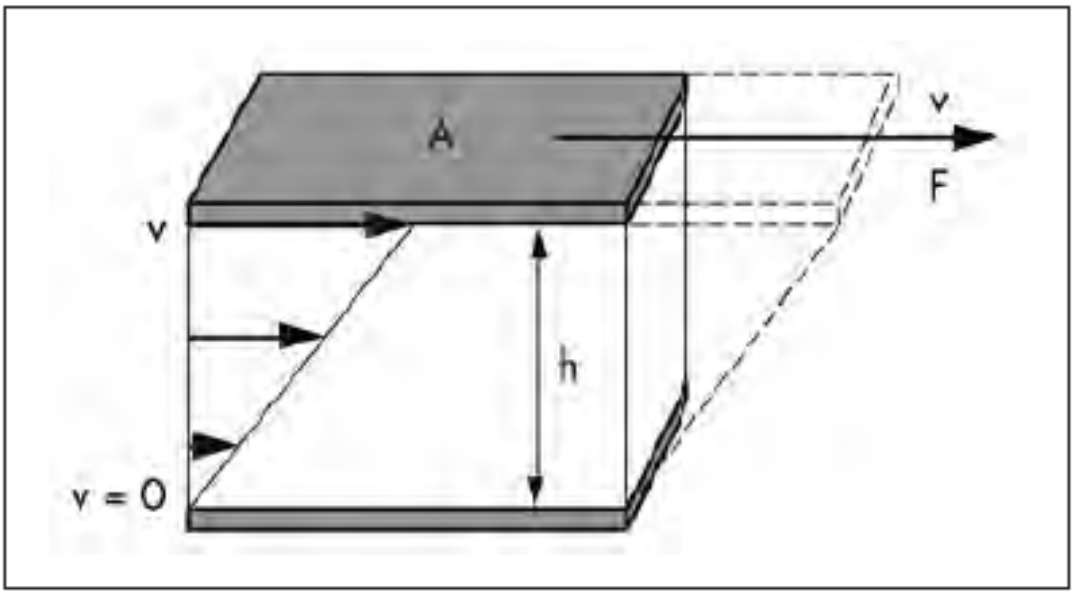

Figure 3. 1: The two-plates-model for shear tests to illustrate the velocity distribution of a flowing fluid in the shear gap [6].

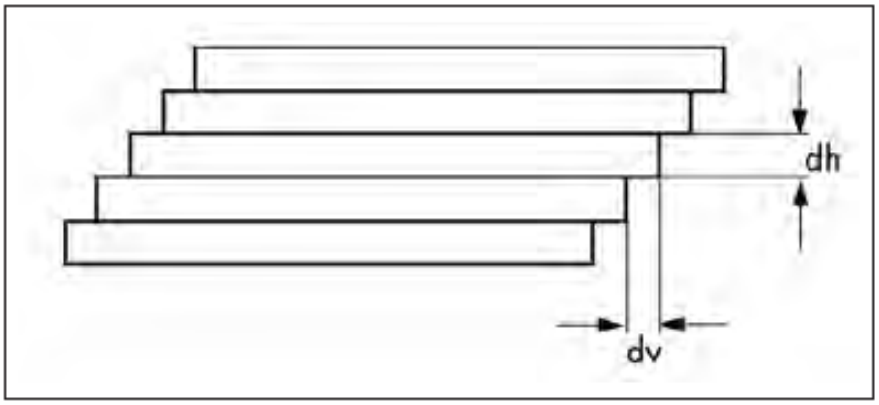

Figure 3. 2: Laminar flow in the form of planar fluid layers [6].

3.1 Shear stress

The equation that describes an average shear stress is force per unit area [9]. The equation 3.1 represents an area *A* between the upper plate and the liquid below being subjected by a tangential force *F* [8]:

$$\tau = \frac{F}{A} \tag{3.1}$$

where:

τ – the shear stress

F – the force applied

A – the cross-sectional area of material with area parallel to the applied force vector

The unit of the shear stress is "*pascal*" [Pa], where [*1 Pa = 1 N / m² = 1 kg / m · s²*] taking into account that previously the unit that was used for expressing shear stress was [*dyne / cm²*], where [*1 dyne / cm² = 0.1 Pa*] [6].

3.2 Shear rate

As follows from the figure 3.1 shown above, which depicts that the shear flow is the continual movement of liquid particles, it represents that the shear stress τ induces the liquid to flow in a specific pattern, where the maximum velocity V_{max} is detected at the upper boundary and the minimum velocity V_{min} = 0 at the lower boundary. Therefore, shear rate is the velocity drop throughout the gap size and mathematically defined by a differential in its general form [8]. In the other words the shear rate is a velocity gradient in the direction at right angle to the flow. For visual representation of the hypothetical layers sliding over each other the reader is referred to figure 3.3 [7].

Simply saying the shear rate is the ratio of the velocity of the upper plate to the distance between the two plates. The unit representing the shear rate is [1 / s] or reciprocal second [s^{-1}] [10].

$$\dot{\gamma} = \frac{v}{h} = \left[\frac{m}{s \cdot m}\right] = \left[\frac{1}{s}\right] = [s^{-1}] \tag{3.2}$$

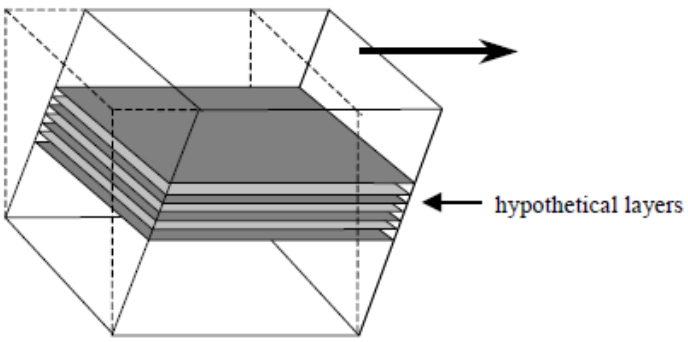

Figure 3. 3: Hypothetical layers in shear flow [7].

3.2.1 Shear rate in industrial practice

Some typical values of the shear rate encountering in industrial practical situations are shown in table 3.1. By dividing a typical velocity in any flow of interest by a typical dimension, one can associate the values in the table to their field of interest [7].

Table 3. 1: Typical shear rates of technical processes [6]:

Process	Shear rates $\dot{\gamma}$ (s^{-1})	Practical examples
Physical aging, long-term creep within days and up to several years	10^{-8} ... 10^{-5}	Polymers, asphalt
Cold flow	10^{-8} ... 0.01	Rubber mixtures, elastomers
Sedimentation of particles	≤ 0.001 0.01	Emulsion paints, ceramic suspensions, fruit juices
Surface leveling of coatings	0.01 ... 0.1	Coatings, paints, printing inks
Sagging of coatings, dripping, flow under gravity	0.01 ... 1	Emulsion paints, plasters, chocolate coatings (couvertures)
Self-leveling at low-shear conditions in the range of the zero-shear viscosity	≤ 0.1	Silicone polymers (PDMS)
Dip coating	1 ... 100	Dip coatings, candy masses
Applicator roller, at the coating head	1 ... 100	Paper coatings
Thermoforming	1 ... 100	Polymers
Mixing, kneading	1 ... 100	Rubber mixtures, elastomers
Chewing, swallowing	10 ... 100	Jelly babies, yogurt, cheese
Spreading	10 ... 1,000	Butter, toothpastes
Extrusion	10 ... 1,000	Polymer melts, dough, ceramic pastes, tooth paste
Pipe flow, capillary flow	10 ... 10^4	Crude oils, paints, juices, blood
Mixing, stirring	10 ... 10^4	Emulsions, plastisols, polymer blends
Injection moulding	100 ... 10^4	Polymer melts, ceramic suspensions
Coating, painting, brushing, rolling, blade coating (manually)	100 ... 10^4	Brush coatings, emulsion paints, wall paper paste, plasters
Spraying	1,000 ... 10^4	Spray coatings, fuels, nose spray aerosols, adhesives
Impact	1,000 ... 10^5	Solid polymers
Milling pigments in fluid bases	1,000 ... 10^5	Pigment pastes for paints and printing inks
Rubbing	1,000 ... 10^5	Skin creams, lotions, ointments
Spinning process	1,000 ... 10^5	Polymer melts, polymer fibers
Blade coating (by machine), high-speed coating	1,000 ... 10^7	Paper coatings, adhesive dispersions
Lubrication of engine parts	1,000 ... 10^7	Mineral oils, lubricating greases

3.2.2 Definition of the shear rate using differential variables

Velocity drop shows a linear pattern over the shear gap which creates a linear velocity distribution between the plates. Therefore, velocity difference between the adjacent layers for ideally viscous and laminar flow will be constant (*dv = const*). Assuming that all the layers are of the same thickness (i.e. *dh = const*), the shear rate will show a constant value throughout the whole shear gap of the two-plate-model since (this is illustrated in figure 3.4) [6]:

$$\dot{\gamma} = \frac{dv}{dh} = \frac{const}{const} = const \tag{3.3}$$

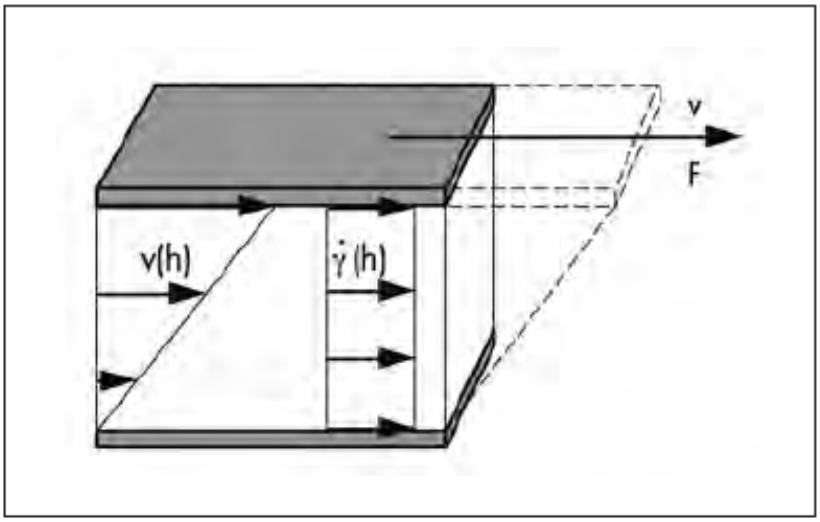

Figure 3. 4: Velocity distribution and shear rate in the shear gap of the two-plates-model [6].

The velocity information of a flowing fluid is provided by both $\dot{\gamma}$ and *v*, however by opting for the shear rate, an advantage will present because of the constant value throughout the whole shear gap, which makes the shear rate act independently of the position of any flowing layer in the shear gap. However, one should take into account the conditions that have to be met that were mentioned previously in chapter 3 as well as understanding that this cannot be applicable to velocity *v*, as it decreases from the maximum value in the upper boundary of the system in downward direction to its lowest value in the very bottom, where the velocity equals to zero (i.e. $V_{min} = 0$). That is why sometimes a term *velocity gradient* is used as a synonym for the shear rate [6].

3.2.3 Some basic dimensions and units

In order to avoid mistakes and misunderstandings it is very easy to become confused, it is worth spending some time on this subject. Moreover, it arises very frequently in rheology. The

convention to be followed is SI system and it is basically built around five units, namely length, mass, temperature, time and amount of substance (which is shown in the table 3.2), following that all other units of rheological interest can be derived from the ones mentioned before (which is shown in the table 3.3) [7].

Table 3. 2: SI based units used in rheology [7]:

Quantity	Unit Name	Unit Symbol
Mass	kilogram	kg
Length	metre	m
Time	second	s
Temperature	kelvin	K
Amount of substance	mole	mol

Table 3. 3: Some derived SI units with special names [7]:

Quantity	Special Name	Symbol	Equivalent
Frequency	hertz	Hz	s^{-1}
Force	newton	N	$kg\ m/s^2$
Pressure or stress	pascal	Pa	N/m^2
Work, energy, heat	joule	J	$N\ m, kg\ m^2 s^{-2}$
Power	watt	W	J/s

The units that are used the most often in rheology are shown in table 3.4:

Table 3. 4: Some commonly used rheological quantities and their units [7]:

Quantity	Symbol	Units
Shear	γ (pronounced gamma)	-
Shear rate	$\dot{\gamma}$ (pronounced gamma dot)	s^{-1}
Shear stress	τ (pronounced tau)	Pa
Shear viscosity	η (pronounced eta)	Pa·s (Pascal-seconds)

Note that usually shear viscosity is referred simply as viscosity, however sometimes it is better to distinguish it from the extensional viscosity [7].

3.3 Viscosity

One of the fundamental characteristic parameter of all liquids is viscosity, which acts as a measure of the internal resistance to flow or shear while liquids are flowing [11]. In other words, a certain flow resistance will always be present in fluids that are in motion and this resistance can be defined in terms of viscosity [6]. Although being a function of temperature and pressure, they affect the viscosity in a different manner [11]. Behaviour of solid materials is specified as elastic and liquids as viscous. However, in real life most of the time we come across materials and substances that are neither completely elastic nor entirely viscous (i.e. viscoelastic materials). Scientists classify these as viscoelastic solids (e.g. jellies) and viscoelastic liquids (e.g. shower gels). Low-viscosity fluids are those which show a low resistance to deformation, while high-viscosity fluids highly resist to deformation and consequently do not flow easily. Such cases are depicted in the following figures [10]:

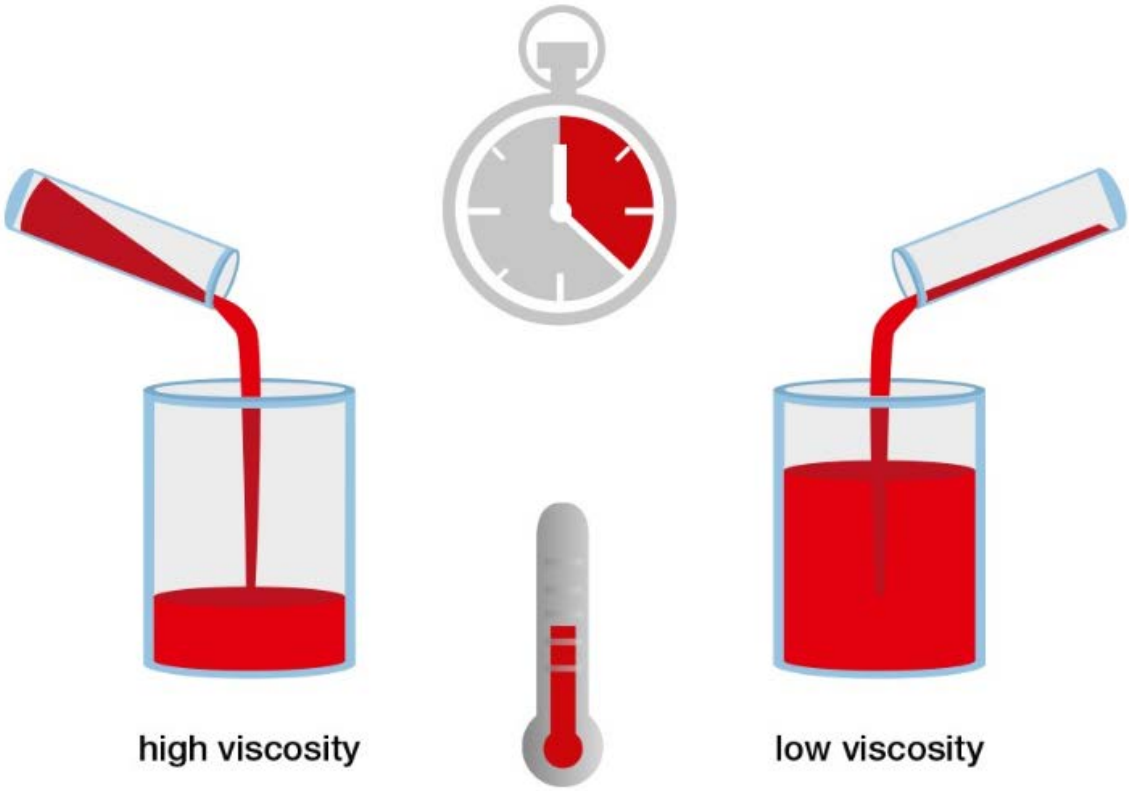

Figure 3. 5: Example of high viscosity fluids and low-viscosity fluids, where the former ones flow slower than the latter ones at the same temperature [10].

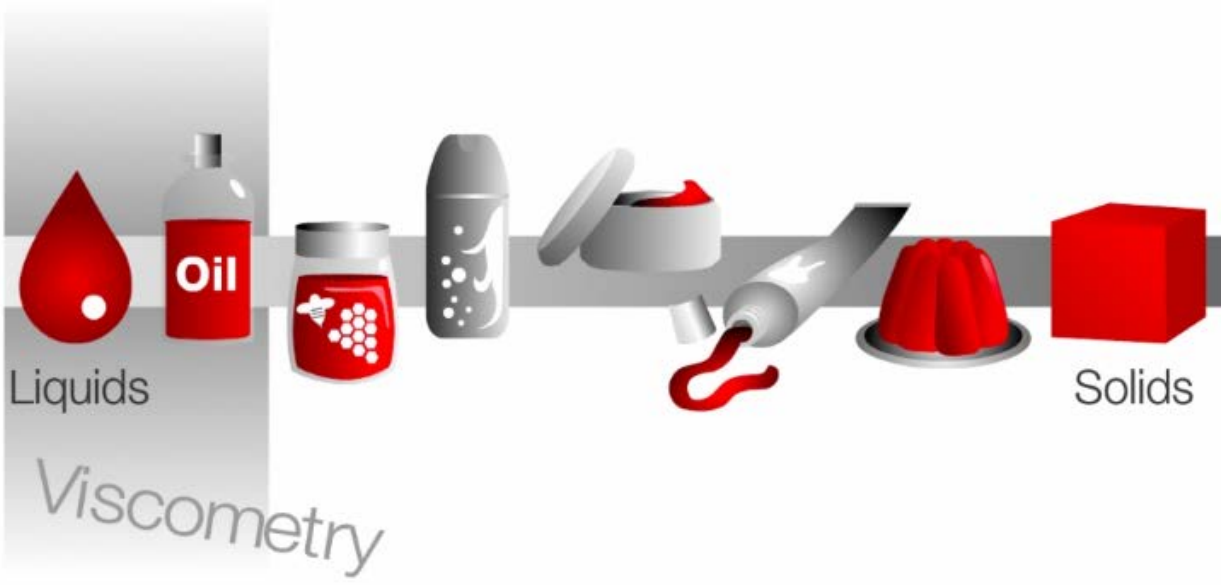

Figure 3. 6: Viscoelastic materials in everyday life (from ideally viscous liquids to elastic solids) [10].

3.3.1 Dynamic (shear) viscosity

Dynamic viscosity also known as shear viscosity is represented by a Greek symbol η (eta) [10]. As can be seen from figure 3.7, dynamic viscosity is the tangential force per unit area that is required to move one layer *(A)* against another layer *(B)* while both of the layers are sustained at a unit distance. From this figure it can be seen that a certain force *F* drifts the layers *A* and *B* and therefore, slides them at certain velocities V_1 and V_2, respectively [11].

Figure 3. 7: Simple shear of a liquid film [11].

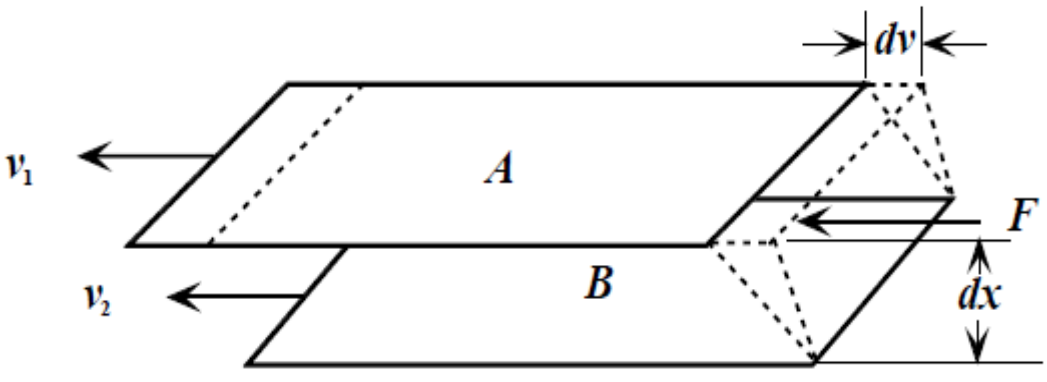

If τ is the shear stress and $\dot{\gamma}$ is the shear rate, then the expression becomes:

$$\tau = \eta \cdot \dot{\gamma} \Rightarrow \eta = \frac{\tau}{\dot{\gamma}} \tag{3.4}$$

Units to be used for dynamic viscosity:

a) SI units (International system of units) [12]:

Pascal-seconds [*Pa·s*] or millipascal-seconds [*mPa·s*],

$$\eta = \frac{N}{m^2} \cdot s = Pa \cdot s \tag{3.5}$$

where *1 Pa·s = 1000 mPa·s*

b) Other common units:

Poise [*P*] or centipoise [*cP*] (named after Jean Poiseuille [13]):

where *1 P = 100 cP*

c) Relation between the units [10]:

1 mPa.s = 1 cP

Some typical values of viscosity at 20°C [mPa·s] are shown in the table 3.5 [6].

At the viscosity values greater than 10^4 Pa·s (i.e. $\eta > 10^4$ Pa·s), the elastic portion has to be taken into account, as the samples of these kinds should not be considered simply as viscous , but visco-elastic [6].

3.3.2 Kinematic viscosity

Viscosity in the capillary viscometer tests is defined in units of kinematic viscosity ν and this viscosity shows how gravitational force impacts on a substance's flow [8, 10]. One other parameter that is required for kinematic viscosity is density of the liquid at that pressure and temperature [11]. Therefore, the relation between kinematic and dynamic viscosity is linked in the following equation:

$$\nu = \frac{\eta}{\rho} = \left[\frac{mm^2}{s}\right] \text{ ; where } \rho = \frac{m}{V} = \left[\frac{kg}{m^3}\right] = \left[\frac{N \cdot s^2}{m^4}\right] \tag{3.6}$$

where, ν – kinematic viscosity,

ρ – density

Stokes [*St*] and centistokes [*cSt*] were previously used as units of kinematic viscosity [8]:

$$1\ St = 100\ cSt\ ;\ 1\ \frac{mm^2}{s} = 1\ cSt$$

Table 3. 5: Some viscosity values at 20°C, when without further specification [6, 14-16]:

Material	Viscosity η [mPas]
Gases/air	0.01 to 0.02 / 0.018
Pentane/acetone/gasoline, petrol (octane)/ethanol	0.230 / 0.316 / 0.538 / 1.20
Water at 0 / +10 / +20 / +30 / +40 / +50 / +60 / + 70 / +80 / +90 / +100°C	1.79 / 1.31 / 1.00 / 0.798 / 0.653 / 0.547 / 0.467 / 0.404 / 0.354 / 0.315 / 0.282
Mercury	1.55
Blood plasma at +20 / +37°C	1.7 / 1.2
Wine, fruit juices (undiluted)	2 to 5
Milk, coffee cream	2 to 10
Blood (from a healthy body) at +20 / +37°C	5 to 120 / 4 to 15 (at $\dot{\gamma}$ = 0.01 to 1000s^{-1})
Light oils	10
Glycol	20
Sulphuric acid	25
Sugar solutions (60%)	57
Motor oils SAE 10W-30, at +23 / +50 / +100°C	50 to 1000 175 / 52 / 20
Olive oils	Approx. 100
Gear oils	300 to 800
Glycerine	1480
Honey, concentrated syrups	Approx. 10Pas
Polymer melts (at processing conditions, e.g. between T = + 150 and 300°C, and at $\dot{\gamma}$ = 10 bis 1000s^{-1})	10 to 10,000Pas
Polymer melts: zero-shear viscosity at $\dot{\gamma} \leq 0.1s^{-1}$ and at T = +150 to 300°C	1kPas to 1MPas
Silicone (PDMS, unlinked, zero-shear viscosity)	10 to 100kPas
Hotmelts (maximum processing viscosity for melt extruders)	100kPas
Bitumen (example): at T = +80 / +60 / +40 / +20°C and at T = 0°C	200Pas / 1kPas / 20kPas / 0.5MPas and 1MPas, i.e., then almost like a viscoelastic solid

3.3.3 Relative viscosity

One of the vital parameters while measuring dissolved polymers is relative viscosity [17]. Molar mass of polymers highly affects to their quality and majority of them act distinctively with

respect to molar mass and viscosity. Therefore, by measuring viscosity of polymers, one can define their molar mass [10].

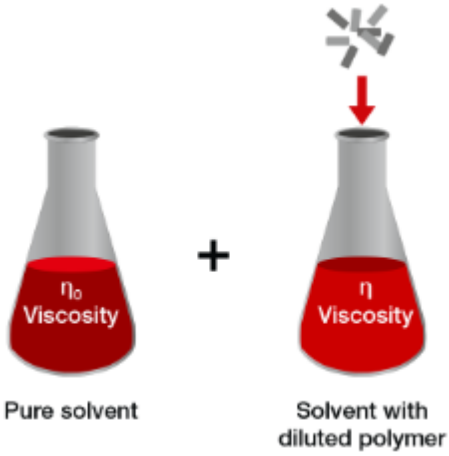

Figure 3. 8: Viscosity measurement of pure solvent and polymer solution of defined concentration

Although polymer viscosity increases with increasing molar mass and being polymer solutions shear-dependent (i.e. acting as a non-Newtonian liquids), in a range of extremely low shear rates, they behave as Newtonian fluids. Thus, in order to get relative viscosity, one should divide viscosity of the polymer solution (η) by the viscosity of the pure solvent (η_o) [10]

$$\eta_r = \frac{\eta}{\eta_o} \tag{3.7}$$

As was mentioned before, relative viscosity is a vital parameter for polymer quality as well as being fundamental for calculating other relevant parameters for polymer quality control [10]:

- **Molar mass** (which is defined as a ratio of the mass of the certain substance and the amount this substance)
- **K-value**
- **Intrinsic viscosity** (also known as Staudinger Index or limiting viscosity number (LVN))
- **Reduced viscosity** (also known as Staudinger Function or viscosity number (VN))
- **Specific viscosity** (also known as relative viscosity increment)
- **Logarithmic viscosity number** (also known as inherent viscosity) [10].

Viscosity-related quantities are often quoted and also worth noting with their assigned units and symbols [7]:

- Continuous phase or viscosity of the solvent, η_s , *Pa·s;*
- Dimensionless relative viscosity, η_r , which represent the ratio between the viscosity of a suspension and its continuous phase viscosity, i.e. (η / η_s);

- The dimensionless specific viscosity, η_{sp} , which is given by $(\eta_r - 1)$;
- The intrinsic viscosity, $[\eta]$ (with dimensions $m^3 \cdot kg^{-1}$) which shows the ratio of the specific viscosity to the concentration c of a dispersed phase, $(\eta_r - 1)/c$;
- The kinematic viscosity, $\nu = \eta/\rho$ [7].

3.3.4 Apparent viscosity

Viscosity of the Newtonian or ideally viscous fluids are constant for all shear rates. However, the viscosity of fluids that depend on shear rate will vary and one should specify at which shear rate the viscosity value was defined. This viscosity value is called '*apparent viscosity*' or '*apparent shear viscosity*'. An example of this case is depicted in figure 3.9 [10]:

$$\eta_a\ (\dot{\gamma} = 60 s^{-1}) = 398\ mPa \cdot s$$

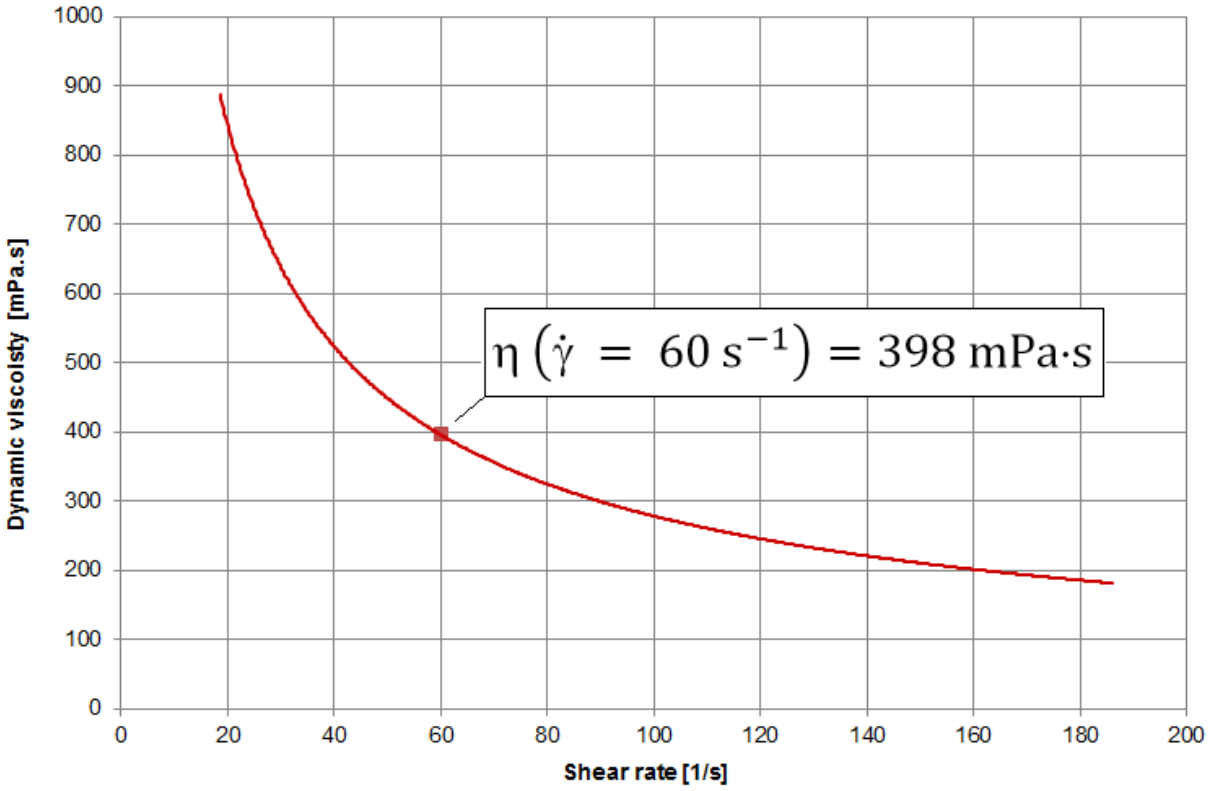

Figure 3. 9: Viscosity function of a shear-thinning fluid. An example is taken at shear rate of $60s^{-1}$ [10].

4. Polymers

Polymers are the substances that consist of long chains of repeating groups of atoms. All the water-soluble polymers can be divided into two major groups [1]:

1. **Synthetic polymers** – those that are produced synthetically.
2. **Biopolymers (including polysaccharides)** – where the biopolymers are the natural products from seeds, wood etc. and the polysaccharides those that are produced by bacteria or fungi [1].

4.1 Synthetic polymers

In overwhelming majority of synthetic polymers are polyacrylamides, which are available from different manufacturers [18].

4.1.1 Polyacrylamides

These are the water-soluble polymers that are used in many ways and for different purposes. One of the major compound, acrylamide, is a monomer derived from acrylic acid. Some most common representatives of the chemical group that acrylic acid belongs to are [1]:

- $CH_2 = CH - COOH$ → acrylic acid
- $CH_2 = CH - CN$ → acrylnitril
- $CH_2 = CH - COOR$ → acrylic acid ester
- $CH_2 = CH - CONH_2$ → acrylamide
- $CH_2 = CH - CHO$ → acrolein

The molecular weight and the size of the molecules of polyacrylamides depend on the type of the polymer and range between $1 \cdot 10^6 - 8 \cdot 10^6$ MDa for molecular weight and 0.1 – 0.3 μm for the size of the molecules. There are 2 main types of polyacrylamides i.e. hydrolyzed and not hydrolyzed (see Fig. 4.1 for chemical structure). The degree of hydrolysis is stated by the percentage of acrylic acid in the molecular chain of the polymer, which is usually 25-30% for most EOR products (but products with hydrolysis level approximating zero are also available). The products with high hydrolysis degree exhibit a strong sensitivity to salts unlike those approximating zero and can be used for preconditioning reservoirs [1].

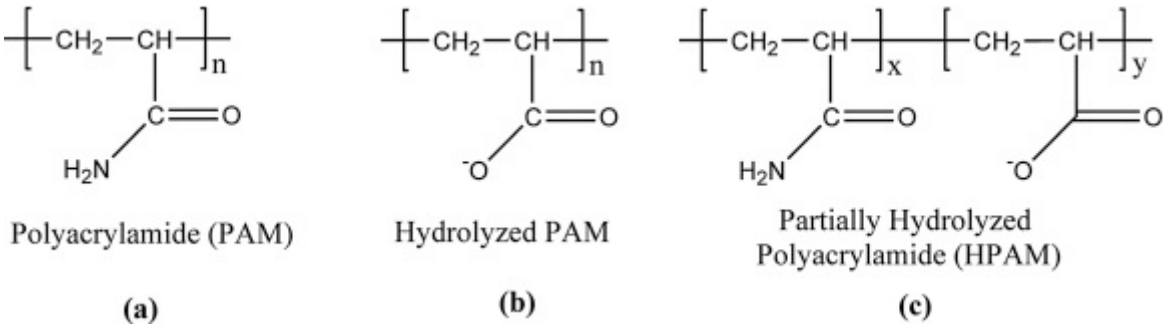

Figure 4. 1: Chemical structure of polyacrylamides with different hydrolysis level [19].

In the table below standard polymer are presented which co-polymers of acrylamide and acrylate are suitable for reservoirs with temperature up to 70°C (158°F) [20]:

Table 4. 1: Polymers that are best suitable for reservoirs up to 70°C [20].

		Anionicity	MW
Flopaam	1430 S	Low	Low
Flopaam	1530 S	Low	Medium
Flopaam	1630 S	Low	High
Flopaam	2430 S	Low	Low
Flopaam	2530 S	Low	Medium
Flopaam	2630 S	Low	Medium-High
Flopaam	3130 S	Medium to High	Ultra Low
Flopaam	3230 S	Medium to High	Very Low
Flopaam	3330 S	Medium to High	Low
Flopaam	3430 S	Medium to High	Medium
Flopaam	3530 S	Medium to High	Medium-High
Flopaam	3635 S	Medium to High	High
Flopaam	3630 S	Medium to High	High
Flopaam	6030 S	High	Very High
Flopaam	6040 D	High	Very High

ATBS-based polymers exhibit less sensitivity to salinity and temperature and are suitable for the reservoirs with temperature up to 95°C. These polymers are listed in table 4.2 and table 4.3 [20]:

Table 4. 2: Co-polymers of ATBS and acrylamide [20].

	Anionicity	MW
Flopaam AN 105	Very Low	Low
Flopaam AN 105 SH	Very Low	High
Flopaam AN 105 VHM	Very Low	Very High
Flopaam AN 110	Low	Low
Flopaam AN 110 SH	Low	High
Flopaam AN 110 VHM	Low	Very High
Flopaam AN 113	Low	Low
Flopaam AN 113 SH	Low	High
Flopaam AN 113 VHM	Low	Very High
Flopaam AN 118	Medium	Low
Flopaam AN 118 SH	Medium	High
Flopaam AN 118 VHM	Medium	Very High
Flopaam AN 125 VLM	Medium	Very low
Flopaam AN 125	Medium	Low
Flopaam AN 125 SH	Medium	High
Flopaam AN 125 VHM	Medium	Very High
Flopaam AN 132	High	Low
Flopaam AN 132 SH	High	High
Flopaam AN 132 VHM	High	Very High

Table 4. 3: Acrylamide / ATBS / Acrylic acid polymers [20].

	Anionicity	MW
Flopaam 5205	Medium	Medium
Flopaam 5205 SH	Medium	High
Flopaam 5115 VLM	Medium	Very Low
Flopaam 5115 BPM	Medium	Low
Flopaam 5115 MPM	Medium	Medium
Flopaam 5115	Medium	Medium
Flopaam 5115 SH	Medium	High
Flopaam 5115 VHM	Medium	Very High
Flopaam 5220	High	Medium
Flopaam 5220 SH	High	High
Flopaam 5220 VHM	High	Very High

4.2 Polysaccharides

It is important to understand a general description of saccharide chemistry in order to understand the properties of such polysaccharides as hydroxyethyl cellulose or xanthan gum.

Polysaccharides being the wealthiest material, are present ax cellulose to provide material for cell walls or as starch, etc. [1].

4.2.1 Hydroxyethyl cellulose (HEC)

Cellulose is the basic component of HEC. There are three positions for an addition or possible reaction with other chemicals without destroying the character of the molecule (i.e. two OH groups and the CH_2OH group). The chemical structure of the polymer is shown on Fig. 4.2 [1].

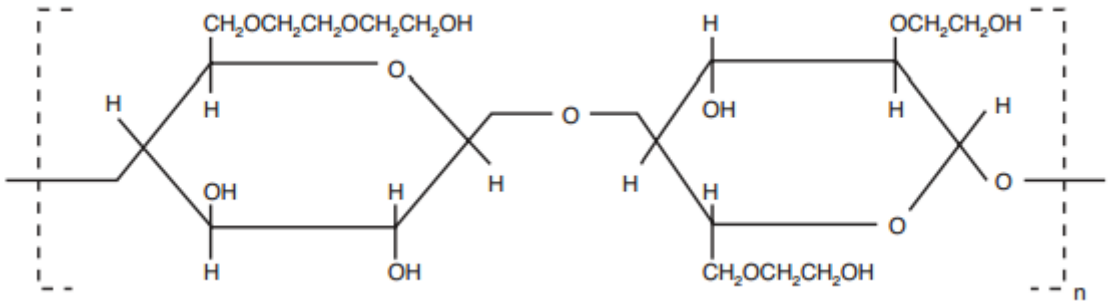

Figure 4. 2: Molecular structure of hydroxyethyl cellulose

There is also a possibility to get other polymers by just adding methyl, ethyl or carboxyl groups, which will give such polymers as carboxylmethyl cellulose (CMC) or ethylhydroxyethyl cellulose [1].

4.2.2 Xanthan

Xanthan is another kind of polysaccharides and it is produced by a type of bacteria called xanthomonas campestris, which is assumed to produce the polymer as a protection mechanism against dehydration. The chemical composition of the polymer is a complex structure where a cellulose chain with two different side chains at every second glucose ring (β – L glucose) being the backbone. As basic elements, side chains have saccharide rings as well and these side chains are made up of three monosaccharides. Mannose is located at the beginning of the end of the first side chain, which is followed by gluceron acid, after which again mannose with an acethyl group at the sixth carbon atom. The same way is structured the second side chain but at the end mannose it contains pyruvate unit. Fig 4.3 gives an example of molecular structure of xanthan [1].

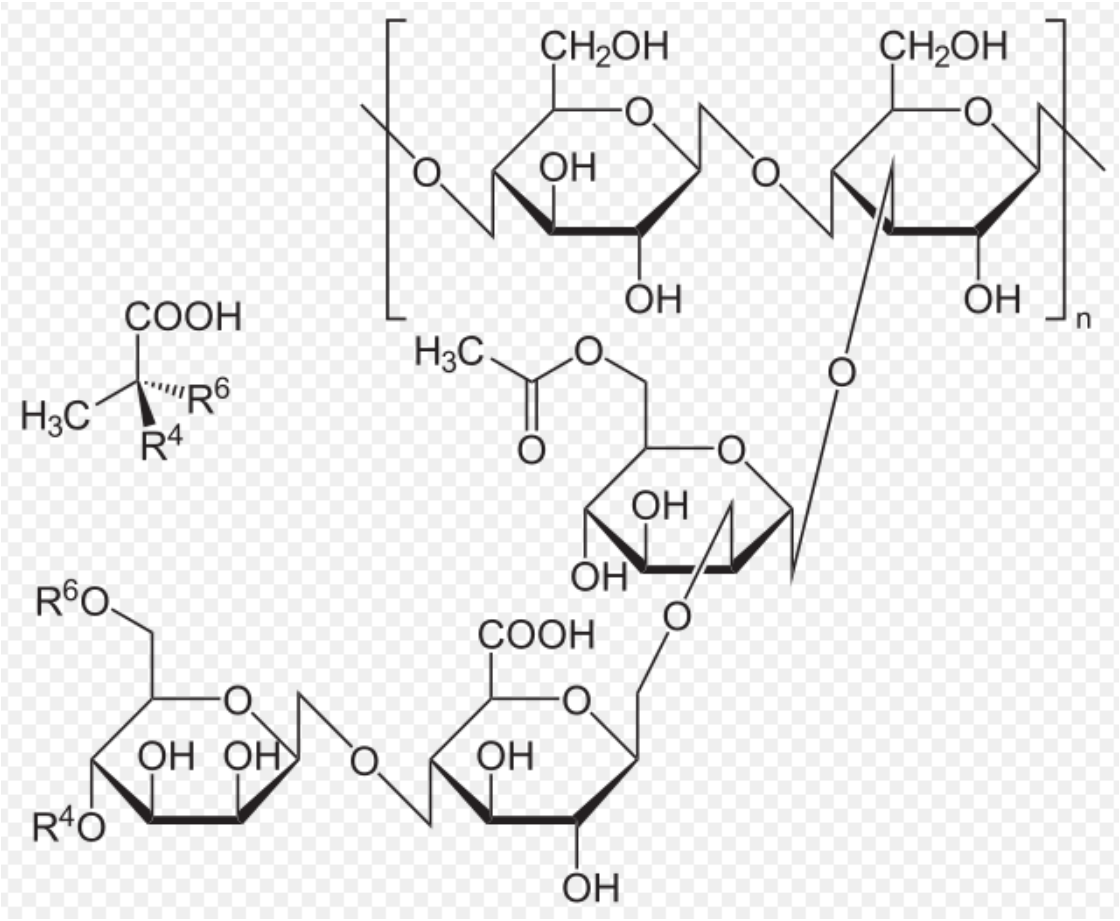

Figure 4. 3: Molecular structure of xanthan.

4.2 The main types of degradation and their mechanisms

Three basic types of degradation mechanisms exist i.e. chemical, mechanical and biological degradation [1].

4.2.1 Chemical degradation

Chemical degradation occurs when free radicals react with the polymer backbone resulting in decreasing molecular weight as well as viscosity drop because of in hydrodynamic volume. The reason for such radicals to form is the presence of chemicals or impurities in the water together with oxygen [21]. Moreover, divalent cations like Ca^{2+}, Mg^{2+} etc., impact the solution stability of polyacrylamides and their hydrolysis as well as influencing their tendency to flocculate. One of the facts that accelerates the mechanism of chemical degradation is temperature, which means that one should be aware of while choosing the right polymer for the right conditions [1].

4.2.2 Mechanical degradation

Mechanical degradation is tightly linked to shear conditions namely high shear conditions that can occur during mixing of polymers at high rates or during in the formations near the well where the polymer solutions flow at high velocities [1]. An example can be a polymer flowing through a capillary tube at different velocities (with high flow rate) [22]. And as was stated before the choice of polymer is very important as polymers with high molecular weight exhibit more sensitivity to mechanical degradations. Figures 4.4 and 4.5 show how different polymers are affected by shear degradation [21].

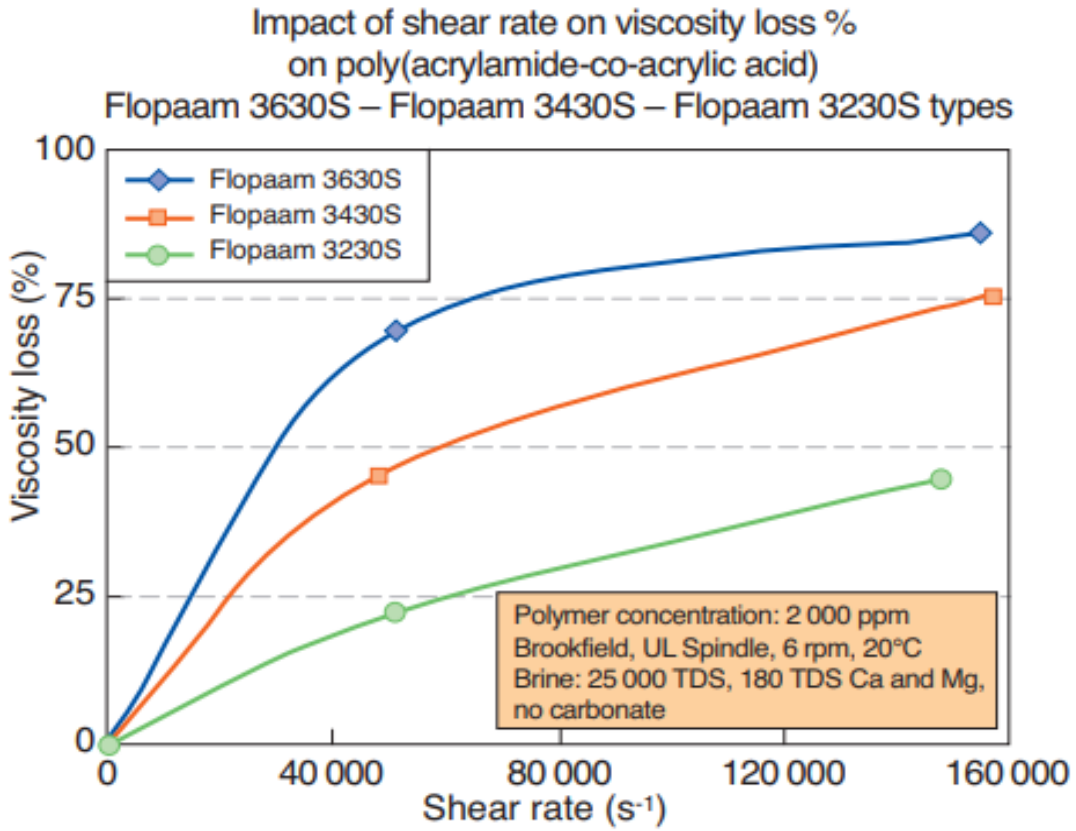

Figure 4. 4: Impact of shear rate on three copolymers with decreasing molecular weights: FP 3630S (high molecular weight), FP 3430S (medium molecular weight) and FP 3230S (low molecular weight) [21].

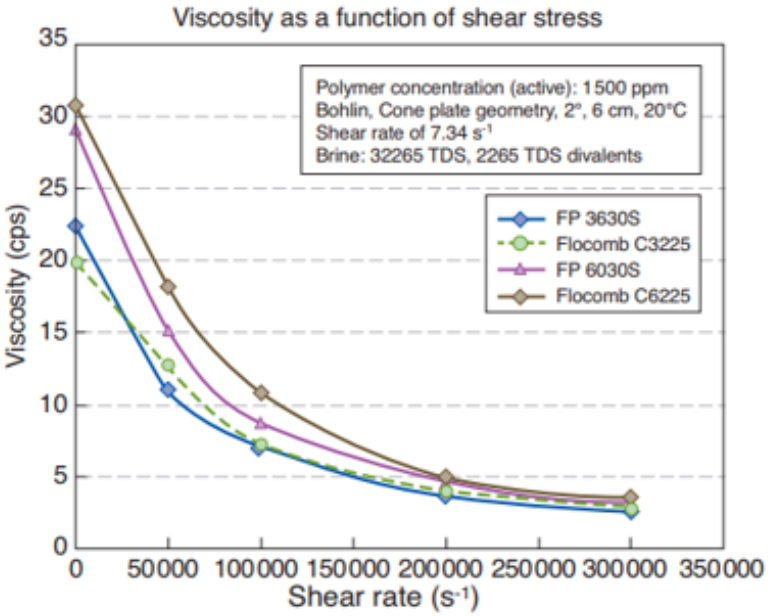

Figure 4. 5: Impact of mechanical degradation on a copolymer (FP3630S), a post-hydrolized polymer (FP6030S) and salt tolerant polymers (Flocomb C3525 and Flocomb C6225) [21].

An important point to note is that polyacrylamides are sensitive to mechanical degradation to some extent, while polysaccharides are not and can be mixed at very high shear rates [1].

4.2.3 Biological degradation

This type of degradation basically occurs in biopolymers mostly at low temperatures and salinities. There are two main things that cause biological degradation: when molecule is attacked by bacteria or by chemical processes governed by enzymes. Especially well enzymes can degrade cellulose polymers [1].

The most important factor affected by the biodegradability of polymers is their chemical structure which is liable for reactivity, functional group stability, hydrophilicity and swelling behaviour) [23]. Fig. 4.6 illustrates a pathway during biological degradation:

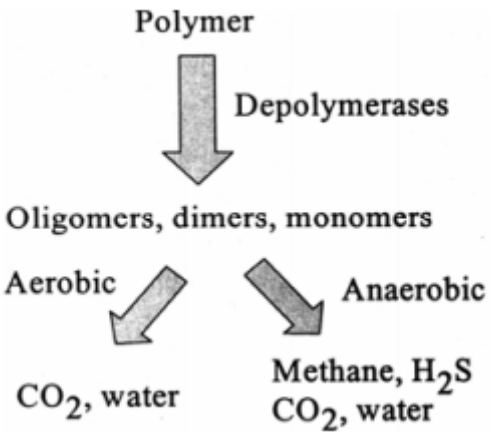

Figure 4. 6: Reaction pathways during biodegradatiuon of polymers [24].

5. Flow behaviour and flow curves and governing equations of fluid dynamics

This chapter will be devoted to different types of flow behaviour such as shear-thinning and shear-thickening and to derivation of the fundamental equations that govern the flow of fluids as well as examining their nature and appropriate boundary and initial conditions.

5.1 What influences flow behaviour?

There are three factors responsible for a substance's flow behaviour, they are:

1. Inner-molecular structure i.e. materials with high viscosity result in tightly linked molecules, which resist deformation (also defines Newtonian and non-Newtonian fluid dynamics).
2. Outside or external forces i.e. shear stress or shear rate, which compiles all types of actions (pulling, pushing or most commonly – gravity). The strength and the duration of the external force constitutes the further impact.
3. The ambient conditions i.e. pressure and temperature, which governs conditions under which a substance flows and what flow it develops [10].

One should also know that laminar flow is required in order to measure viscosity [10].

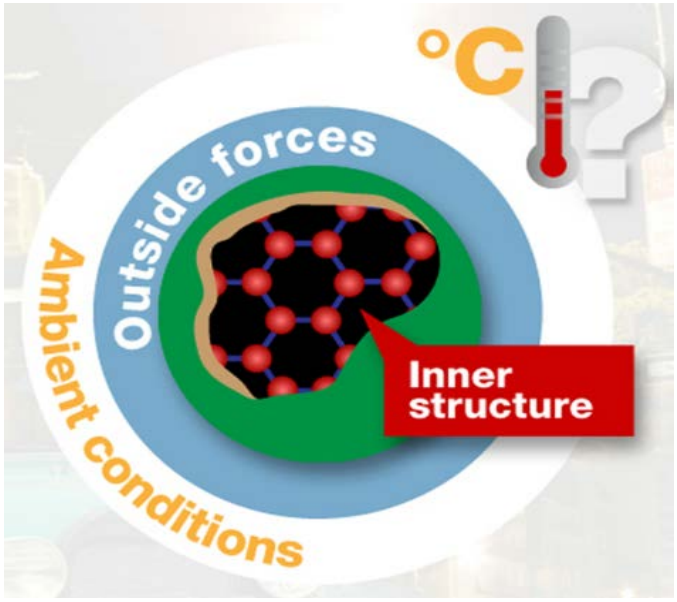

Figure 5. 1: Factors responsible for a substance's flow behaviour [10]

5.2 Laminar or turbulent flow

Laminar flow means a flow where molecules form a regular pattern and flow in determined direction and do not flow from one layer to another, which can be illustrated as imaginary thin layers (see Fig. 5.2) [10].

Turbulent flow means the flow where molecules have no a regular pattern and flow in random directions which leads to vortices and eddies and therefore, causes erroneous results during measurements. This happens because the device measuring viscosity, register the random movement of molecules as high flow resistance. One of the reasons of turbulent flow while measurements can be submitting a fluid to a too high shear rate [10].

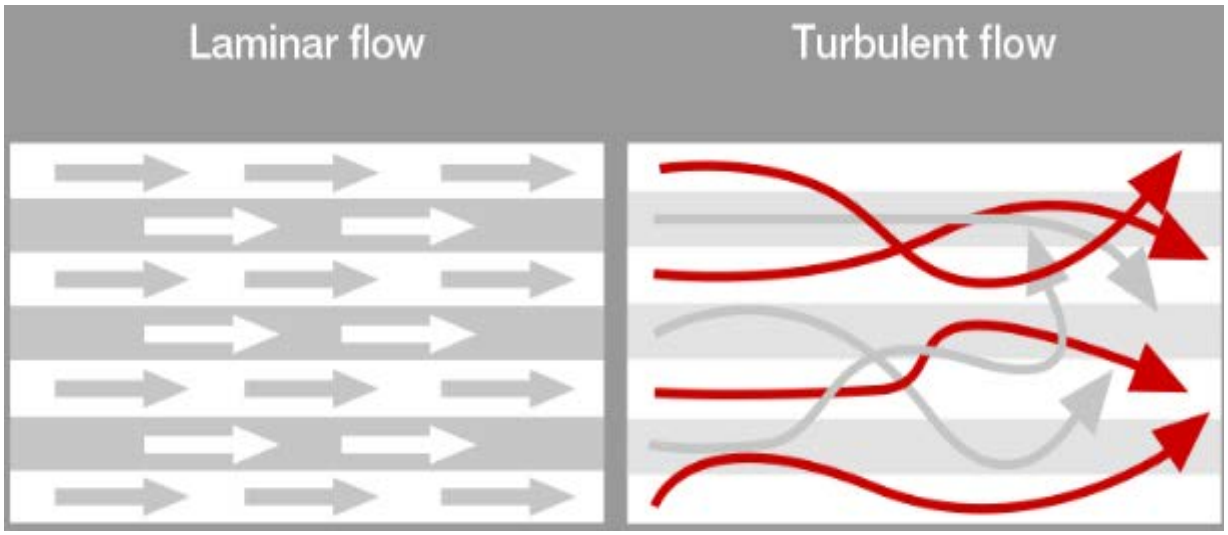

Figure 5. 2: Movement of molecules while laminar and tubulent flow [10].

5.3 Flow curves of ideally viscous substances

Figure 5.3 shows examples of ideally viscous or so-called Newtonian samples and the relation of shear stress and shear rate. As can be seen from this figure, viscosity of the samples does not change with the change in shear rate [25]:

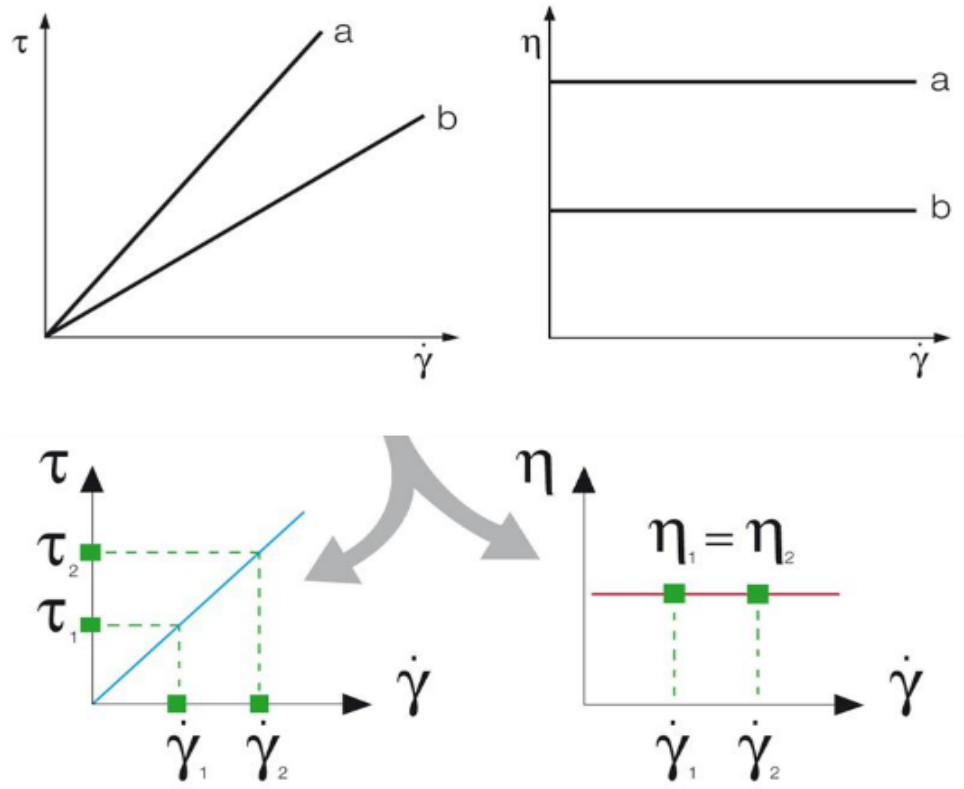

Figure 5. 3: Flow curves of two different ideally viscous fluids [25].

5.4 Flow curve of shear-thinning substances

The higher shear rates the lower the gradient of shear stress for the substances that show shear-thinning behaviour, which simply means with higher shear rates the viscosity of the material becomes lower. Many materials from daily life show this type of behaviour e.g. cosmetics such as creams, food samples such as ketchup, molten chocolate and etc. This is illustrated in figure 5.4 [25]:

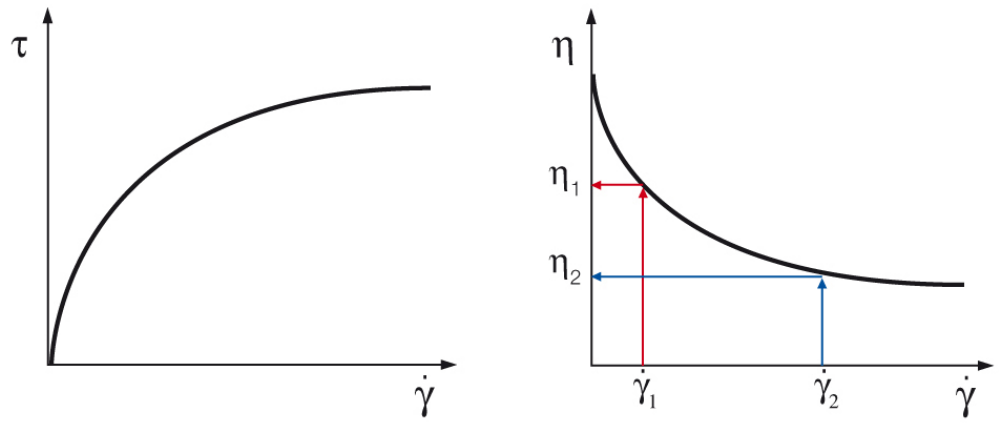

Figure 5. 4: Flow curve of a shear-thinning material [25].

5.5 Flow curve of shear-thickening substances

In this case, on the contrary to the first one, the gradient of shear stress increases with the increasing shear rate values, which means that the viscosity of the sample becomes higher with increasing shear rates. This type of flow behaviour is relatively rare which is encountered in the materials with the high solid content i.e. ceramic suspensions, starch dispersions, or dental composites. Figure 5.5 represents this type of flow behaviour [25].

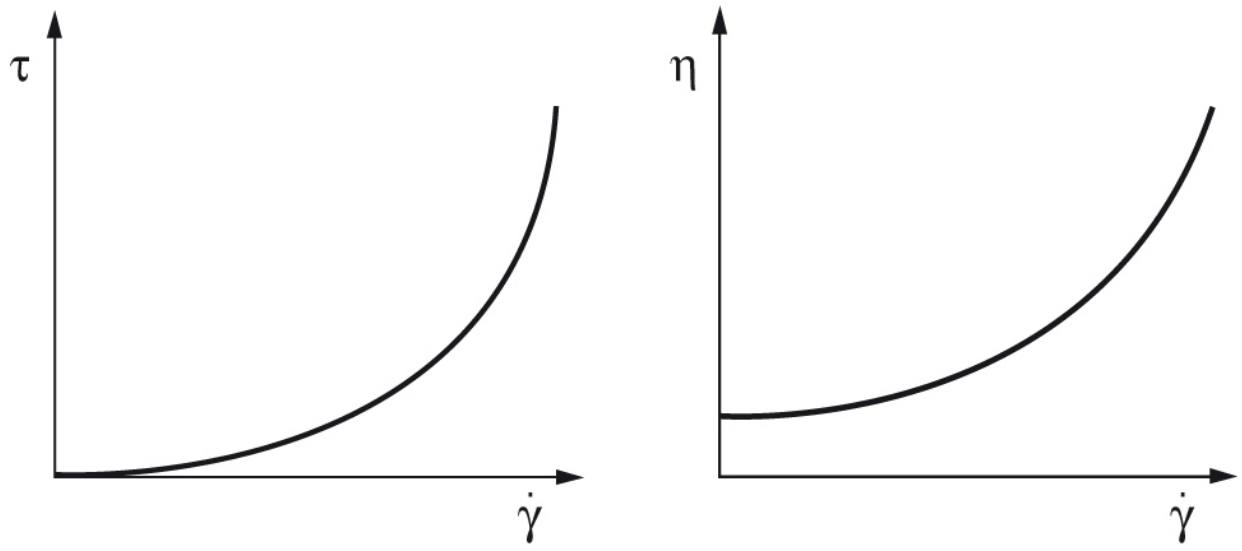

Figure 5. 5: Flow curve of a shear-thickening material [25].

5.6 Concepts of system and volume control

In fluid mechanics theory, it is determined that an identity of any fluid does not change in a system while the course of flow. And by identity, it means that the system consists of the same fluid particles as it flows. In other words, the mass of the fluid remains constant since it consists of the same fluid particles. Considering Fig. 5.6, the highlighted oval is assumed as a system that moves in the left direction. As different particles have different velocities, the size and the shape of the system may change, however the particles inside the oval will not change.

A control volume is a so-called region whose identity varying while fluid enters and leaves the control surface. The size and shape of the control volume depends on coordinate system used to analyze flow situation [26].

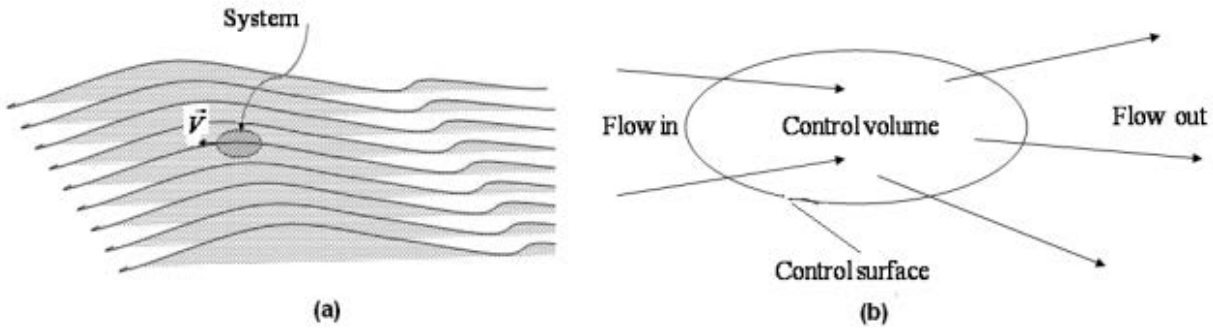

Figure 5. 6: Concept of system and control volume [26].

5.7 The substantial derivative

The major purpose of this chapter is to identify the physical meaning of substantial derivative and establish common notations.

Considering the model of infinitesimally small fluid element moving with the flow and unit vectors along *x*, *y* and *z* axes being $\vec{\imath}, \vec{\jmath}$ and $\vec{k}$ respectively, the vector velocity field then will be [27]:

$$\vec{V} = u\vec{\imath} + v\vec{\jmath} + w\vec{k} \tag{5.1}$$

where the *x, y* and *z* components are given by

$$u = u(x, y, z, t)$$

$$v = v(x, y, z, t)$$

$$w = w(x, y, z, t)$$

One should bear in mind that we are considering unsteady flow, which means that *u, v* and *w* are functions of both space and time. Scalar density is given by

$$\rho = \rho(x, y, z, t)$$

Fig. 5.7 illustrates fluid element moving in the flow field; where at initial time t_1 the density of the fluid is ρ_1 and after moving to point 2 at time t_2 the density of the fluid will be ρ_2

$$\rho_1 = \rho(x_1, y_1, z_1, t_1)$$

$$\rho_2 = \rho(x_2, y_2, z_2, t_2)$$

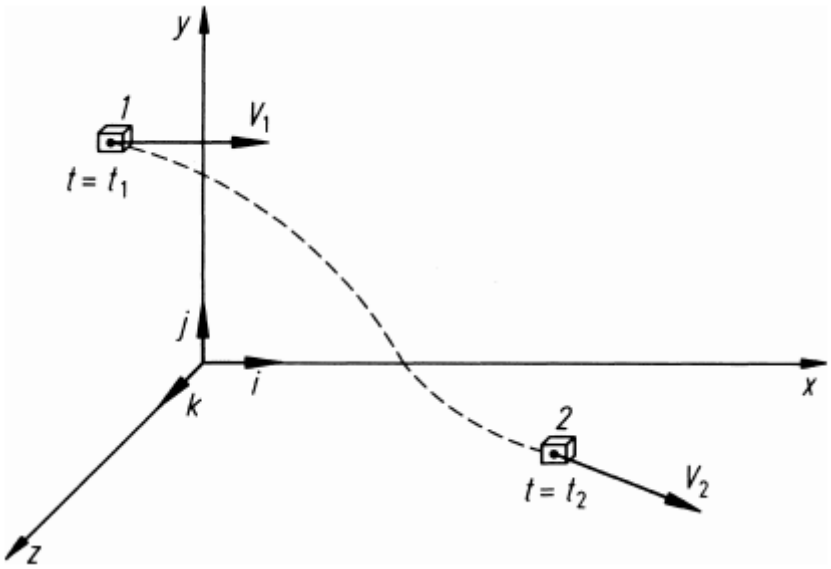

Figure 5. 7: Fluid element moving in the flow field (illustration for substantial derivative) [27].

By expanding the function in a Taylor's series around point 1, we obtain

$$\rho_2 = \rho_1 + \left(\frac{\partial \rho}{\partial x}\right)_1 (x_2 - x_1) + \left(\frac{\partial \rho}{\partial y}\right)_1 (y_2 - y_1) + \left(\frac{\partial \rho}{\partial z}\right)_1 (z_2 - z_1) + \left(\frac{\partial \rho}{\partial t}\right)_1 (t_2 - t_1) + (higher\ order\ terms)$$

Dividing the equation above by $(t_2 - t_1)$ and ignoring the terms with higher order, we get

$$\frac{(\rho_2 - \rho_1)}{(t_2 - t_1)} = \left(\frac{\partial \rho}{\partial x}\right)_1 \frac{(x_2 - x_1)}{(t_2 - t_1)} + \left(\frac{\partial \rho}{\partial y}\right)_1 \frac{(y_2 - y_1)}{(t_2 - t_1)} + \left(\frac{\partial \rho}{\partial z}\right)_1 \frac{(z_2 - z_1)}{(t_2 - t_1)} + \left(\frac{\partial \rho}{\partial t}\right)_1 \quad (5.2)$$

Taking right-hand-side of the Eq. 5.2 in the limit, as t_2 approaches t_1, we obtain

$$\lim_{t_2 \to t_1} \left(\frac{\rho_2 - \rho_1}{t_2 - t_1}\right) \equiv \frac{d\rho}{dt}$$

Here, $d\rho/dt$ stands for instantaneous time rate of change of density of the fluid element while movement through the point 1 and this is called substantial derivative. However, we should distinguish $(d\rho/dt)$ which is change of density of the given fluid element through space, from $(\partial\rho/\partial t)_1$ which is change of density at the fixed point 1. Hence, physically and numerically $(d\rho/dt)$ and $(\partial\rho/\partial t)$ are different quantities [27].

Returning to Eq. 5.2, we should note that

$$\lim_{t_2 \to t_1} \left(\frac{x_2 - x_1}{t_2 - t_1}\right) \equiv u$$

$$\lim_{t_2 \to t_1} \left(\frac{y_2 - y_1}{t_2 - t_1}\right) \equiv v$$

$$\lim_{t_2 \to t_1} \left(\frac{z_2 - z_1}{t_2 - t_1} \right) \equiv w$$

So, limiting Eq. 5.2 as $t_2 \to t_1$, we obtain

$$\frac{d\rho}{dt} \equiv u \frac{\partial \rho}{\partial x} + v \frac{\partial \rho}{\partial y} + w \frac{\partial \rho}{\partial z} + \frac{\partial \rho}{\partial t} \tag{5.3}$$

An expression for the substantial derivative in cartesian coordinates, then will look like

$$\frac{d}{dt} \equiv u \frac{\partial}{\partial x} + v \frac{\partial}{\partial y} + w \frac{\partial}{\partial z} + \frac{\partial}{\partial t} \tag{5.4}$$

In cartesian coordinates, the vector operator ∇ is defined as

$$\nabla \equiv \vec{\imath} \frac{\partial}{\partial x} + \vec{\jmath} \frac{\partial}{\partial y} + \vec{k} \frac{\partial}{\partial z} \tag{5.5}$$

Thus, Eq. 5.4 can be rewritten as

$$\frac{d}{dt} \equiv \frac{\partial}{\partial t} + (\vec{V} \cdot \nabla) \tag{5.6}$$

Equation 5.6 defines the substantial derivative operator in vector notation (which means that it is applicable for any coordinate system) [27].

5.7 Physical meaning of $\nabla \cdot \vec{V}$

As this term often appears in the equations of fluid dynamics, it is important to consider its physical meaning. Considering Fig. 5.8, the control volume moves with the flow hence it is always made up of the same fluid particles, which means that the mass is fixed and does not depend on time. However, as it flows to different places and regions with different densities ρ, its control surface *S* and volume *V* change with time [27].

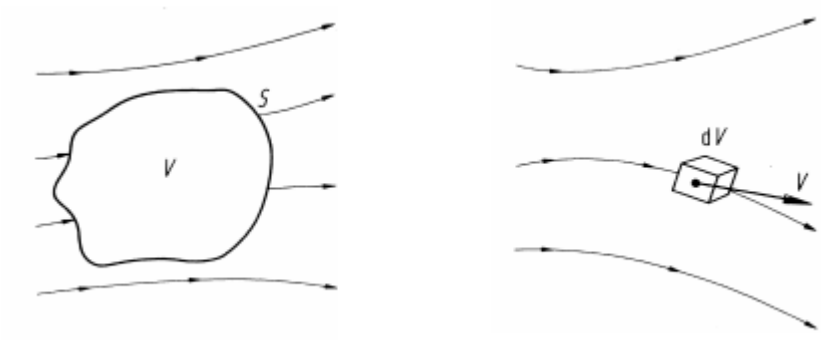

Figure 5. 8: Infinitesimal fluid element approach [27].

The control volume described above, is shown on Fig. 5.9 at some instant in time, considering infinitesimal surface element dS, moving at local velocity $\vec{V}$. Due to a movement of dS over a time increment Δt, the control volume ΔV will be equal to the volume of the cylinder with base area dS and altitude $(\vec{V}\Delta t)\cdot\vec{n}$, where $\vec{n}$ is a unit vector perpendicular to the surface dS and directed outwards [27].

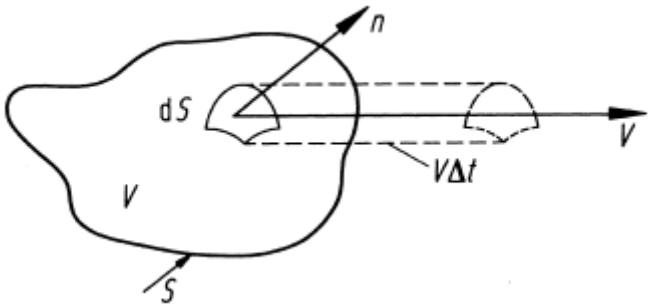

Figure 5. 9: Moving control volume used for the physical interpretation of the divergence of the velocity [27].

Thus,

$$dV = \left[(\vec{V}\Delta t)\cdot\vec{n}\right]dS = (\vec{V}\Delta t)\cdot dS \tag{5.7}$$

where $d\vec{S} \equiv \vec{n}dS$, and the total change in volume equals to the sum of Eq. 5.1 over the total control surface. By setting the limits $dS \to 0$, the summation will become the surface integral [27]:

$$\oiint_S (\vec{V}\Delta t)\cdot dS \tag{5.8}$$

If one simply divides Eq. 5.2 by Δt the result will be denoted by *dV/dt* as the time rate of change of the control volume

$$\frac{dV}{dt} = \frac{1}{\Delta t}\oiint_S (\vec{V}\Delta t)\cdot d\vec{S} = \oiint_S \vec{V}\cdot d\vec{S} \tag{5.9}$$

It is important to note that we have taken the substantial derivative of *V* for the left-hand-side of Eq. 5.3 as we are dealing with the time rate of the control volume (i.e. the volume moves with the flow). Then we can apply the divergence theorem from vector calculus and get

$$\frac{dV}{dt} = \iiint_V (\nabla\cdot\vec{V})dV \tag{5.10}$$

Considering Fir. 5.8, let's imagine that the moving control volume decreases to a very small volume δV and eventually becoming an infinitesimal fluid element as was shown in Fig. 5.7. then, we can rewrite Eq. 5.4 as

$$\frac{d(\delta V)}{dt} = \oiiint_{\delta V} (\nabla \cdot \vec{V}) dV \tag{5.11}$$

Finally, by assuming that δV is small enough i.e. $\nabla \cdot \vec{V}$ is constant throughout δV, the integral from Eq. 5.5 can be approximated to $(\nabla \cdot \vec{V})\delta V$ [27]:

$$\frac{d(\delta V)}{dt} = (\nabla \cdot \vec{V})\delta V$$

or

$$\nabla \cdot \vec{V} = \frac{1}{\delta V}\frac{d(\delta V)}{dt} \tag{5.12}$$

Eq. 5.6 illustrates the physical meaning of divergence of the velocity, which physically means that $\nabla \cdot \vec{V}$ *is the time rate of change of the volume of a moving fluid element per unit volume* [27].

5.8 Basic physical laws

In the theory of fluid dynamics, basically the flow properties are predicted without even measuring it. One should know the initial values of certain minimum numbers in order to obtain the values from different locations by using certain fundamental relationships. It is important to note that as they are strictly local and, therefore, cannot be used for different set of conditions. These are empirical relationships and there are certain of them that are widely applicable in a general flow field. Referring to the theory of fluid dynamics, one should highlight three most relevant laws i.e. [26]:

- **Conservation of mass (continuity equation)**
- **Conservation of momentum (Newton's second law of motion)**
- **Conservation of energy (first law of thermodynamics)**
- **Second law of thermodynamics**

All the laws stated above compile thermodynamic state relations i.e. equations of state, fluid property relation etc. for a particular fluid [26].

5.8.1 Conservation of mass (equation of continuity)

This chapter is devoted to show the physical nature of both the finite control volume and the infinitesimal fluid element models of the flow. The former model will be fixed in space, while the infinitesimal fluid element model will be moving with the flow (this is done in order to see the difference between the conservation and non-conservation forms).

First, considering a moving fluid element where the mass is fixed and is given by δm and the volume of the element is given δV [27].

$$\delta m = \rho \delta V \tag{5.13}$$

Since mass is conserved, it will remain constant in time (i.e. time derivative will be equal to zero), while the element is moving along the flow

$$\frac{d(\delta m)}{dt} = 0 \tag{5.14}$$

Taking equations (5.13) and (5.14) together, we obtain

$$\frac{d(\rho \delta V)}{dt} = \delta V \frac{d\rho}{dt} + \rho \frac{d(\delta V)}{dt} = 0$$

or,

$$\frac{d\rho}{dt} + \rho \left[\frac{1}{\delta V} \frac{d(\delta V)}{dt} \right] = 0 \tag{5.15}$$

As was discussed in section 5.7, the term in brackets stands for the physical meaning of the divergence of the velocity. Thus, combining equations (5.12) and (5.15) we have:

$$\frac{d\rho}{dt} + \rho \left(\nabla \cdot \vec{V} \right) = 0 \tag{5.16}$$

The equation that we obtained above is called *continuity equation* in *non-conservation form*. It took a non-conservation form because:

- The infinitesimal fluid element model was used, and we obtained Eq. 5.16, which is directly in partial differential form

- As the moving with the flow model was opted, we came to the *non-conservation* form of the continuity equation.

Now, we are taking the model with the finite control volume fixed in space, where velocity is $\vec{V}$, the vector elemental surface area is $d\vec{S}$ and the elemental volume inside the finite control volume is dV (as illustrated in Fig. 5.10). Fundamental physical principle of the mass being conserved then will look like:

$$\begin{Bmatrix} Net\ mass\ flow\ out \\ of\ control\ volume \\ through\ surface\ S \end{Bmatrix} = \begin{Bmatrix} Time\ rate\ of \\ decrease\ of\ mass \\ inside\ control\ volume \end{Bmatrix} \tag{5.17a}$$

or,

$$B = C \tag{5.17b}$$

where *B* and *C* were used for the left-hand-side and right-hand-side respectively in order to make further derivations more convenient.

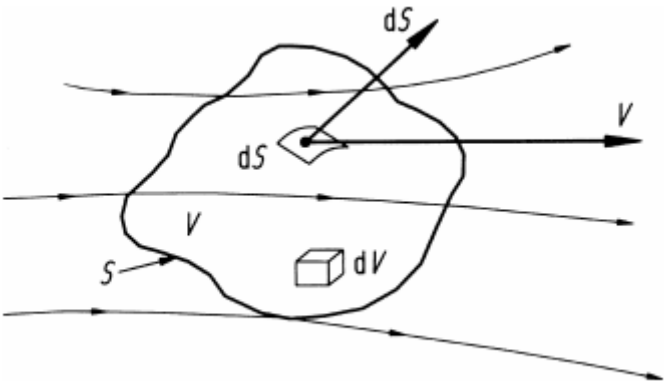

Figure 5. 10: Finite control volume fixed in space [27].

The elemental mass flow across the area dS will look like:

$$\rho V dS = \rho \vec{V} d\vec{S} \tag{5.18}$$

Note that $d\vec{S}$ is always directed out of the control volume, which means that when $\vec{V}$ also points out, the resulting $\rho\vec{V} \cdot d\vec{S}$ will be positive (i.e. *outflow* is seen). But when $\vec{V}$ points into the control volume, the product of $\rho\vec{V} \cdot d\vec{S}$ will be negative and hence, showing an *inflow.* Hence, a positive $\rho\vec{V} \cdot d\vec{S}$ denotes an *outflow*, whereas the negative – *inflow*. The sum over the control surface *S* of the elemental mass flows from Eq. (5.18) is the net mass flow *out* of the

entire control volume and after setting the limit over control surface *S*, we will obtain a surface integral, which physically represents the left-hand-side of Eq. (5.17b) [27].

$$B = \oiint_S \rho \vec{V} d\vec{S} \tag{5.19}$$

Now, considering the right-hand-side of Eq. (5.17b), the mass within dV is ρdV. Then, the total mass will be

$$\oiiint_V \rho dV$$

The time rate of *increase* of mass inside *V* will then be

$$\frac{\partial}{\partial t} \oiiint_V \rho dV$$

Then, the time rate of *decrease* will be the negative of that above which is equal to the right-hand-side of Eq. (5.17b)

$$-\frac{\partial}{\partial t} \oiiint_V \rho dV = C \tag{5.20}$$

Thus, by changing *B* and *C* from Eq. (5.17b) with equations (5.19) and (5.20), we get

$$\oiint_S \rho \vec{V} d\vec{S} = -\frac{\partial}{\partial t} \oiiint_V \rho dV$$

or,

$$\frac{\partial}{\partial t} \oiiint_V \rho dV + \oiint_S \rho \vec{V} d\vec{S} = 0 \tag{5.21}$$

Eq. (5.21) is in *conservation* form and in the integral form of the continuity equation.

If we set Eq. (5.21) in differential equation form then, as the control volume is fixed in space, the limits of integration will be constant, which allows to place the time derivative $\partial/\partial t$ inside the integral:

$$\oiiint_V \frac{\partial \rho}{\partial t} dV + \oiint_S \rho \vec{V} d\vec{S} = 0 \tag{5.22}$$

Using the divergence theorem from the vector calculus, we can express the surface integral from Eq. (5.22) as a volume integral

$$\oiint_S (\rho\vec{V})d\vec{S} = \iiint_V \nabla(\rho\vec{V})dV \tag{5.23}$$

Taking Eq. (5.23) into Eq. (5.22), we have

$$\iiint_V \frac{\partial\rho}{\partial t}dV + \iiint_V \nabla(\rho\vec{V})dV = 0 \tag{5.24}$$

or,

$$\iiint_V \left[\frac{\partial\rho}{\partial t} + \nabla\cdot(\rho\vec{V})\right]dV = 0 \tag{5.25}$$

The finite control volume is randomly featured in space which means that the only way for the integral to be equal to zero is for the integrand to be zero at every point within the control volume i.e.

$$\frac{\partial\rho}{\partial t} + \nabla\cdot(\rho\vec{V}) = 0 \tag{5.26}$$

Eq. (5.26) now is the *conservation form of the continuity equation* [27].

As for liquids $\overline{\nabla}\vec{V} = 0$, we have

$$\frac{\partial V_x}{\partial x} + \frac{\partial V_y}{\partial y} + \frac{\partial V_z}{\partial z} = 0 \tag{5.27}$$

5.8.2 Conservation of momentum (Generalized Navier-Stokes equations)

There are two forces acting on a body, namely body forces (acting at a distance) and surface forces (or tractions) [28]. The fundamental physical principle of this section is Newton's 2nd Law.

$$\vec{F} = m\frac{d\vec{V}}{dt} = m\vec{a}$$

Fig. 5.11 illustrates the sketch which says that mass times the acceleration of the element equals to its net force on the fluid element. As this is the vector relation, we can split it into three scalar relations along *x, y* and *z* axes. Considering only x-component, we get

$$F_x = ma_x \tag{5.28}$$

In this case F_x and a_x are the scalar components.

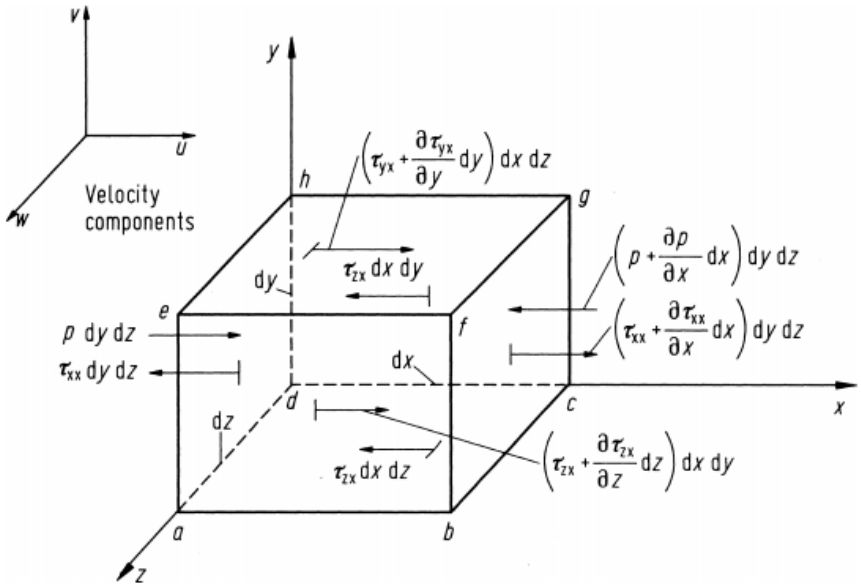

Figure 5. 11: X-direction forces of the infinitesimally small moving fluid element [27].

As was stated before there are two sources of the force acting on the moving fluid element:

- Body forces – acting directly on the volumetric mass of the fluid element (e.g. magnetic, gravitational etc.)
- Surface forces – acting directly on the surface of the fluid element [27].

Let us assume that $\vec{f}$ is the body force per unit mass acting on the fluid element and f_x is its x-component, where $(d_x\ d_y\ d_z)$ is the volume of the fluid element, then

$$\left\{ \begin{matrix} Body\ force\ on\ the \\ fluid\ element\ acting \\ in\ the\ x-direction \end{matrix} \right\} = \rho f_x \left(d_x\ d_y\ d_z\right) \tag{5.29}$$

for the moving fluid element, we then can write

$$\begin{aligned} \left\{ \begin{matrix} net\ surface\ force \\ in\ the\ x-direction \end{matrix} \right\} &= \left[p - \left(p + \frac{\partial p}{\partial x} dx\right)\right] dydz \\ &+ \left[\left(\tau_{xx} + \frac{\partial \tau_{xx}}{\partial x} dx\right) - \tau_{xx}\right] dydz \\ &+ \left[\left(\tau_{yx} + \frac{\partial \tau_{yx}}{\partial y} dy\right) - \tau_{yx}\right] dxdz \\ &+ \left[\left(\tau_{zx} + \frac{\partial \tau_{zx}}{\partial z} dz\right) - \tau_{zx}\right] dxdy \end{aligned} \tag{5.30}$$

where τ_{xx} – normal stress and τ_{yx}, τ_{zx} – shear stresses.

By adding equations (5.29) and (5.30) and cancelling terms, we obtain the total force in the x-direction i.e.

$$F_x = \left(-\frac{\partial p}{\partial x} + \frac{\partial \tau_{xx}}{\partial x} + \frac{\partial \tau_{yx}}{\partial y} + \frac{\partial \tau_{zx}}{\partial z}\right) dxdydz + \rho f_x dxdydz \tag{5.31}$$

Eq. (5.31) stands for the left-hand-side of Eq. (5.28) and in order to determine the right-hand-side we need to recall that the mass of the fluid element is fixed and equals

$$m = \rho \, dxdydz \tag{5.32}$$

Let us denote the acceleration in the x-direction as a_x and since the acceleration is the time-rate-of-change of its velocity, we have

$$a_x = \frac{du}{dt} \tag{5.33}$$

Combining equations (5.28), (5.31), (5.32) and (5.33), we have

$$\rho \frac{du}{dt} = -\frac{\partial p}{\partial x} + \frac{\partial \tau_{xx}}{\partial x} + \frac{\partial \tau_{yx}}{\partial y} + \frac{\partial \tau_{zx}}{\partial z} + \rho f_x \tag{5.34a}$$

Eq. (5.34a) is the x-component of the momentum equation for a viscous flow. In the same way we can obtain equations for the y- and z-components i.e.

$$\rho \frac{dv}{dt} = -\frac{\partial p}{\partial y} + \frac{\partial \tau_{xy}}{\partial x} + \frac{\partial \tau_{yy}}{\partial y} + \frac{\partial \tau_{zy}}{\partial z} + \rho f_y \tag{5.34b}$$

and

$$\rho \frac{dw}{dt} = -\frac{\partial p}{\partial z} + \frac{\partial \tau_{xz}}{\partial x} + \frac{\partial \tau_{yz}}{\partial y} + \frac{\partial \tau_{zz}}{\partial z} + \rho f_z \tag{5.34c}$$

It is important to note that as the fluid element is moving, equations (5.34a, b and c) are in *non-conservation* form. They are also called *Navier-Stokes equations*, after two scientists – the Frenchman M. Navier and the Englishman G. Stokes [27].

5.8.2.1 Navier-Stokes equations in conservation form

The equations derived above can be obtained in conservation form as well. To do so, let us take the left-hand-side of Eq. (5.34a) in terms of definition of the substantial derivative i.e.

$$\rho \frac{du}{dt} = \rho \frac{\partial u}{\partial t} + \rho \vec{V} \cdot \nabla u \tag{5.35}$$

Now, let us expand the derivative

$$\frac{\partial(\rho u)}{\partial t} = \rho \frac{\partial u}{\partial t} + u \frac{\partial \rho}{\partial t} \tag{5.36}$$

or,

$$\rho \frac{\partial u}{\partial t} = \frac{\partial(\rho u)}{\partial t} - u \frac{\partial \rho}{\partial t} \tag{5.37}$$

Recalling the vector identity for the divergence of the product, we get

$$\nabla \cdot \left(\rho u \vec{V}\right) = u \nabla \cdot \left(\rho \vec{V}\right) + \left(\rho \vec{V}\right) \cdot \nabla u \tag{5.38}$$

or,

$$\left(\rho \vec{V}\right) \cdot \nabla u = \nabla \cdot \left(\rho u \vec{V}\right) - u \nabla \cdot \left(\rho \vec{V}\right) \tag{5.39}$$

Now, let us substitute equations (5.39) and (5.37)

$$\begin{aligned} \rho \frac{du}{dt} &= \frac{\partial(\rho u)}{\partial t} - u \frac{\partial \rho}{\partial t} - u \nabla \cdot \left(\rho \vec{V}\right) + \nabla \cdot \left(\rho u \vec{V}\right) \\ \rho \frac{du}{dt} &= \frac{\partial(\rho u)}{\partial t} - u \left[\frac{\partial \rho}{\partial t} + \nabla \cdot \left(\rho \vec{V}\right)\right] + \nabla \cdot \left(\rho u \vec{V}\right) \end{aligned} \tag{5.40}$$

Examining Eq. (5.40) we can see that the term in the brackets is the continuity equation (which was derived in Eq. (5.26)). Hence, we can reduce Eq. (5.40) as the term in the brackets simply equals to zero and get

$$\rho \frac{du}{dt} = \frac{\partial(\rho u)}{\partial t} + \nabla \cdot \left(\rho u \vec{V}\right) \tag{5.41}$$

Now, in order to obtain Navier-Stokes equations in the *conservation form*, we should simply substitute Eq. (5.41) into Eqs. (5.34a), (5.34b) and (5.34c) to derive expressions for x-, y- and z-components i.e.

$$\frac{\partial(\rho u)}{\partial t} + \nabla \cdot \left(\rho u \vec{V}\right) = -\frac{\partial p}{\partial x} + \frac{\partial \tau_{xx}}{\partial x} + \frac{\partial \tau_{yx}}{\partial y} + \frac{\partial \tau_{zx}}{\partial z} + \rho f_x \tag{5.42a}$$

$$\frac{\partial(\rho v)}{\partial t} + \nabla \cdot \left(\rho v \vec{V}\right) = -\frac{\partial p}{\partial y} + \frac{\partial \tau_{xy}}{\partial x} + \frac{\partial \tau_{yy}}{\partial y} + \frac{\partial \tau_{zy}}{\partial z} + \rho f_y \tag{5.42b}$$

$$\frac{\partial(\rho w)}{\partial t} + \nabla \cdot \left(\rho w \vec{V}\right) = -\frac{\partial p}{\partial z} + \frac{\partial \tau_{xz}}{\partial x} + \frac{\partial \tau_{yz}}{\partial y} + \frac{\partial \tau_{zz}}{\partial z} + \rho f_z \qquad (5.42c)$$

Equations (5.42a, b and c) are the Navier-Stokes equations in *conservation form* [27].

5.8.2.2 Complete Navier-Stokes equations

In the late 17th century Isaac Newton stated that *Newtonian* fluids (that time they were not yet called *Newtonian* fluids) are those where shear stress is proportional to the velocity gradient i.e. time-rate-of-strain. Similarly, those fluids where τ is not proportional to the velocity gradient are *non-Newtonian* fluids. In 1845, Stokes obtained the following equations for the *Newtonian* fluids:

$$\tau_{xx} = \lambda \nabla \cdot \vec{V} + 2\mu \frac{\partial u}{\partial x} \qquad (5.43a)$$

$$\tau_{yy} = \lambda \nabla \cdot \vec{V} + 2\mu \frac{\partial v}{\partial y} \qquad (5.43b)$$

$$\tau_{zz} = \lambda \nabla \cdot \vec{V} + 2\mu \frac{\partial w}{\partial z} \qquad (5.43c)$$

$$\tau_{xy} = \tau_{yx} = \mu \left(\frac{\partial v}{\partial x} + \frac{\partial u}{\partial y}\right) \qquad (5.43d)$$

$$\tau_{xz} = \tau_{zx} = \mu \left(\frac{\partial u}{\partial z} + \frac{\partial w}{\partial x}\right) \qquad (5.43e)$$

$$\tau_{yz} = \tau_{zy} = \mu \left(\frac{\partial w}{\partial y} + \frac{\partial v}{\partial z}\right) \qquad (5.43f)$$

where, μ – molecular viscosity coefficient

λ – bulk viscosity coefficient

Stokes, then made a hypothesis that is often used in practice, however which has not been precisely confirmed to the present day.

$$\lambda = -\frac{2}{3}\mu$$

Now, in order to obtain the complete Navier-Stokes equations in conservation form, we should substitute equations (5.43) into equations (5.42)

$$\frac{\partial(\rho u)}{\partial t}+\frac{\partial(\rho u^2)}{\partial x}+\frac{\partial(\rho uv)}{\partial y}+\frac{\partial(\rho uw)}{\partial z}= \tag{5.44a}$$

$$=-\frac{\partial p}{\partial x}+\frac{\partial}{\partial x}\left[\lambda\nabla\cdot\vec{V}+2\mu\frac{\partial u}{\partial x}\right]+\frac{\partial}{\partial y}\left[\mu\left(\frac{\partial v}{\partial x}+\frac{\partial u}{\partial y}\right)\right]+\frac{\partial}{\partial z}\left[\mu\left(\frac{\partial u}{\partial z}+\frac{\partial w}{\partial x}\right)\right]+\rho f_x$$

$$\frac{\partial(\rho v)}{\partial t}+\frac{\partial(\rho uv)}{\partial x}+\frac{\partial(\rho v^2)}{\partial y}+\frac{\partial(\rho vw)}{\partial z}= \tag{5.44b}$$

$$=-\frac{\partial p}{\partial y}+\frac{\partial}{\partial x}\left[\mu\left(\frac{\partial v}{\partial x}+\frac{\partial u}{\partial y}\right)\right]+\frac{\partial}{\partial y}\left[\lambda\nabla\cdot\vec{V}+2\mu\frac{\partial v}{\partial y}\right]+\frac{\partial}{\partial z}\left[\mu\left(\frac{\partial w}{\partial y}+\frac{\partial v}{\partial z}\right)\right]+\rho f_y$$

$$\frac{\partial(\rho w)}{\partial t}+\frac{\partial(\rho uw)}{\partial x}+\frac{\partial(\rho vw)}{\partial y}+\frac{\partial(\rho w^2)}{\partial z}= \tag{5.44c}$$

$$=-\frac{\partial p}{\partial z}+\frac{\partial}{\partial x}\left[\mu\left(\frac{\partial u}{\partial z}+\frac{\partial w}{\partial x}\right)\right]+\frac{\partial}{\partial y}\left[\mu\left(\frac{\partial w}{\partial y}+\frac{\partial v}{\partial z}\right)\right]+\frac{\partial}{\partial z}\left[\lambda\nabla\cdot\vec{V}+2\mu\frac{\partial w}{\partial z}\right]+\rho f_z$$

The equations obtained above (i.e. (5.44a, 5.44b and 5.44c)) are the complete Navier-Stokes equations in conservation form [27].

5.8.3 First law of thermodynamics

The first law of thermodynamics constitutes the energy conservation law which states that energy cannot be created, nor can it be destroyed but can change its form from one to another. For a closed system, the expression of this law will be [26]

$$\delta Q = dE + \delta W \tag{5.45}$$

where, δQ – the heat exchange with the system,

δW – the work done by the system,

dE – the change in energy of the system.

5.8.4 Second law of thermodynamics

The second law or as it is also said the *'total entropy'* of thermodynamics is the second fundamental concept of thermodynamics. By introducing a new property i.e. entropy (*S*) we can express the unidirectional nature of a process [29].

$$dS \geq \frac{\delta Q}{T} \tag{5.46}$$

where, S – entropy,

dS – change in the entropy,

δQ – heat transfer,

T – absolute temperature.

As it is experienced losses due to friction, viscous dissipation and other non-recoverable losses, the inequality sign was used [26].

5.9 Poiseuille flow and Hagen-Poiseuille equation

In this section a flow resulting from pressure gradients in a tube will be covered. Hagen-Poiseuille flow is the one describing pressure-driven flow in a tube with circular cross section (Fig. 5.12). Here, we will assume a flow in z direction (i.e. $V_r = V_\theta = 0$) $\Longrightarrow$ velocity gradients in the θ and z directions are zero. Recalling Navier-Stokes equation [30],

$$\rho \frac{\partial \vec{V}}{\partial t} + \rho \vec{V} \cdot \nabla \vec{V} = -\nabla p + \eta \nabla^2 \vec{V} \tag{5.46}$$

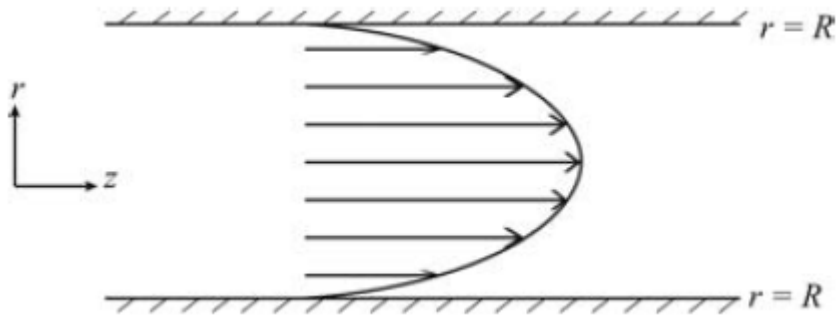

Figure 5. 12: Poiseuille flow in a circular tube [30].

Because of the geometric simplification we can obtain a simplified version Eq. (5.46) by just cancelling the convection and unsteady terms i.e.

$$\nabla p = \eta \nabla^2 \vec{V} \tag{5.47}$$

For radially symmetric flow:

$$\frac{\partial p}{\partial z} = \eta \frac{1}{\zeta} \frac{\partial}{\partial \zeta} \zeta \frac{\partial V_z}{\partial \zeta} \tag{5.48}$$

In order to solve Eq. (5.48) we should assume that $\partial p/\partial z$ is uniform and then, integrate the ζ terms:

$$\frac{\partial p}{\partial z} \frac{1}{2} \zeta^2 + C_1 = \zeta \eta \frac{\partial V_z}{\partial \zeta} \tag{5.49}$$

Now, by simple rearranging, we get

$$\frac{\partial p}{\partial z} \frac{\zeta}{2\eta} + \frac{C_1}{\eta \zeta} = \frac{\partial V_z}{\partial \zeta} \tag{5.50}$$

Finally, after integrating again the term above, we obtain the expression for V_z

$$V_z = \frac{\partial p}{\partial z} \frac{\zeta^2}{4\eta} + \frac{C_1}{\eta} ln\zeta + C_2$$

Now, by bounding V_z at ζ = 0, and V_z= 0 at ζ = R, we can find Poiseuille solution for flow in a tube of radius R:

$$V_z = -\frac{1}{4\eta} \frac{\partial p}{\partial z} (R^2 - r^2) \tag{5.51}$$

We can integrate the distribution spatially in order to express volumetric flow rate Q:

$$Q = -\frac{\pi R^4}{8\eta} \frac{\partial p}{\partial z} \tag{5.52}$$

recalling that

$$Q = \int_A dQ = \int_A V dA$$

We can, write Hagen-Poiseuille equation as follows

$$\int_0^R V_z(r) 2\pi r dr = \frac{\pi R^4}{8\eta} \frac{\partial p}{\partial z} \tag{5.53}$$

6. Newtonian Fluid models

As was discussed in chapter 5, majority of the polymers experience shear thinning effect such as reduction in viscosity at high shear rates. This is easily explained, as at high shear rates the molecular chains of the polymers are disentangled and stretched out, which makes the molecules to slide past each other easier, making the bulk viscosity lower. Taking for an example a polystyrene, Fig. 6.1 illustrates the shear thinning behaviour as well as temperature dependence of the viscosity.

It is common to determine the viscosity η as a function of the strain rate and temperature, and calculate the deviatoric stress tensor such as

$$\underline{\underline{\tau}} = \eta(\dot{\gamma}, T)\underline{\underline{\dot{\gamma}}} \tag{6.1}$$

Eq. (6.1) is often mentioned as the *General Newtonian Fluid model*, where $\underline{\underline{\dot{\gamma}}}$ is the rate of deformation tensor or simply strain rate tensor and is defined as follows:

$$\underline{\underline{\dot{\gamma}}} = \nabla\underline{u} + \nabla\underline{u}^t \tag{6.2}$$

where $\nabla\underline{u}$ is the velocity gradient tensor.

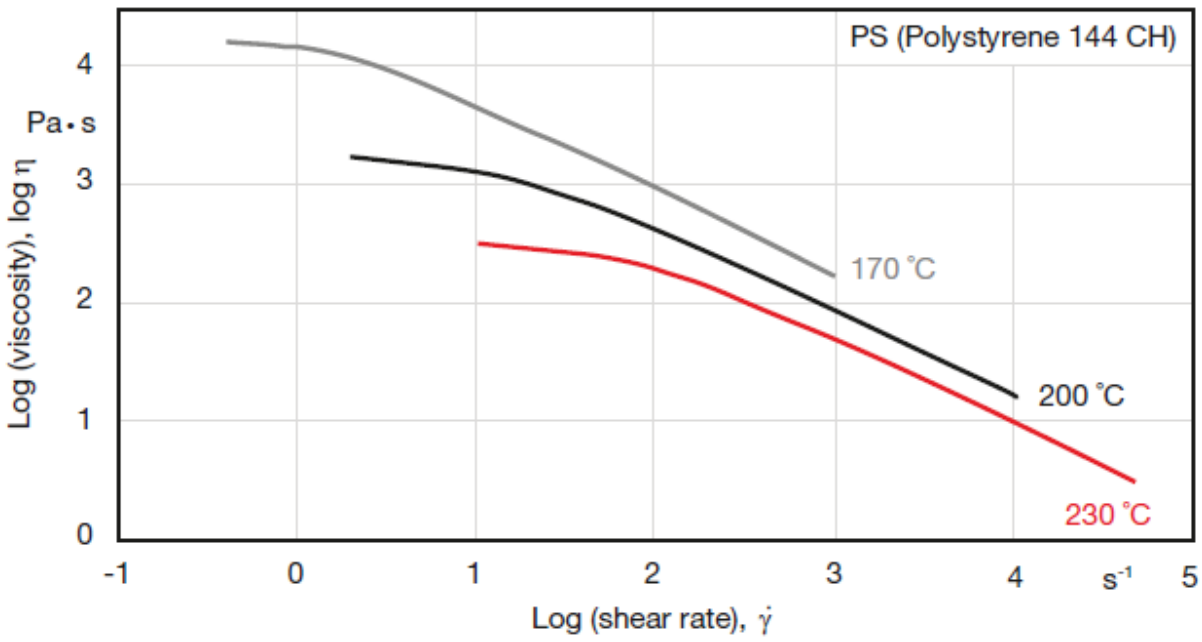

Figure 6. 1: Viscosity curves for polystyrene [31].

6.1 Generalized Newtonian Fluid (GNF) models; Viscous flow models

In this chapter several flow models will be described, those that comply with the *Generalized Newtonian Fluid* assumptions, even though they have different parameters to fit them. The goals of the models are as follows: to get analytical solutions for different flow behaviours in polymer processing and store the data obtained with the minimum number of parameters. As fluids have different flow behaviour (i.e. some can exhibit a strong shear thinning behaviour, others may be sensitive to a yield stress or even experiencing both of the behaviours and so on), there are different models that would best fit them. Cases for different fluids with different flow behaviours are presented on Fig. 6.2 [31].

Taking into account all the behaviour parameters, type of the flow and all the appropriate specification of the process, rheologists are those who responsible to find the most suitable model represented in Eq. (6.1). but one should bear in mind that models that represent complex rheological behaviour, such as those of polymers, append a significant difficulty to the analysis of a flow [31].

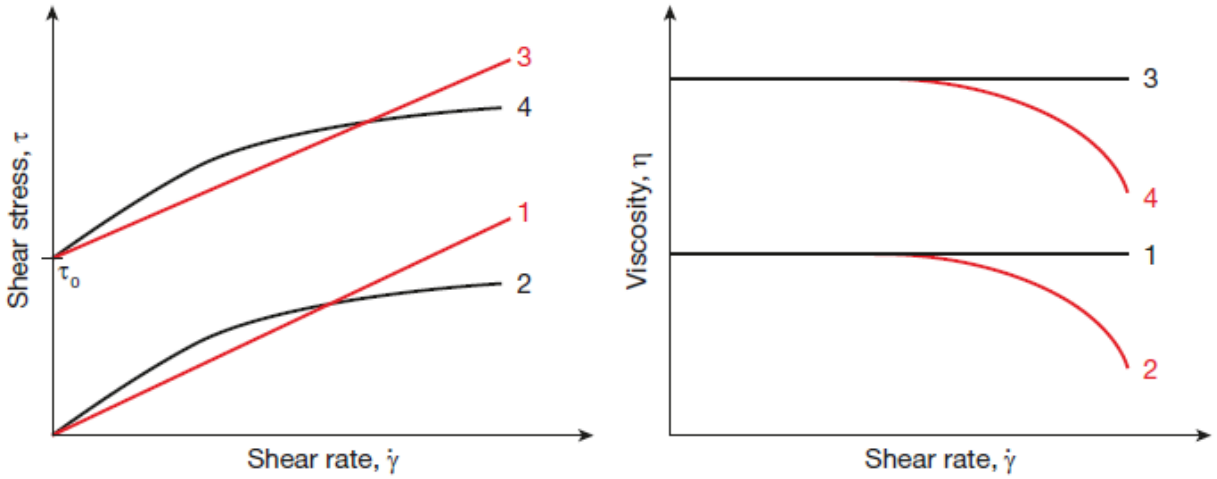

Figure 6. 2: Stress curves (left) and viscosity curves (right) for various fluids: (1) Newtonian fluid, (2) Shear-thinning fluid, (3) Newtonian fluid with yield stress τ_o, (4) shear-thinning fluid with yield stress τ_o [31].

6.1.1 The Power Law model

This is the model that was first proposed by Ostwald and de Waele, which accurately shows the shear thinning region in the viscosity versus shear rate curve. However, the Power Law model

neglects the Newtonian plateau measured at low strain rates (see Fig. 6.3). The basic equation that stands for the Power Law is

$$\tau = m(T)\dot{\gamma}^{n-1} \tag{6.3}$$

where m – consistency index,

n – Power Law or flow index.

Here, n represents behaviour of the shear thinning flow of the polymer for $n < 1$. One should keep in mind that consistency index may contain the temperature dependency of viscosity. Typical values of consistency indices, Power Law indices and temperature dependence parameters for common thermoplastics are shown in Table 6.1. The coefficients presented in the table are not recommended for design purposes and are presented only for a guideline as the values can vary significantly from one sort of polymer to another because the variation in side groups, molecular weight, flowing agents and other processing additives plays a big role. The power Law model has the limits where the infinite viscosity at zero shear strain $\dot{\gamma}$ leads to an erroneous result in the region where the shear rate of zero is encountered i.e.:

$$\eta \to 0 \quad \text{as} \quad \dot{\gamma} \to \infty$$

$$\eta \to \infty \quad \text{as} \quad \dot{\gamma} \to 0.$$

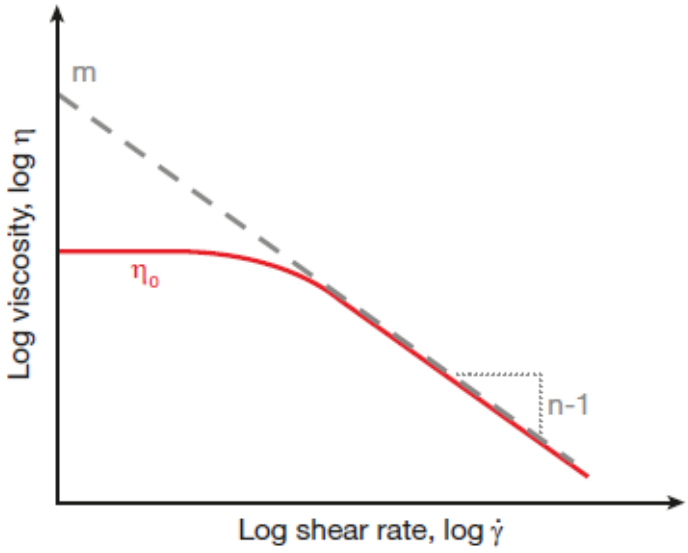

Figure 6. 3: Viscosity curve (solid line) and an approximation by the Power Law model (dashed line) in Eq. (6.3) [31].

Table 6. 1: Power Law and consistency indices *m* and *n* respectively for common thermoplastics [31].

Polymer	m (Pa·s^n)	n	T (°C)
Polystyrene	2.80×10^4	0.28	170
High density polyethylene	2.00×10^4	0.41	180
Low density polyethylene	6.00×10^3	0.39	160
Polypropylene	7.50×10^3	0.38	200
Polyamide 66	6.00×10^2	0.66	290
Polycarbonate	6.00×10^2	0.98	300
Polyvinyl chloride	1.70×10^4	0.26	180

6.1.2 Cross model

This is the model with four constants displays a non-zero bounded viscosity at both the upper and lower limits, and describes both Newtonian and shear thinning behaviour:

$$\frac{\eta - \eta_\infty}{\eta_o - \eta_\infty} = \frac{1}{[1 + (K\dot{\gamma})^{1-n}]} \tag{6.4}$$

where η_o – zero shear rate viscosity,

η_∞ – infinite shear rate viscosity,

K – time constant,

n – Power Law index.

It is important to note that when $\eta \ll \eta_o$ or $\eta \gg \eta_\infty$, then the Cross model reduces to the Power Law model.

We can also rewrite the Cross model, if the infinite shear rate viscosity is negligible, as follows:

$$\eta = \frac{\eta_o}{\left[1 + \left(\frac{\eta_o \dot{\gamma}}{\tau^*}\right)^{1-n}\right]} \tag{6.5}$$

where, τ^* - critical shear stress at the transition from Newtonian plateau, with $K = \eta_o/\tau^*$ [31].

6.1.4 Carreau model

Carreau model is for data over a wide range of shear rates and is similar to Yasuda model where the constant *a* is replaced by 2 i.e. [5]:

$$\frac{\eta - \eta_\infty}{\eta_o - \eta_\infty} = [1 + (\lambda\dot{\gamma})^2]^{\frac{n-1}{2}} \quad (6.7)$$

6.1.3 Carreau-Yasuda model

This model is similar to the Cross model and was proposed by Yasuda and has an extra material constant *a* in order to fit the data [32]:

$$\frac{\eta - \eta_\infty}{\eta_o - \eta_\infty} = [1 + (\lambda\dot{\gamma})^a]^{\frac{n-1}{a}} \quad (6.6)$$

6.1.5 Bird-Carreau-Yasuda model

This model, containing 5 parameters, was developed for a very wide range of shear rates and that accounts for the observed Newtonian plateaus [31]:

$$\frac{\eta - \eta_\infty}{\eta_o - \eta_\infty} = [1 + |\lambda\dot{\gamma}|^a]^{\frac{n-1}{a}} \quad (6.8)$$

Parameter *a* stands for the width of the transition region between zero shear viscosity and the Power Law region. In original Bird-Carreau model this parameter equals 2.

The infinite shear rate viscosity in many cases is negligible, therefore reducing Eq. (6.8) to a three-parameter model [31]:

$$\eta = \frac{\eta_o}{[1 + |\lambda\dot{\gamma}|^a]^{\frac{n-1}{a}}} \quad (6.9)$$

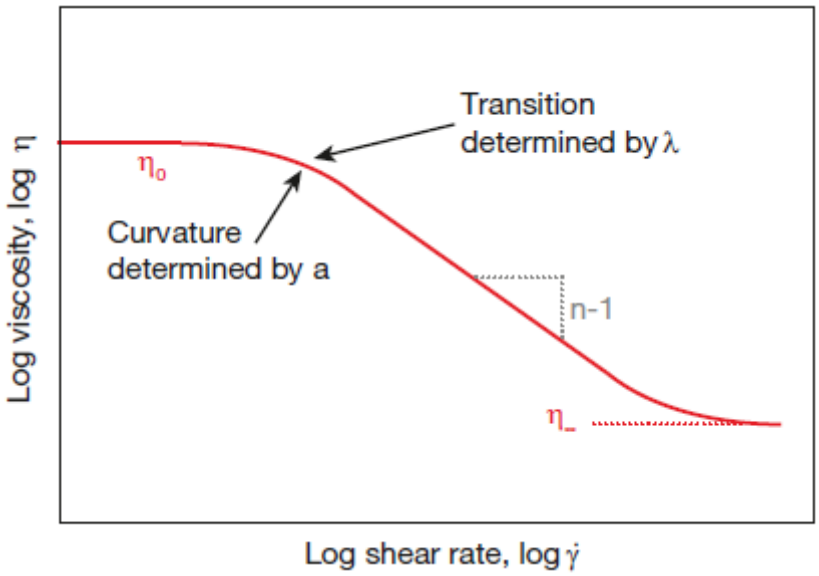

Figure 6. 4: Viscosity approximation using the Bird-Carreau-Yasuda model in Eq. (6.8) [31].

6.2 Advanced fluid models

6.2.1 FENE-P model

The simplest possible approach is when the polymer molecules are modelled similar to dumbbells such as having two beads and a spring connecting them [33]. This is a non-Newtonian fluid model, based on kinetic theory and designed to describe diluted polymer solutions [34]. The simplest model is referred to as Hookean model, as the elastic force between the beads is proportional to the separation between them. Solvent molecules surrounding the beads exert an arbitrary force due to the thermal agitation as well as distort the beads by exerting viscous force. There are some disadvantages of the model due to its simplicity, as it is considered that the shear viscosity is constant, and the dumbbells can be stretched infinitely. For example, considering elongational flow, at finite shear strains, this will lead to an unbounded (infinite) elongational viscosity [35].

In order to overcome these problems, a new model was proposed, where the Hookean spring was replaced by a non-linear spring to limit the dumbbell extension to a maximum value. This spring is finitely extensible non-linear elastic (FENE) spring introduced by Warner [36] and it looks like as follows:

$$F^c = \frac{HQ}{1 - \left(\frac{Q}{Q_o}\right)^2} \tag{6.10}$$

where F^c – connector force,

Q – connector vector between the beads,

H – spring constant,

Q_o – upper limit of the spring extension.

However, we should take into account that one major drawback remains in this model, namely it does not yield a closed-form constitutive equation for the polymer stress, which makes it unsuitable for the calculation of a macroscopic flow. The way out was found by replacing the connector vector in the denominator by its ensemble average value, then it is possible to close the model [35].

$$F^c = \frac{HQ}{1 - \left(\frac{\langle Q \rangle}{Q_0}\right)^2} \tag{6.11}$$

Thus, Eq. (6.11) is the resulting model (i.e. FENE-P model) , where P stands for the Peterlin approximation and usually referred as Peterlin closure [35].

Conservation of mass and momentum for a dilute solution of polymers described by the FENE-P model will then take form [37]:

$$\nabla \vec{V} = 0 \tag{6.12}$$

$$\frac{d\vec{V}}{dt} \equiv \frac{\partial \vec{V}}{\partial t} + \vec{V} \cdot \nabla \vec{V} = -\frac{1}{\rho}\nabla p + \frac{1}{\rho}\nabla \tau^{[s]} + \frac{1}{\rho}\nabla \tau^{[p]} \tag{6.13}$$

where $\vec{V}$ – velocity vector,

ρ – constant fluid density,

p – local pressure,

$\tau^{[s]}$ – Newtonian stress due to the solvent,

$\tau^{[p]}$ – polymer stress.

For a schematic comparison of difference between the experimental and theoretical data of shear viscosity and first normal stress coefficient, the reader is referred to Fig. 6.5. The experiments were conducted at the Department of Chemical Engineering of Katholieke Universiteit Leuven and they based on the rheological characterization of a 0.5% aqueous polyacrylamide. The measurements were done by means of a cone-plate rheometer (RMS 800, Rheometrics) (see Fig. 6.6).

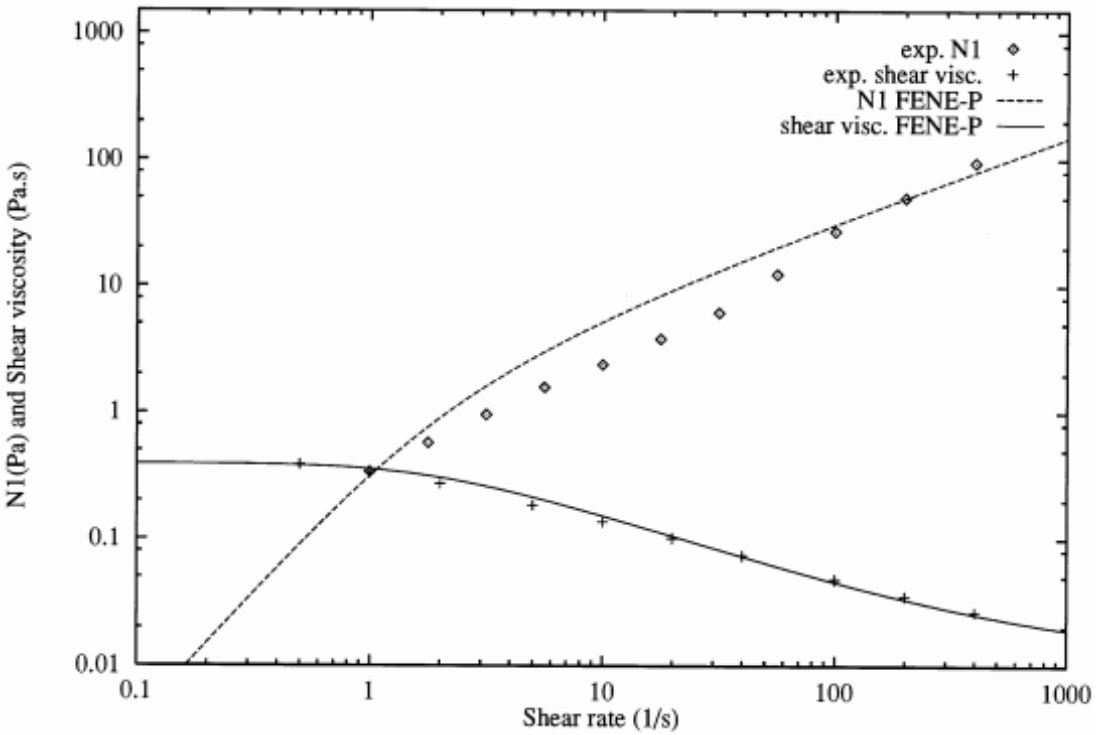

Figure 6. 5: Theoretical and experimental data for shear viscosity and 1st normal stress difference [38].

Figure 6. 6: Rheometer (RMS 800, Rheometrics) [39].

6.2.2 Phan-Thien-Tanner model

The model presented by Phan-Thien and Tanner gives non-linear stresses and is based on network theory (an example of the network we should be concerned is illustrated on Fig 6.7 [40]) and is focused on concentrated polymer solutions and polymer melts. They were successfully used to model complex flows [31].

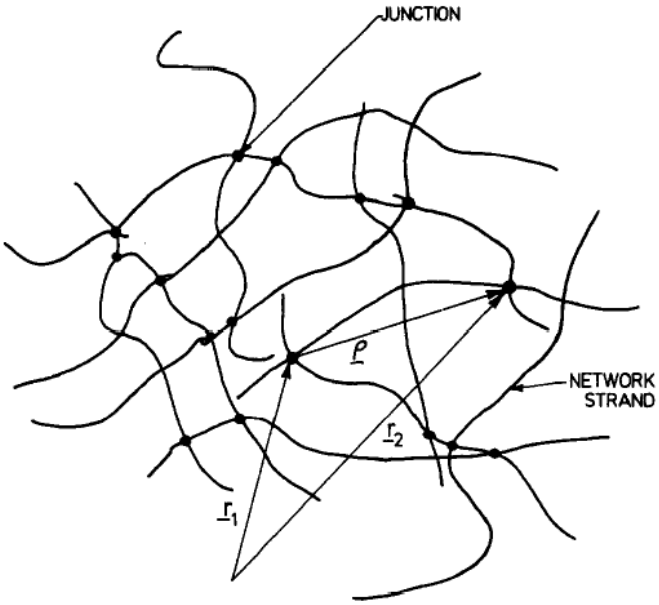

Figure 6. 7: A typical network of polymer solutions [40].

For a simple shear flow the viscometric functions are given by

$$\eta = \sum_{i=1} \frac{G_i \lambda_i}{1 + \xi(2-\xi)\lambda_i^2 \dot{\gamma}^2} \tag{6.14}$$

$$N_1 = 2\sum_{i=1} \frac{G_i \lambda_i^2 \dot{\gamma}^2}{1 + \xi(2-\xi)\lambda_i^2 \dot{\gamma}^2} \tag{6.15}$$

$$\mathrm{N2} = -\frac{\xi}{2}\mathrm{N1} \tag{6.16}$$

where G_i – rigidity modulus spectra, λ_i – relaxation time, N1 and N2 are the first and the second normal stress differences, λ – time constant, ξ – free parameter [41].

The defining equation for the Phan-Thien-Tanner model, then, will look like:

$$\underline{\underline{\tau}}\left(1 + We \cdot \varepsilon\left(\tau_{xx} + \tau_{yy}\right)\right) + We\left(\vec{V} \cdot \nabla\underline{\underline{\tau}} - \nabla\vec{V}^T \cdot \underline{\underline{\tau}} - \underline{\underline{\tau}} \cdot \nabla\vec{V}\right) = \nabla\vec{V} + \nabla\vec{V}^T \tag{6.17}$$

where $\underline{\underline{\tau}}$ – stress tensor, $\vec{V}$– velocity vector, ε – elasticity of the fluid (parameter in PTT model), We – Weissenberg number; [42].

7. Viscoelasticity

7.1 Maxwell Model

Newton and Hooke were the first who proposed models for fluids and solids. After almost two centuries, James Clerk Maxwell tried to model a material that has both viscous and elastic behaviour during deformation. And in 1867, he published a paper "On the Dynamical Theory of Gases" [43], where he presented a model combining both of the two behaviours. Today's Maxwell model represents the linear differential equations that relate stress and strain, which is graphically depicted on Fig. 7.1. Theoretically, the model means that when a stress τ_{xy} is applied to the system, it will be the same for both liquid and solid elements, where the total strain will be equal to the summation of the elastic and the viscous strains i.e. γ_{xy}^{G} and γ_{xy}^{η} respectively [31]:

$$\tau_{xy} = \tau_{xy}^{G} = \tau_{xy}^{\eta} \tag{7.1}$$

and

$$\gamma_{xy} = \gamma_{xy}^{G} + \gamma_{xy}^{\eta} \tag{7.2}$$

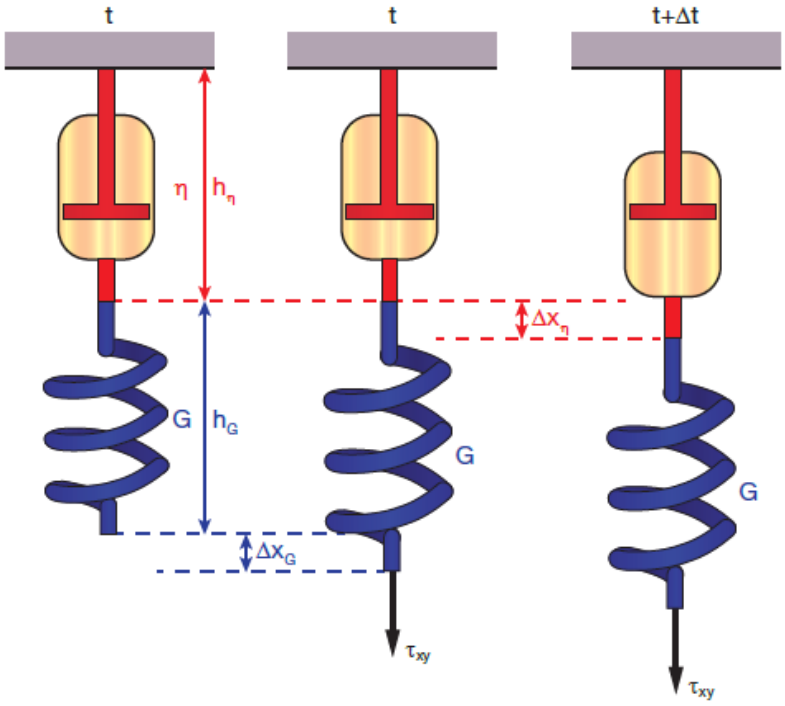

Figure 7. 1: Maxwell's viscoelastic model [31].

By differentiating eq. (7.2) in time, the equation will represent the total rate of deformation i.e. [31]:

$$\dot{\gamma}_{xy} = \dot{\gamma}_{xy}^{G} + \dot{\gamma}_{xy}^{\eta} \tag{7.3}$$

Combining the equations of the constitutive laws with the equations (7.1, 7.2 and 7.3), we will obtain Maxwell's linear differential equation:

$$\frac{d\tau_{xy}}{dt} = G\frac{d\gamma_{xy}}{dt} - \frac{\tau_{xy}}{\lambda} \tag{7.4}$$

where $\lambda = G/\eta$, and represents relaxation time [31].

When stress is constant, the equation, then, is solved for strain:

$$\gamma_{xy} = \frac{\tau_{xy}}{\eta}t + \frac{\tau_{xy}}{G} \tag{7.5}$$

Fig. 7.2 schematically represents Eq. (7.5) where the stress τ_{xy} remains constant from $t = 0$ to $t = \Delta t$.

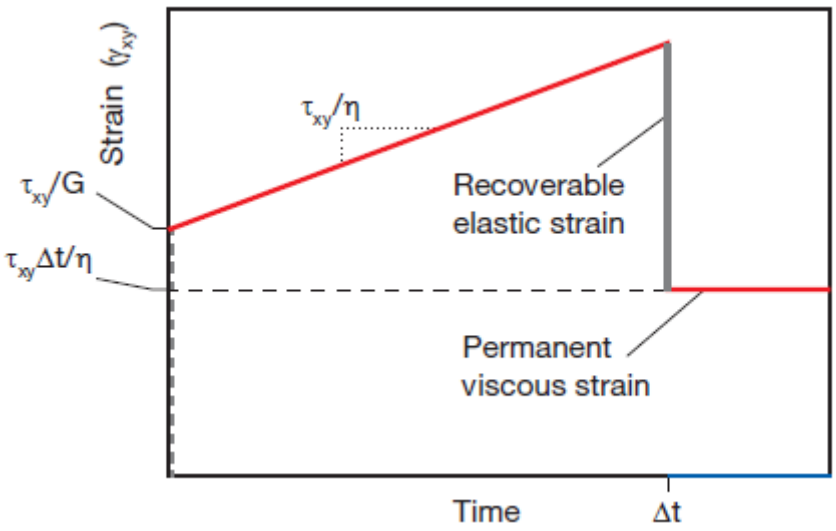

Figure 7. 2: Creep in the Maxwell model [31].

Now, considering that a constant strain applied, the linear differential equation, then, is solved for stress i.e.:

$$\tau_{xy} = G\gamma_{xy}e^{-\frac{t}{\lambda}} \tag{7.6}$$

Fig. 7.3 schematically illustrates Eq. (7.6) as follows:

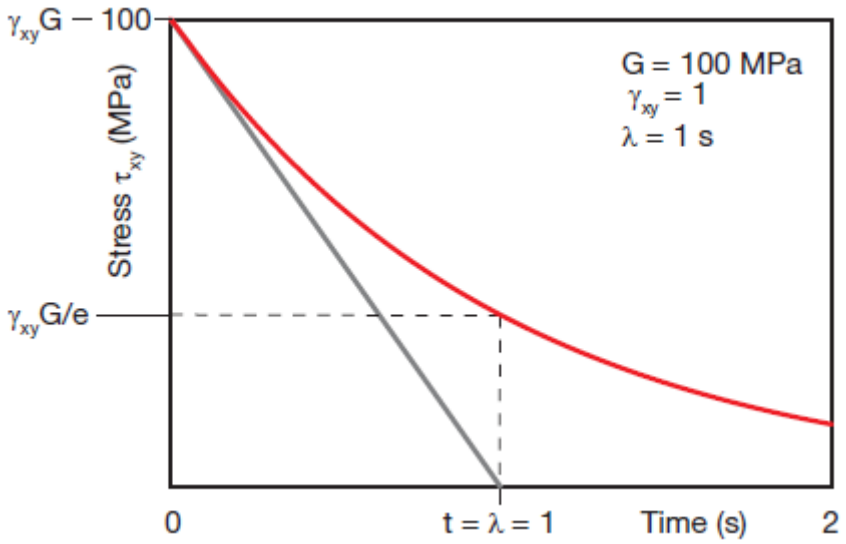

Figure 7. 3: Stress relaxation in the Maxwell model, when G=100 MPa, γ_{xy}=1 and λ=1s [31].

The figure above introduces a phenomenon commonly known as stress relaxation which is depicted as a gradual reduction in stress.

7.2 Time scale and the Deborah Number

While examining any material, besides relaxation time, one should consider the time scale of the process to which the material is subjected i.e. how fast or slow the material is being deformed. For a specific case in Maxwell's model, when the system is deformed at a constant deformation rate $\dot{\gamma}_{xy}$, we can obtain [31]

$$\tau_{xy} = G\dot{\gamma}_{xy}\left(1 - e^{-\frac{t}{\lambda}}\right) \tag{7.7}$$

Comparing three different rates, Fig 7.4 shows the stress being a function of strain, with the same parameters as from Fig 7.3, namely G=100 MPa and λ=1s. The curves on the figure are linked to their own time scales such as for $\dot{\gamma}_{xy} = 10s^{-1}$ it takes 0.1 second to reach $\gamma_{xy} = 1.0$, thus having a time scale of $t_p = 0.1s$. Within such a small time scale the material behaviour will be almost like a solid, as this time is not enough to relax the stress that was built up during deformation. But if material deformation occurs at a much slower rate ($0.1s^{-1}$), the time scale is $t_p = 10s$, hence creating sufficient amount of time for the stress to relax so that the material behaves more like a fluid [31].

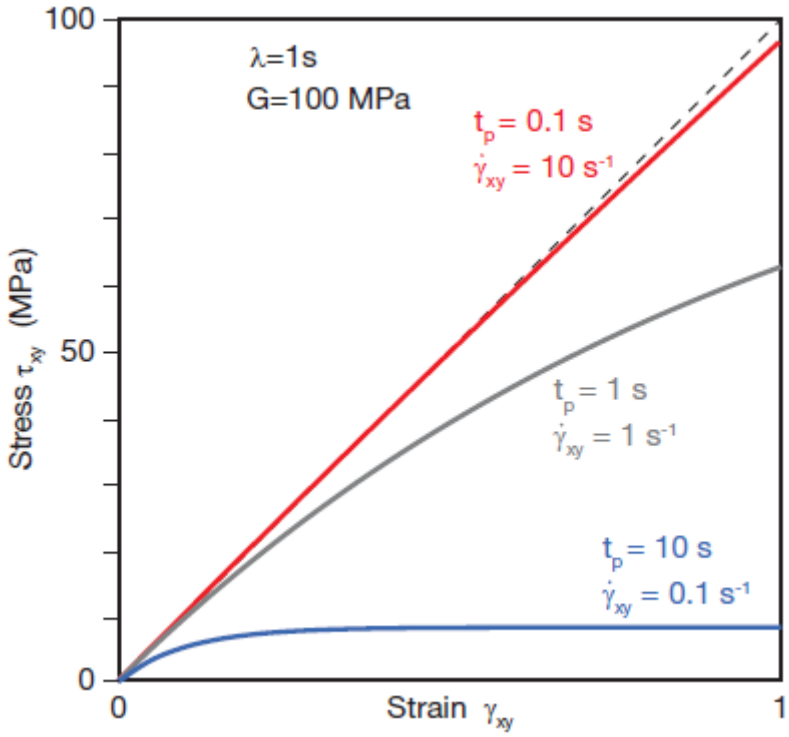

Figure 7. 4: Stress as a function of strain for a Maxwell model at various rates of deformation [31].

Now while studying a material, particularly a polymeric material, should it be considered as a solid, liquid or viscoelastic material? in every specific situation and process we have to take into account the material's behaviour. In 1964, the Deborah number (*De*) was introduced Marcus Reiner. The Deborah number being dimensionless number best represents and captures the effect of process time scale on a material's deformation behaviour [44] and it is defined as [31]:

$$De = \frac{\lambda}{t_p} \tag{7.8}$$

To make it clear, the behaviour of a viscous fluid is observed when the Deborah number is zero, while the behaviour of elastic solid is seen when it equals to infinity [31].

7.3 General concept of viscoelasticity

Let us consider polymers. Above the glass transition or melting temperatures the may be considered as liquids but below these temperatures – solids, however, in reality they are neither liquids nor solids but viscoelastic materials. This means that depending on the time scale and deformation rate, polymers can be either liquids or solids. For visual representation of the relation between time scale, deformation and applicable material behaviour, the reader

is referred to Fig. 7.9, where the Deborah number was used as $De = \lambda\omega$ and the deformation as γ_o. As was discussed previously, at very high values of Deborah number the polymer can be considered as a Hookean solid and at very small Deborah numbers – as a Newtonian fluid [31].

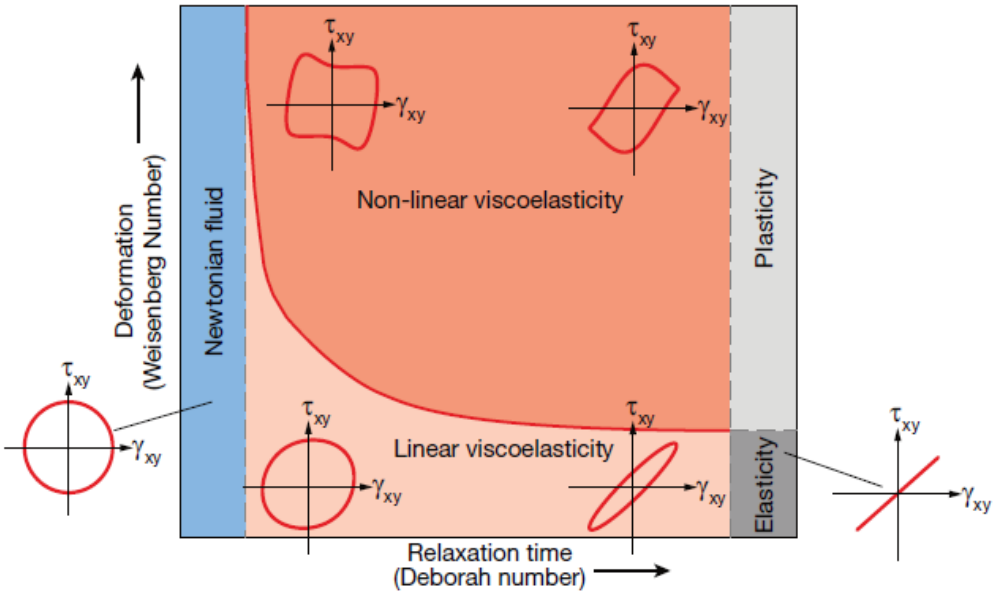

Figure 7. 5: Illustration of different regimes i.e. Newtonian, elastic, linear and non-linear viscoelastic as a function of deformation and relaxation time during deformation of polymeric materials [31].

Viscoelastic region consists of two regions: linear viscoelastic region for small deformations and non-linear – for large deformations, which will be discussed further on.

7.4 Linear viscoelasticity

This field of studies applies to the materials with small deformations (i.e. short-term deformation of polymers) [31]. In chapter 7.1, the most common model of linear viscoelasticity was described, namely Maxwell model.

$$\tau_{xy} + \lambda \frac{d\tau_{xy}}{dt} = -\eta_o \dot{\gamma}_{xy} \tag{7.9}$$

Eq. (7.9) is the governing equation for the Maxwell model [31].

When the deformation is large enough (so that can change the structure of polymer chains) the non-linearities arise and this is described later in chapter 7.5.

7.4.1 Relaxation modulus

Stress relaxation behaviour is the most fundamental principle that defines rheological and mechanical behaviour of polymers. Considering polymers, as being non-linear materials, the decaying stress results in a shear modulus which is also a function of strain $G(\gamma_o, t)$

$$G(\gamma_o, t) = \frac{\tau_{xy}(\gamma_o, t)}{\gamma_o} \tag{7.10}$$

But for small instantaneous deformations the shear modulus is proportional to strain, hence in these cases it is only a function of time i.e [31].

$$G(t) = \frac{\tau_{xy}(t)}{\gamma_o} \tag{7.11}$$

7.5 Non-Linear viscoelasticity

As was mentioned earlier, large deformations are the reason for non-linear viscoelasticity to occur. While processing operations with polymers, large deformations are inevitable and, therefore, use of non-linear viscoelastic models required [31].

7.5.1 Objectivity

A new term introduced in non-linear viscoelasticity is so called '*objectivity*'. In order a constitutive model or a system of equations to be '*objective*' they should not depend on orientation and the movement of coordinate system. This is shown on Fig. 7.6, which illustrates that the force exerted on an elastic spring depends on the spring's stiffness and amount of stretching but not on the orientation of its principal axis [31].

To present a non-objective rheological model, we should consider the tensor form of Maxwell's linear elastic model (that was discussed previously in chapter 7.1) and the experimental setup illustrated in Fig. 7.6.

$$\underline{\underline{\tau}} + \lambda \frac{\partial}{\partial t} \cdot \underline{\underline{\tau}} = -\eta_o \underline{\underline{\dot{\gamma}}} \tag{7.12}$$

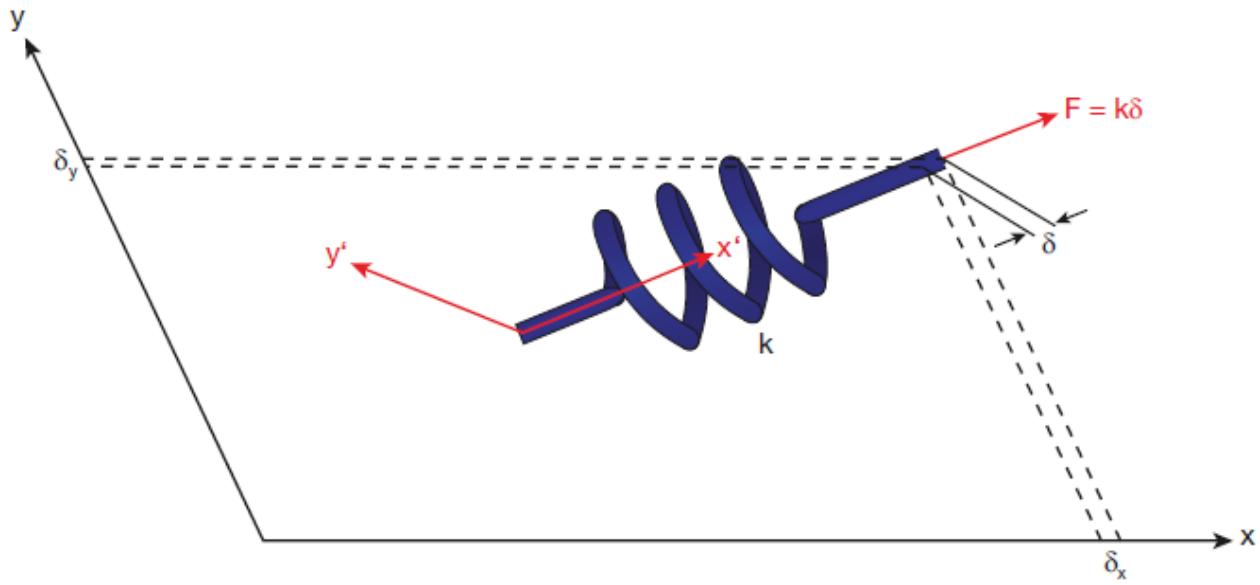

Figure 7. 6: Objective spring system [31].

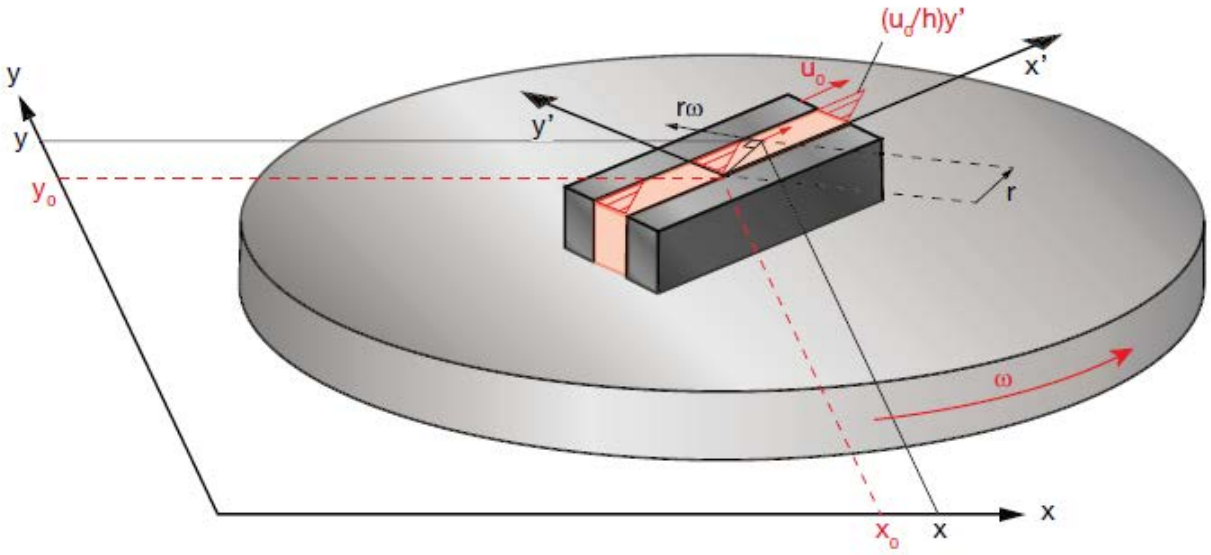

Figure 7. 7: Simple shear flow on a rotating disc [31].

The experiment consists of a rotating disc and a setup of a simple shear flow assembled above. The setup domain has its own coordinate system (i.e. $x'y'$) which rotates with the disc at an angular speed ω. Flow field can be shown within the $x'y'$ coordinate system using [31]:

$$u(y') = \frac{u_o}{h} y' \tag{7.13}$$

and the resulting velocity because of the rotation

$$U = r\omega \tag{7.14}$$

8. Salinity, shear rate dependence and concentration effect on viscometric functions of IOR polymers

Generally, there are two polymers that are commonly used in EOR operations i.e. synthetic material polymers (polyacrylamides) and biopolymers (xanthan and HEC) [45]. HPAMs are favorably used in the reservoirs with low salinity concentrations, while xanthan is used for high salinity ones [46]. In this chapter, different parameters affecting the viscometric functions of polymers will be discussed.

8.1 Shear rate dependence

M. Rashidi et al. (2010) took a sulfonated polyacrylamide polymer in their study (i.e. AN 125). As follows from Fig. 8.1, the viscosity shows shear-independent scenario in polymers with low concentrations such as behaving like a Newtonian fluid (yet, bearing in mind that they are not Newtonian fluids), while for high concentrations the viscosity drops as for pseudo-plastic fluids (known as shear-thinning) [47].

As can be seen from Fig 8.1, the viscosity is higher in the polymers with higher concentrations and also more shear-rate dependent. Extension of shear thinning region also appears, as the macromolecule chains exhibit more entanglements [48].

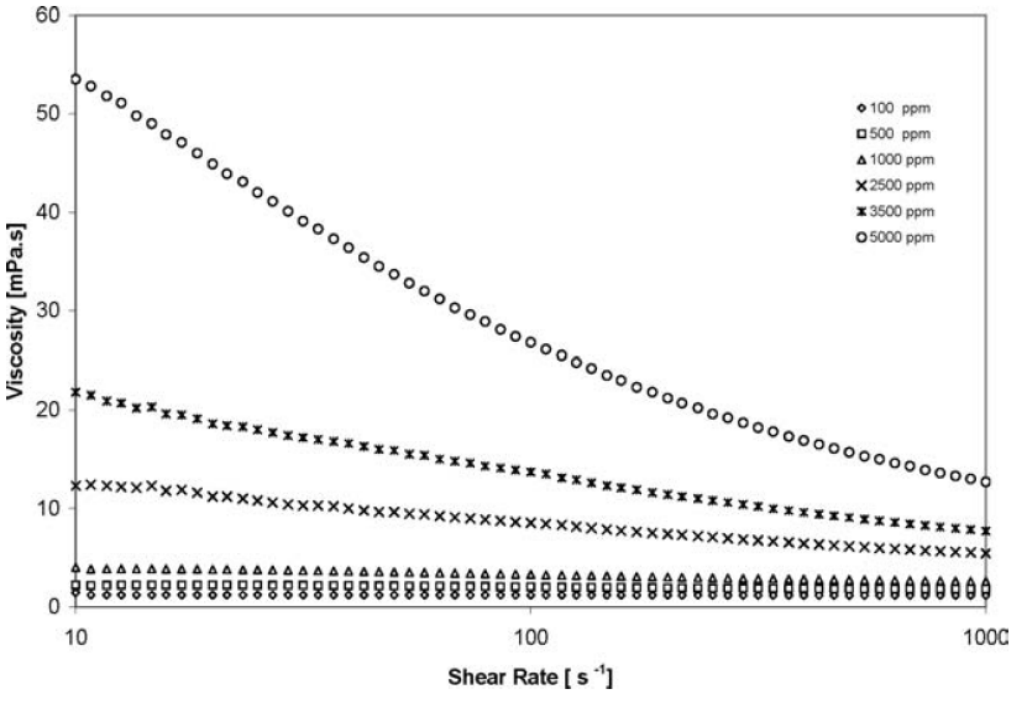

Figure 8. 1: The viscosity of sulfonated polyacrylamide polymer as a function of shear rate for AN125 in 5 wt % NaCl at different polymer concentrations, *T = 20°C* [47].

8.2 Concentration dependence

There is a simple dependence between the concentration of the polymer and its viscosity, which simply means that the more polymer was added to the solution the more viscous it will be. For a visual example of the viscosity as a function of the polymer concentration, Fig. 8.2 obtained by M. Rashidi et al. (2010) is presented below [47].

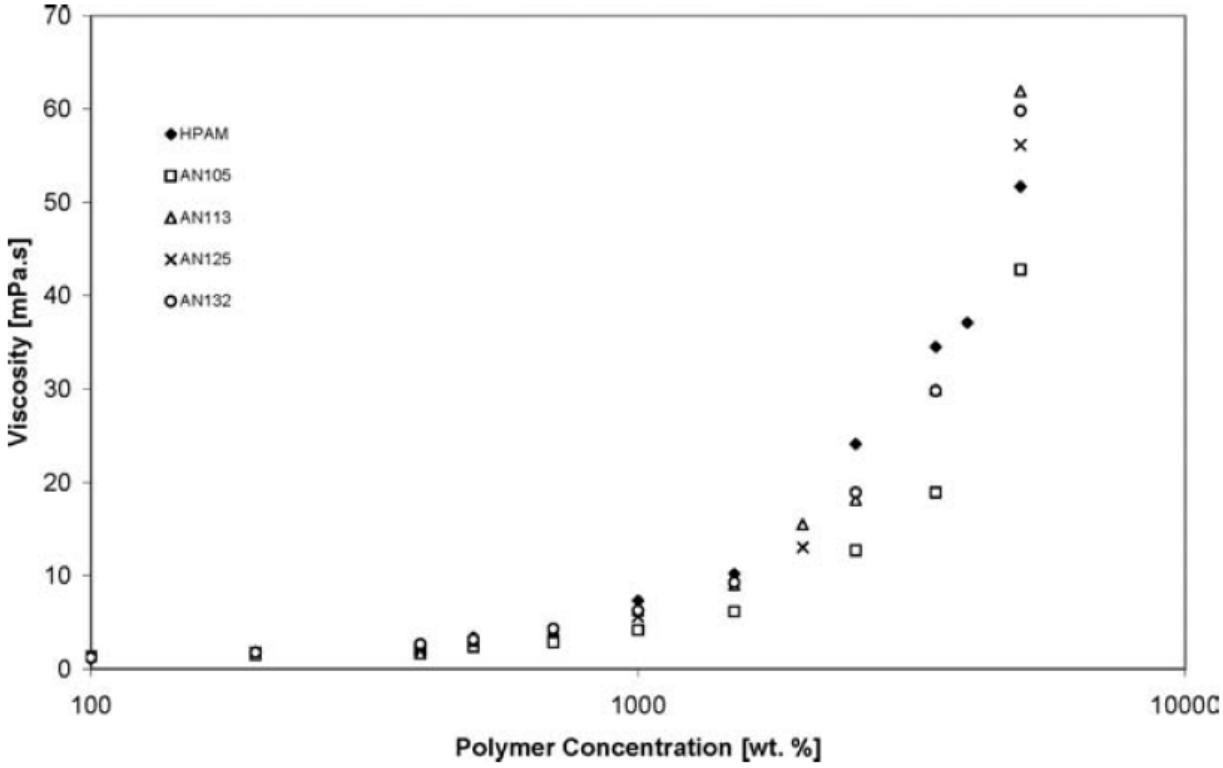

Figure 8. 2: The viscosity as a function of polymer concentration in 0.1 wt % NaCl concentration of sulfonated polyacrylamide polymers and of HPAM; shear rate = 100 s^{-1}; T = 20°C [47].

8.3 Salinity dependence

In order to consider salinity effect on polymers, let us first take a closer look at HPAM polymers. As was stated before they are basically used in low salinity reservoirs such as Daqing (the largest oil field in China), Bohai and so on, because they have limitations in high salinity reservoir as well as being easily shear degradable. According to M. Rashidi et al. (2010), salinity has an opposite effect on polymer viscosity i.e. with the increasing salinity concentrations, viscosity of polymers decreases, and this phenomenon has a stronger effect on HPAMS than on PAMS (which means that PAMS are more salt tolerant and therefore, could be used for higher salinity reservoirs than HPAMS) [47].

Fig. 8.3 outlines an example of sulfonated polymers regarding the effect of salinity on the shear rate dependence, where it is seen that with increasing salinity concentration the solutions act more like Newtonian fluids. And this stands inline with the rheological properties of PAM and HPAM studied by other authors [49]. The presented results are most likely due to the charges of the polymer chains and the decrease of the entanglements at high salt concentrations [47].

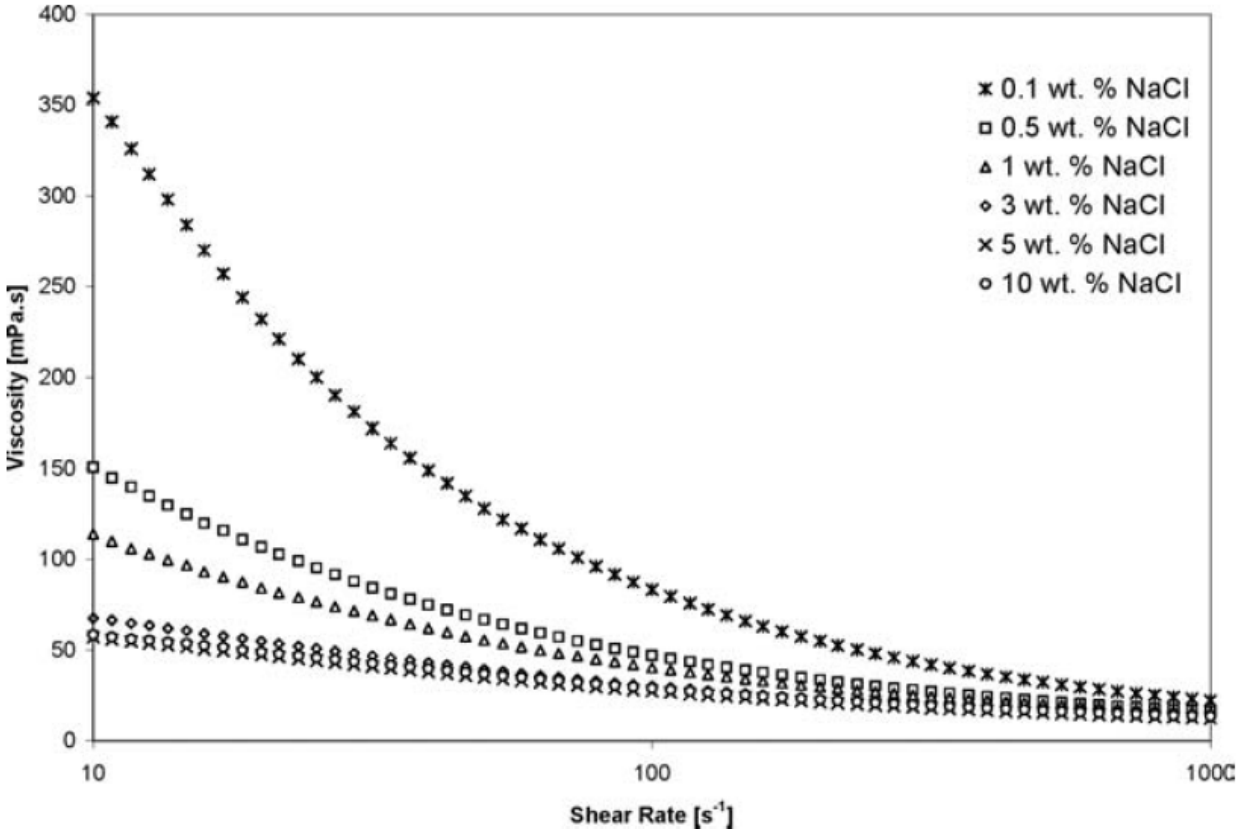

Figure 8. 3: Salinity effect on the viscosity as a function of shear rate of the sulfonated polyacrylamides with polymer concentration of 5000 ppm [47].

Now considering salt concentration dependence of viscosity, polymers with different molecular weight were tested including HPAM. The shear rate was set to 100 s^{-1} and the concentration of all polymers were taken of 5000 ppm in all cases. After increasing salinity in the polymer solutions, the charges on the polymer chains were shielded, and the molecules curled up. This phenomenon occurs due to the charge density on the polymer chain. An important point to be noted is that after certain salinity concentration, the viscosity decreasing rate levels off, which is explained due to the fact that the charges on the polymer chain have been screened by the NaCl ions. And after adding more of NaCl, there will be only a slight effect on the polymer viscosity due to the growth of the solvent viscosity [47]. For the resulting plot, see Fig. 8.4:

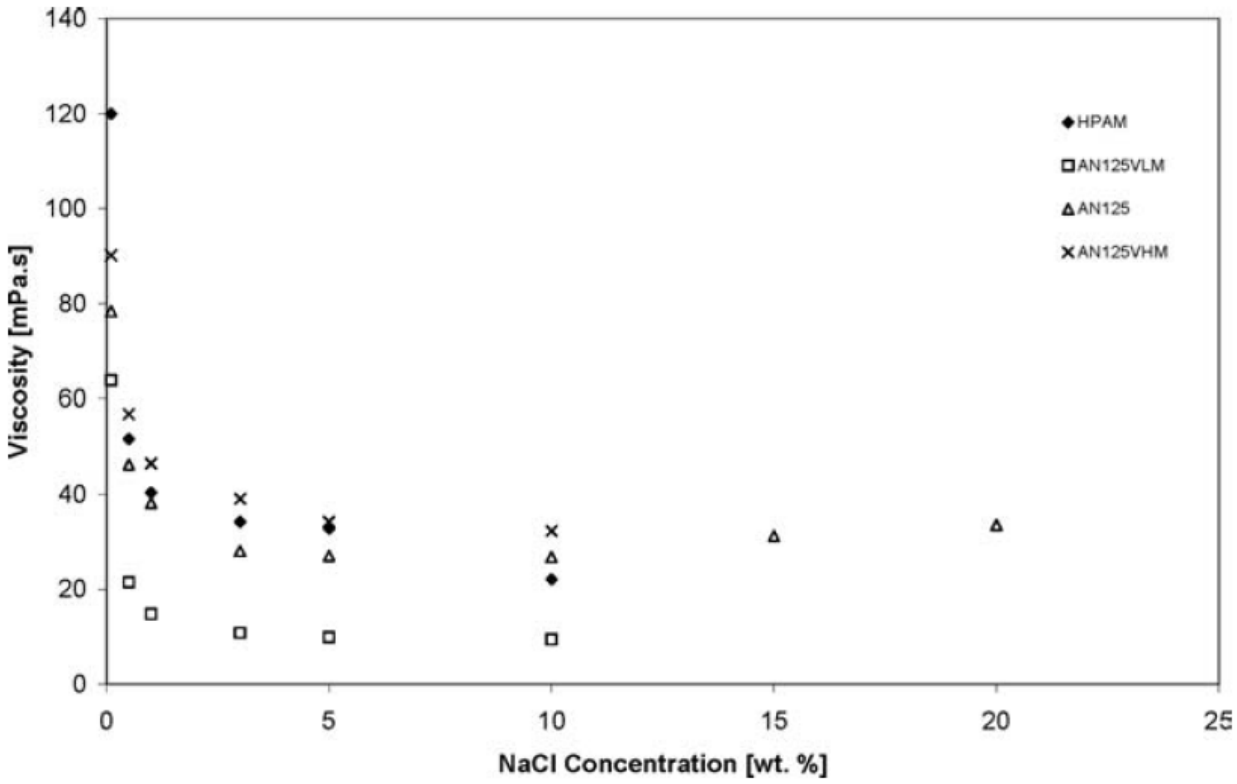

Figure 8. 4: The viscosity of sulfonated polyacrylamides with different molecular weight together with HPAM as a function of NaCl concentration; polymer concentration – 5000 ppm, shear rate – 100 s^{-1}; temperature – 20°C [47].

9. Experimental work

9.1 Materials

The experimental work consists of a number of dry polymer powders which were mixing in solvents such as distilled water and brines with different salinity concentrations as well as several equipment and devices that are stated further on.

9.1.1 Polymers

All in all, during the entire experimental work, 9 polymers have been used and tested, two of which polysaccharides and 7 synthetic polymers (6 of which are polyacrylamides), they are:

- Xanthan Gum
- Hydroxyethyl Cellulose (HEC)
- 5115 VHM
- 5115 VLM

- PolyPak
- AN 125 VHM
- AN 125 VLM
- 3630S VHM
- 3130S VLM

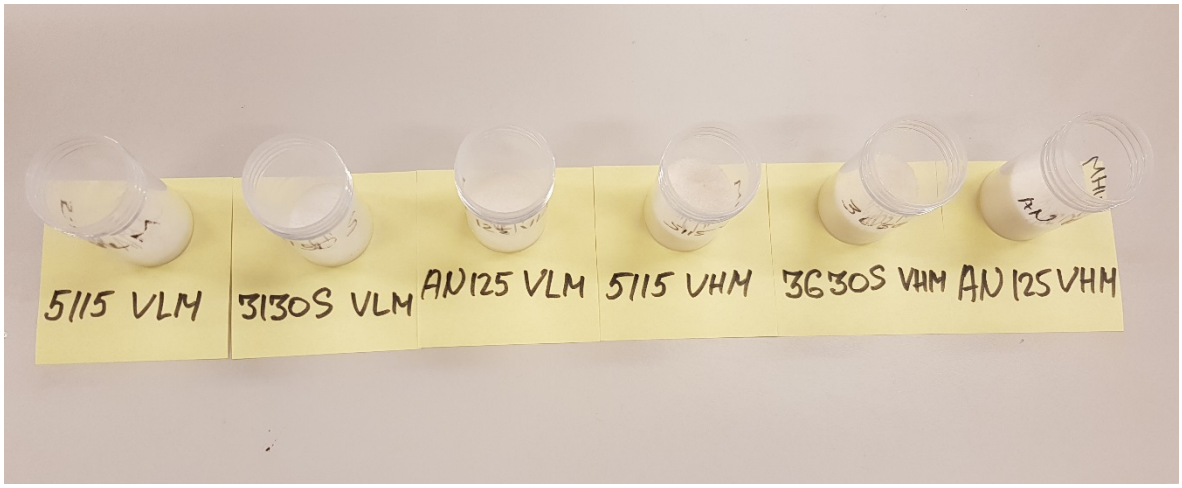

Figure 9. 1: Polyacrylamides used during experimental work.

Figure 9. 2: HEC, PolyPak and Xanthan Gum.

9.1.2 Solvents

There were 6 solvents used in the work, namely distilled water and brines with different salinity concentrations. As the purpose was to examine the influence of monovalent ions, NaCl has been chosen. The highest salinity concentration used in the experiment was the one of the seawater i.e. 38.41 g of NaCl per liter of distilled water. The other concentrations were taken as 1/5, 2/5, 3/5 and 4/5 of the highest concentration. The procedure of making brines is described further.

9.2 Equipment used

9.2.1 Mixers

In order to mix the polymers with the solvents 2 types of mixers were used i.e. 'Heidolph' mixer (see Fig. 9.4) and 'VWR' stirrer or magnet stirrer (see Fig. 9.3)

Figure 9. 3: VWR stirrer

Figure 9. 4: Heidolph mixer.

9.2.2 Filter

The filter (see Fig. 9.5) was used in order to purify the brine solutions.

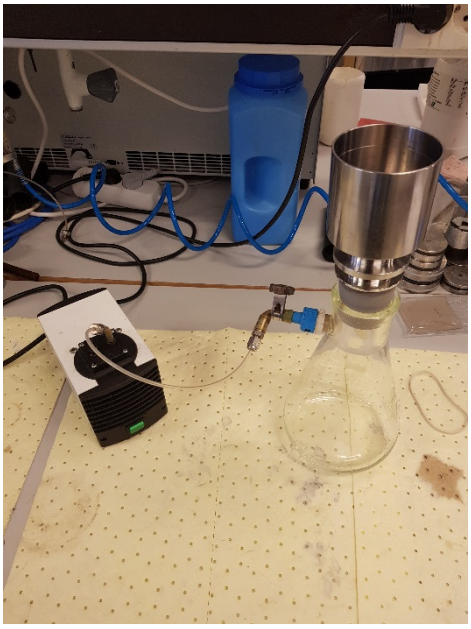

Figure 9. 5: Filtration setup, used to purify brine solutions

9.2.3 Rheometer

Rheometer that was used for all the samples during the entire experimental work was Anton Paar Rheometer 'MCR 302' (see Fig.9.6)

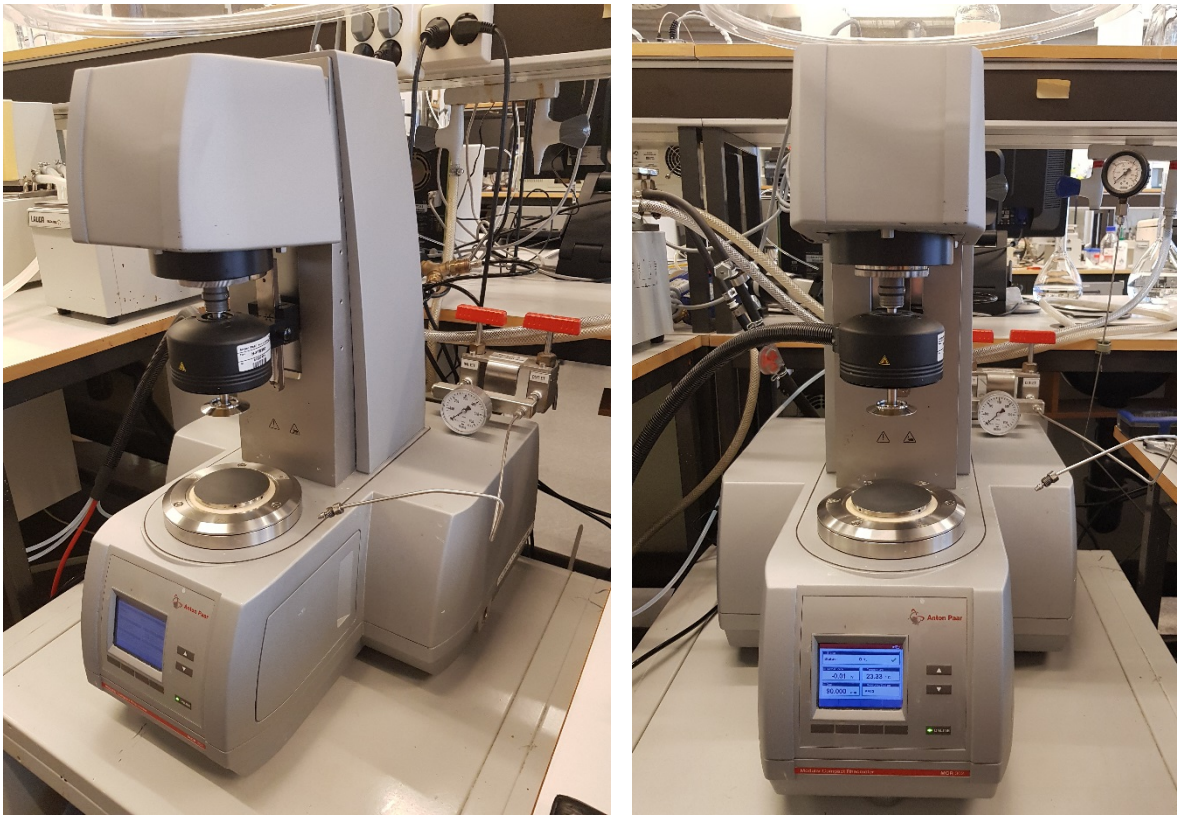

Figure 9. 6: Anton Paar Rheometer 'MCR 302'

9.3 Experimental procedure

This chapter is devoted to a more detailed procedure of the experimental work and the use of the materials and equipment mentioned in previous chapters.

9.3.1 Brine solutions

As was mentioned before, the objective was to find out the effect of monovalent ions, so NaCl has been used as a solvent for making brine solutions. The first salinity that was determined was the one as of the seawater, namely 38.41 g/l of NaCl. Three liters of distilled water (i.e. 3×1 liters) were predetermined and put to the magnetic stirrer, and then the NaCl was gradually introduced. The solutions were left on the stirrer at ambient temperature for approximately 25 minutes in order to get a complete dissolution. Once the NaCl was dissolved, the solutions were filtered, using the filter that was show in Fig. 9.5. A filter screen, together with the filter paper of 1.8μm was used in the filter assembly. Finally, after filtering all of the solutions, they were ready to be used in further mixing with polymers.

Total, there were 5 brine concentrations i.e. 1/5, 2/5, 3/5 and 4/5 of the highest salinity and this was approximately accounted for 7.68 g/l, 15.37 g/l, 23.05 g/l and 30.73 g/l of NaCl. Exactly the same procedures were carried out with the other salinity concentrations.

9.3.2 Polymer mixing

All in all, there were 6 solutions to be used for polymer mixing, such as five brines of different salinity concentrations and one of distilled water. The procedure of making polymeric solutions is as follows. Once brine solution or distilled water were ready to be used, they were started to mix by means of propeller stirrer, which is shown in Fig. 9.3. Then, the polymer powder was slowly introduced into the side of the vortex in order to avoid formation of fisheyes, which can be formed if the powder is not wetted evenly. The solution then was stirred approximately 2 hours under the propeller mixer and then moved to magnetic stirrer. It is also important to note which type of polymer was mixing as the settings for different types varied i.e. polymers with low molecular weight took less time and less rounds per minute (RPM) than those of high

molecular weight. Table 9.1 is introduced to have the complete overview of how much time and under what RPM the polymers were mixing.

Table 9. 1: Concentration, time and rate of the polymers in question.

	Polymer concentration	Propeller stirrer		Magnetic stirrer	
		Time	RPM	Time	RPM
Xanthan Gum	15000 ppm	2(18)	1000(500)	–	–
HEC	15000 ppm	2(18)	1000(500)	–	–
PolyPak	100000 ppm	2(18)	1000(500)	–	–
AN 125 VLM	10000 ppm	2	475	15	250
AN 125 VHM	10000 ppm	2	700	15	200
5115 VLM	10000 ppm	2	475	15	250
5115 VHM	10000 ppm	2	700	15	200
3130S VLM	10000 ppm	2	475	15	250
3630S VHM	10000 ppm	2	700	15	200

After propeller stirrer polymers were set on the magnetic stirrer for much longer time in order to reach a complete dissolution. In case of Xanthan Gum, HEC and PolyPak, means that propeller stirrer was the only mixer used as these polymers were viscous to such an extent that magnetic stirrers would not able to perform as intended. Regarding FLOPAAMS, as the polymeric solutions with high molecular weight are more viscous than those of low molecular weight, they required more RPM under the propeller stirrer in order to get the best result of dissolution and a bit less RPM on the magnetic stirrer in order magnets to rotate well without any fluctuations.

Let us now look a bit closer to the mixing procedure of the polymers. The initial polymer concentrations were set as it is shown in Table 9.1. Once the mixing procedure started, after already some minutes, the solutions started to show the Weissenberg effect, which is common for polymeric liquids. Weissenberg effect is an effect when viscoelastic fluids climb up a rotating rod. The phenomenon of fluid rising up to a rotating rod was first reported by Garner and Nissan in 1946 and by Weissenberg in 1947. Since that time, there were a number of reports of rod climbing effect in polymeric solutions [50]. Some pictures were taken during the mixing

procedure to show the Weissenberg effect (see Fig. 9.7). Xanthan, HEC and PolyPak did not exhibit a very strong effect, while FLOPAAMS with high molecular weight showed a significant rod climbing.

a) Xanthan Gum b) PolyPak c) HEC

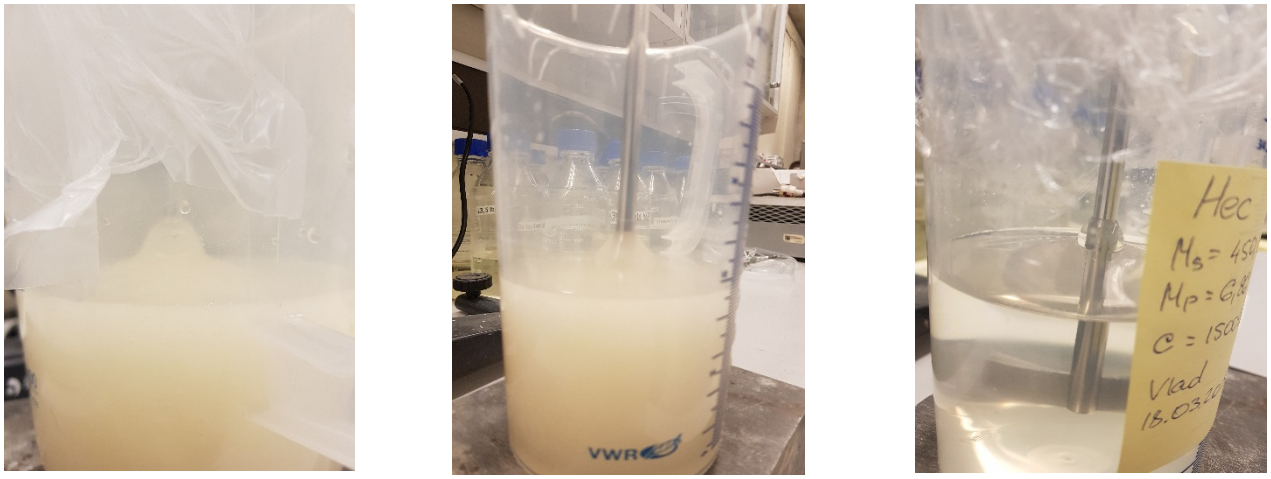

d) 3630S VHM e) AN 125 VHM f) 5115 VHM

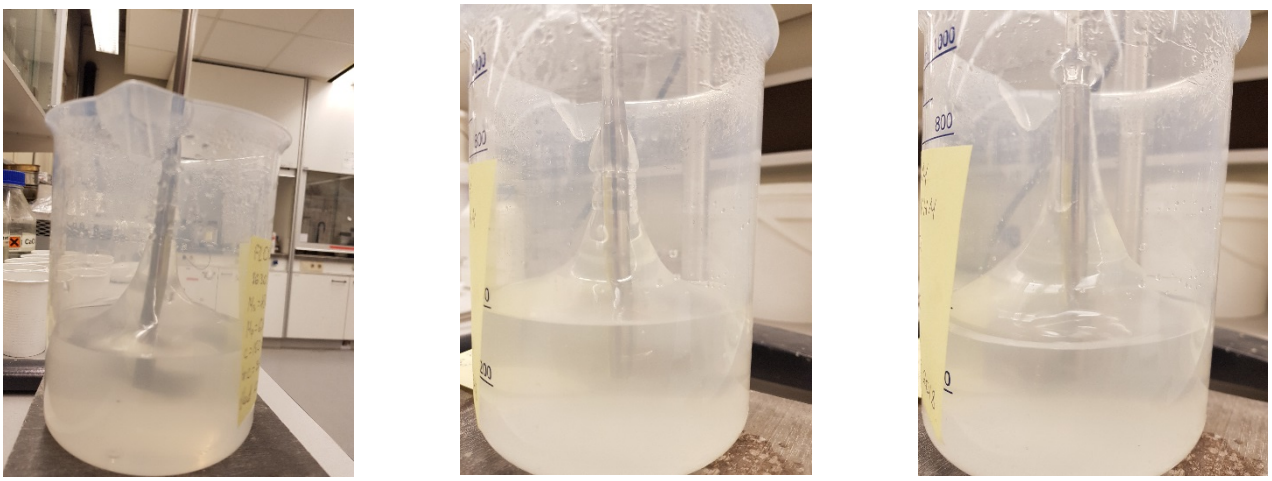

Figure 9. 7: Rod climbing effect (i.e. Weissenberg effect) on different polymers.

As can be seen from Fig. 9.7 (f), the polymer '5115 VHM' experienced the strongest Weissenberg effect among all the polymers. But it is also interesting to note that PolyPak had the strongest intermolecular bonding (most probable due to the highest polymer concentration used). As illustrated on Fig. 9.8, the solution does not flow easily out of the bottle and one needs either to cut the liquid jet with scissors or wait for a couple of minutes.

Figure 9. 8: Illustration of strong intermolecular bonding in PolyPak polymer.

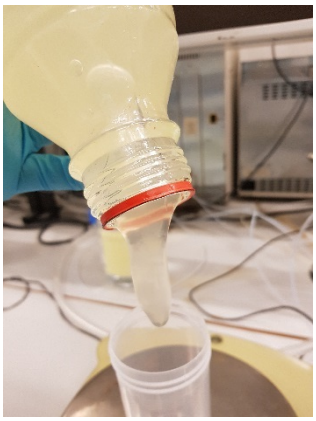

While diluting polymers in order to get solutions of less concentrations, magnet stirrer was used. And there are some polymers i.e. PolyPak and HEC which experienced the strongest liquid climb effect despite they had not had so strong Weissenberg effect. Such cases are depicted in Fig. 9.9.

a) PolyPak

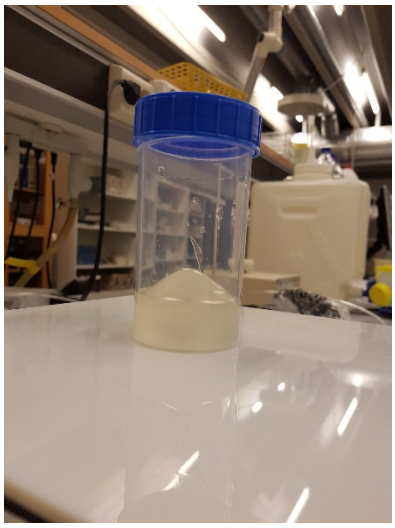

b) HEC

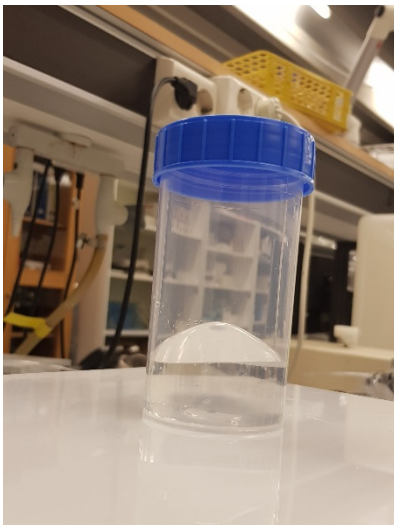

Figure 9. 9: Liquid climbing during mixing on magnetic stirrer.

9.3.3 Rheological measurements

Once the solutions mixed and reached the complete dissolution, they are ready to be used in the rheological measurements. As was stated before, Anton Paar Rheometer 'MCR 302' was used for the measurements, which is illustrated on Fig. 9.6. First, preliminary settings are predefined and set in the Rheoplus application. In this work, after testing different settings for different polymers, it was predetermined to use a two-way fractional design, with the time lap of early and late measurements of 60 … 7s → 7 … 60s, and with the shear rate varying from

0.01 … 200 → 200 … 0.01 s^{-1} and from 0.1 … 2000 → 0.1 … 2000 s^{-1}, where the advantage was given to the latter shear rate intervals in order to have the best results for high shear rates.

After all the settings were predefined and set for further measurements, a certain amount of liquid was introduced between the parallel plates and the upper plate was lowered till 0.096mm distance is reached between the plates, as it is shown on Fig. 9.10. Once the needed distance is reached there is a sudden increase of normal stress due to the liquid pressure, which have to be reseted before the start of the measurements. After meeting all the statements mentioned above the liquid is ready to be measured.

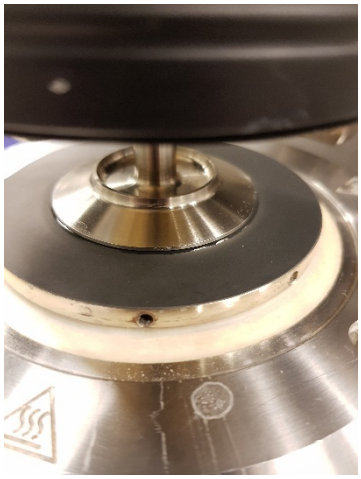

Figure 9. 10: An illustration of rheometer while measuring rheological properties of a given liquid.

9.3.4 Scope of the work

As the work consists of measurements of polymeric liquids in distilled water and in the brines with 5 different salinity concentrations, there were plenty of experiments done resulting with more than 270 samples made and left to be stored in a refrigerator (see Fig. 9.11). The best and the most appropriate results are presented further in chapter 10.

Figure 9. 11: Samples made during the experimental work.

10. Main results and discussion

As was stated before, the main device to conduct the experiment was Anton Paar Rheometer 'MCR 302'. The results presented in this chapter are aimed to show if the tested polymers with the different concentrations follow the models discussed previously in chapter 6. Viscosities and shear rates for these results were normalized in order to illustrate the trend of polymeric liquids together with the models used. Together with these results, the original ones will be shown to give a better view of the change of viscosity for the different polymer concentrations. Furthermore, the effect of salinity on viscometric functions of different polymers together with the results of those in distilled water are illustrated. And finally, plots of the viscosity loss of a given polymer against the shear rate are depicted.

As salinity has a bigger impact on polyacrylamides, they were undergone most of the experimental manipulations in this work, but Xanthan Gum, HEC and PolyPak being more tolerant to salts, were tested with the highest salinity i.e. that of 38.41 g/l of NaCl.

The trends for high molecular weight polymers showed very similar pattern, so AN 125 VHM was decided to be illustrated in the main part, while the rest will be put in the Appendix.

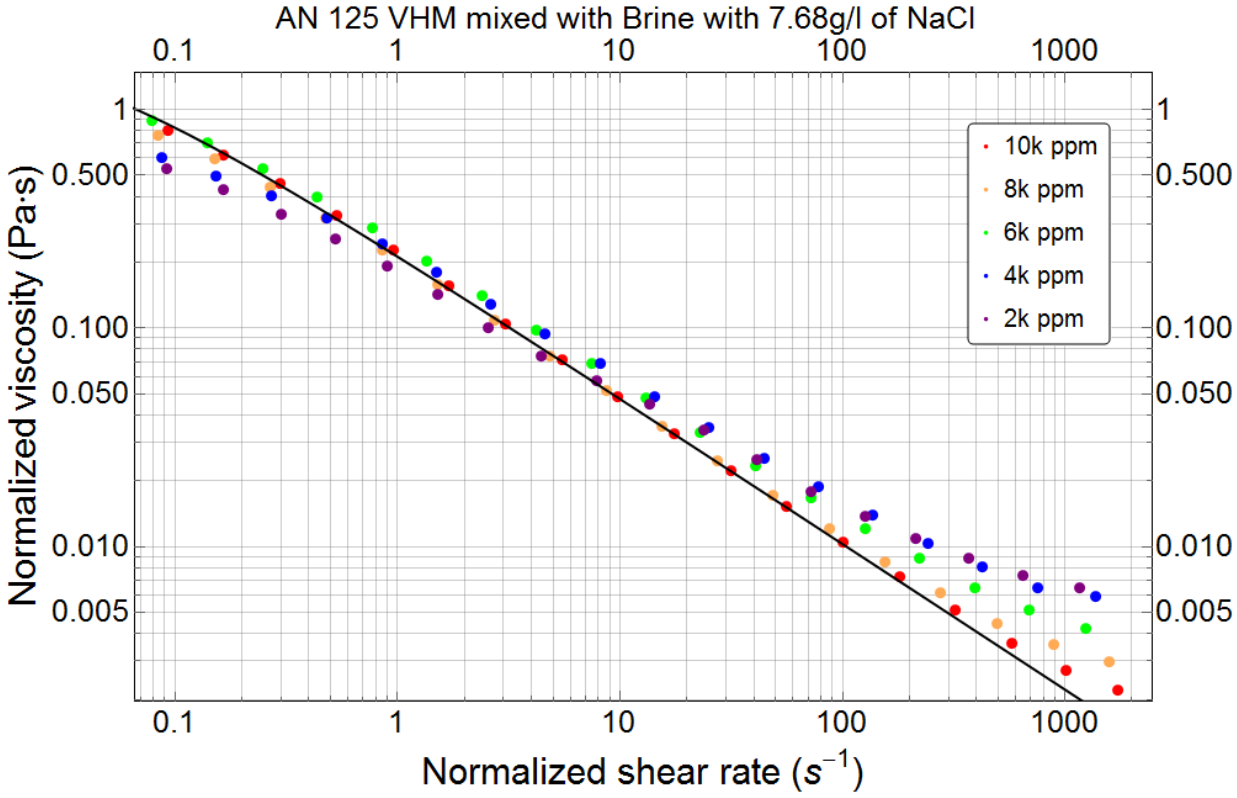

Figure 10. 1: Normalized viscosity vs normalized shear rate for AN 125 VHM mixed with Brine with 7.68 g/l of NaCl.

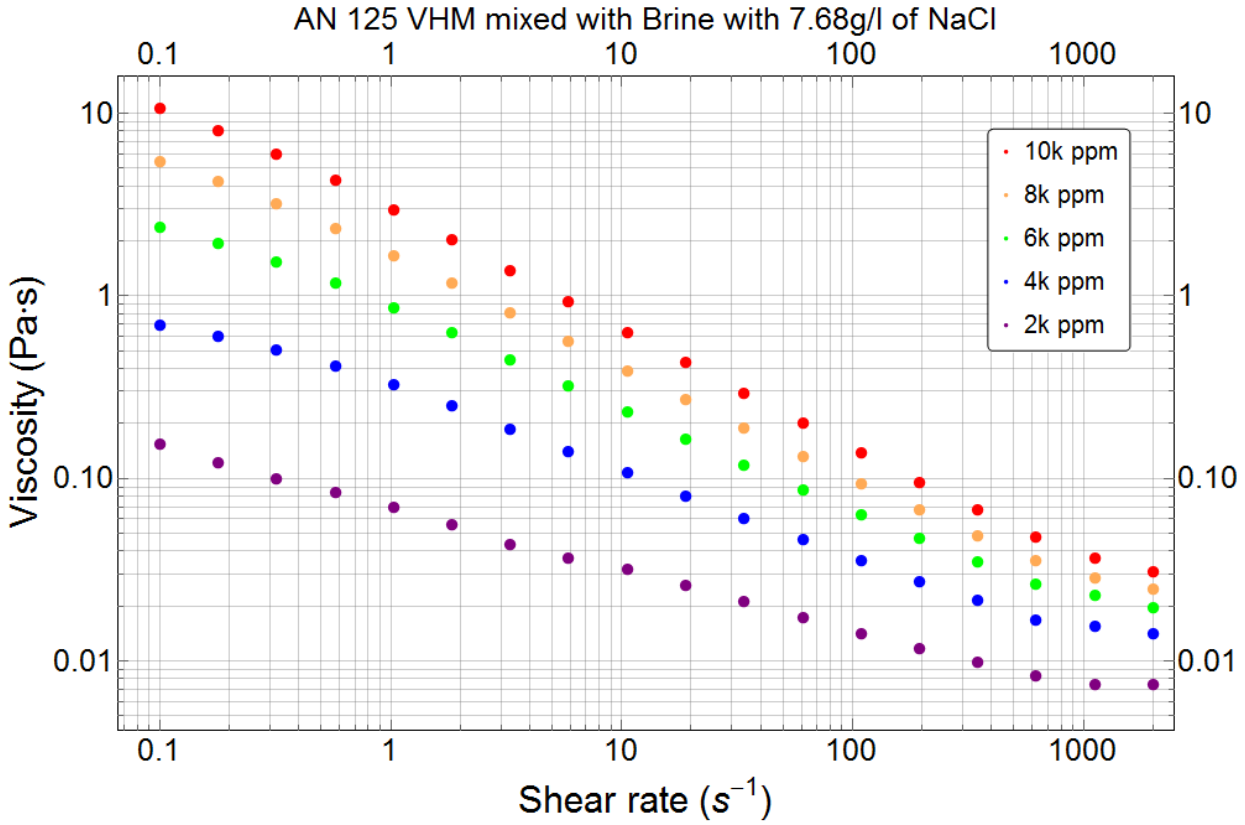

Figure 10. 2: Viscosity vs Shear rate for AN 125 VHM mixed with Brine with 7.68 g/l of NaCl.

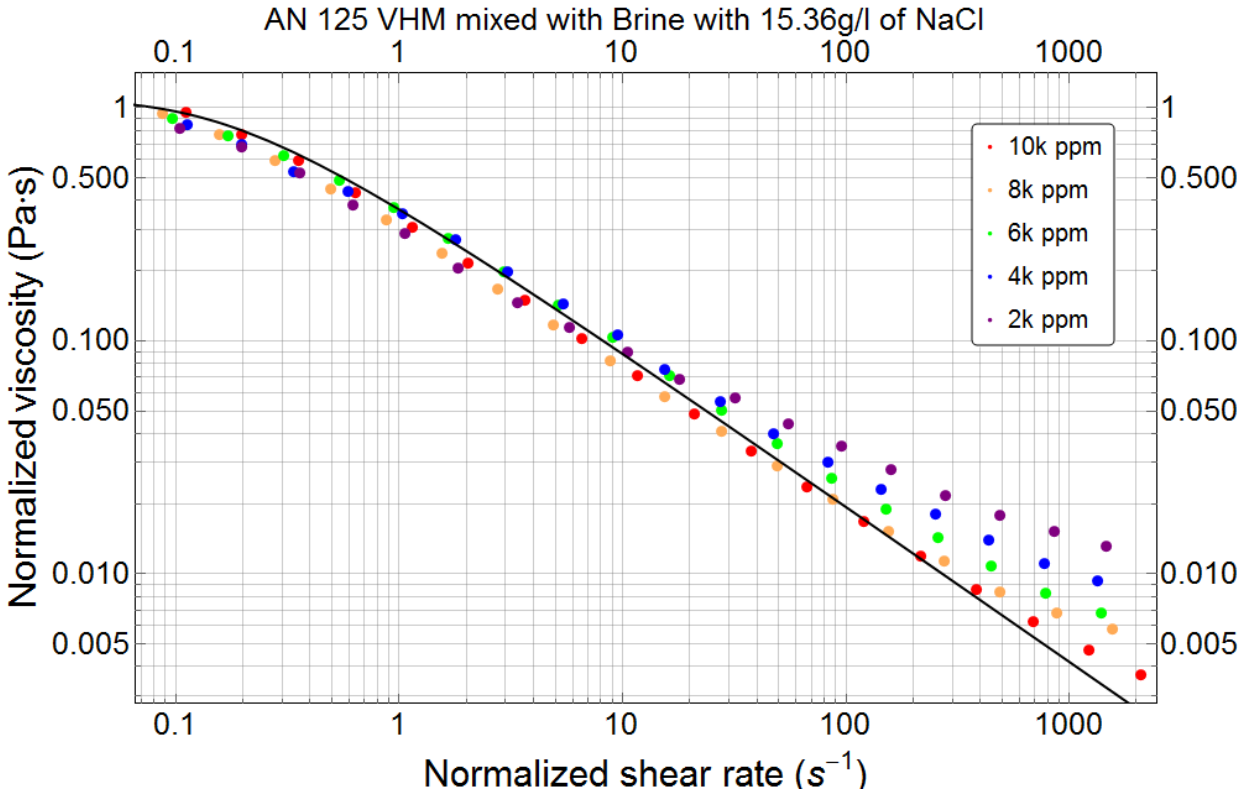

Figure 10. 3: Normalized viscosity vs normalized shear rate for AN 125 VHM mixed with Brine with 15.36 g/l of NaCl.

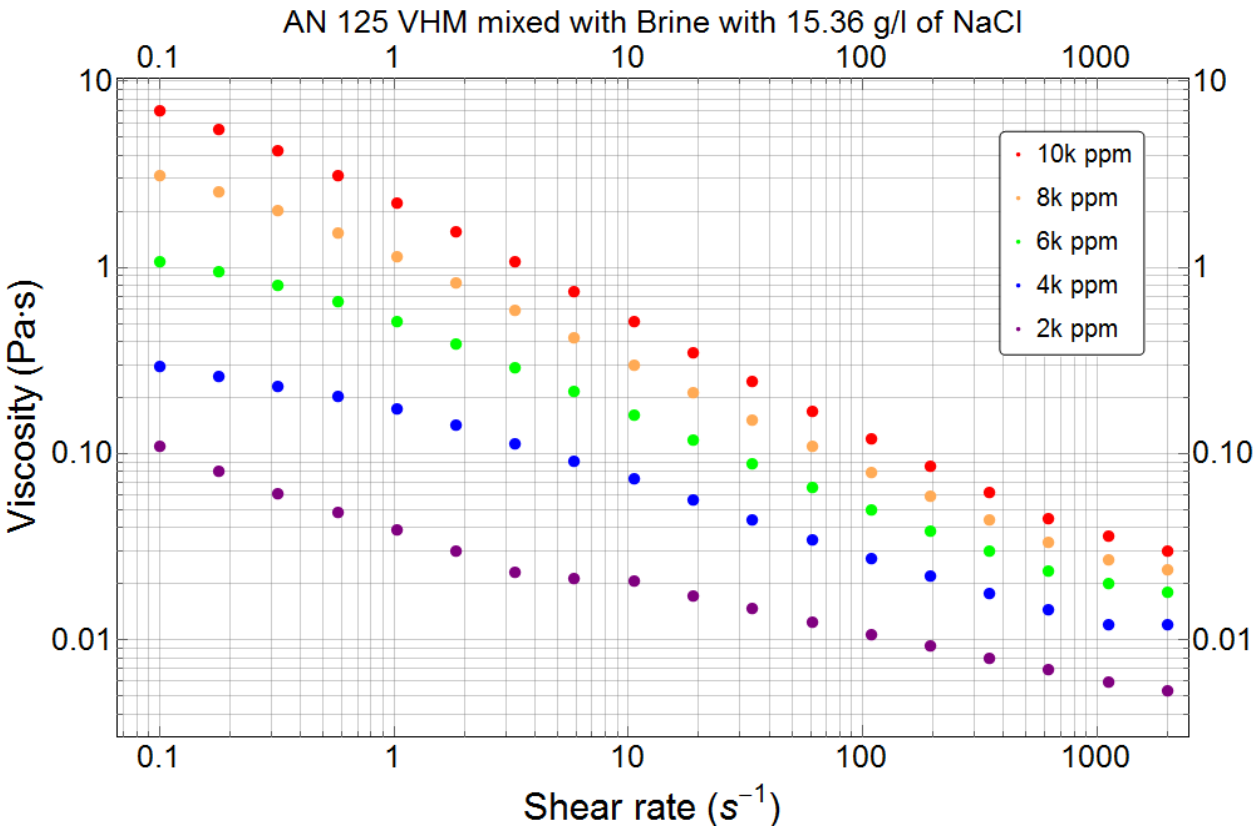

Figure 10. 4: Viscosity vs Shear rate for AN 125 VHM mixed with Brine with 15.36 g/l of NaCl.

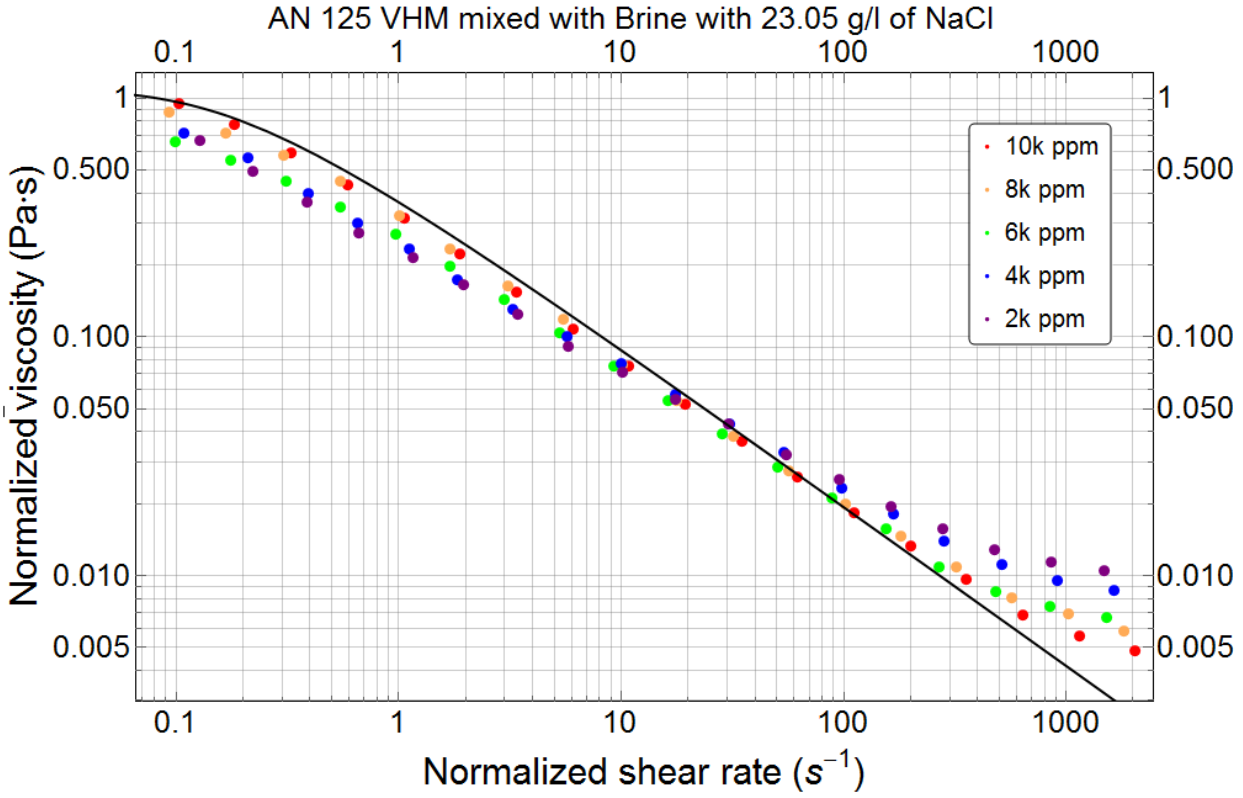

Figure 10. 5: Normalized viscosity vs normalized shear rate for AN 125 VHM mixed with Brine with 23.05 g/l of NaCl.

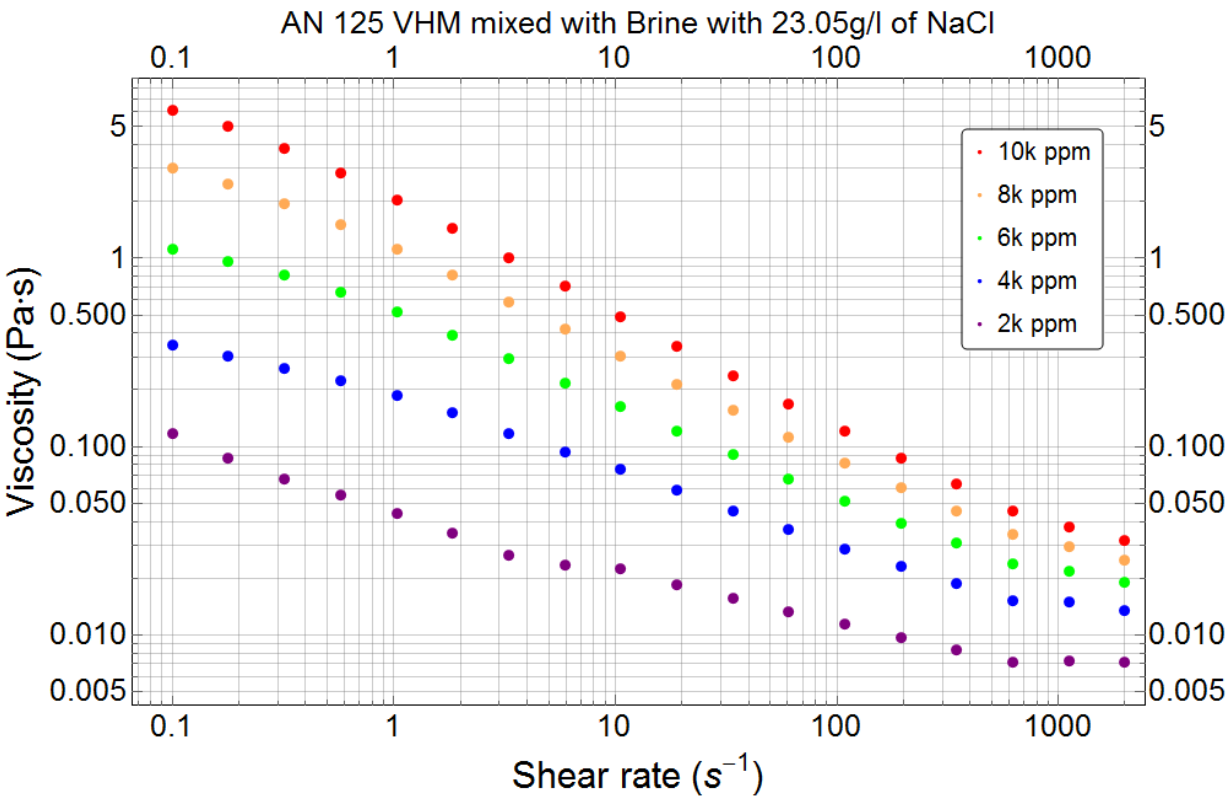

Figure 10. 6: Viscosity vs Shear rate for AN 125 VHM mixed with Brine with 23.05 g/l of NaCl.

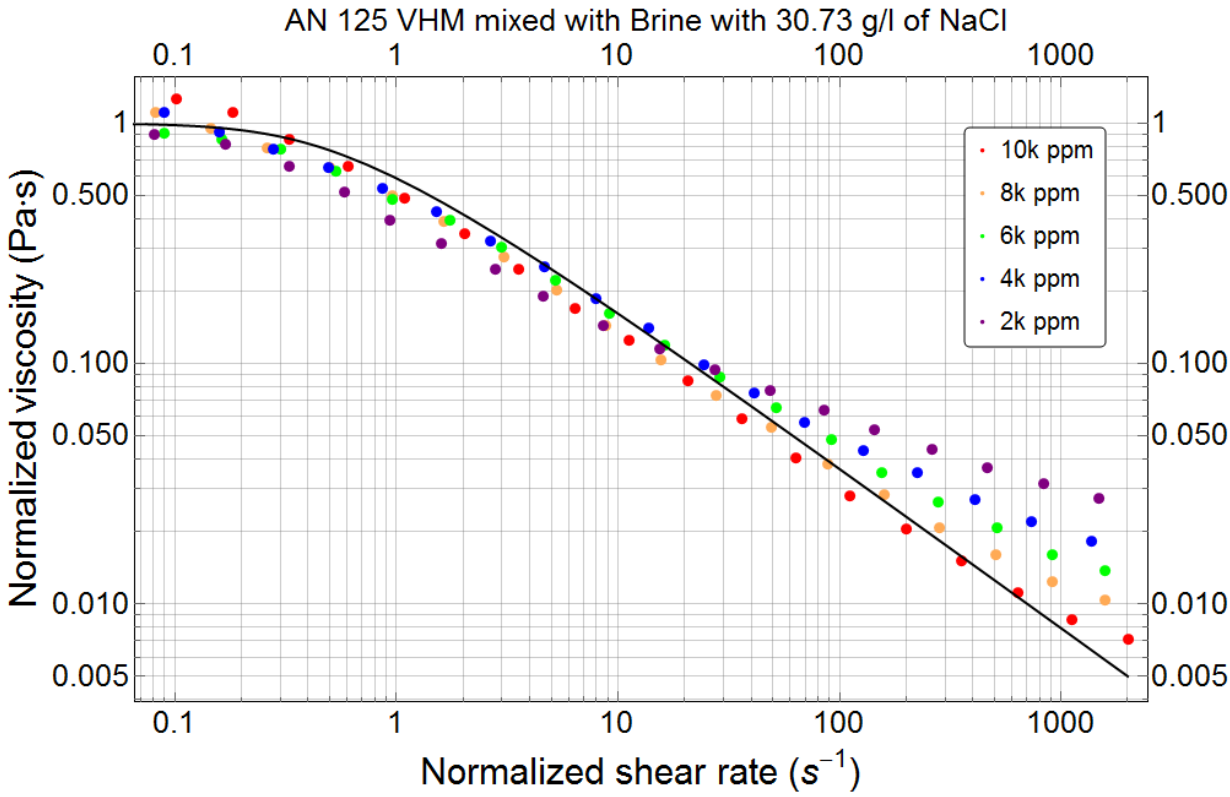

Figure 10. 7: Normalized viscosity vs normalized shear rate for AN 125 VHM mixed with Brine with 30.73 g/l of NaCl.

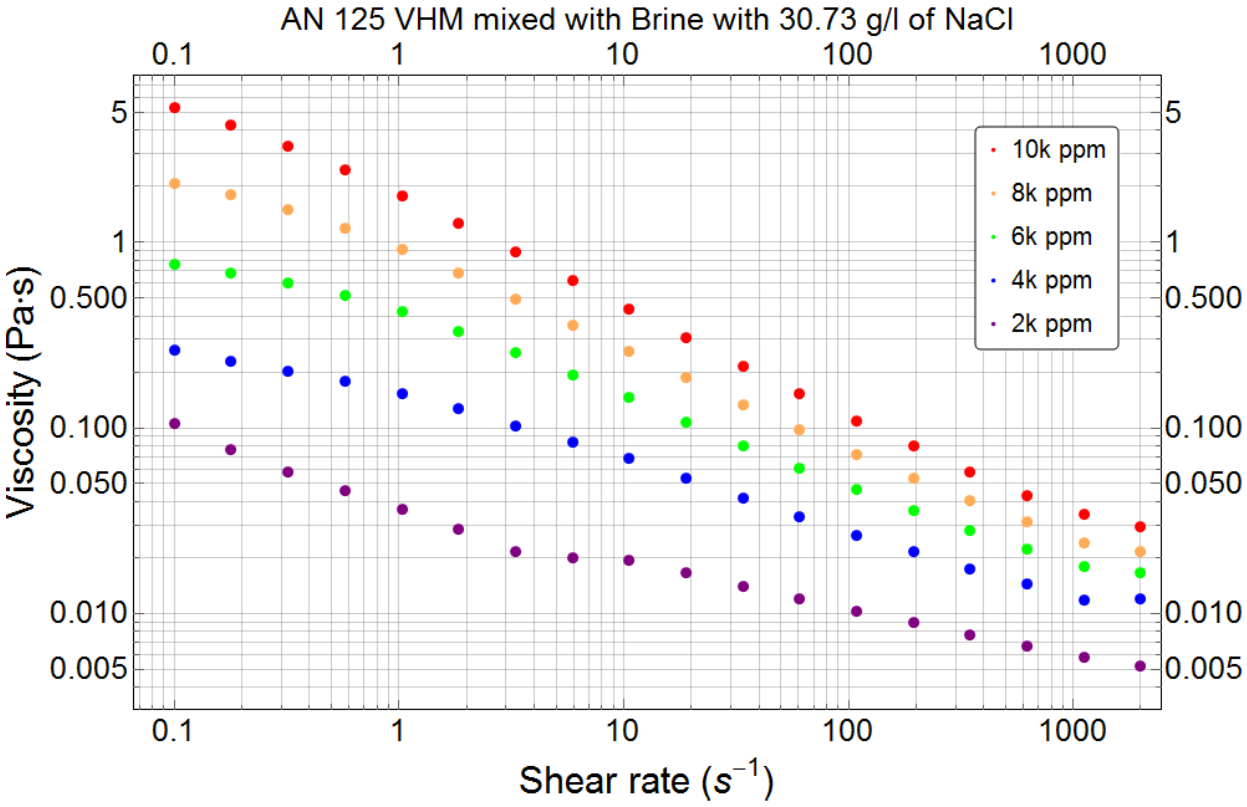

Figure 10. 8: Viscosity vs Shear rate for AN 125 VHM mixed with Brine with 30.73 g/l of NaCl.

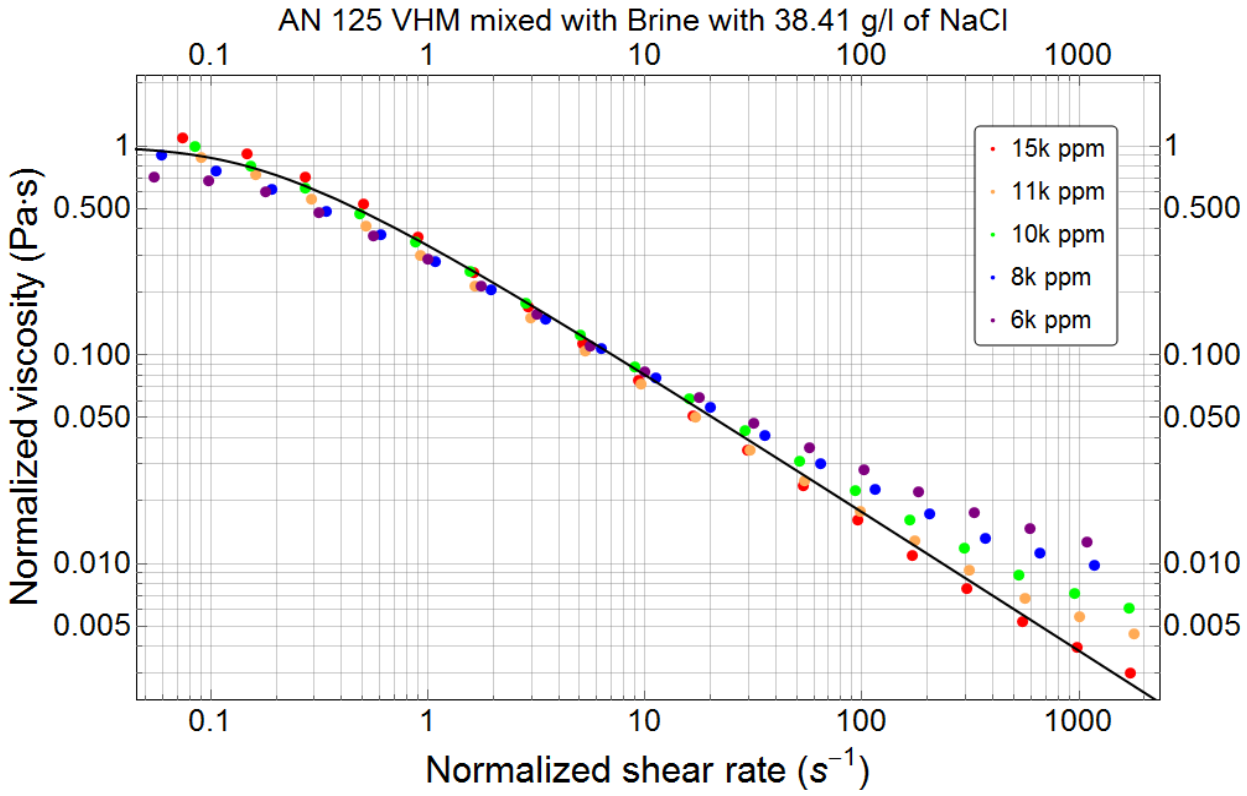

Figure 10. 9: Normalized viscosity vs normalized shear rate for AN 125 VHM mixed with Brine with 30.73 g/l of NaCl.

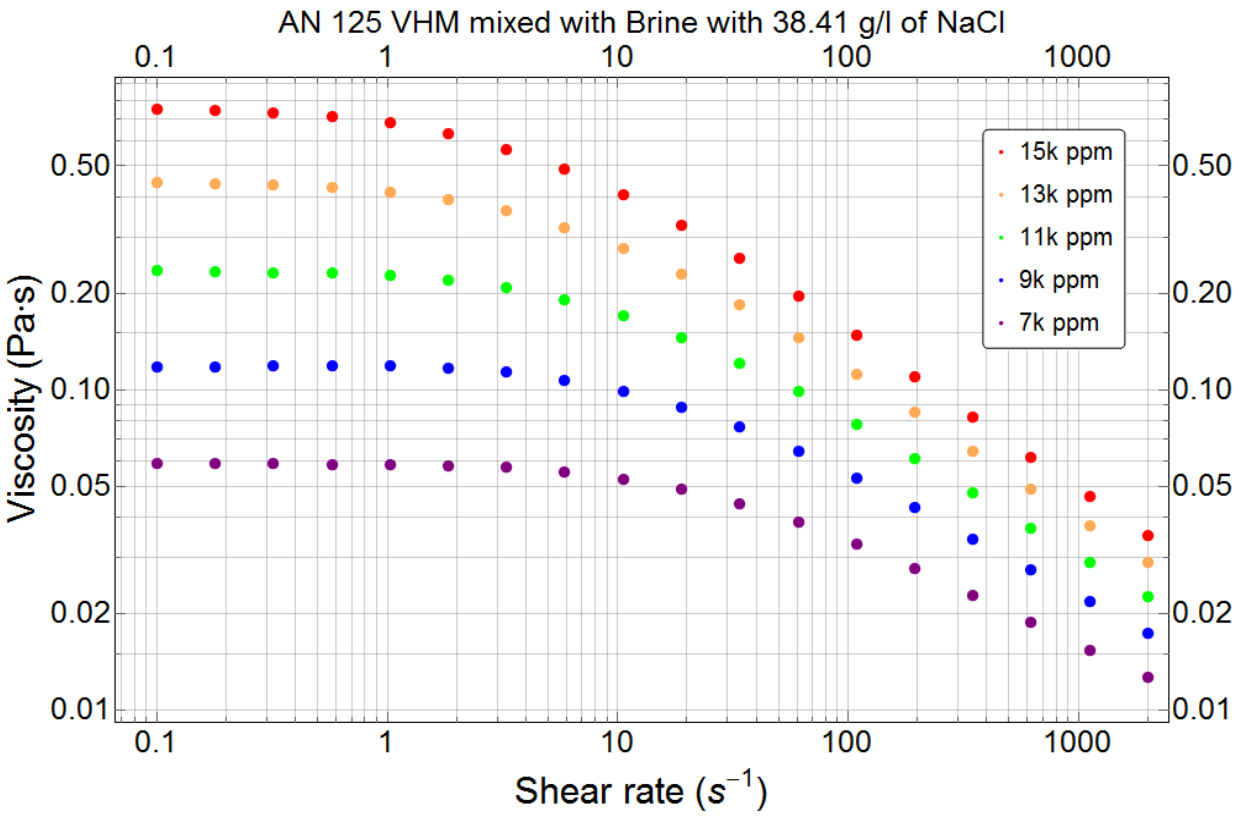

Figure 10. 10: Viscosity vs Shear rate for AN 125 VHM mixed with Brine with 38.41 g/l of NaCl.

The figures depicted above (i.e. fig. 10. 1 – 10. 10) are paired respectively, where the second graphs represent viscosity against shear rate values for different polymer concentrations within the original dataset. While the viscosity and shear rate values on the first graphs were normalized in order to see which model is the best fitted for a given dataset.

FENE-P model was chosen as the best fit for all 5 salinity concentrations. From the graphs depicting normalized viscosity and shear rate, it is clearly seen that the polymer solutions with greater polymer concentrations tend to better follow the model, whereas those of lower polymer concentrations have a greater deviation from the presented model. This is, most probable, due to polymers with lower concentrations experiencing less viscosity drop and having less shear thinning effect.

Similarly, the polymers with the low molecular weight were tested and the results were compared with the models discussed before, and are illustrated as follows:

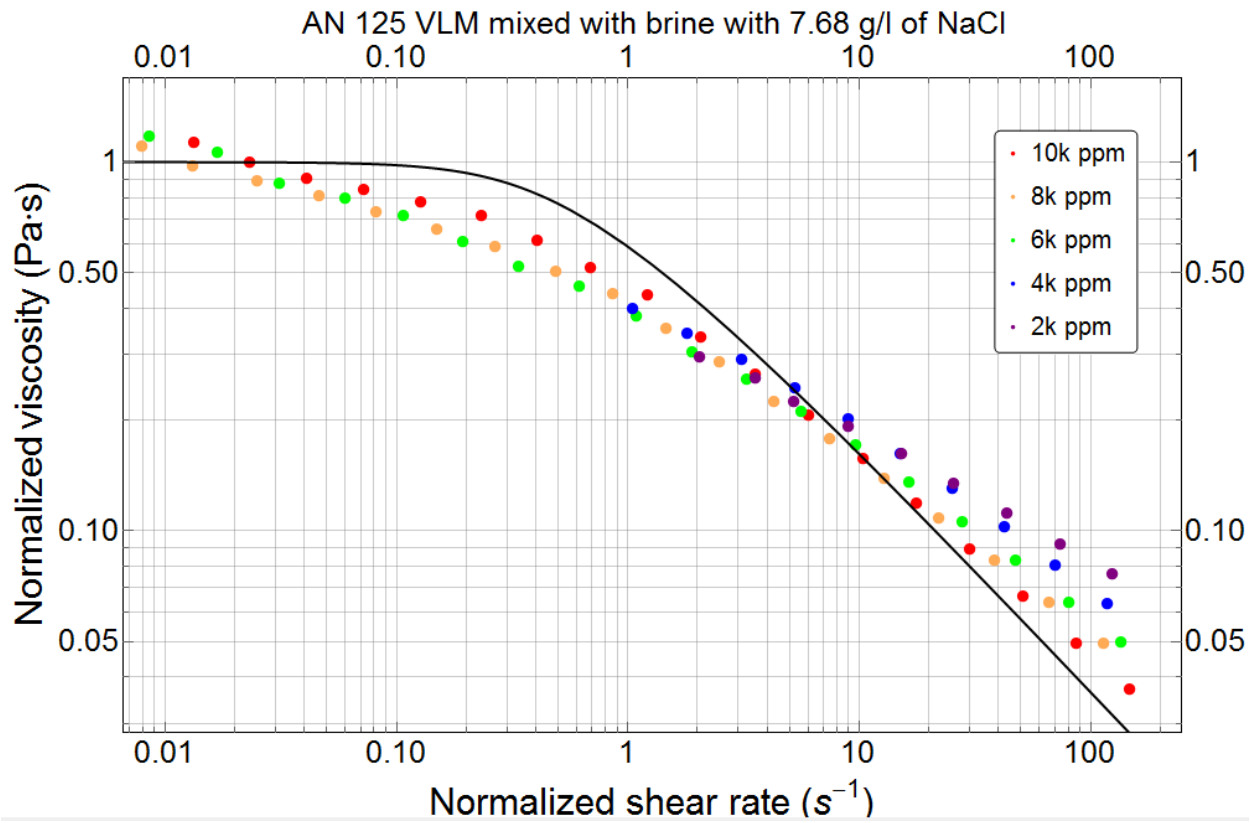

Figure 10. 11: Normalized viscosity vs normalized shear rate for AN 125 VLM mixed with Brine with 7.68 g/l of NaCl.

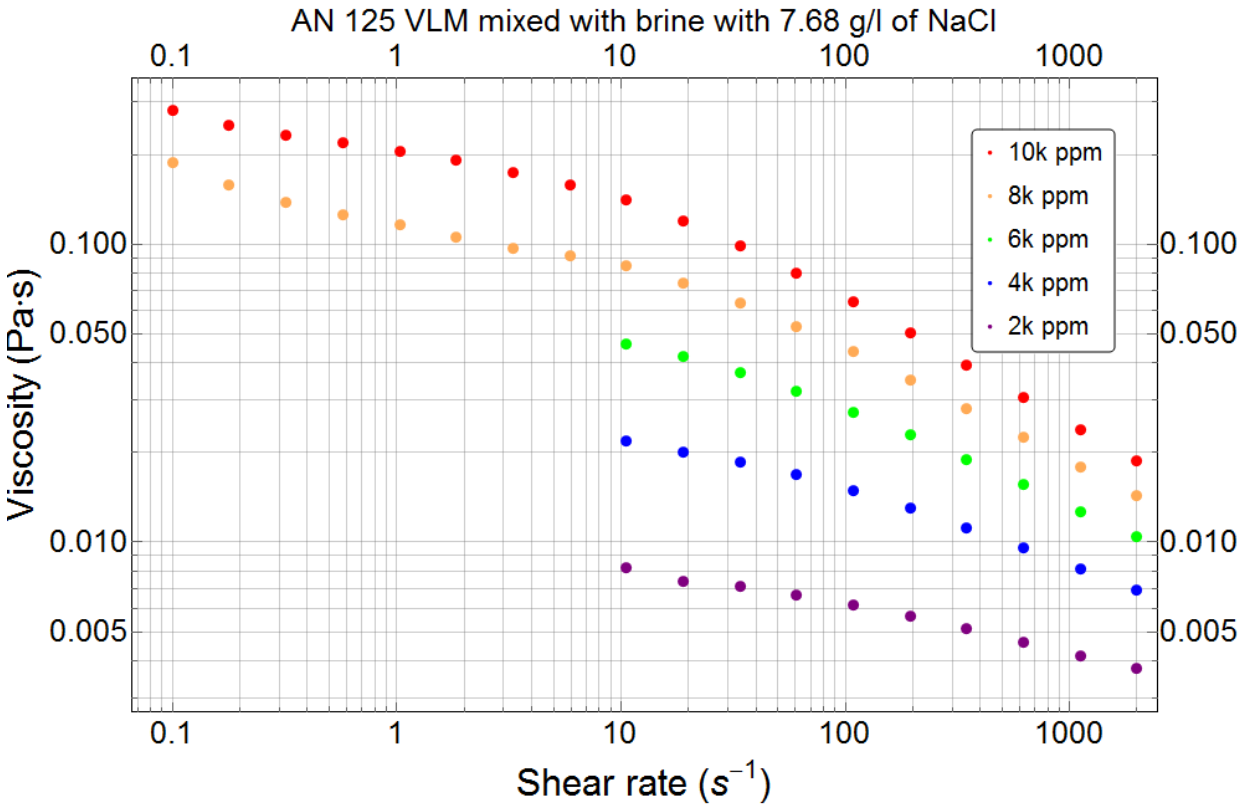

Figure 10. 12: Viscosity vs Shear rate for AN 125 VHM mixed with Brine with 38.41 g/l of NaCl.

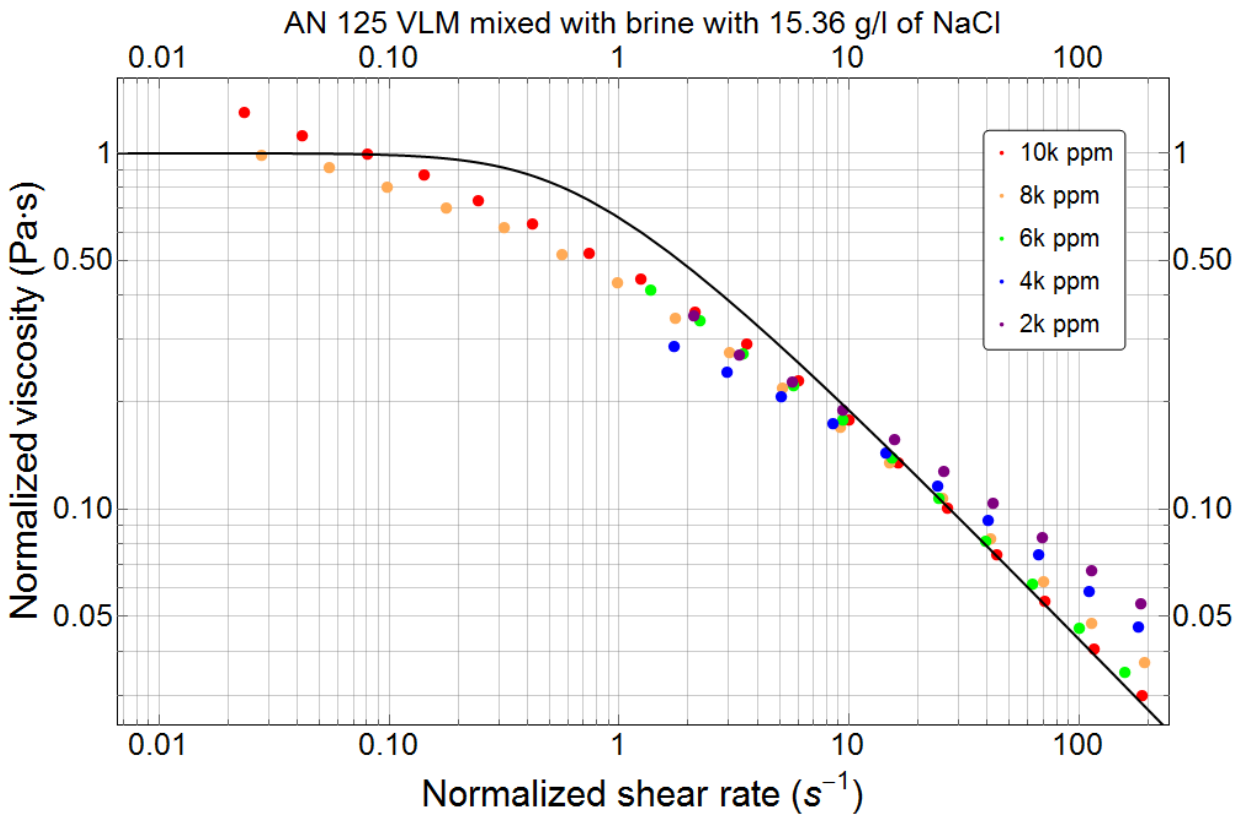

Figure 10. 13: Normalized viscosity vs normalized shear rate for AN 125 VLM mixed with Brine with 15.36 g/l of NaCl.

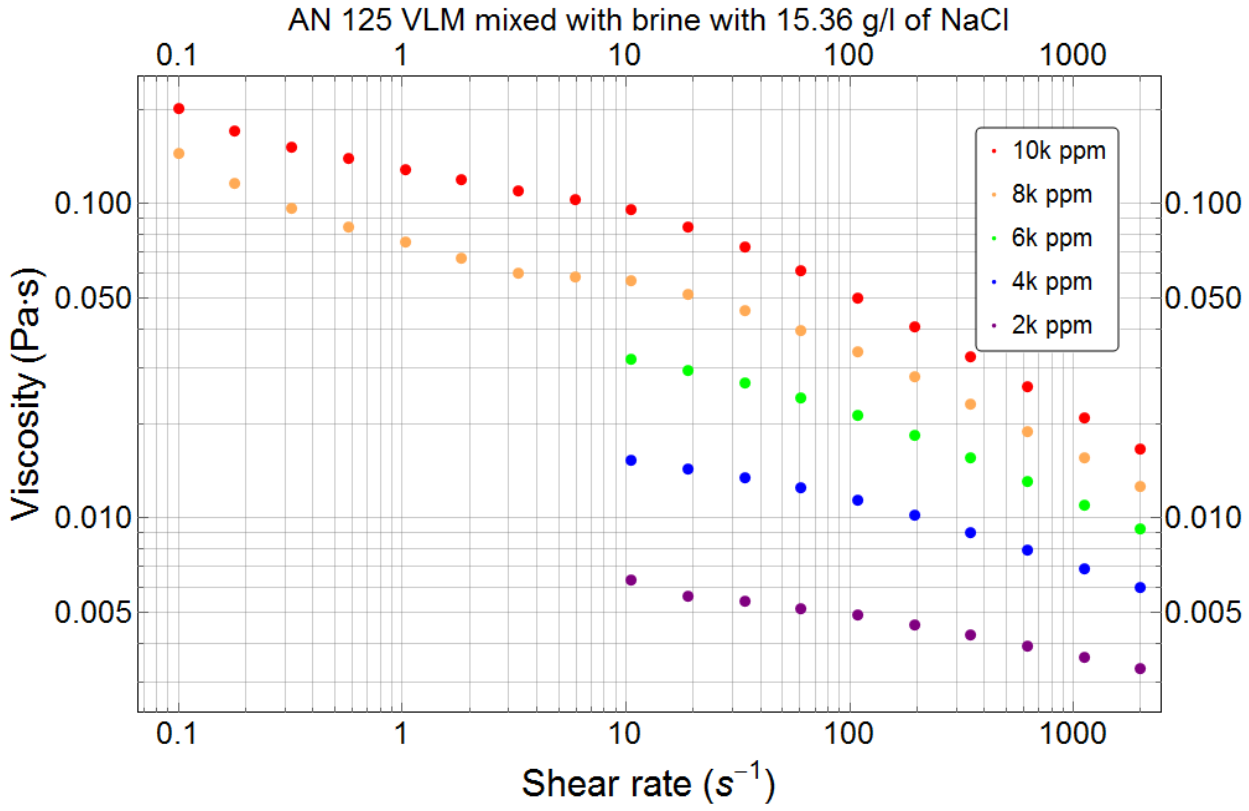

Figure 10. 14: Viscosity vs Shear rate for AN 125 VLM mixed with Brine with 15.36 g/l of NaCl.

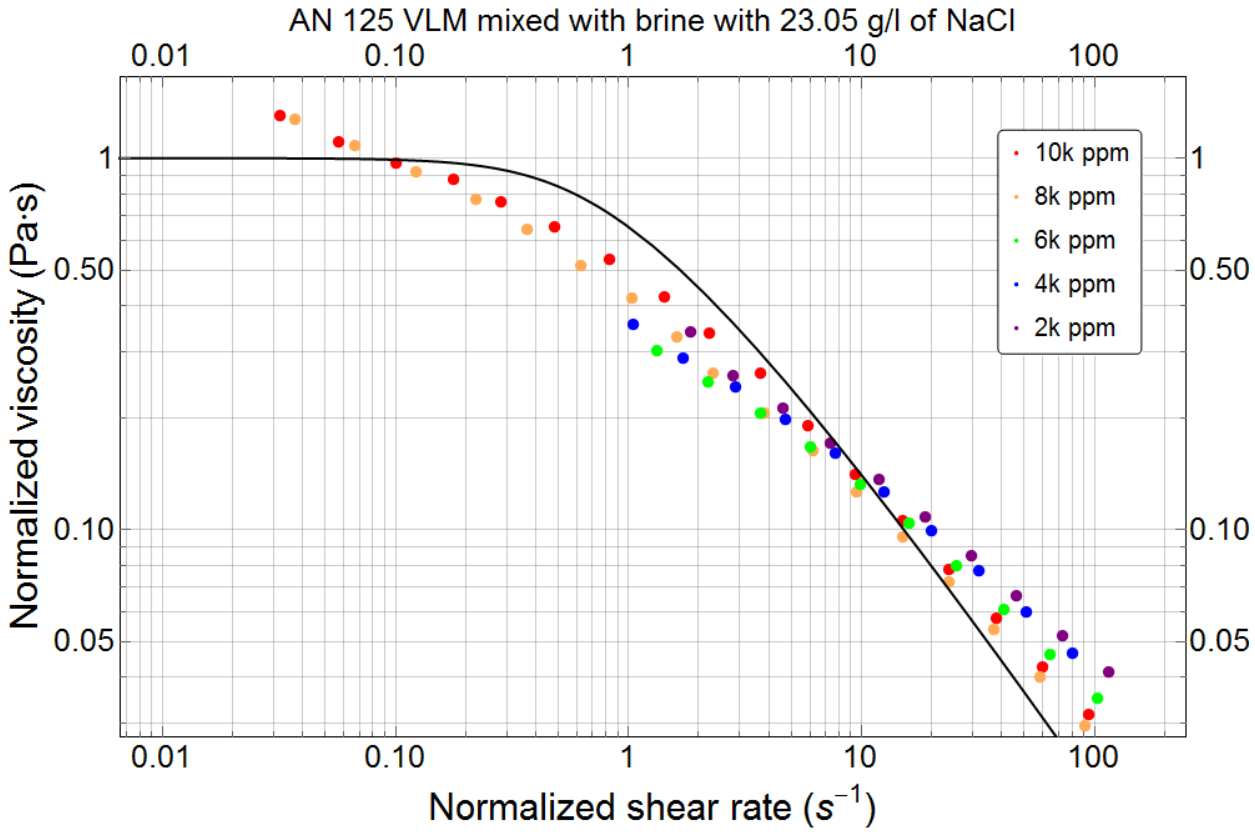

Figure 10. 15: Normalized viscosity vs normalized shear rate for AN 125 VLM mixed with Brine with 23.05 g/l of NaCl.

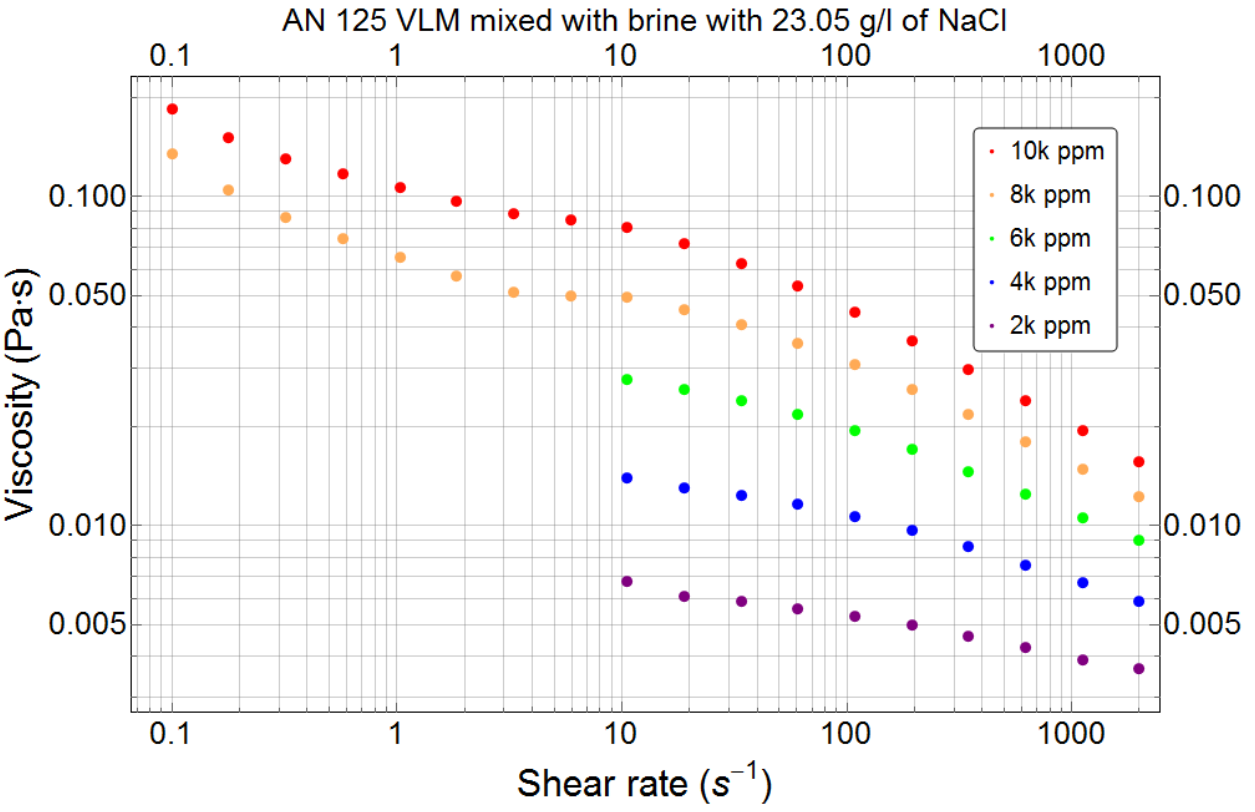

Figure 10. 16: Viscosity vs Shear rate for AN 125 VLM mixed with Brine with 23.05 g/l of NaCl.

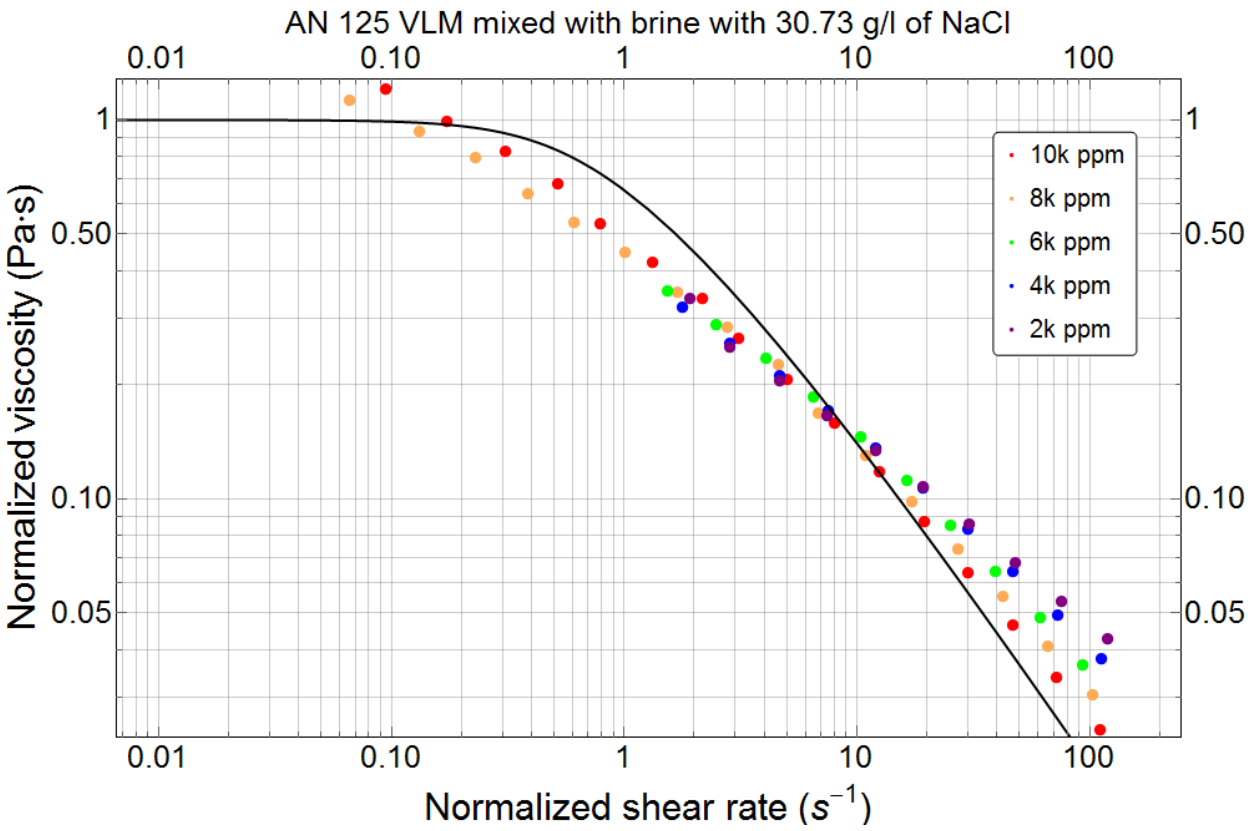

Figure 10. 17: Normalized viscosity vs normalized shear rate for AN 125 VLM mixed with Brine with 30.73 g/l of NaCl.

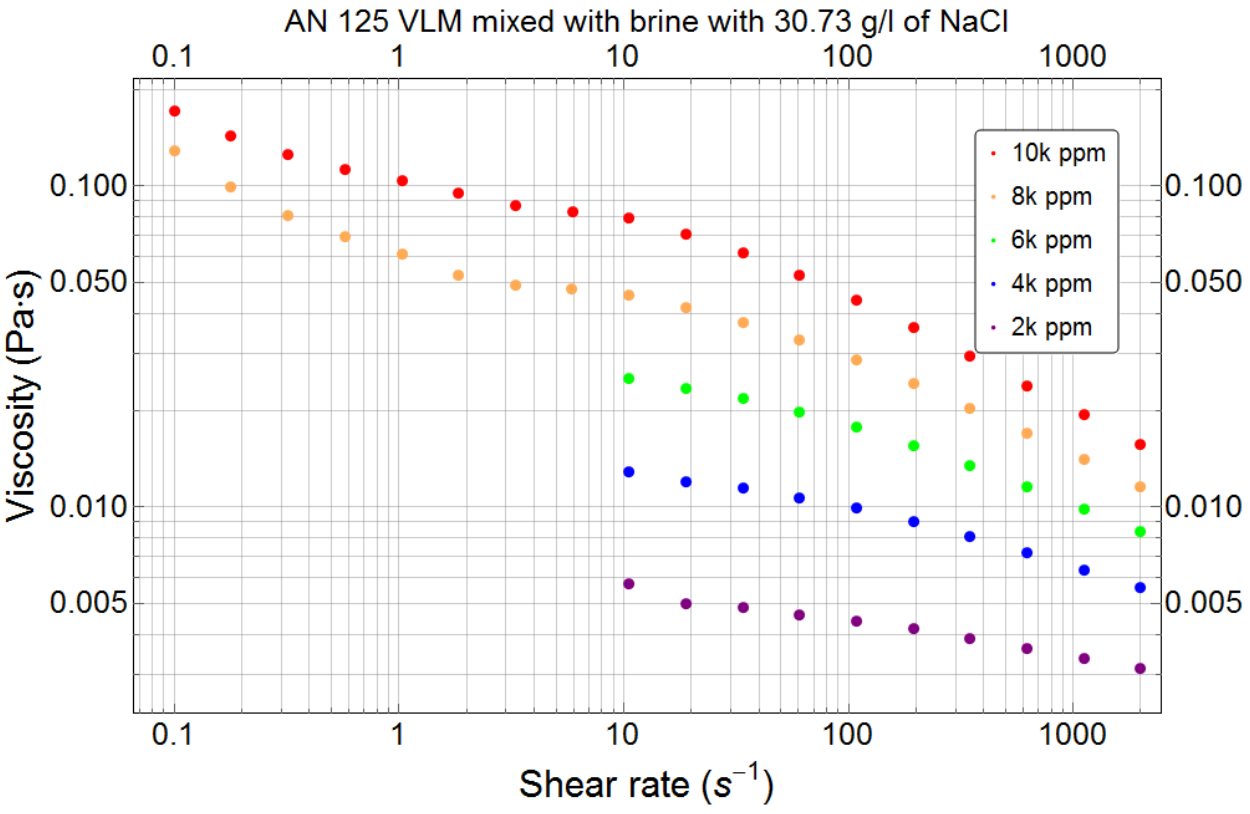

Figure 10. 18: Viscosity vs Shear rate for AN 125 VLM mixed with Brine with 30.73 g/l of NaCl.

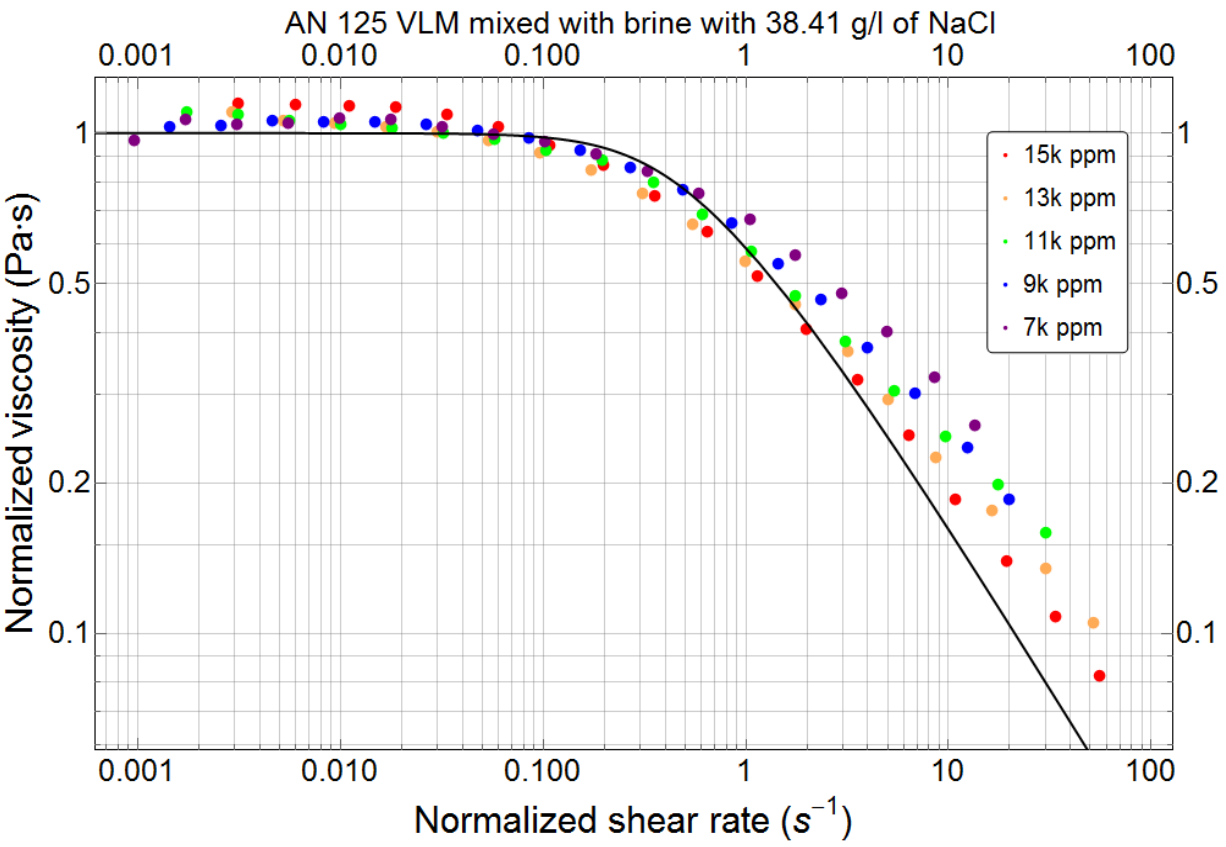

Figure 10. 19: Normalized viscosity vs normalized shear rate for AN 125 VLM mixed with Brine with 38.41 g/l of NaCl.

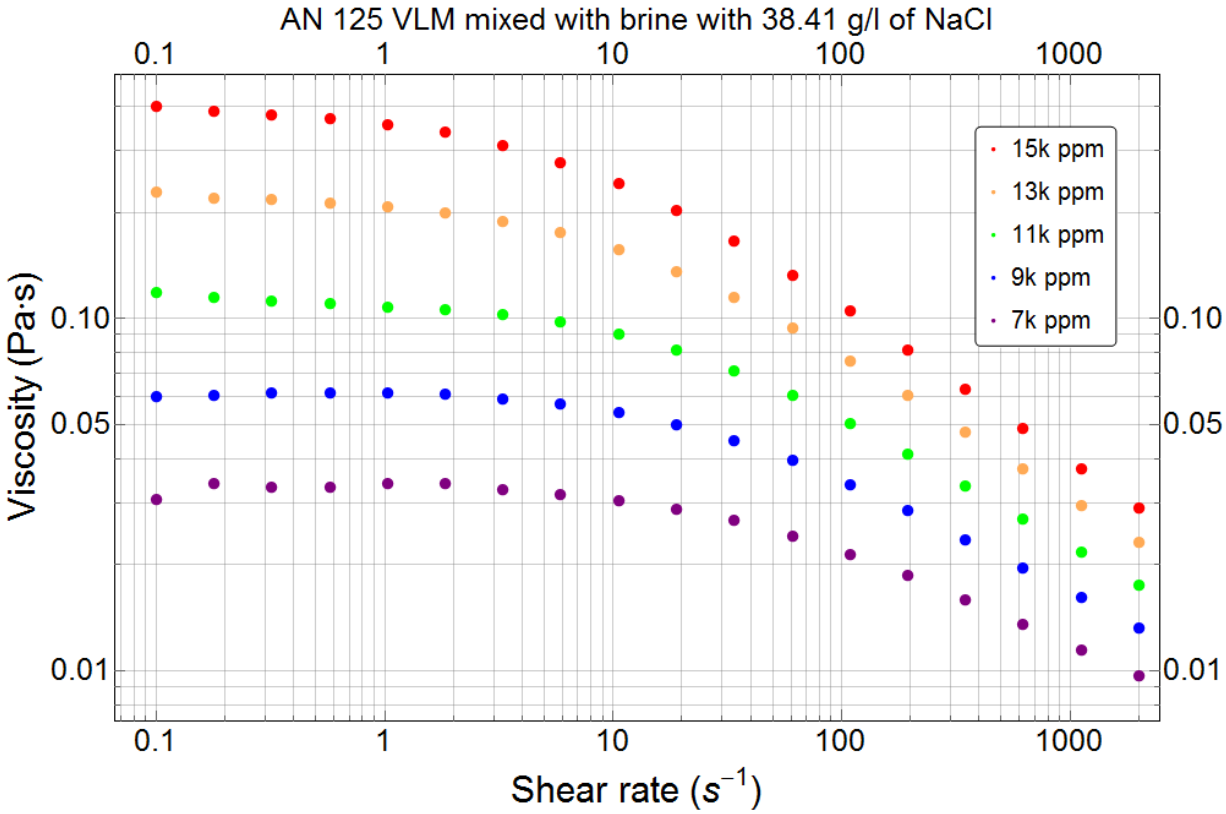

Figure 10. 20: Viscosity vs Shear rate for AN 125 VLM mixed with Brine with 38.41 g/l of NaCl.

Considering low molecular weight polymers (taking as an example of AN 125 VLM), it was noticed that the FENE-P model was the best fitted one, as in the case with the high molecular weight polymers. However, the trends for the low molecular weight polymers were not as close as they were for the latter ones, which is explained as the VLM polymers exhibit less sensitivity to shear thinning effect rather than VHM polymers, therefore having less viscosity drop. In figures (10.11-10.18), the first half of the data was dropped out as it was not consistent and had no reasonable values. This happens due to small amount of time that were set up for the low shear rate experiments, however the same amount of time was quite a lot for the high molecular weight polymers. The experiments for the higher salinity concentration were set up with the twice as much amount of time than for the solutions with lower salinity concentrations. And eventually the results obtained were quite consistent and showed the best stick to the FENE-P model with the further deviation on the higher shear rates.

Similarly to the experiments presented above, Xanthan Gum and HEC were tested, but as they show much less sensitivity to salt, it was decided to test them in the brine with highest salinity.

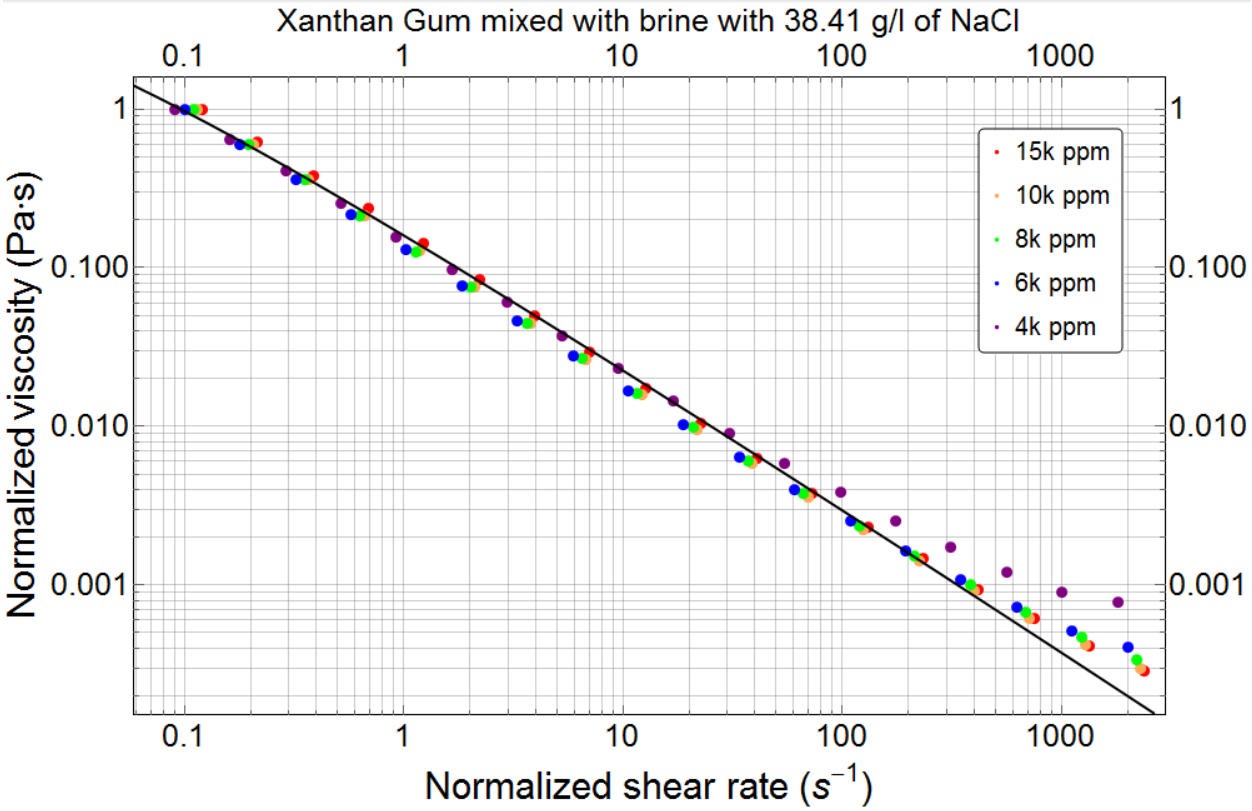

Figure 10. 21: Normalized viscosity vs normalized shear rate for Xanthan Gum mixed with Brine with 38.41 g/l of NaCl.

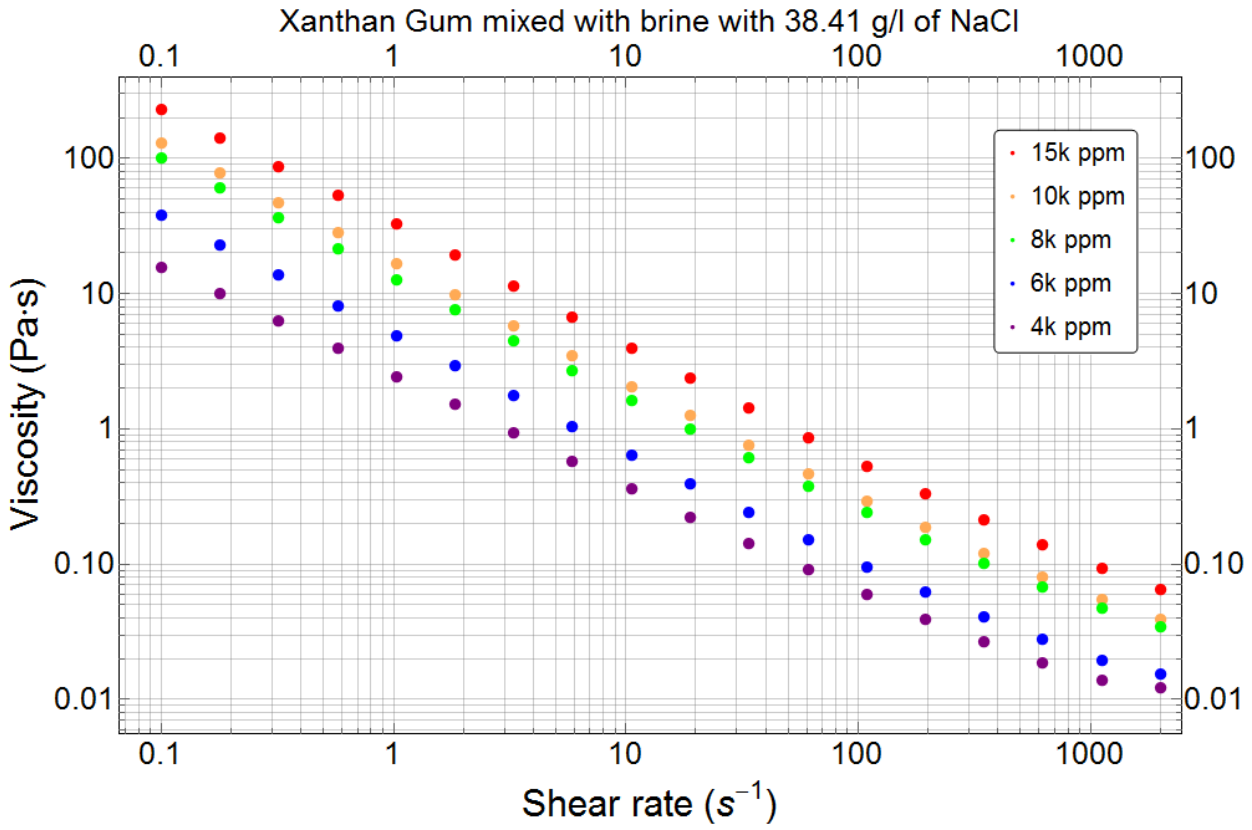

Figure 10. 22: Viscosity vs Shear rate for Xanthan Gum mixed with Brine with 38.41 g/l of NaCl.

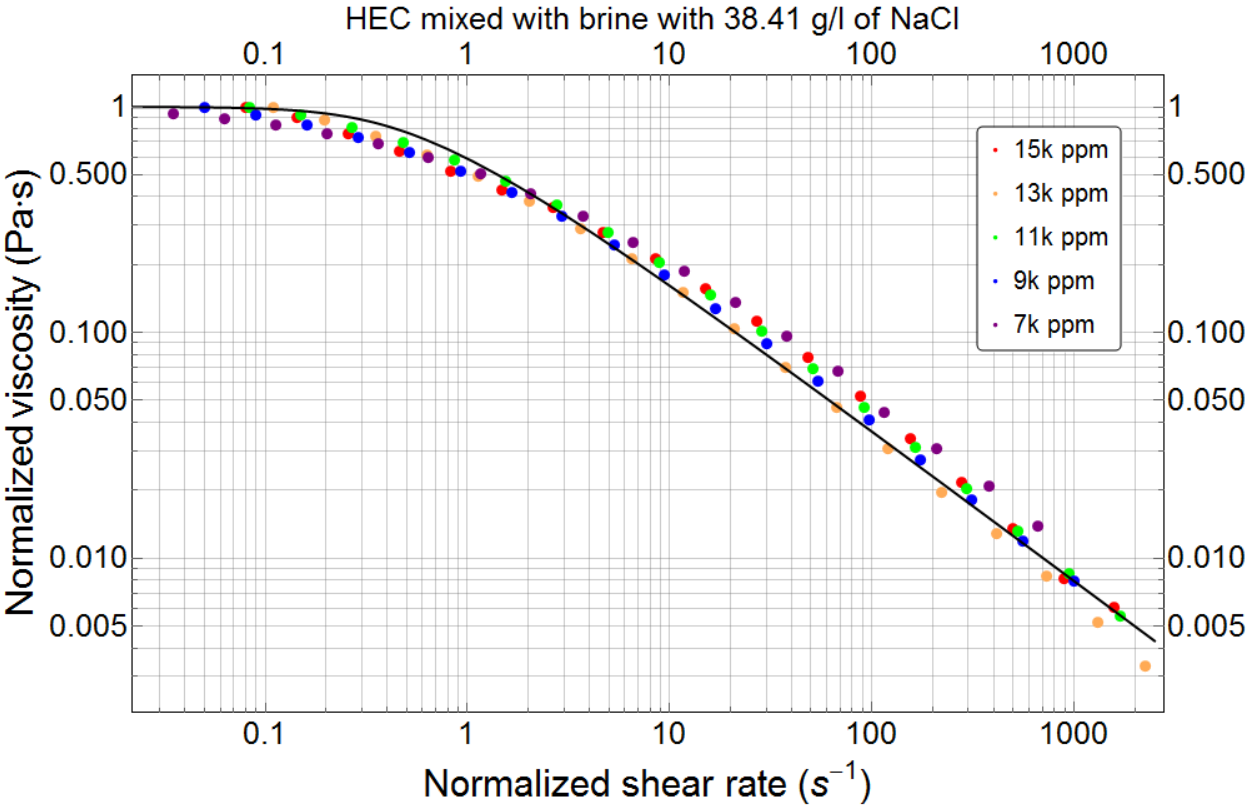

Figure 10. 23: Normalized viscosity vs normalized shear rate for HEC mixed with Brine with 38.41 g/l of NaCl.

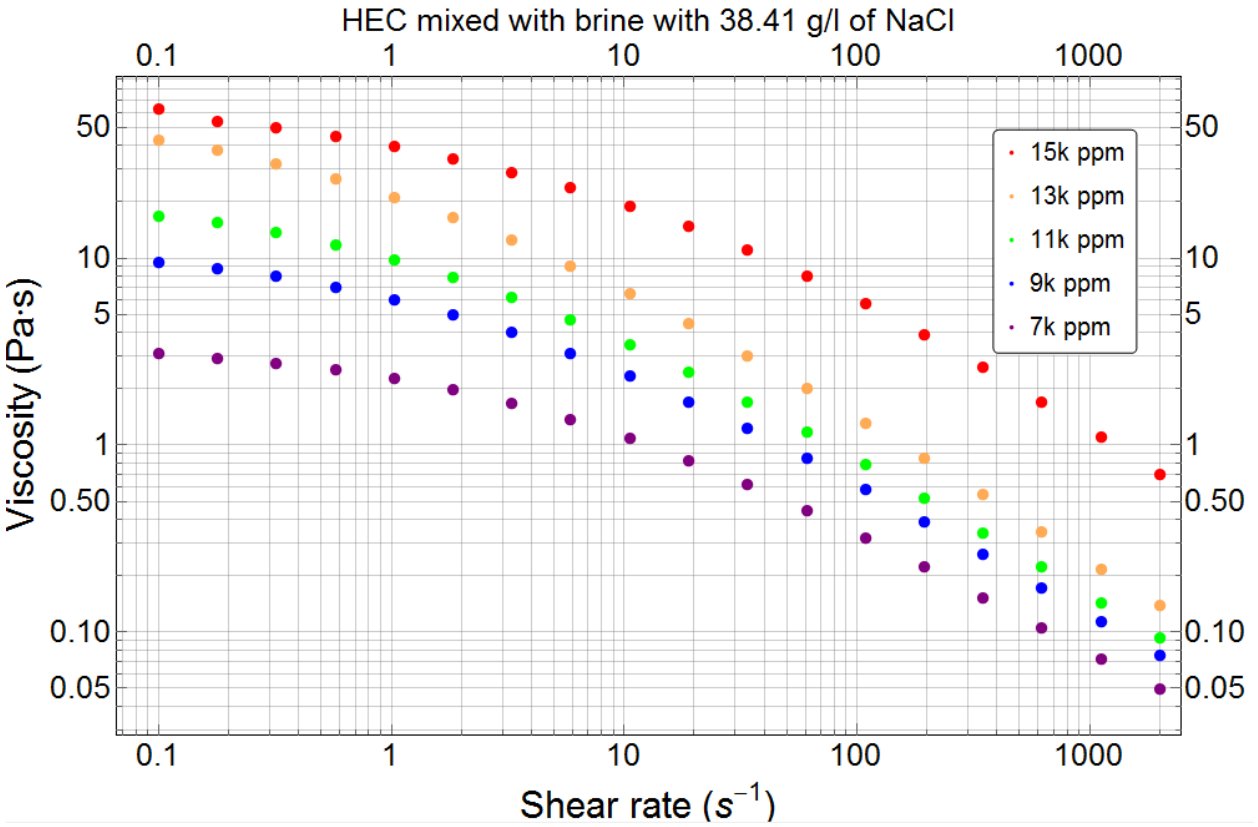

Figure 10. 24: Viscosity vs Shear rate for Xanthan Gum mixed with Brine with 38.41 g/l of NaCl.

An important point to be mentioned is that in case of Xanthan Gum Phan-Thien & Tanner model was used, as it shows the best fit for this polymer, while hydroxyethyl cellulose was more compatible with FENE-P model. It is also clearly seen that polysaccharides are more consistent with the models than polyacrylamides. The most likely explanation of less deviation from the models is that Xanthan Gum and HEC are salt tolerant polymers and undergo much less viscosity drop even in the brine with high salinity concentration.

In case of PolyPak polymer, the data obtained from the experiments did not match neither of the models presented above. However, the original results for the viscosity vs shear rate plot showed a quite reasonable trends and are illustrated in Fig. 10.25. It was decided to take high concentrations for PolyPak polymer as it showed almost Newtonian behaviour for lower concentrations. And this can be clearly seen from the Fig.10.25, when the trend tends to flatten out while reaching lower concentrations and, already, for 20 000 ppm it showed a trend similar to shear independent.

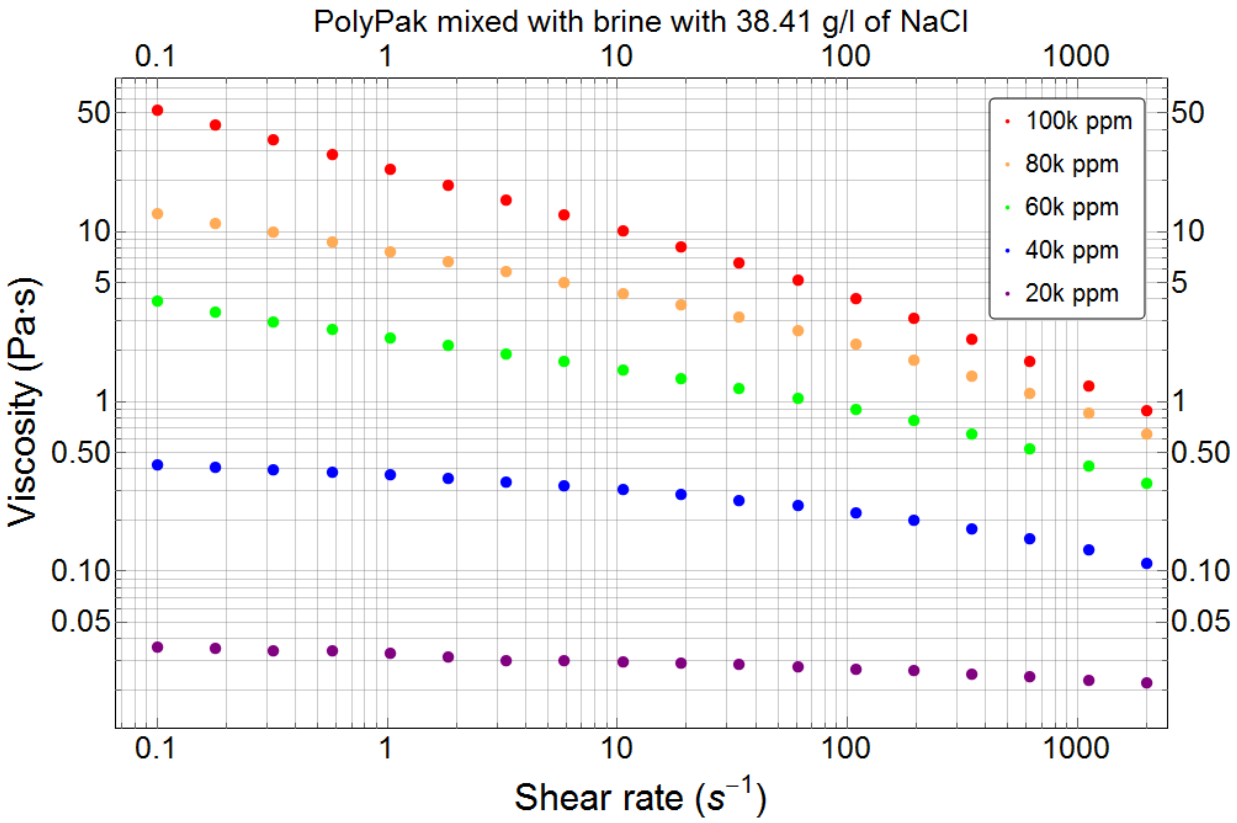

Figure 10. 25: Viscosity vs Shear rate for PolyPak mixed with Brine with 38.41 g/l of NaCl.

As one can see, all the data for every polymer obtained is quite similar and broadly consistent with the major trends corresponding to two models, namely FENE-P and Phan-Thien & Tanner models.

After presenting viscosity dependency phenomena of polymers with different concentrations, it is reasonable to show the viscosity difference between a given polymer solution mixed with brines and those mixed with distilled water. This is illustrated on Fig. (10. 26) – Fig (10. 34) as follows:

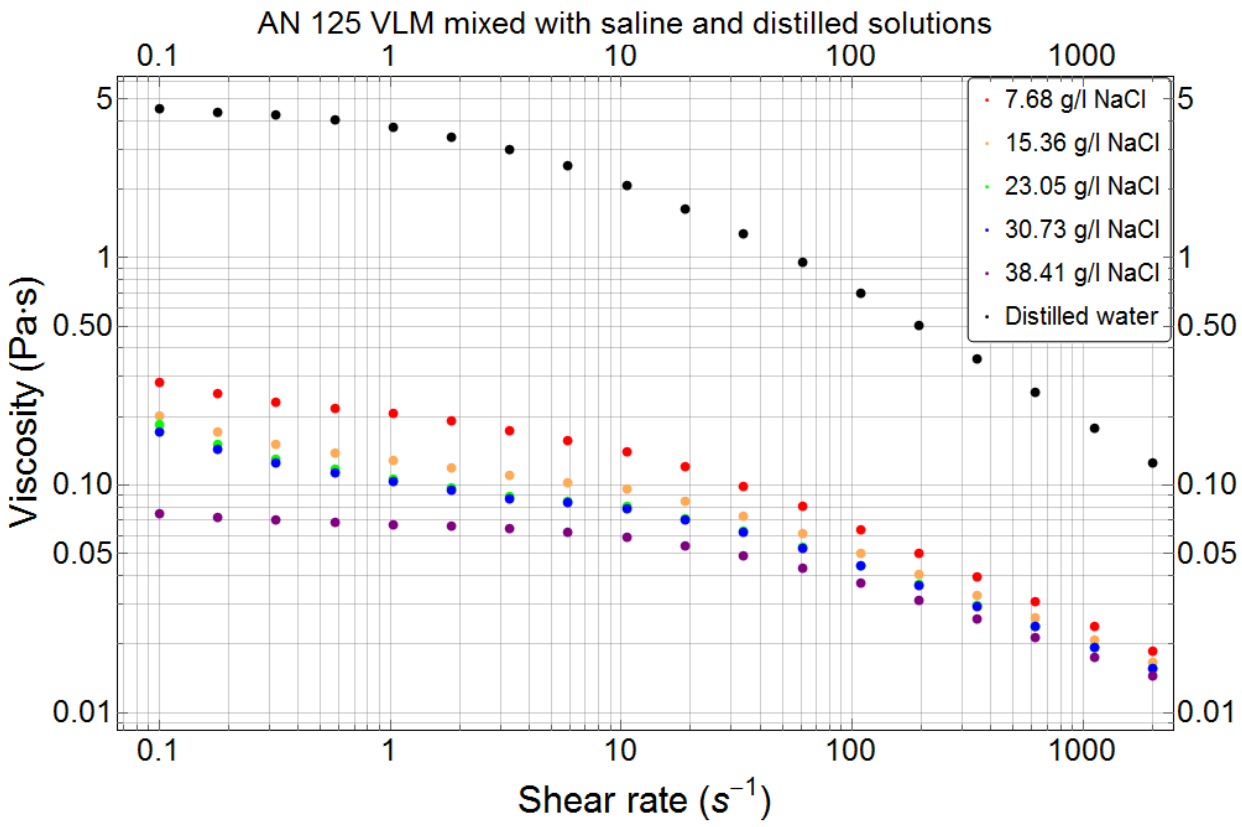

Figure 10. 26: Viscosity difference of AN 125 VLM (10 000 ppm) for saline and distilled water.

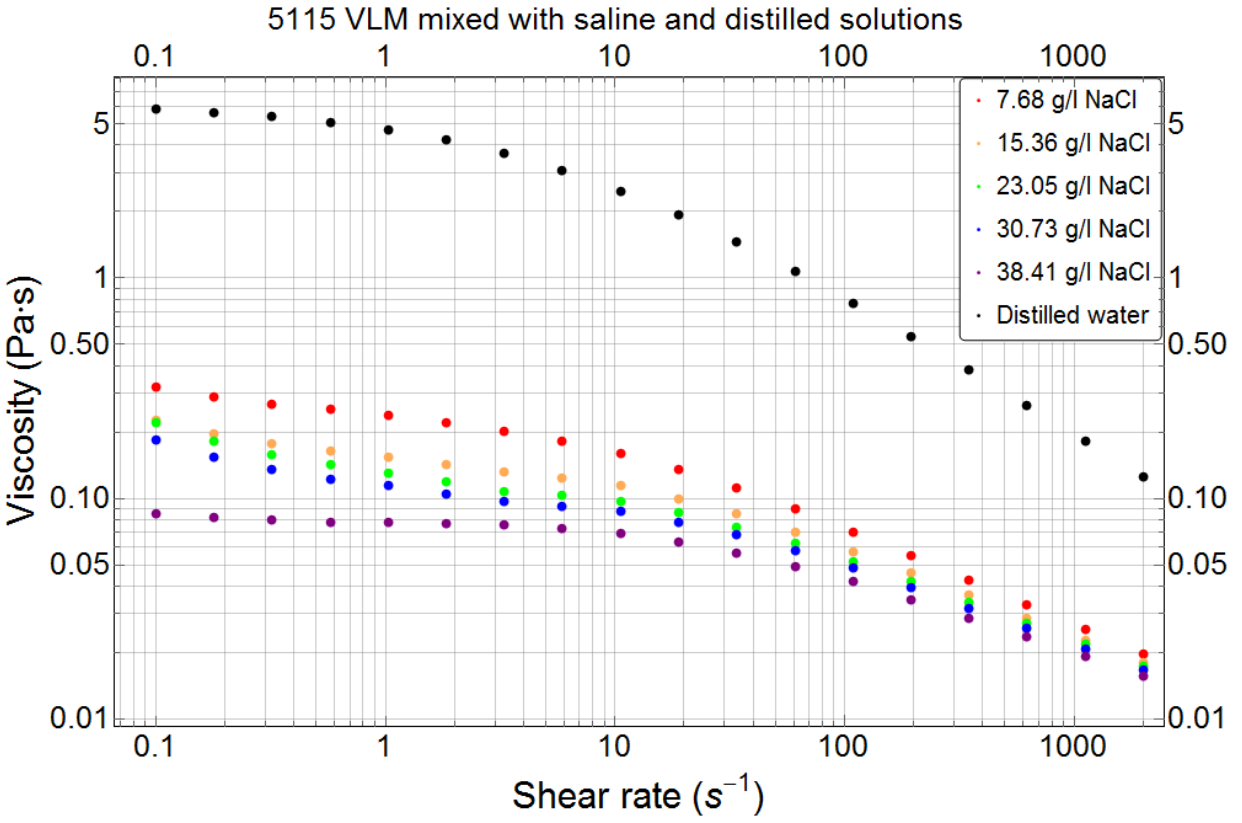

Figure 10. 27: Viscosity difference of 5115 VLM (10 000 ppm) for saline and distilled water.

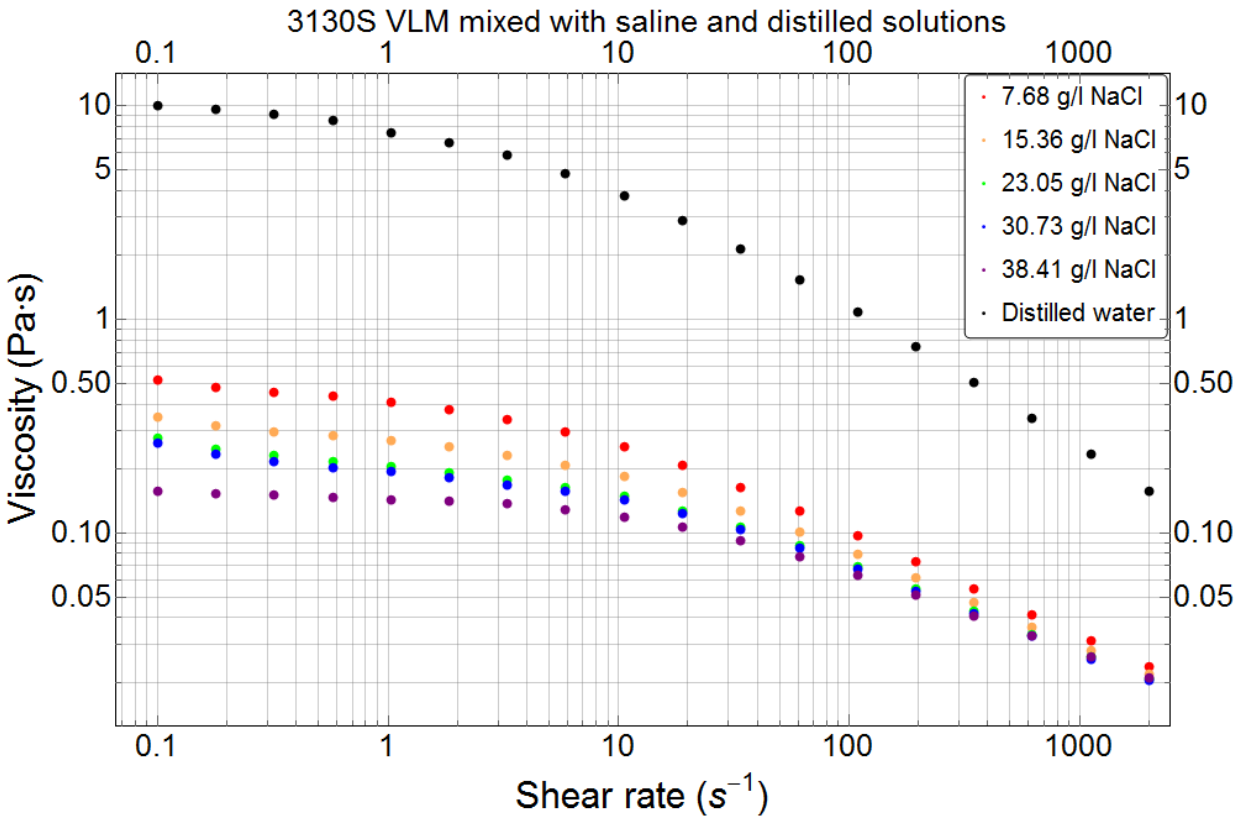

Figure 10. 28: Viscosity difference of 3130S VLM (10 000 ppm) for saline and distilled water.

Fig. 10. 26 – Fig. 10. 28 illustrate how big the impact of salinity is on polymers with low molecular weight. Comparing the results between solutions with 38.41 g/l of NaCl and those of distilled water, one can see that the difference is huge and account for more than 70 times for AN 125 VLM and 5115 VLM and even more than 80 times in case of 3130S VLM.

Similarly, the experiments were conducted for the high molecular weight polymers. VHM polymers also showed a significant viscosity drop due to salinity effect, but in this case, it was not less than those found in low molecular weight polymers. Again, comparing the highest salinity solution with the distilled water solutions, we can see that for AN 125 VHM the effect of salinity was a huge reaching almost 55 times difference. But in case of 5115 VHM and 3630S VHM, the difference in viscosity was 2.5 times less, however, also reaching a significant value of more than 20 times. Fig. 10. 29 – Fig. 10. 31 are presented to show this phenomenon:

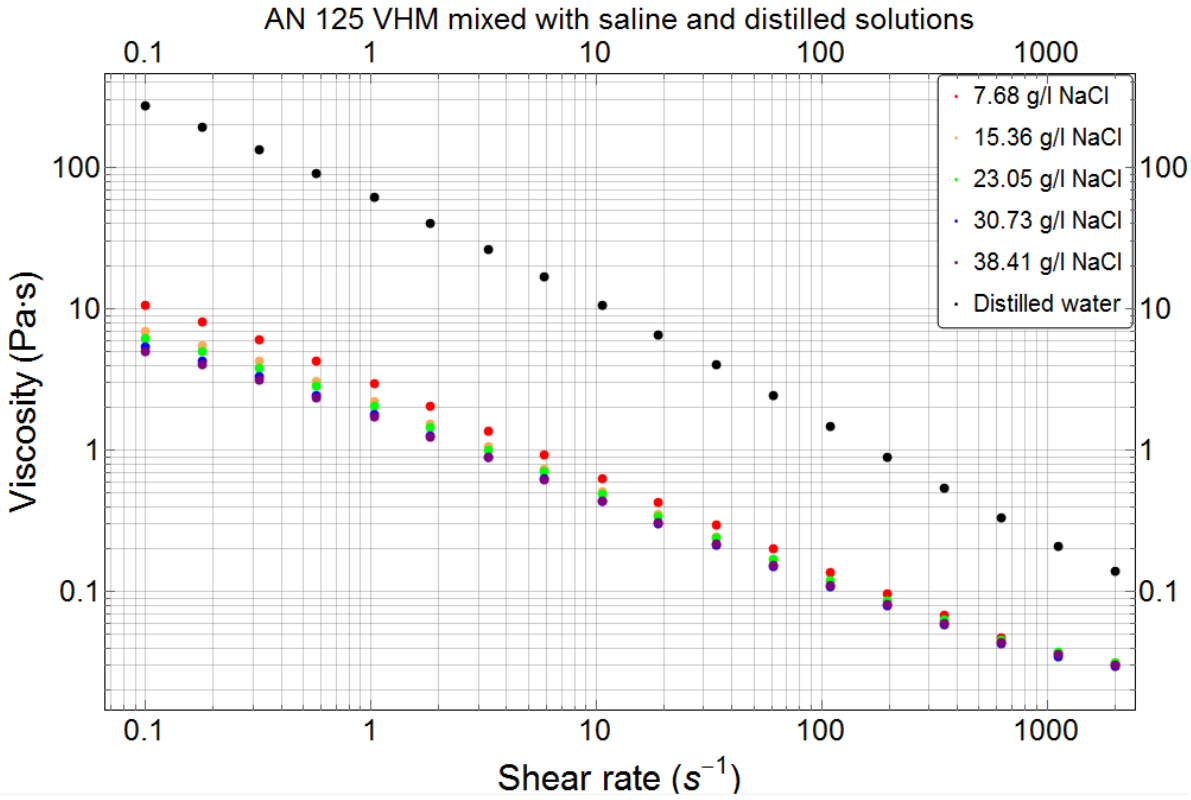

Figure 10. 29: Viscosity difference of AN 125 VHM (10 000 ppm) for saline and distilled water.

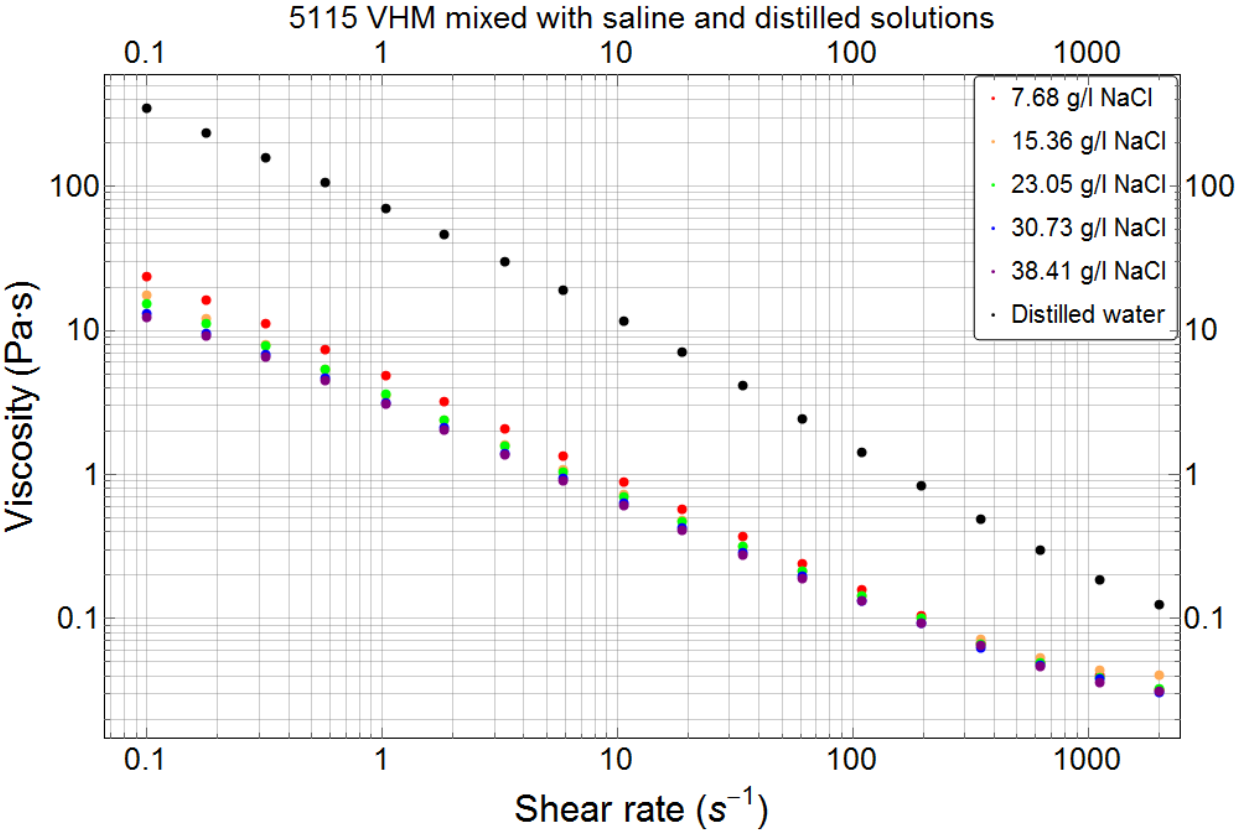

Figure 10. 30: Viscosity difference of 5115 VHM (10 000 ppm) for saline and distilled water.

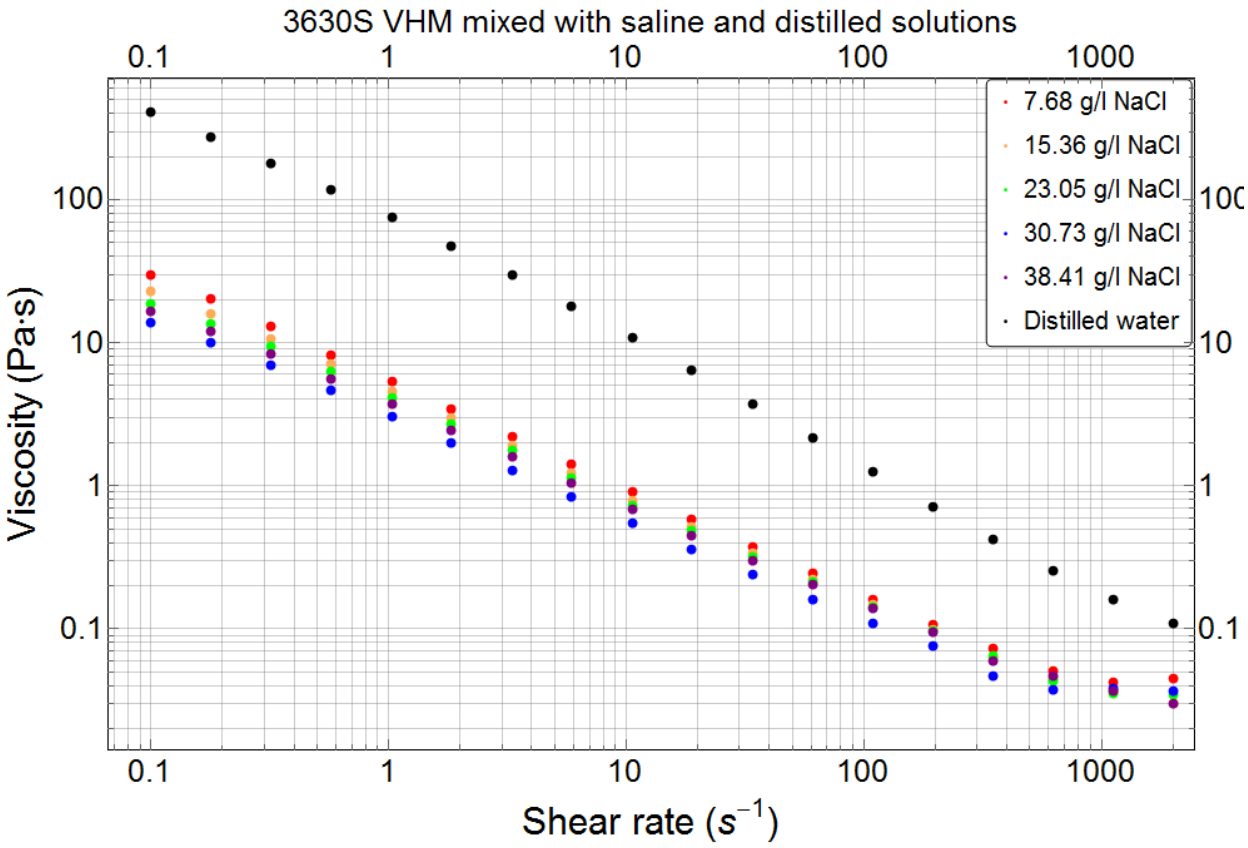

Figure 10. 31: Viscosity difference of 3630S VHM (10 000 ppm) for saline and distilled water.

As was discussed previously, Xanthan Gum, Hydroxyethyl cellulose and PolyPak were the polymers exhibiting less sensitivity to salinity. So, the highest salinity of brine was used directly to compare the results to those of distilled water.

As can be seen from Fig. 10.32 – Fig. 10.34, Xanthan Gum, HEC and PolyPak experience the least effect of water salinity among all the polymers, where the viscosity of distilled water 2-3 times greater than that of solution with 38.41 g/l of NaCl for high shear rates. For the low shear rate values the solutions showed a similar trend, except HEC polymer which showed almost no difference in viscosity. In other words, these polymers are the most salt tolerant polymers tested throughout this work and are illustrated as follows:

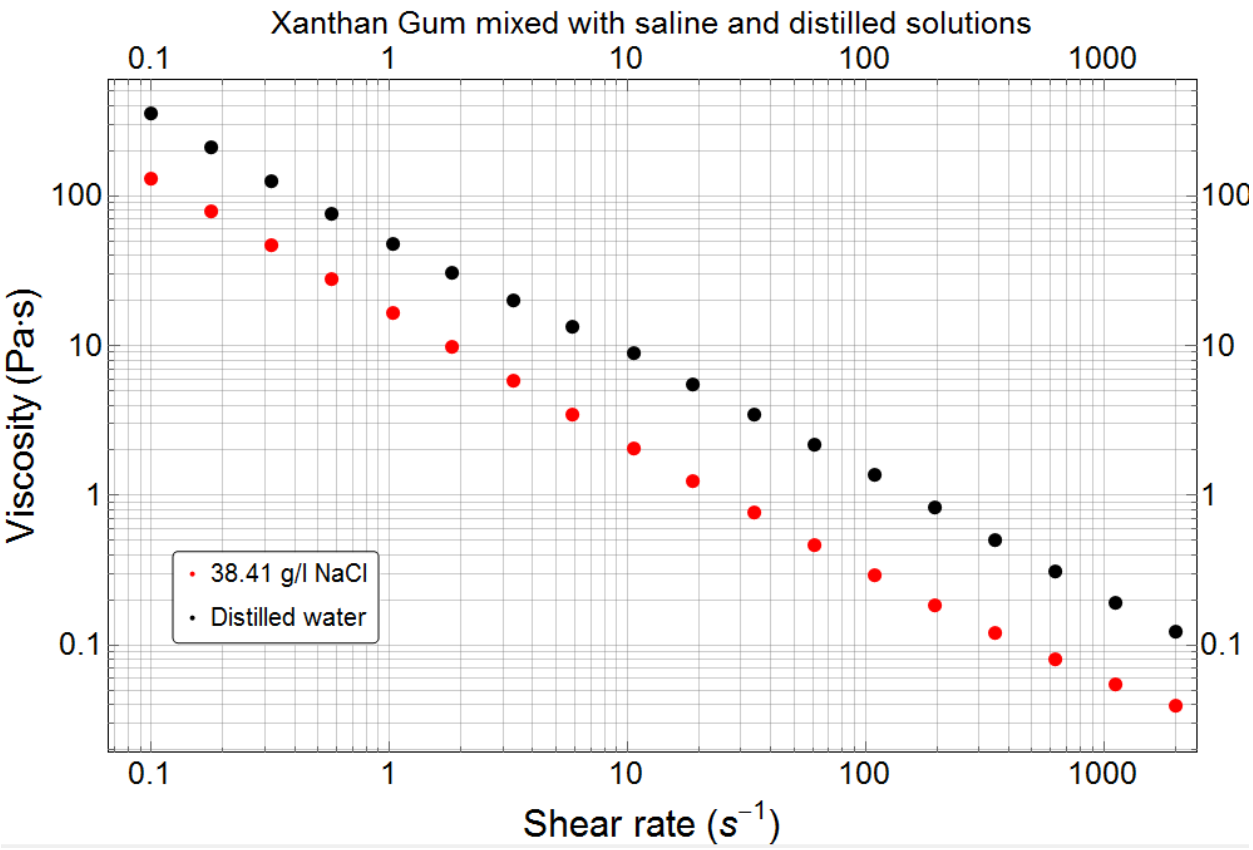

Figure 10. 32: Viscosity difference of Xanthan Gum (10 000 ppm) for saline and distilled water.

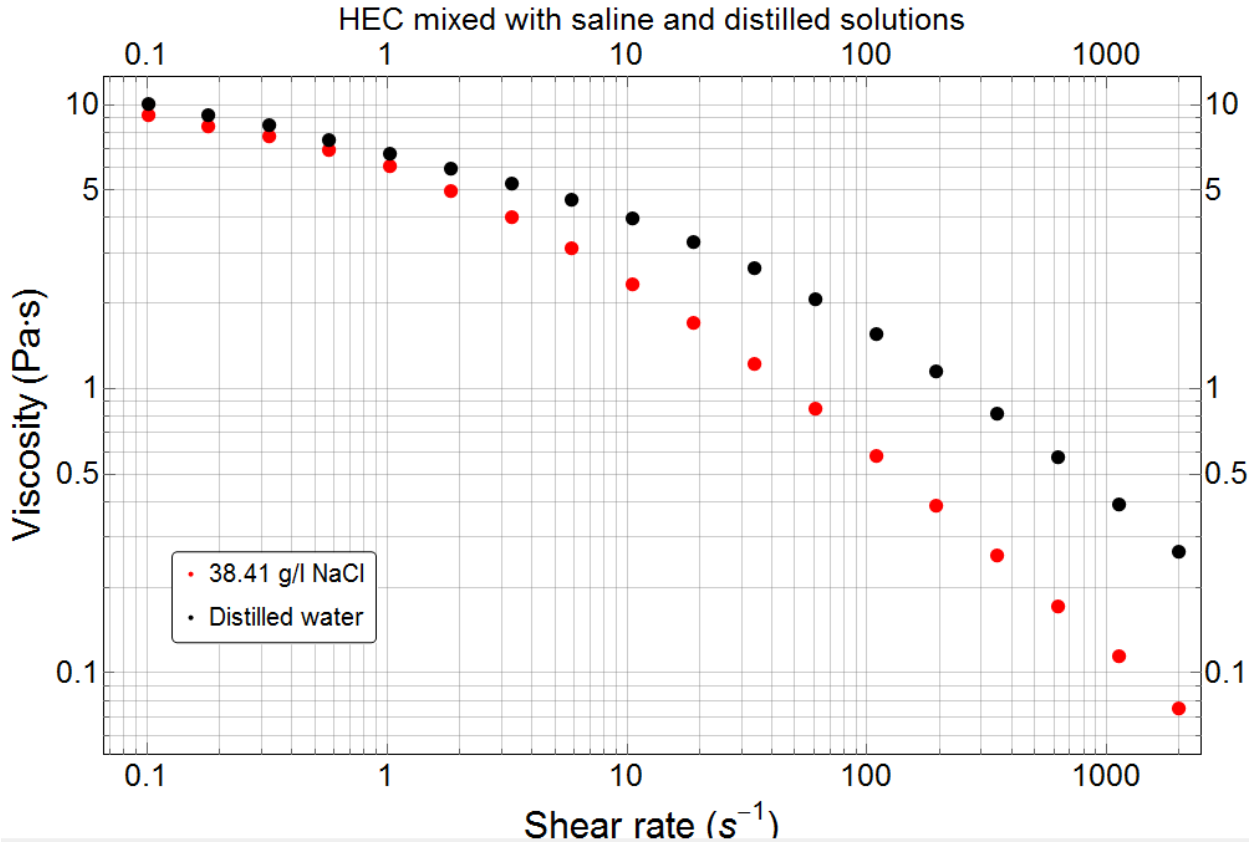

Figure 10. 33: Viscosity difference of HEC (9 000 ppm) for saline and distilled water.

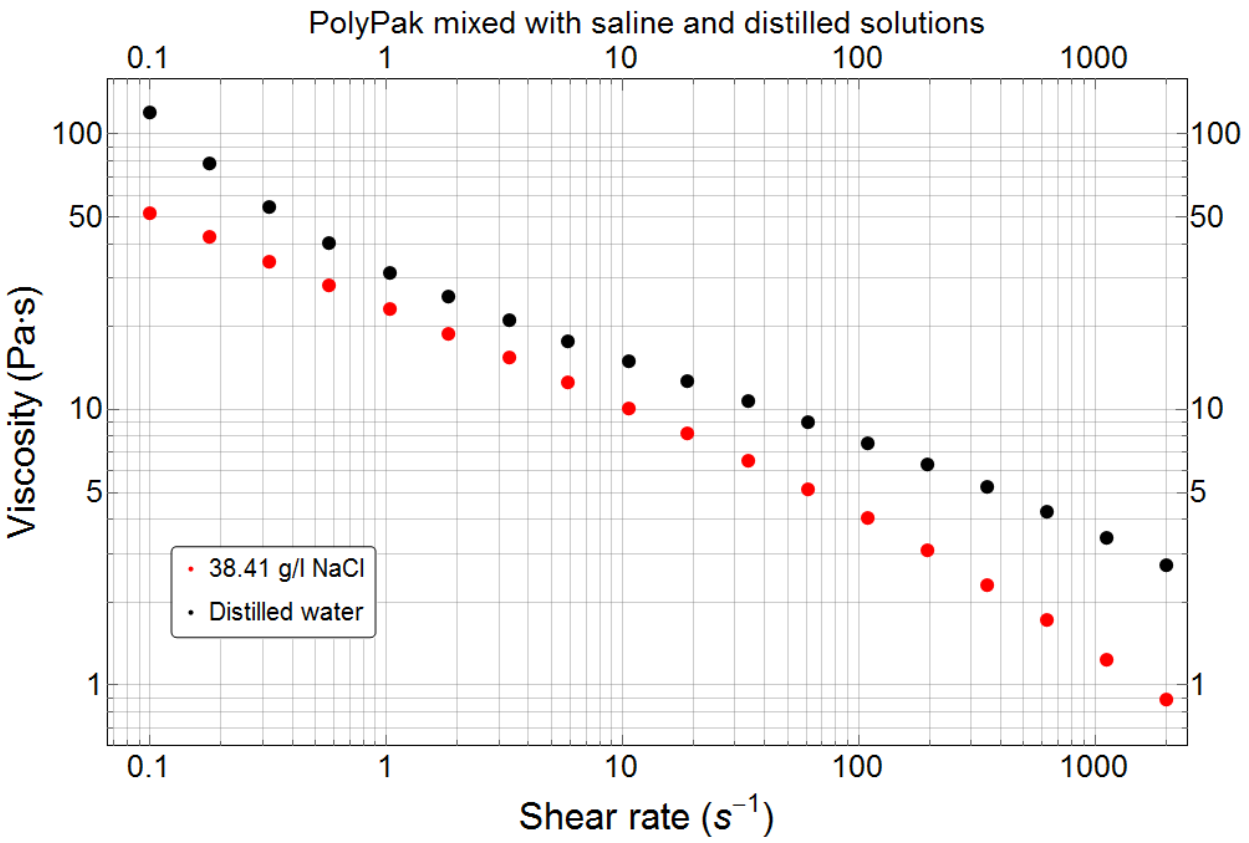

Figure 10. 34: Viscosity difference of PolyPak (100 000 ppm) for saline and distilled water.

And finally, after defining and illustrating the relations among viscosities of different polymer solutions together with the presented models, it would be reasonable to investigate the viscosity loss of every polymer in order to understand which polymers are the most stable ones and therefore resistant to shear-thinning.

Figures 10. 35 – 10. 43 visually represent dependency of viscosity loss against shear rate. Considering first the polymers with low molecular weight, it is obvious that they experience a huge viscosity loss, and the results obtained from the experimental data are compatible with those presented above (Fig.10. 26 – 10.34). The data also proves that salinity has a great effect, and the polymer solutions with higher salt concentrations undergo severe viscosity losses.

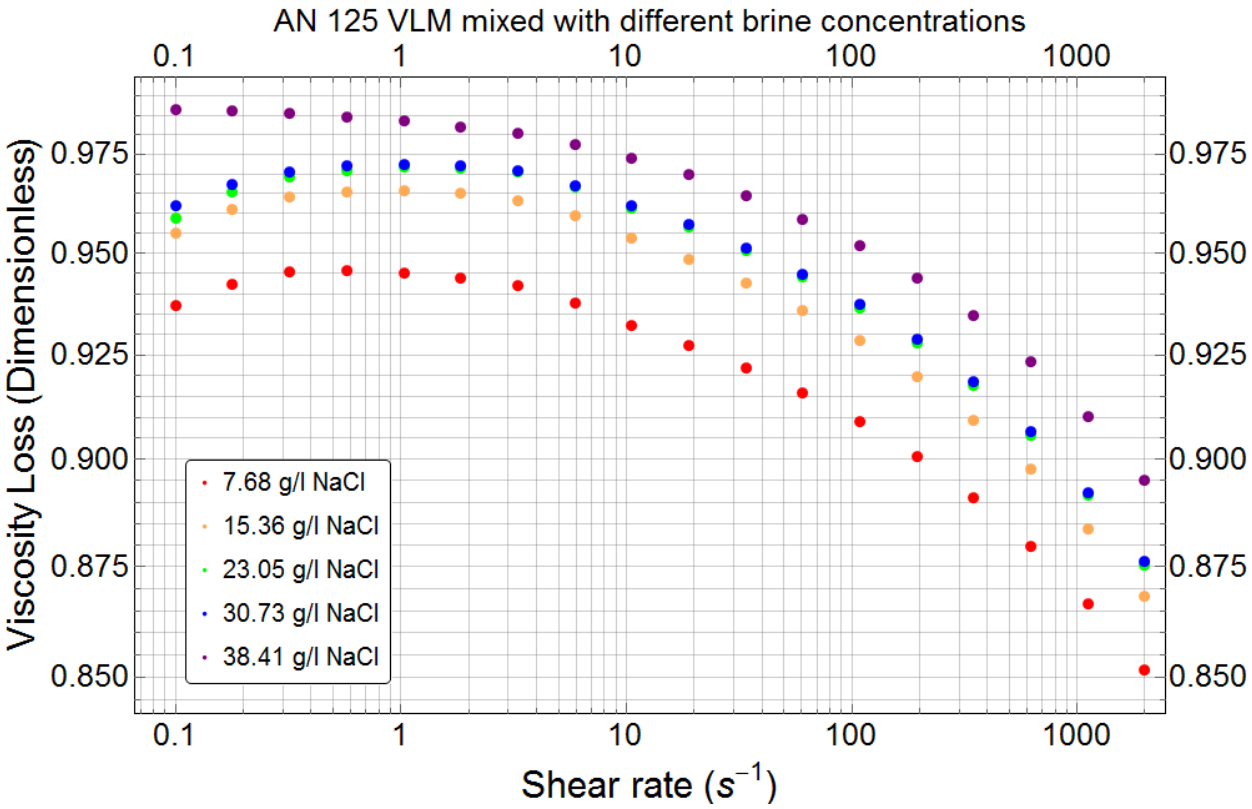

Figure 10. 35: Viscosity loss against shear rate of AN 125 VLM (10 000 ppm) for various brine concentrations.

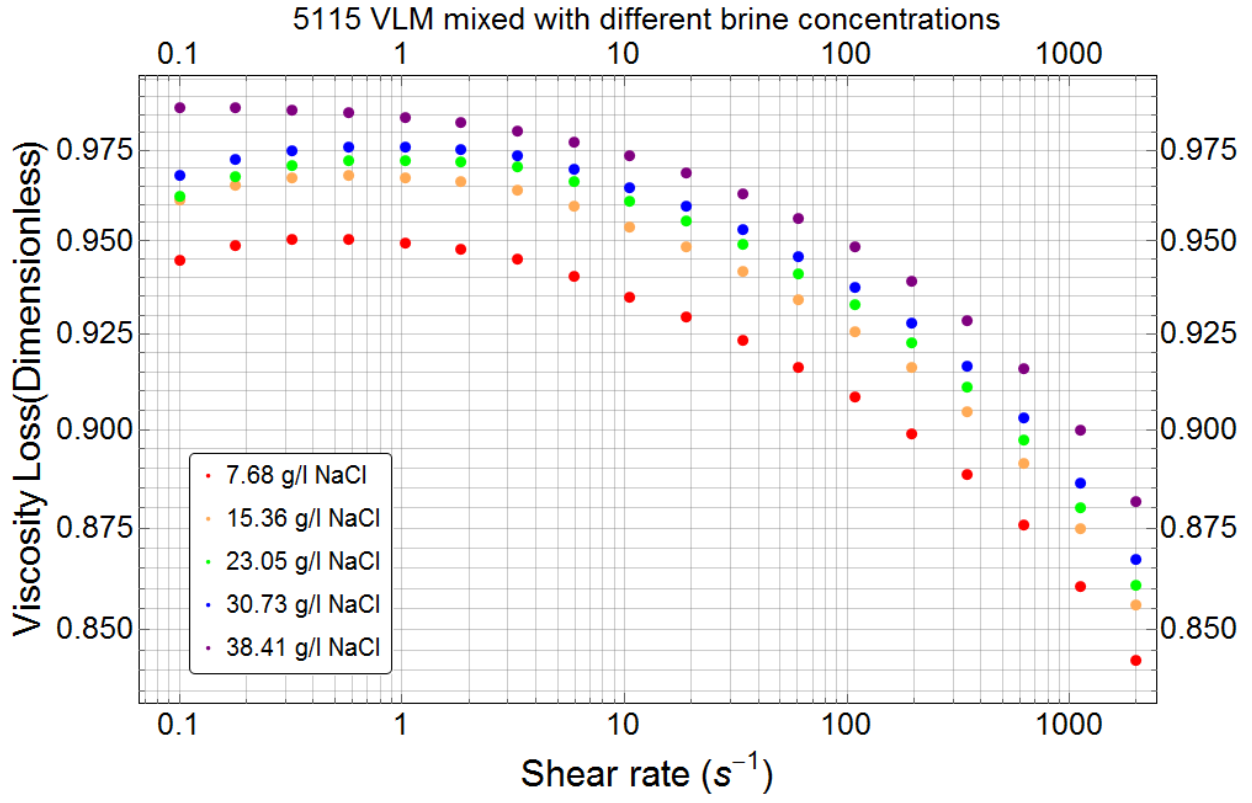

Figure 10. 36: Viscosity loss against shear rate of 5115 VLM (10 000 ppm) for various brine concentrations.

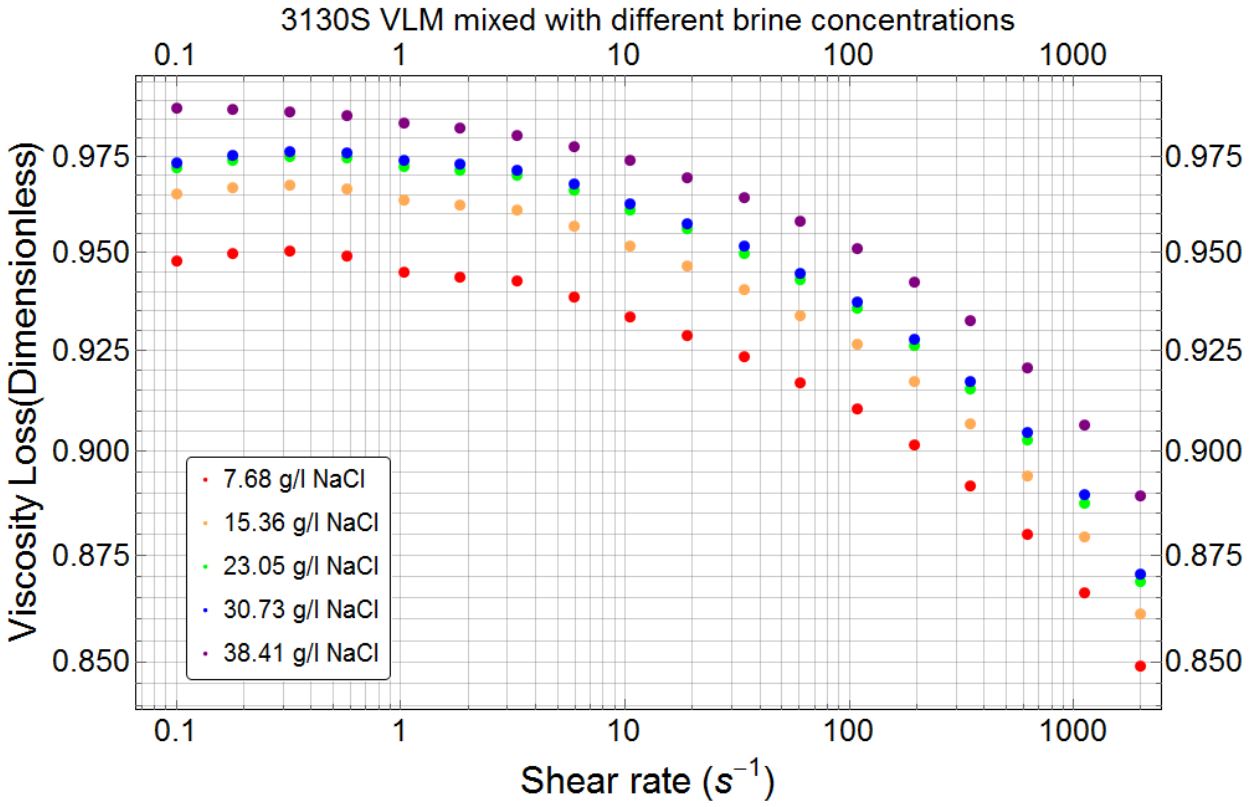

Figure 10. 37: Viscosity loss against shear rate of 3130S VLM (10 000 ppm) for various brine concentrations.

Now, taking a closer look into polymers with high molecular weights, one can notice that salinity has much less effect on viscosity loss, which was also predicted on Fig. 10.29 –Fig 10.31. Moreover, these polymers showed a much stronger resistance against viscosity loss than those of low molecular weight, which simply means that the former ones are more resistant to shear-thinning effect that the later ones (see Fig. 10. 38 – Fig. 10. 40).

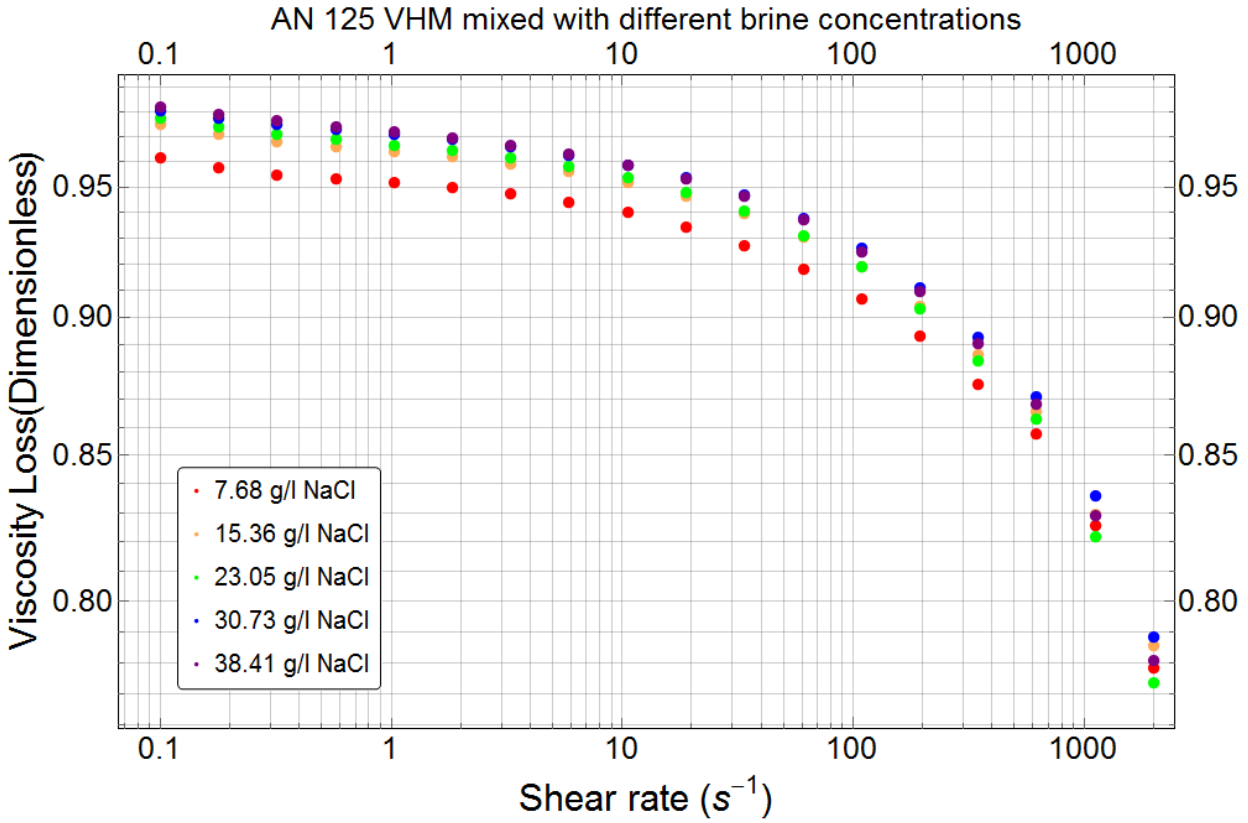

Figure 10. 38: Viscosity loss against shear rate of AN 125 VHM for various brine concentrations.

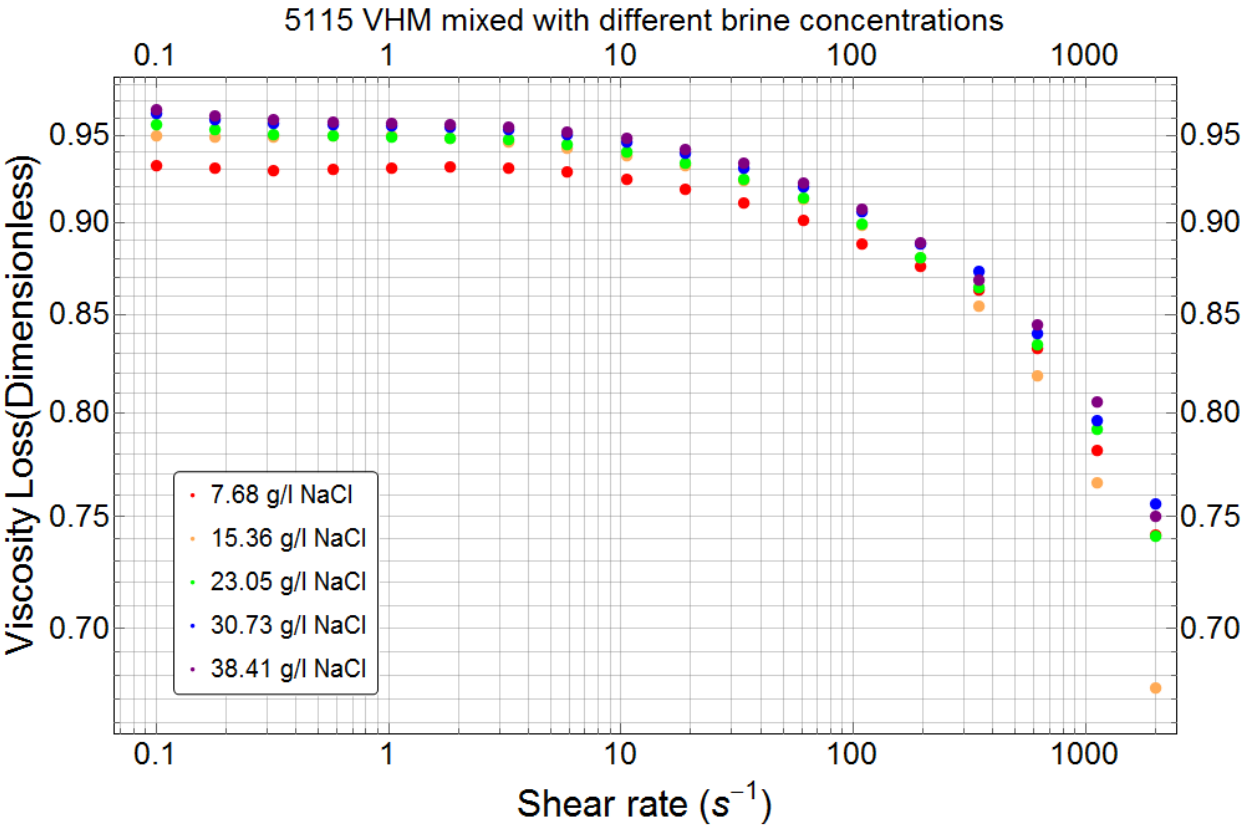

Figure 10. 39: Viscosity loss against shear rate of 5115 VHM for various brine concentrations.

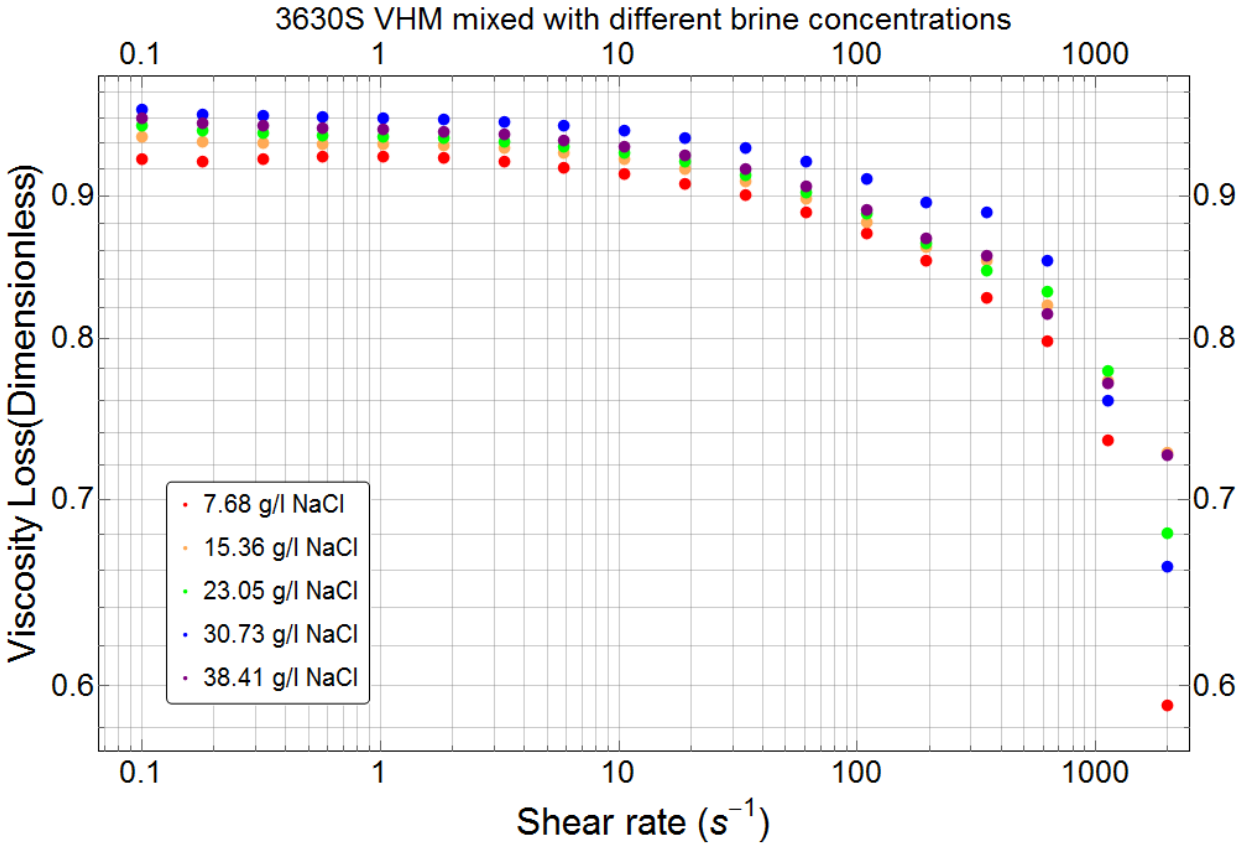

Figure 10. 40: Viscosity loss against shear rate of 3630S VHM for various brine concentrations.

What it comes to Xanthan Gum, HEC and PolyPak the final trends were unpredictable and contradicts the measurement conducted before. The most possible explanation for that may be that the polymers are the most salt tolerant ones, which makes the viscosity loss deviate from the general trend. This phenomenon is yet to be examined, as the polymers are widely used in industrial purposes.

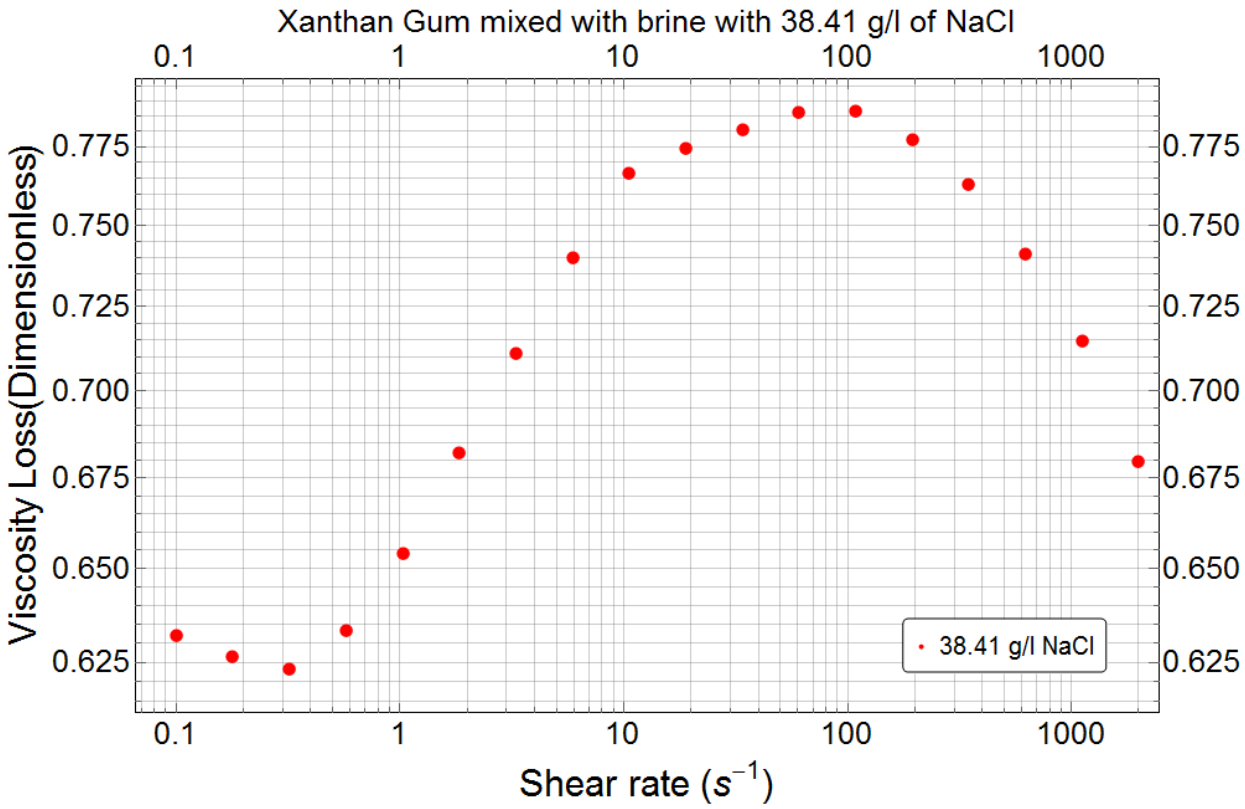

Figure 10. 41: Viscosity loss against shear rate of Xanthan Gum mixed with brine with 38.41 g/l of NaCl.

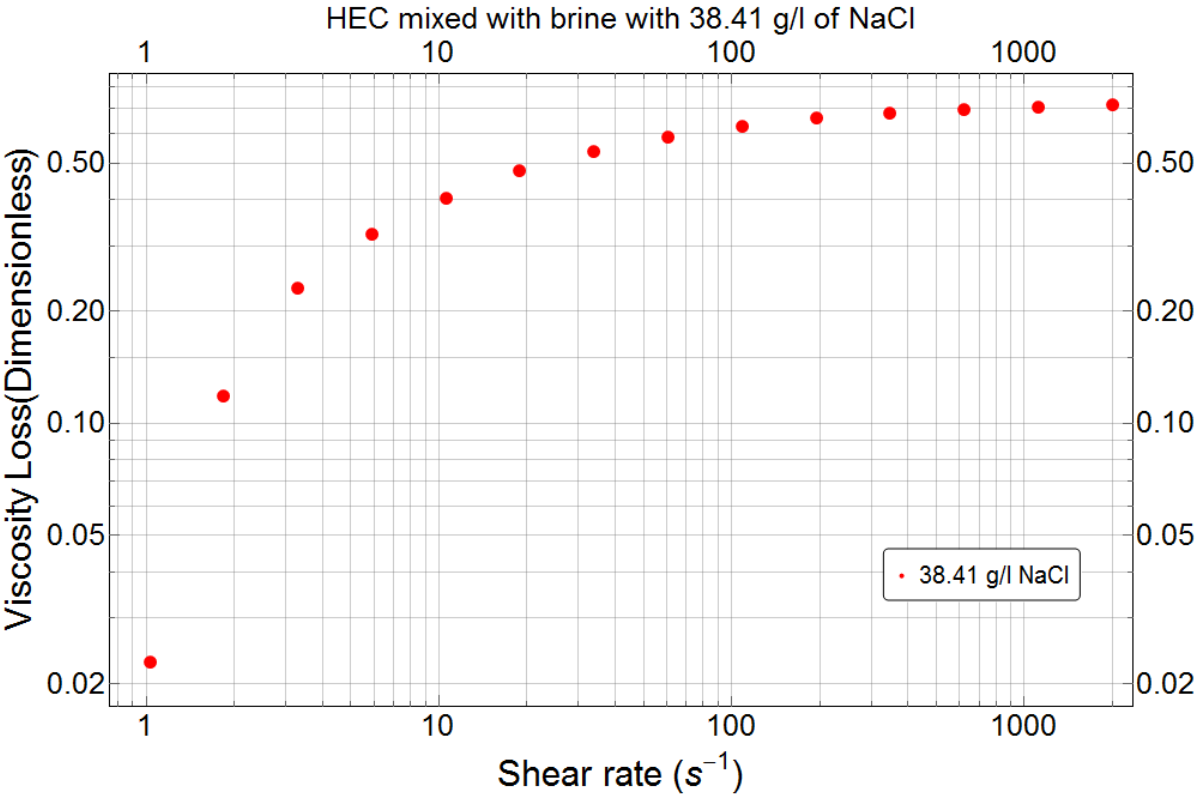

Figure 10. 42: Viscosity loss against shear rate of HEC mixed with brine with 38.41 g/l of NaCl.

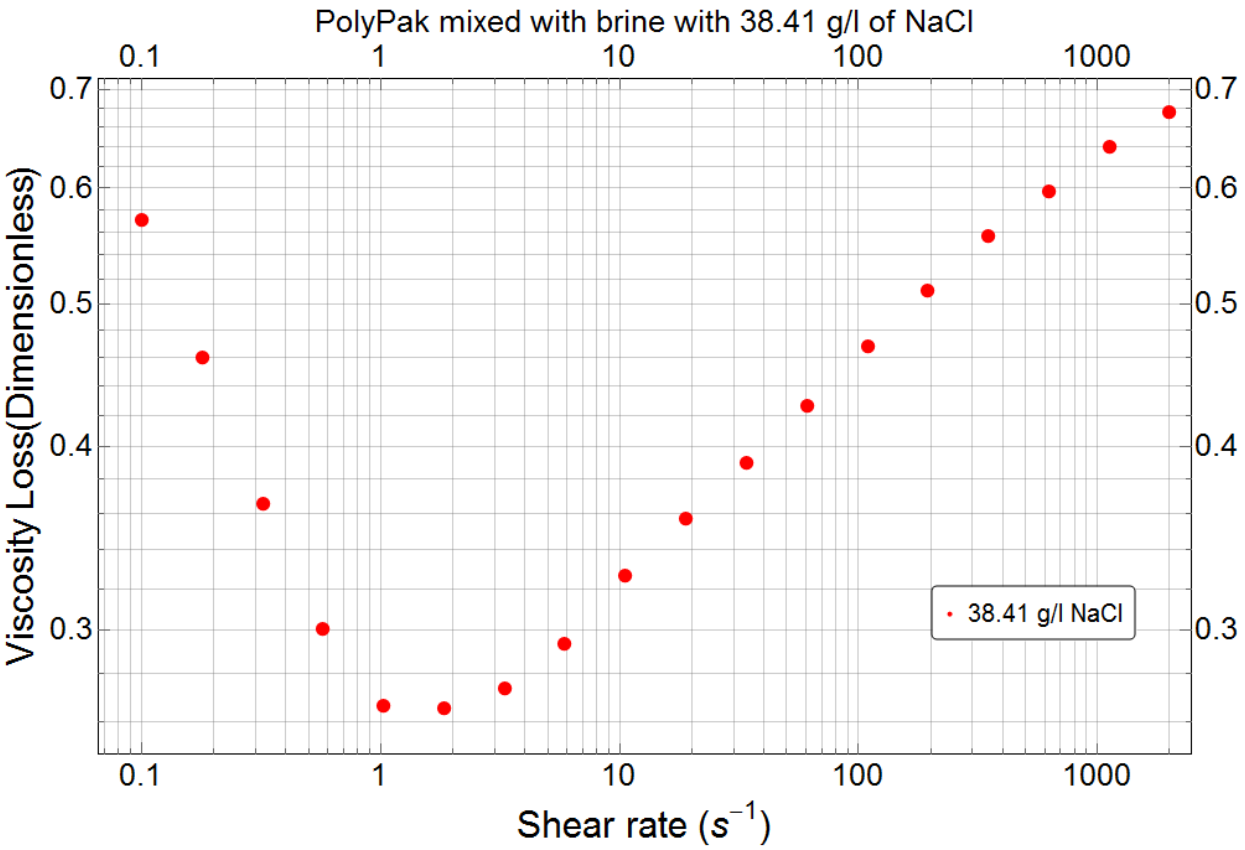

Figure 10. 43: Viscosity loss against shear rate of PolyPak mixed with brine with 38.41 g/l of NaCl.

11. Conclusion

General observations:

Summing up the results, it would be reasonable to pick the polymers tested into three group. The representatives of the same group generally showed very similar trends. Let us assume the first group consisting of polymers with low molecular weight (i.e. AN 125 VLM, 5115 VLM and 3130S VLM), the second consisting of those with high molecular weight (i.e. AN 125 VHM, 5115 VHM and 3630S VHM) and the third one with the remaining polymers (i.e. Xanthan Gum, HEC and PolyPak).

From the research that has been carried out it is possible to conclude that generally, all the tested polymers are sensitive to salt, however some of them exhibit a very strong sensitivity even in the solutions with small amount of salt, while the others are relatively stable with high salinity concentrations.

What it comes to non-Newtonian fluid models, there was just one polymer, namely Xanthan Gum that followed the Elongational Phan-Thien & Tanner model, while the best fitted model for all the rest polymers was FENE-P model.

The findings of the research are quite convincing, and eventually the following conclusions can be drawn:

1) **Viscosity vs shear rates:**
   - Regardless the assumed polymer group on high shear rates the viscosity was decreasing drastically;
   - Basically polymers from the first group had the greater decrease in viscosity than that of the second and third group;
2) **Viscosity vs salinity**
   - Salinity has a great impact on the viscometric functions of the first group of polymers, which cannot be ignored while performing polymers in industry. In the solutions with even small amount of salt these group of polymers shows a huge decrease in viscosity. So while performing this type of polymers in the EOR techniques even with small amount of salt, it would be reasonable first to perform a preflush i.e. preconditioning the reservoir;

- High molecular weight polymers also illustrated a big impact of salinity on the viscometric functions, but the results did not account for the abnormal values as they did in case of VLM polymers;
- Despite experiencing a small drop in viscosity as well, the third group of polymers showed the strongest resistance to salinity among all the polymers tested in the work. These polymers would show the best performance in high saline reservoir i.e. the ones located in Middle East.

3) Models prediction

- As was stated before the best fitted model that was predicted for almost all the polymers is FENE-P dumbbell model, which clearly shows the behaviour as well as the rheological properties of a given polymer;
- Xanthan Gum was the only polymer which had the best follow of Elongational Phan-Thien & Tanner model.

Some interesting points to be mentioned:

- HEC polymer had almost the same viscosity in the solutions with distilled water and brine with 38.41 g/l of NaCl for small shear rate values, which simply means that in practical situations with small shear rates HEC would show the best performance;
- The findings of viscosity loss for Xanthan Gum, HEC and PolyPak were quite unexpected and suggest deviatoric viscosity drop, which contradicts the results obtained before.

12. References

1. Littmann, W., *Polymer flooding*. Developments in petroleum science. Vol. 24. 1988, Amsterdam: Elsevier.
2. Wever, D.A.Z., Picchioni, F., & Broekhuis, A. A., *Polymers for enhanced oil recovery: A paradigm for structure–property relationship in aqueous solution.* Progress in Polymer Science, 2011. **36**: p. 1558-1628.
3. Lake, L.W., *Enhanced Oil Recovery*. 1989, Englewood Cliffs, N.J: Prentice Hall Inc.
4. Khisamov R.S., G.A.A., Gazizov A.Sh., *Enhanced oil recovery technologies*. 2005, Moscow: OJSC "VNIIOENG".
5. Bird, R.B. and O. Hassager, *Dynamics of Polymeric Liquids: Fluid mechanics*. 2nd ed. Vol. 1. 1987, USA & Canada: John Wiler & Sons, Inc.
6. Mezger, T.G., *The Rheology Handbook*. 4th ed. 2014, Hannover: Vincentz Network.
7. Barnes, H.A., *Handbook of elementary rheology*. 2000, Wales: University of Wales,Institute of Non-Newtonian Fluid Mechanics.
8. Schramm, G., *A Practical Approach to Rheology and Rheometry*. 2nd ed. 1994, Karlsruhe, Federal Republic of Germany: Gebrueder Haake.
9. R.C., H., *Mechanics of Materials*. 10th ed. 2016, New Jersey USA: Pearson Education.
10. Paar, A. *Basics of viscometry*. 2018 [cited 2018 15th of May]; Available from: https://wiki.anton-paar.com/en/basic-of-viscometry/.
11. Viswanath, D.S., *Viscosity of Liquids*. 1st ed. 2006: Springer.
12. Wikipedia. *International System of Units*. 14th of May, 2018 [cited 2018 20th May]; Available from: en.wikipedia.org/wiki/International_System_of_Units.
13. Pfitzner, J., *Poiseuille and his law*. 1976, Anaesthesia. p. 273-275.
14. Kulicke, W.M., *Fließverhalten von Stoffen und Stoffgemischen*. 1986, Basel: Hüthig & Wepf.
15. M. Pahl, W.G., H.-M. Laun, *Praktische Rheologie der Kunststoffe und Elastomere*. 1995, Düsseldorf: VDI.
16. W.M. Kulicke, C.C., *Viscosimetry of polymers and electrolytes*. 2004, Berlin: Springer.
17. Kulicke, W.-M. and C. Clasen, *Viscosimetry of polymers and polyelectrolytes*. 2013: Springer Science & Business Media.
18. A.Z. Abidin, T.P., W.A.Nugroho, *Polymers for Enhanced Oil Recovery Technology.* Procedia Chemistry, 2012. **4**: p. 11-16.
19. Qisheng Ma. Patrick J. Shuler, C.W.A., Yongchun Tang, *Theoretical studies of hydrolysis and stability of polyacrylamide polymers.* Polymer Degradation and Stability, 2015. **121**: p. 69-77.
20. Floerger, S., *Enhancing Polymer Flooding Performance*. 2012, Altavia St Etienne: Andrézieux, France.
21. Dominique Langevin, M.C., *Challenges and New Approaches in EOR.* OGST, 2013. **67**(6): p. 883-1039.
22. de Melo, M. and E. Lucas, *Characterization and selection of polymers for future research on enhanced oil recovery.* Chemistry & chemical technology, 2008. **2**(4).
23. Katarzyna Leja, G.L., *Polymer Biodegradation and Biodegradable Polymers – a Review* Polish Journal of Environmental Studies, 2010. **19**(2): p. 255-266.
24. Premraj R., M.D., *Biodegradation of polymers.* Indian Journal of Biotechnology, 2005. **4**: p. 186-193.
25. Paar, A. *Flow curve and yield point determination with rotational viscometry*. 2018 [cited 2018 18th of May]; Available from: https://wiki.anton-paar.com/en/flow-curve-and-yield-point-determination-with-rotational-viscometry.
26. Vinayak Kulkarni, N.S., *Principle of Fluid Dynamics*. 2014, National Programme on Technology Enhanced Learning (NPTEL): India, Assam.
27. J.D. Anderson, J., *Governing Equations of Fluid Dynamics*, in *Computational fluid dynamics*, J.F. Wendt, Editor. 2009, Springer-Verlag Berlin Heidelberg. p. 15-51.

28. Phan-Thien, N., *Understanding viscoelasticity: basics of rheology*. 2002, Berlin; New York: Springer.
29. Petrowiki. *Second law of thermodynamics*. 2015 16.07.2015 [cited 2018 25.05]; Available from: http://petrowiki.org/Second_law_of_thermodynamics.
30. Kirby, B., *Micro- and nanoscale fluid mechanics*. 2010, USA, New York: Cambridge University Press.
31. A.Tim Osswald, N., *Polymer rheology : fundamentals and applications*. 2015, Munich: Hanser Publications.
32. K. Yasuda, R.C.A., R. E. Cohen, *Shear flow properties of concentrated solutions of linear and star branched polystyrenes.* Rheologica Acta, 1981. **20**(2): p. 163-178.
33. D. Shogin, P.A.A., A. Hiorth, M.V. Madland, *Physical Modeling of Rheological Properties of Polymer Solutions for Enhanced Oil Recovery*. 2017, The National IOR Centre of Norway: Norway, Stavanger.
34. D. Shogin, P.A.A., A. Hiorth, M.V. Madland, *Modeling the Rheology of Two-phase Polymer Flow*. 2017, The National IOR Centre of Norway: Norway, Stavanger.
35. Van Heel, A., M. Hulsen, and B. Van den Brule, *On the selection of parameters in the FENE-P model.* Journal of non-newtonian fluid mechanics, 1998. **75**(2-3): p. 253-271.
36. Harold R. Warner, J., *Kinetic theory and rheology of dilute suspensions of finitely extendible dumbbells.* Industrial & Engineering Chemistry Fundamentals, 1972. **11**(3): p. 379-387.
37. Vincenzi, D., et al., *Stretching of Polymers in Isotropic Turbulence: A Statistical Closure.* Physical Review Letters, 2007. **98**(2): p. 024503.
38. Purnode, B. and M.J. Crochet, *Polymer solution characterization with the FENE-P model.* Journal of Non-Newtonian Fluid Mechanics, 1998. **77**(1): p. 1-20.
39. Center, F.-F.M.R.; Available from: https://www.fmf.uni-freiburg.de/service/dienstleistungen/details/rms_800/view?set_language=en.
40. Thien, N.P. and R.I. Tanner, *A new constitutive equation derived from network theory.* Journal of Non-Newtonian Fluid Mechanics, 1977. **2**(4): p. 353-365.
41. Phan-Thien, N., *A nonlinear network viscoelastic model.* Journal of Rheology, 1978. **22**(3): p. 259-283.
42. Griffith, A., *Phan-Thien-Tanner Modeling of a Viscoelastic Fluid in the Stick-Slip Scenario*. 2007, Department of Chemical Engineering, University of Washington.
43. Macosko, C.W., *Rheology: principles, measurements, and applications*. 1st ed. Advances in Interfacial Engineering. 1994, New York: Wiley-VCH.
44. Dealy, J.M., *Rheometers for Molten Plastics*. 1982, New York: Van Nostrand Reinhold Company.
45. Sorbie, K.S., *Polymer-improved oil recovery*. 2013: Springer Science & Business Media.
46. Algharaib, M., A. Alajmi, and R. Gharbi, *Investigation of Polymer Flood Performance in High Salinity Oil Reservoirs*, in *SPE/DGS Saudi Arabia Section Technical Symposium and Exhibition*. 2011, Society of Petroleum Engineers: Al-Khobar, Saudi Arabia.
47. Rashidi, M., A.M. Blokhus, and A. Skauge, *Viscosity study of salt tolerant polymers.* Journal of applied polymer science, 2010. **117**(3): p. 1551-1557.
48. Ait-Kadi, A., P. Carreau, and G. Chauveteau, *Rheological properties of partially hydrolyzed polyacrylamide solutions.* Journal of Rheology, 1987. **31**(7): p. 537-561.
49. Lewandowska, K., *Comparative studies of rheological properties of polyacrylamide and partially hydrolyzed polyacrylamide solutions.* Applied Polymer Science, 2007. **103**: p. 2235.
50. Dealy, J.M. and T.K.P. Vu, *The Weissenberg effect in molten polymers.* Journal of Non-Newtonian Fluid Mechanics, 1977. **3**(2): p. 127-140.

Appendix

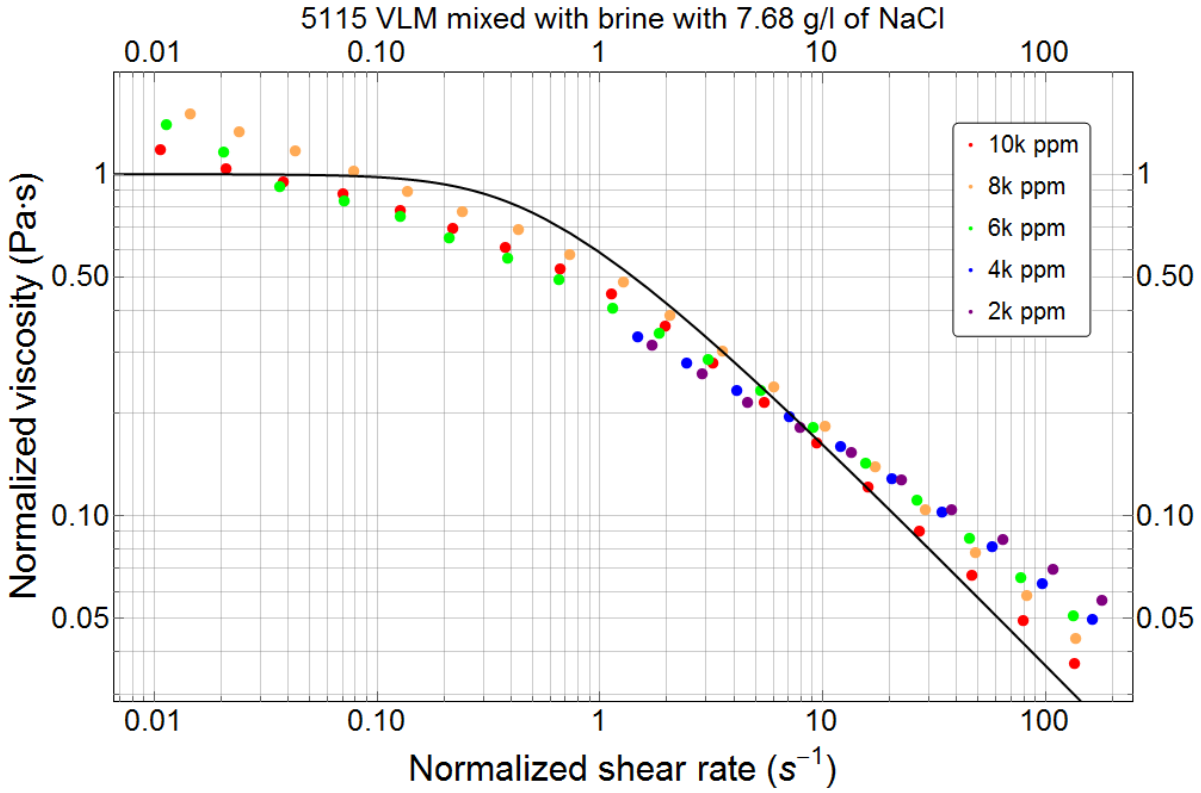

Figure A. 1: Normalized viscosity vs normalized shear rate for 5115 VLM mixed with Brine.

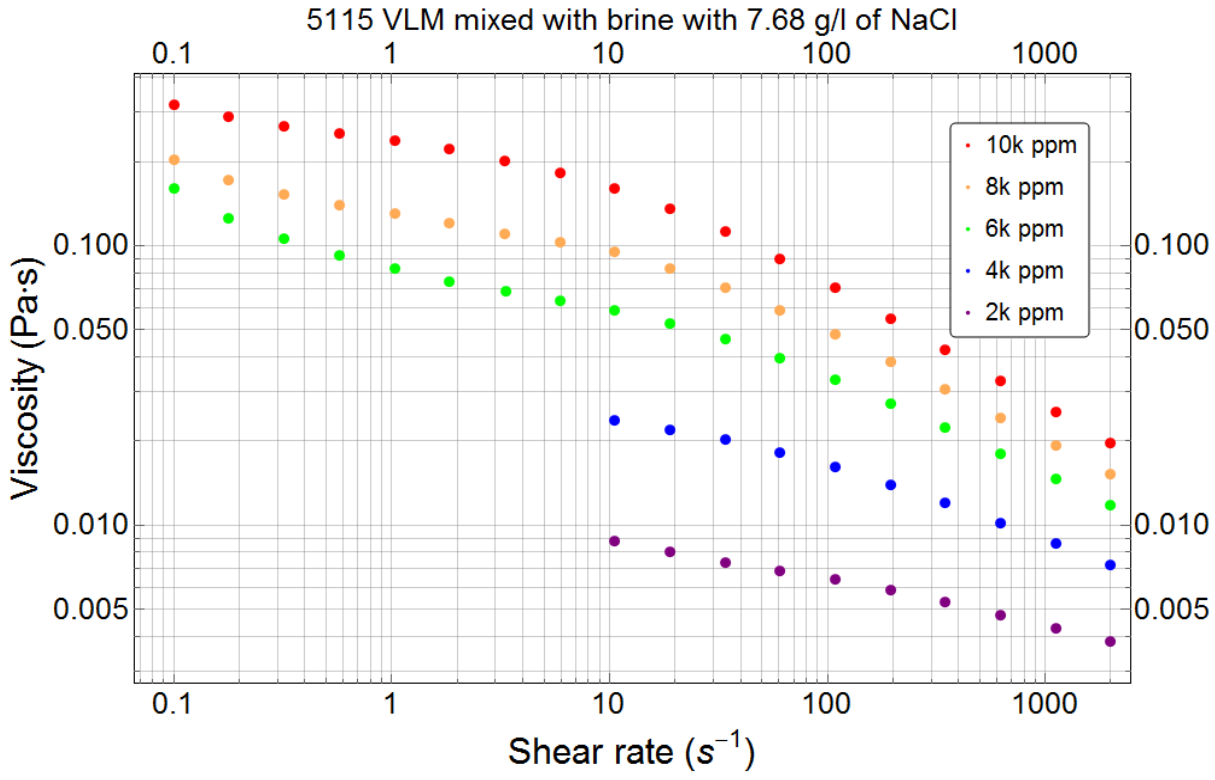

Figure A. 2: Viscosity vs shear rate for 5115 VLM mixed with Brine with 7.68 g/l of NaCl.

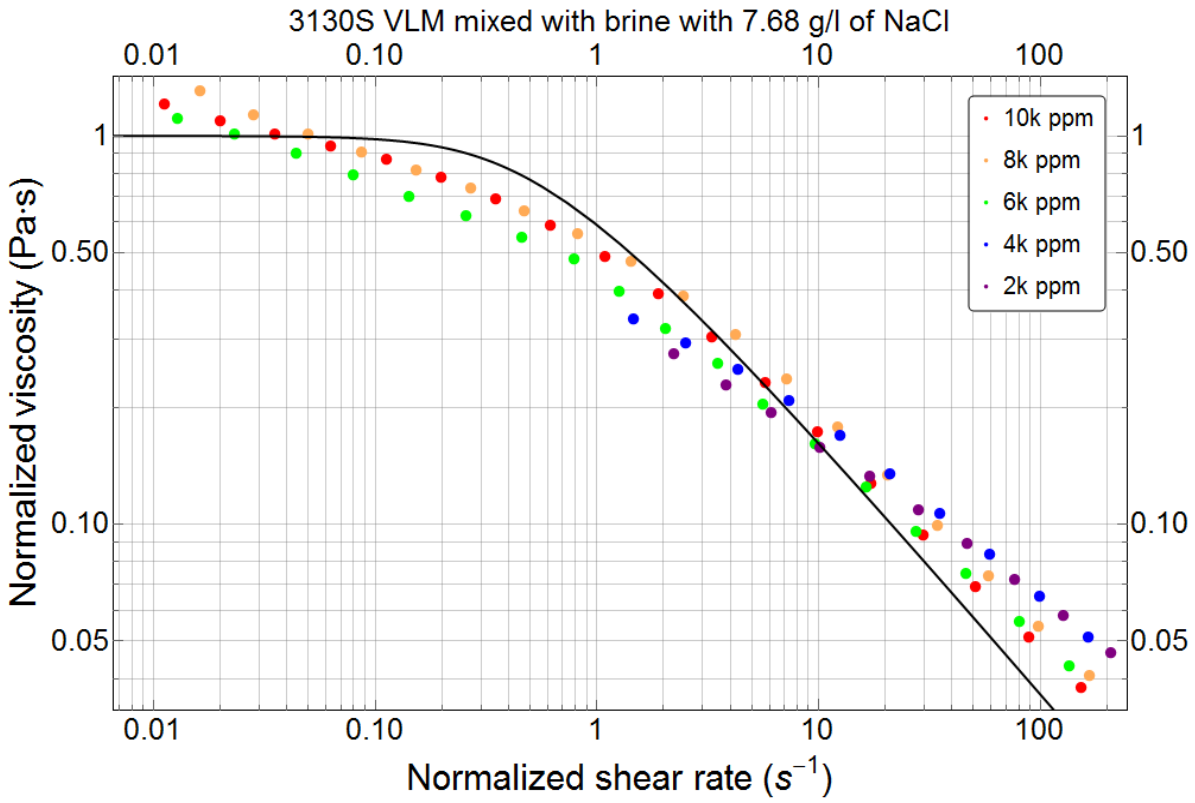

Figure A. 3: Normalized viscosity vs normalized shear rate for 3130S VLM mixed with Brine with 7.68 g/l of NaCl.

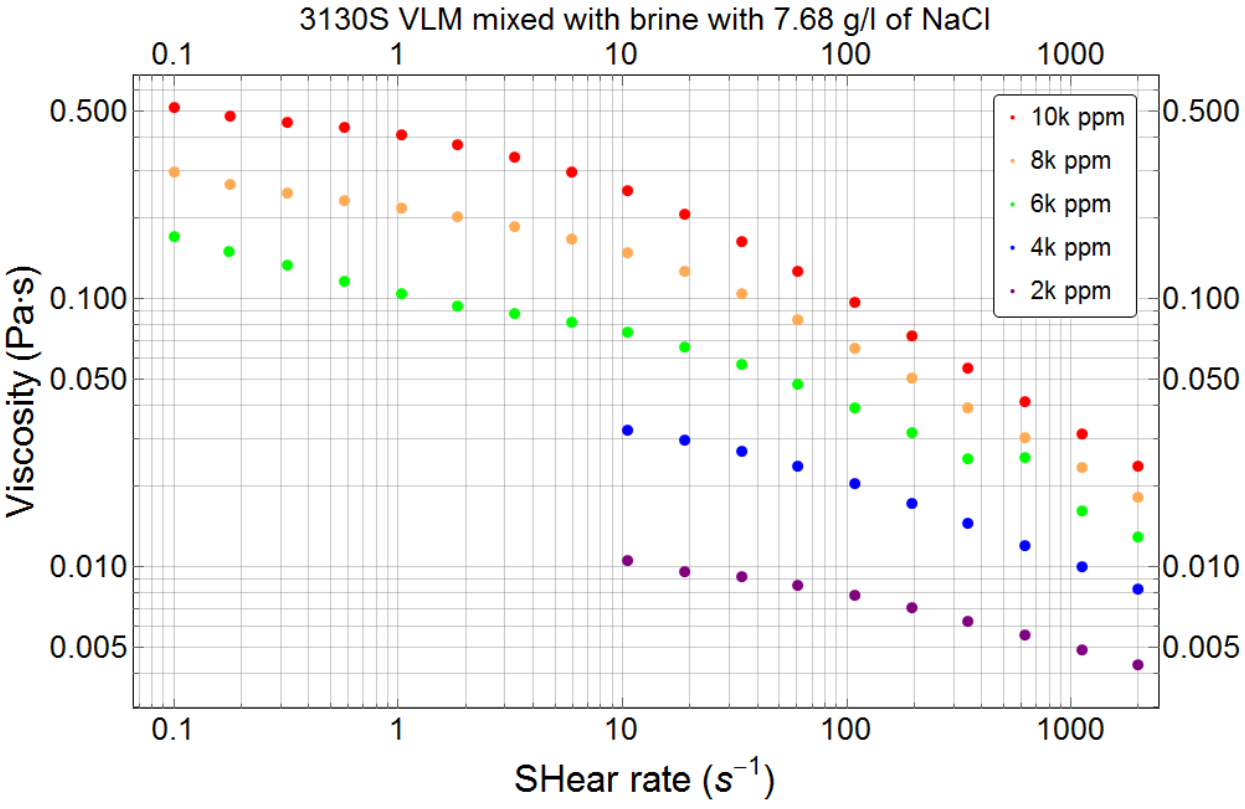

Figure A. 4: Viscosity vs shear rate for 3130S VLM mixed with Brine with 7.68 g/l of NaCl.

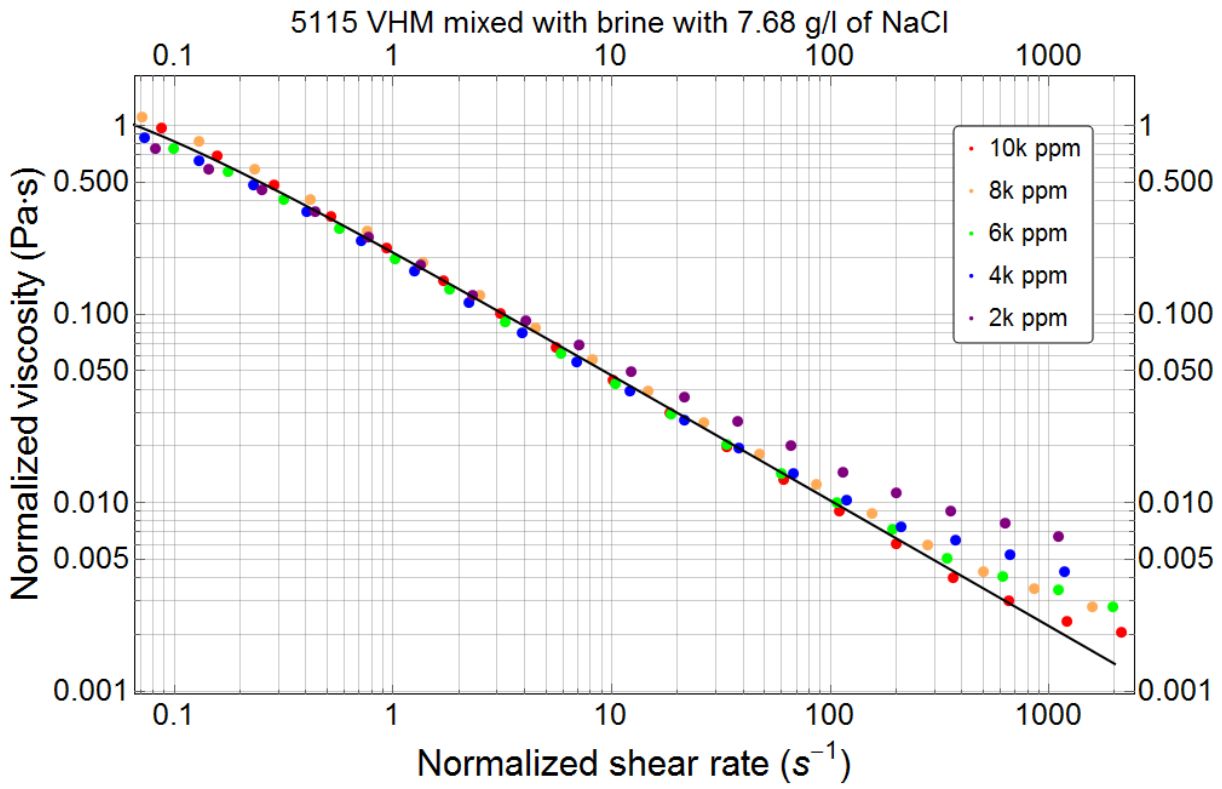

Figure A. 5: Normalized viscosity vs normalized shear rate for 5115 VHM mixed with Brine with 7.68 g/l of NaCl.

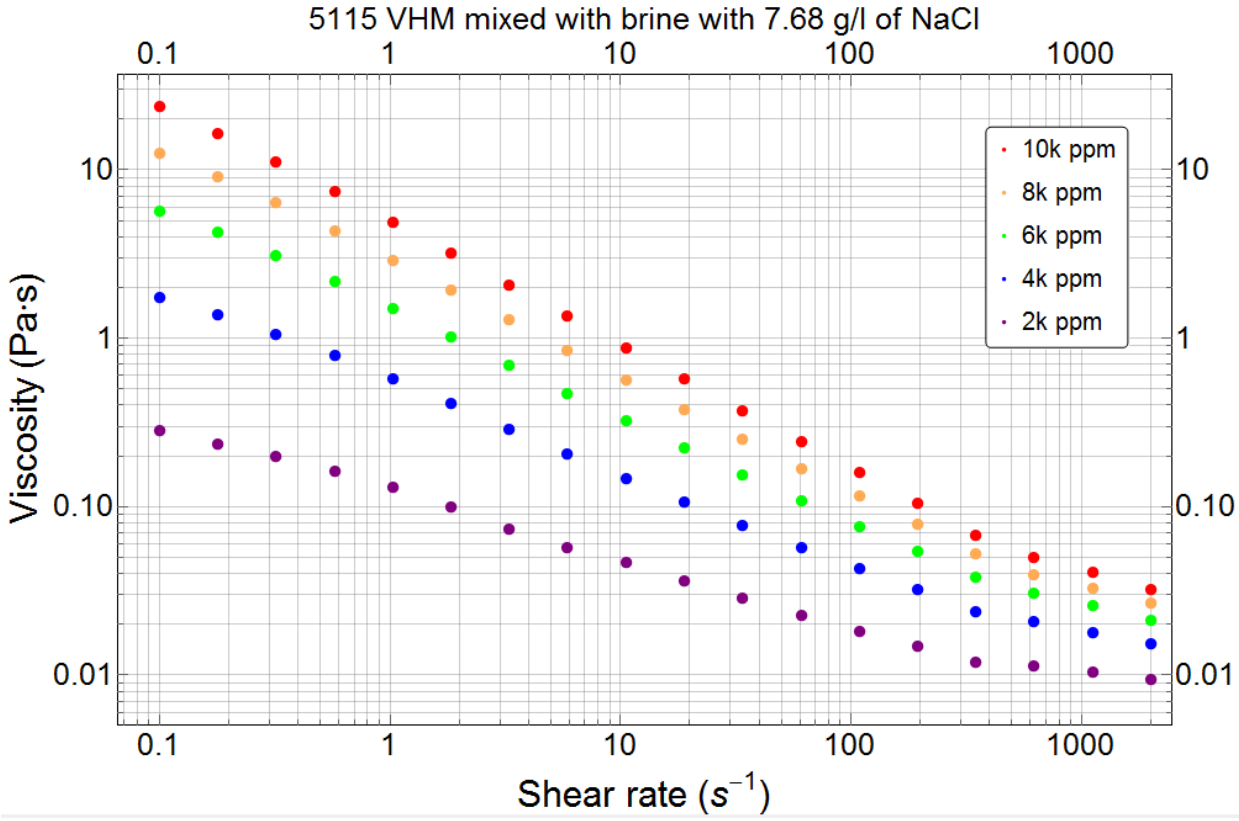

Figure A. 6: Viscosity vs shear rate for 5115 VHM mixed with Brine with 7.68 g/l of NaCl.

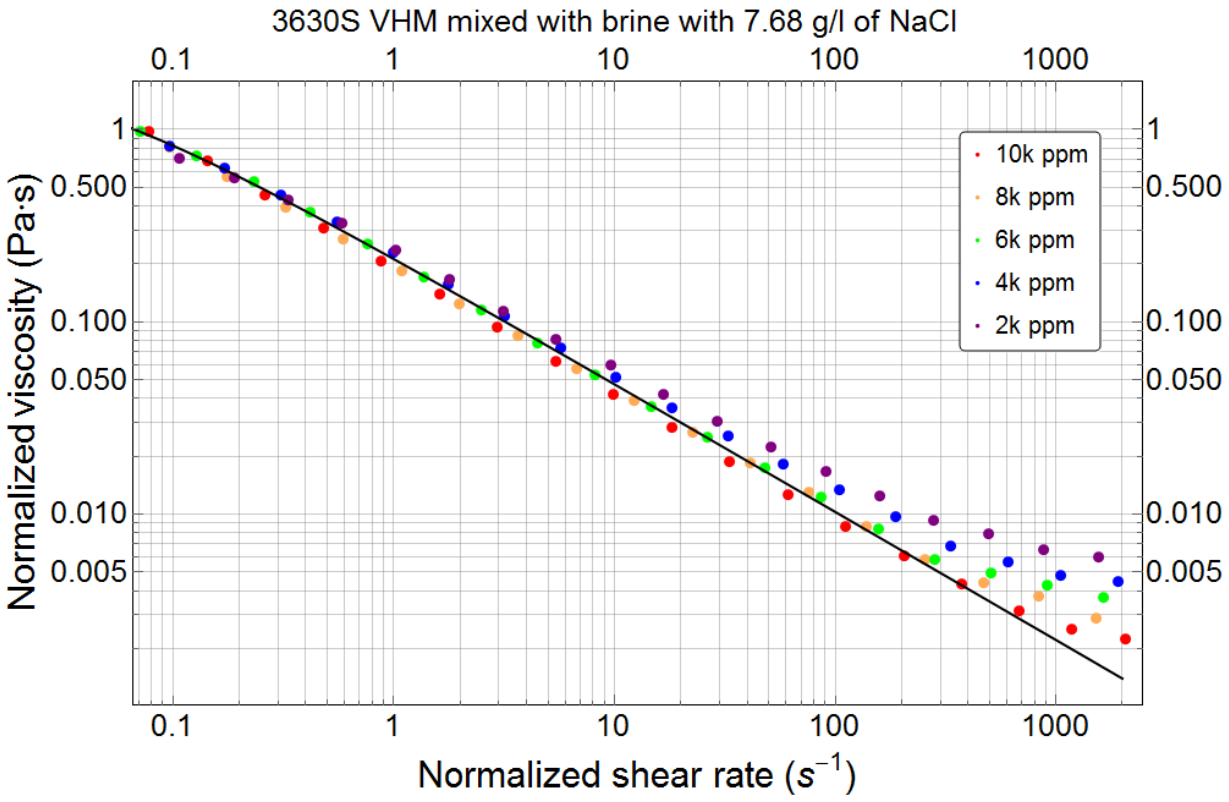

Figure A. 7: : Normalized viscosity vs normalized shear rate for 3630S VHM mixed with Brine with 7.68 g/l of NaCl.

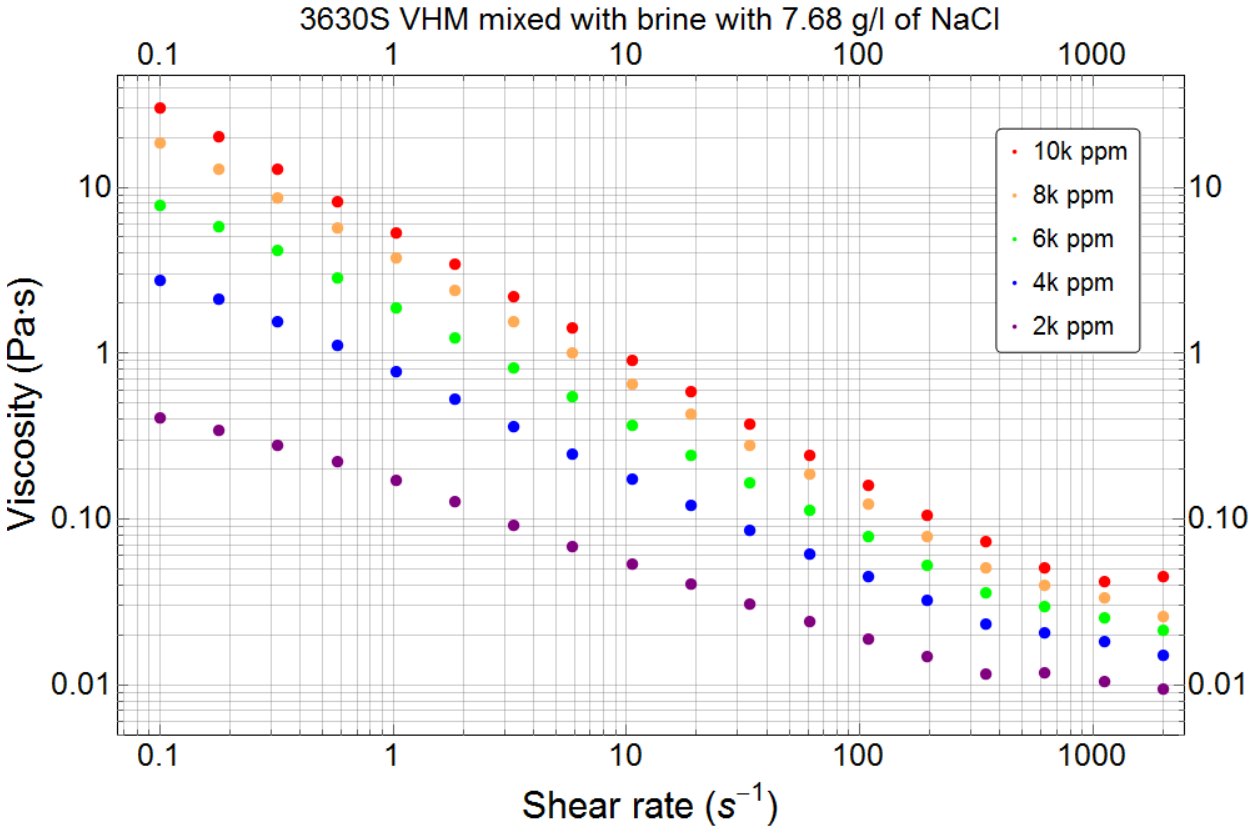

Figure A. 8: Viscosity vs shear rate for 3630S VHM mixed with Brine with 7.68 g/l of NaCl.

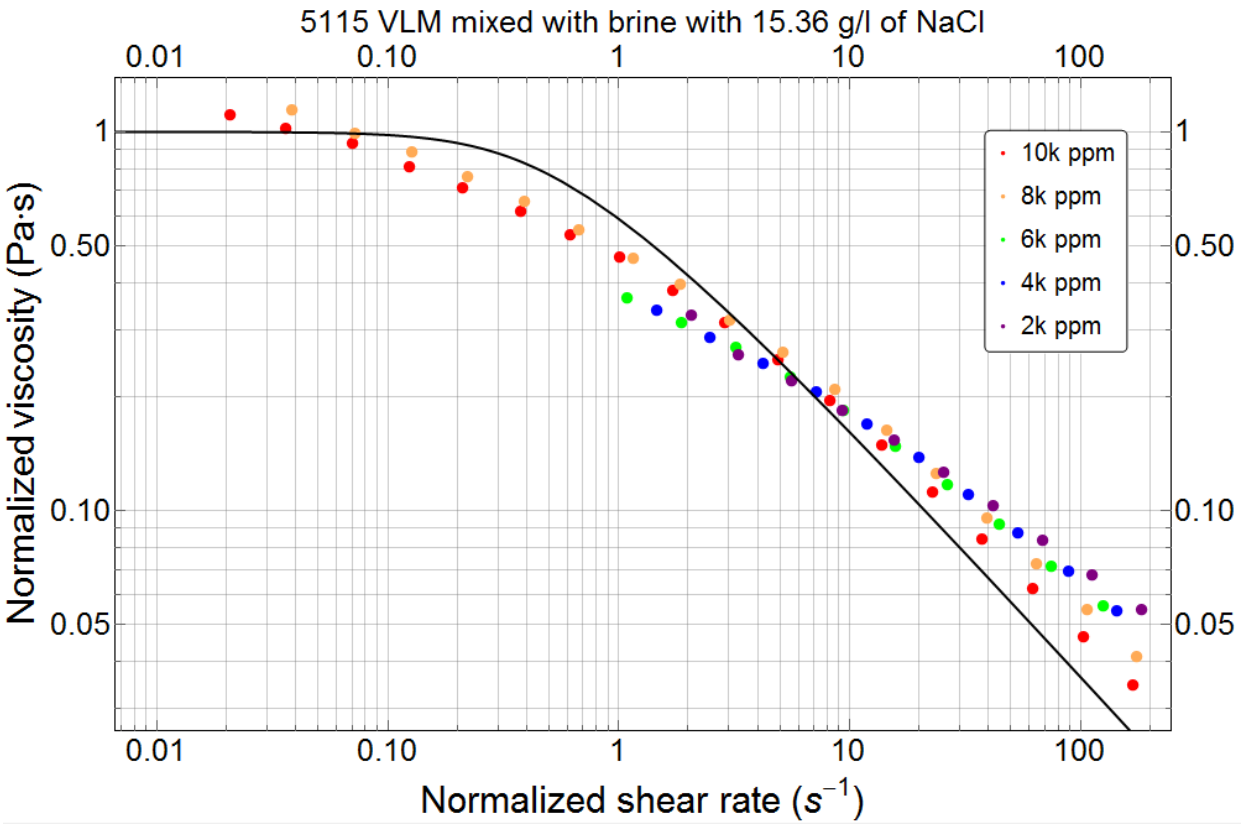

Figure A. 9: Normalized viscosity vs normalized shear rate for 5115 VLM mixed with Brine with 15.36 g/l of NaCl.

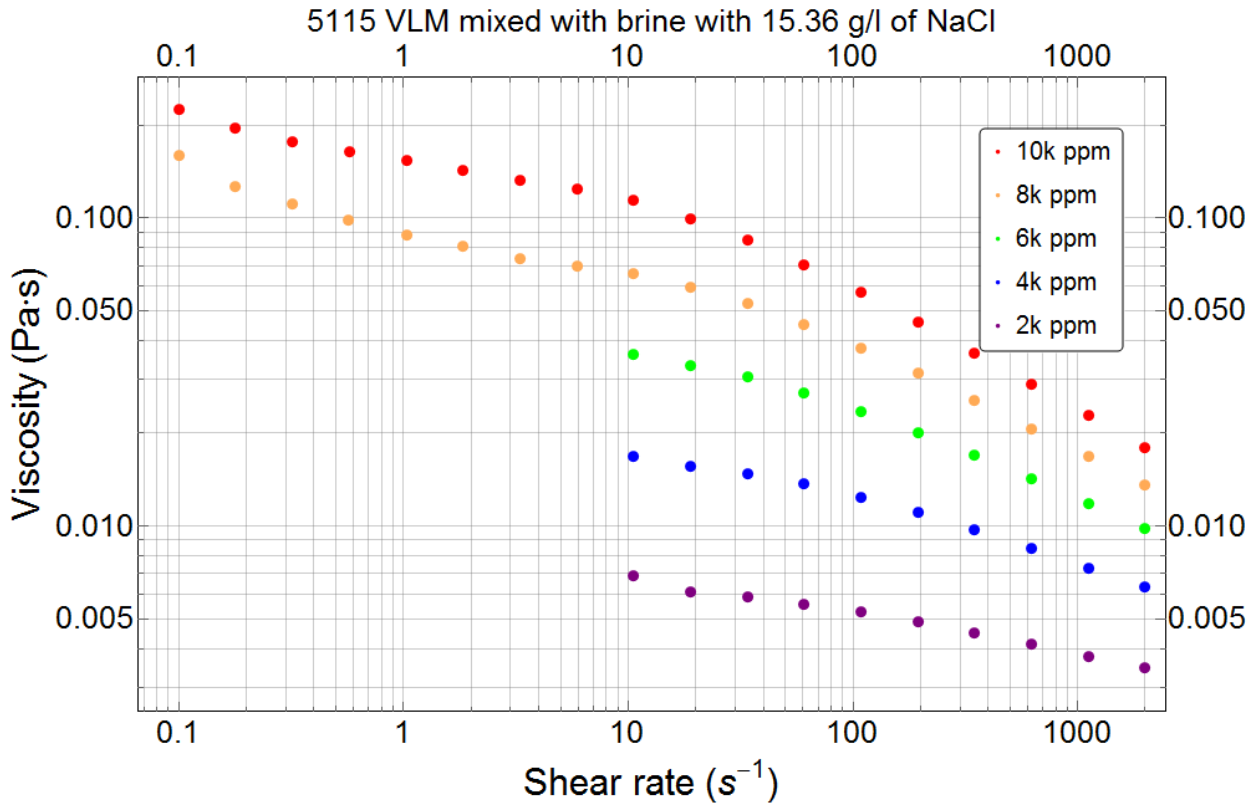

Figure A. 10: Viscosity vs shear rate for 5115 VLM mixed with Brine with 15.36 g/l of NaCl.

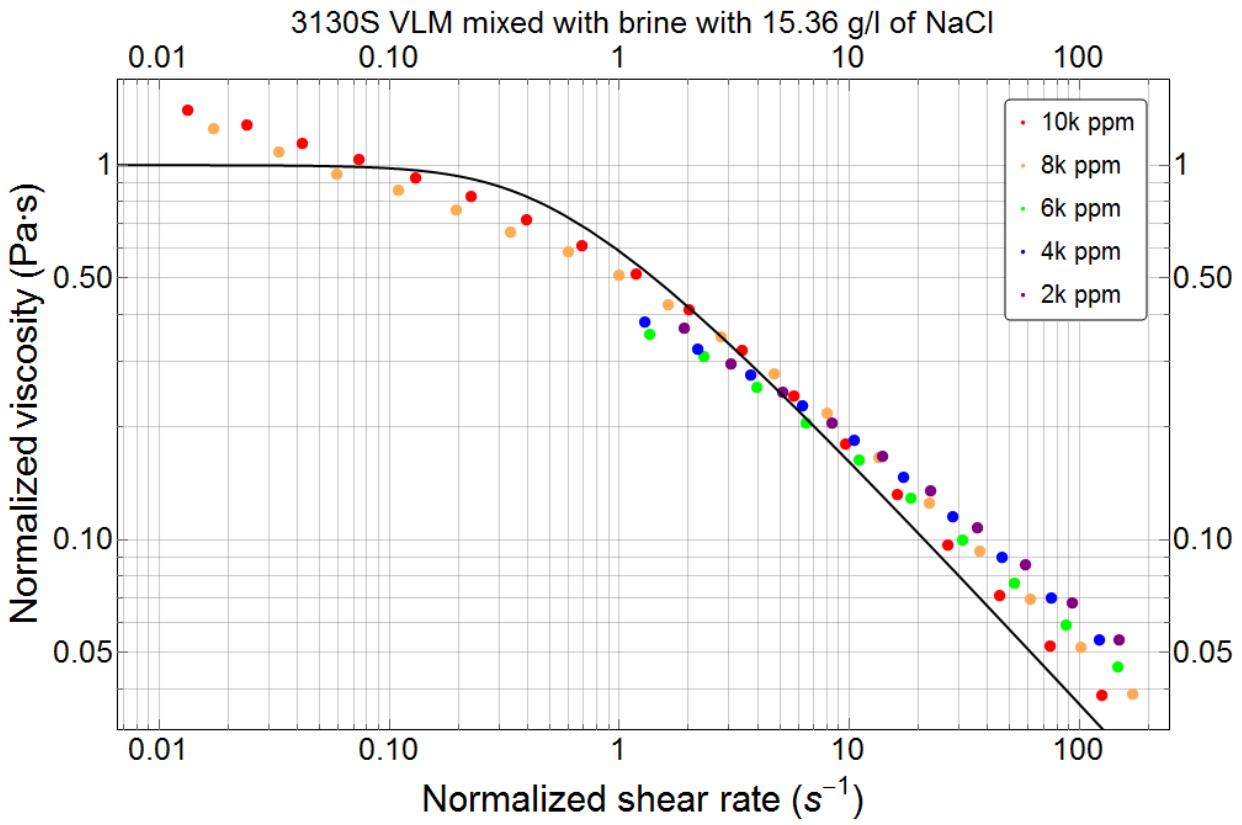

Figure A. 11: Normalized viscosity vs normalized shear rate for 3130S VLM mixed with Brine with 15.36 g/l of NaCl.

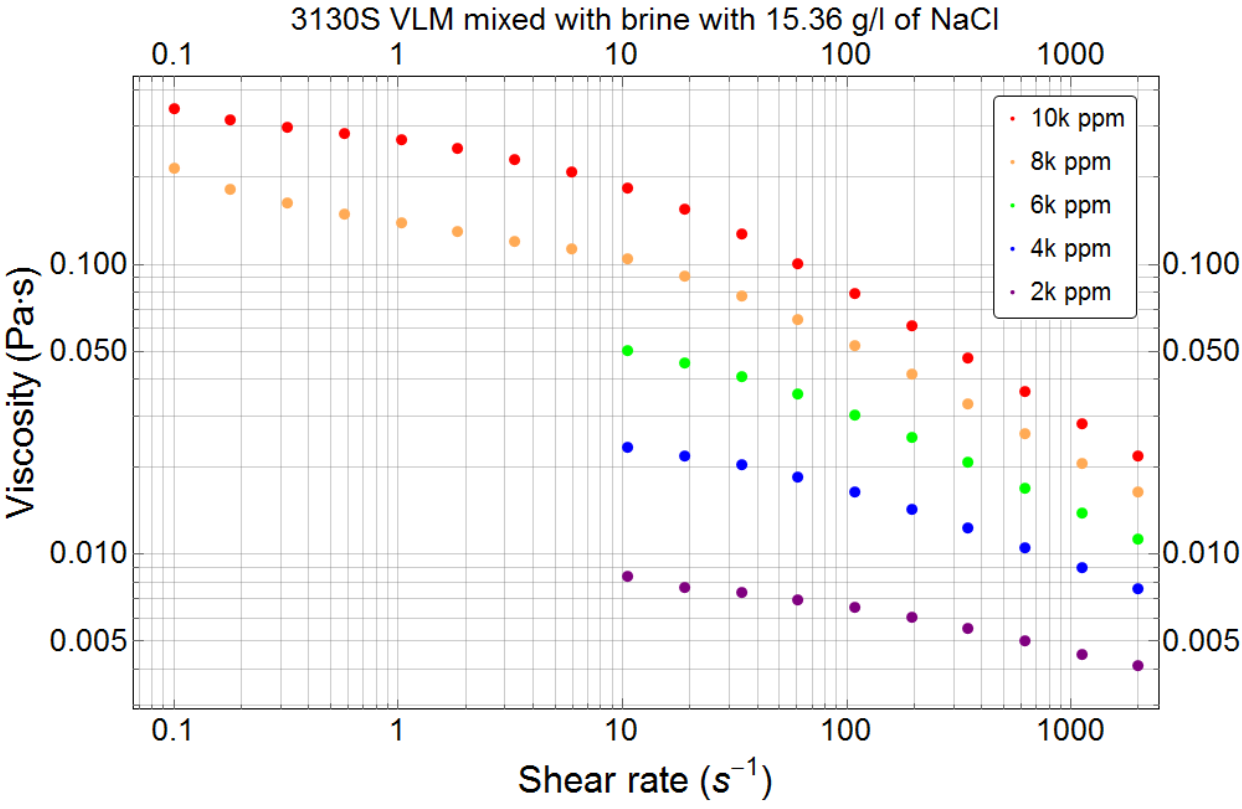

Figure A. 12: Viscosity vs shear rate for 3130S VLM mixed with Brine with 15.36 g/l of NaCl.

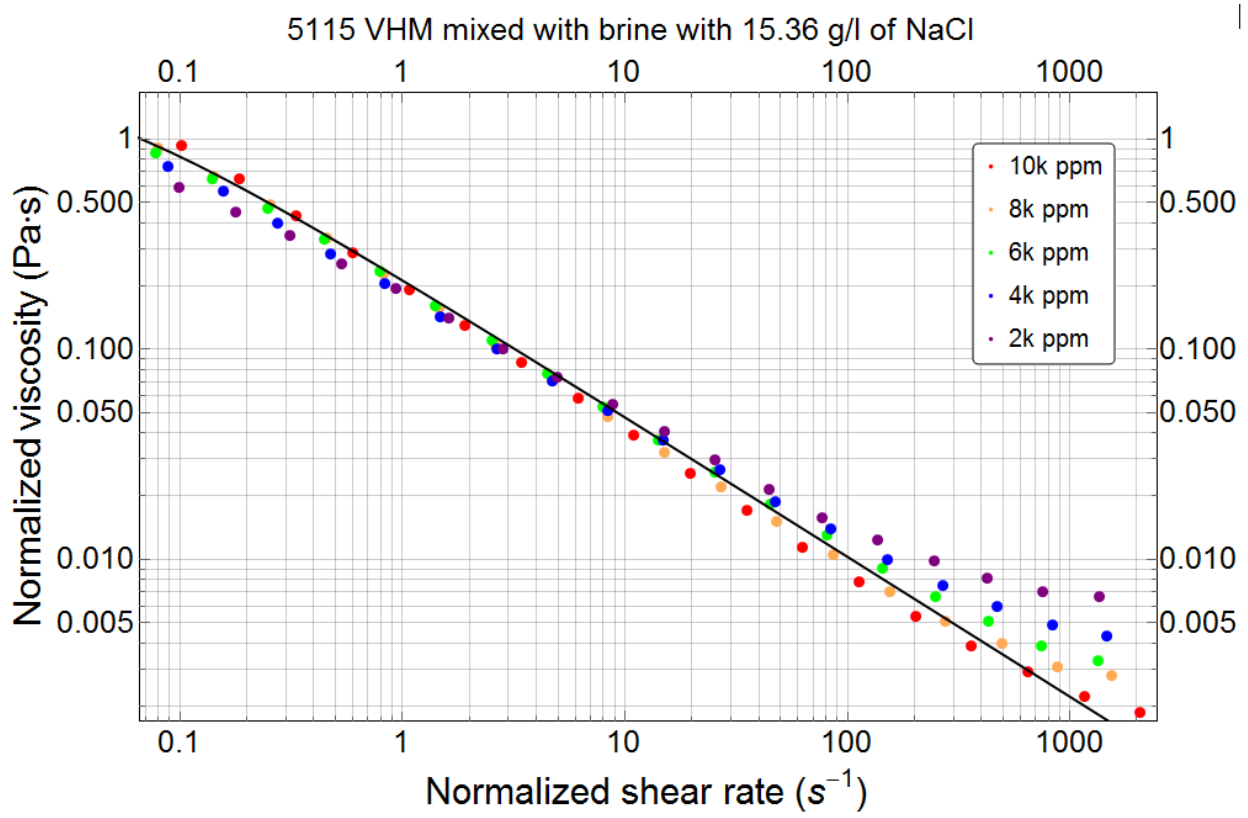

Figure A. 13: Normalized viscosity vs normalized shear rate for 5115 VHM mixed with Brine with 15.36 g/l of NaCl.

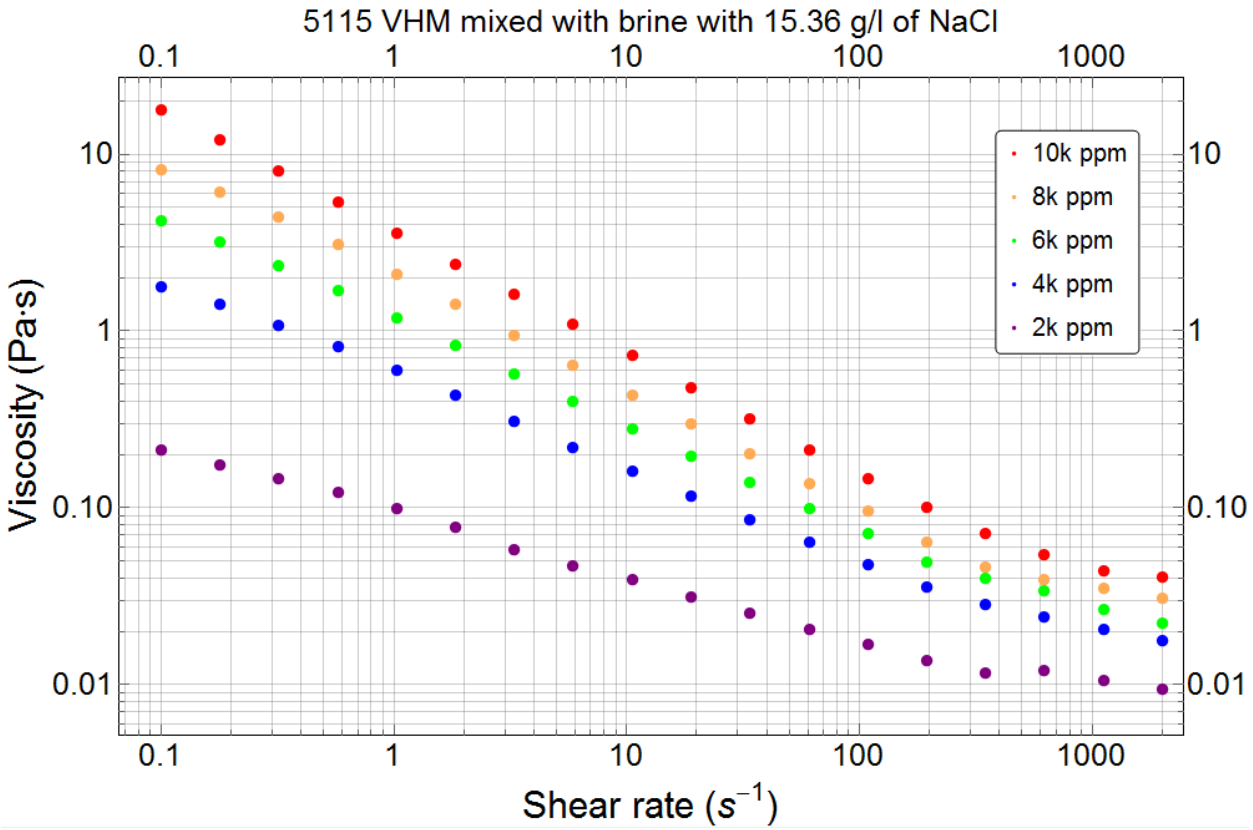

Figure A. 14: Viscosity vs shear rate for 5115 VHM mixed with Brine with 15.36 g/l of NaCl.

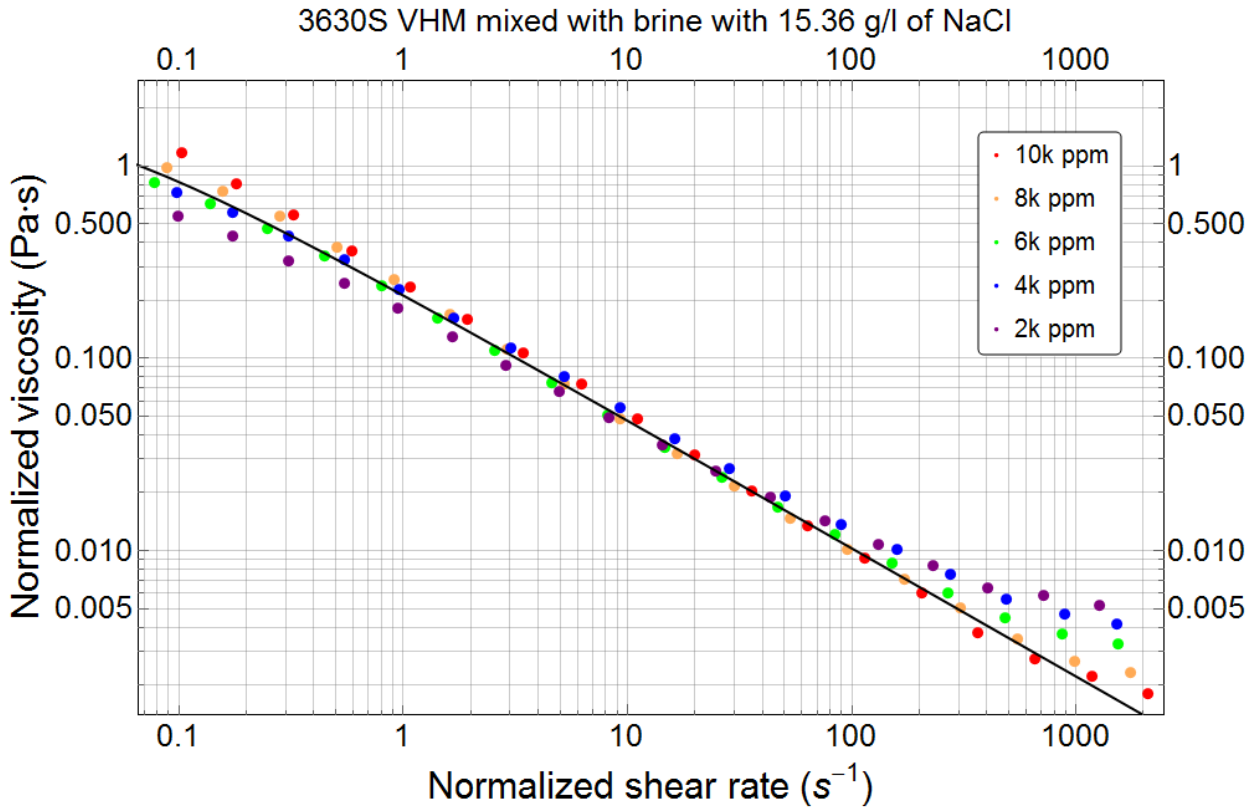

Figure A. 15: Normalized viscosity vs normalized shear rate for 3630S VHM mixed with Brine with 15.36 g/l of NaCl.

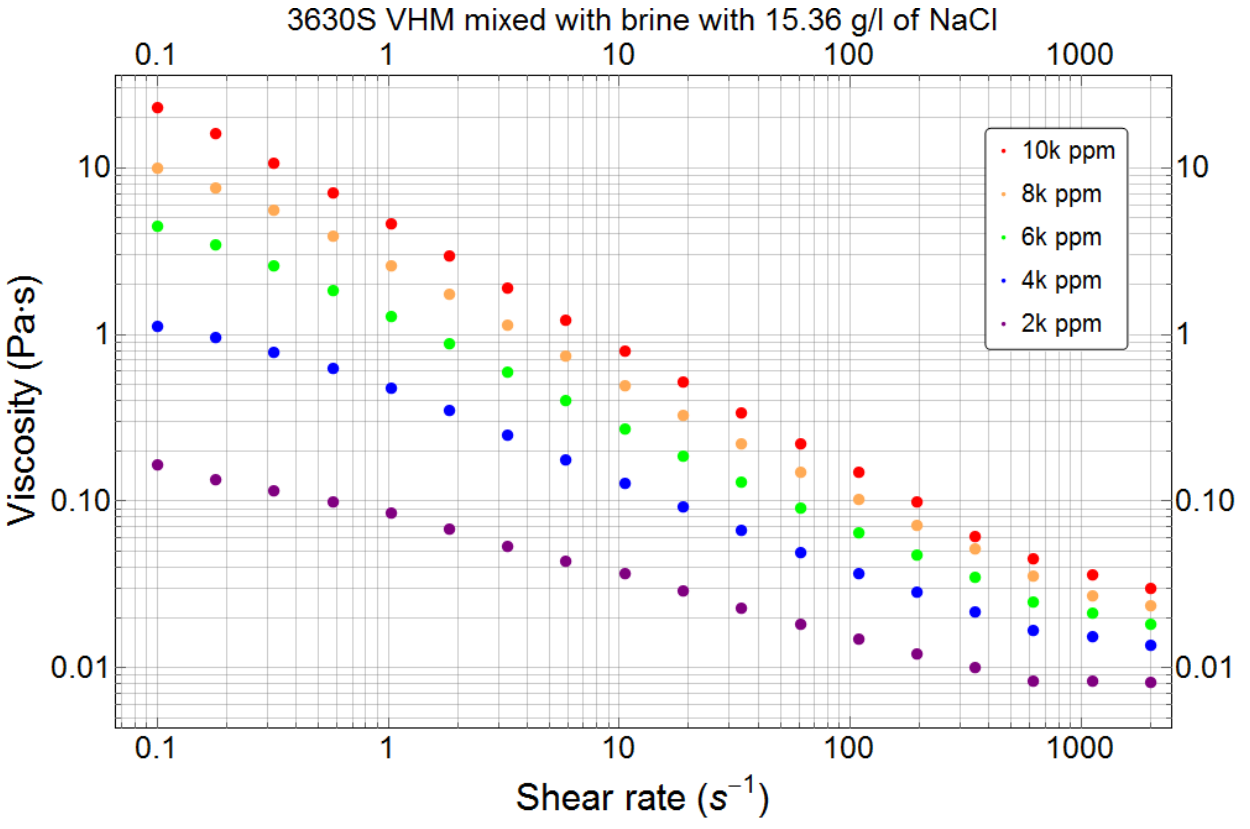

Figure A. 16: Viscosity vs shear rate for 3630S VHM mixed with Brine with 15.36 g/l of NaCl.

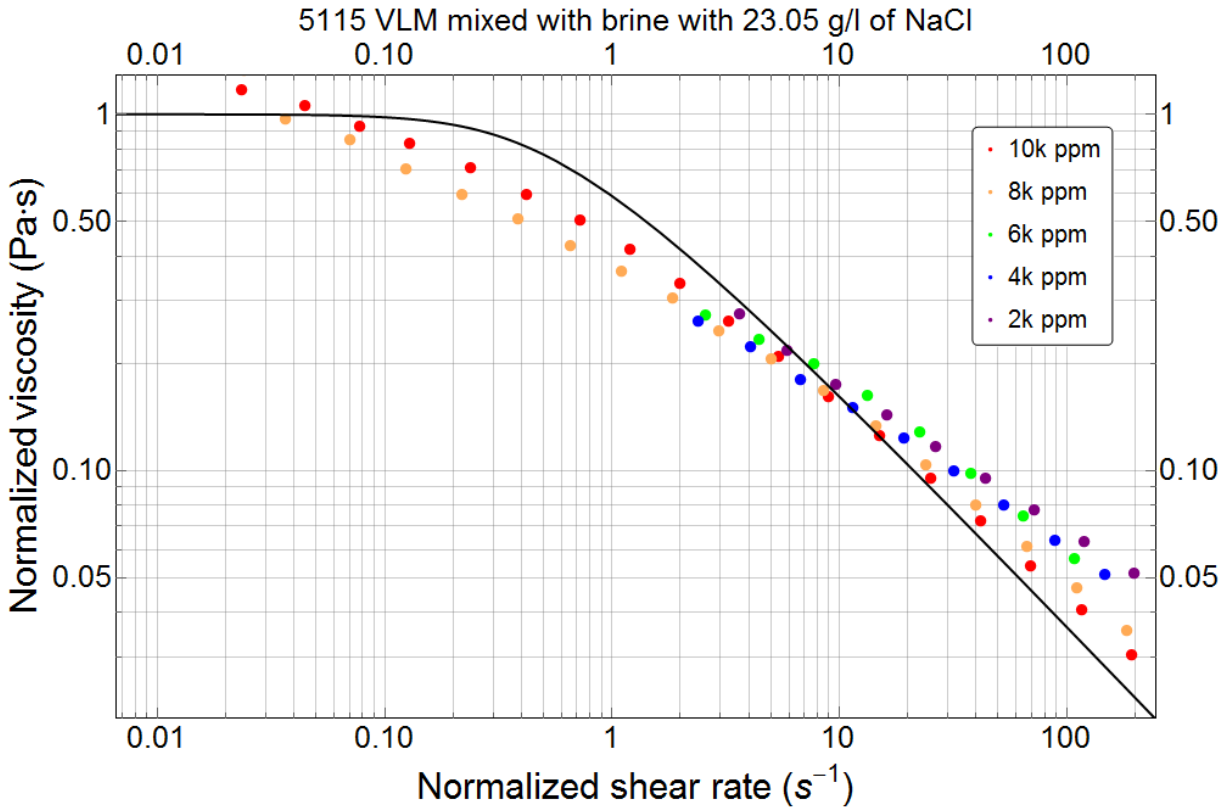

Figure A. 17: Normalized viscosity vs normalized shear rate for 5115 VLM mixed with Brine with 23.05 g/l of NaCl.

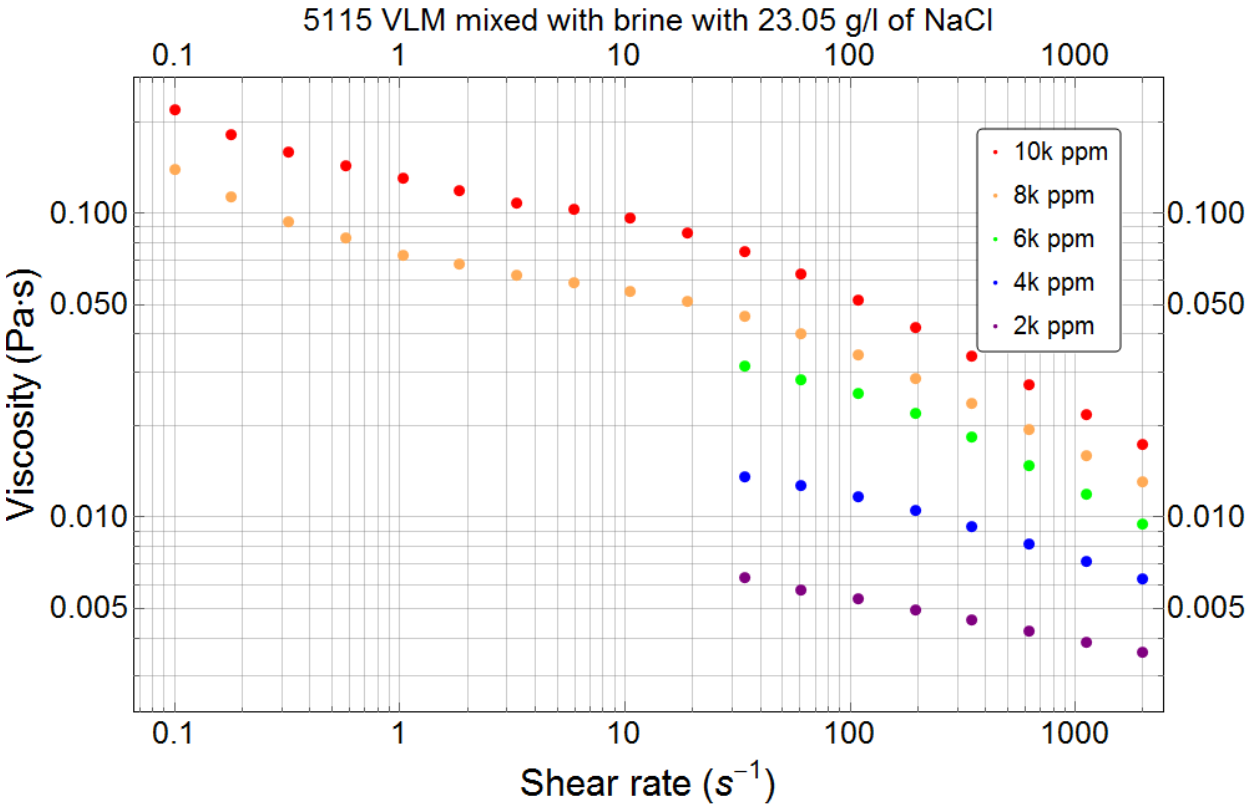

Figure A. 18: Viscosity vs shear rate for 5115 VLM mixed with Brine with 23.05 g/l of NaCl.

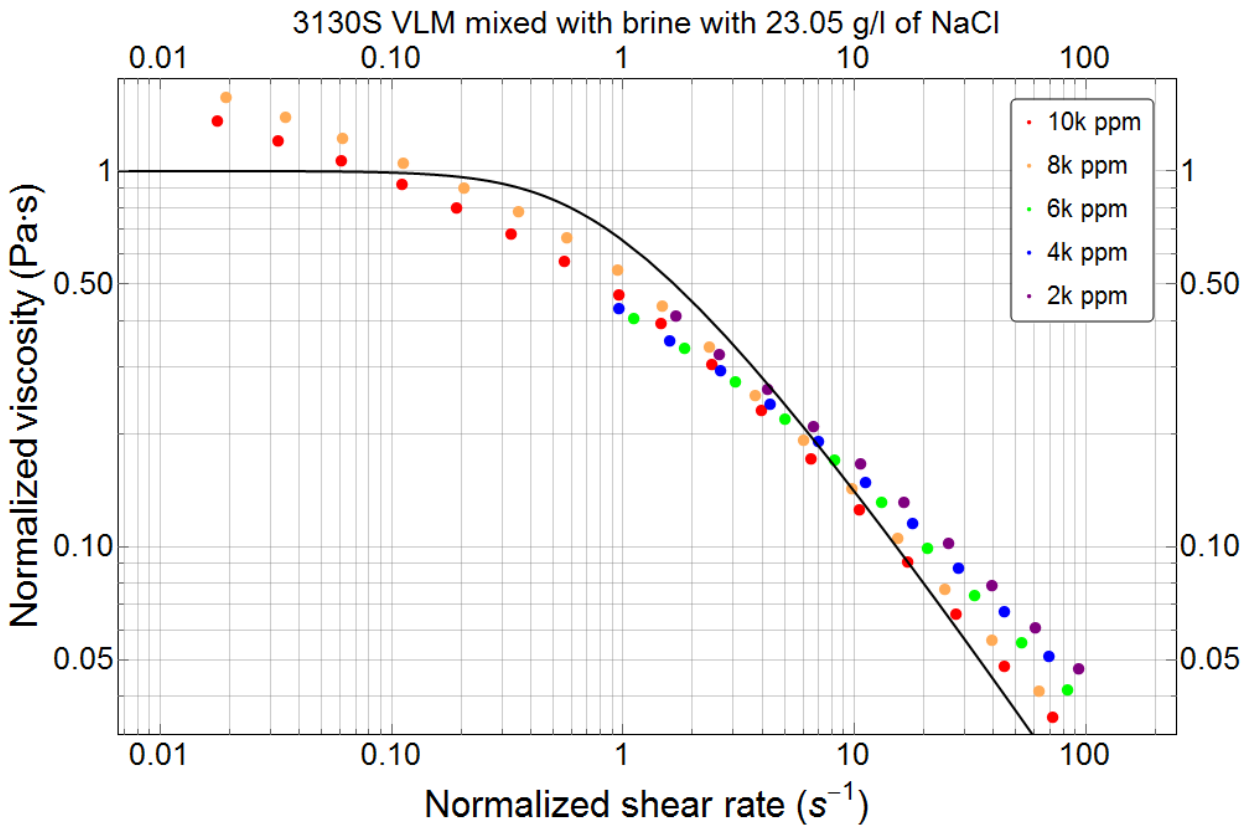

Figure A. 19: Normalized viscosity vs normalized shear rate for 3130S VLM mixed with Brine with 23.05 g/l of NaCl.

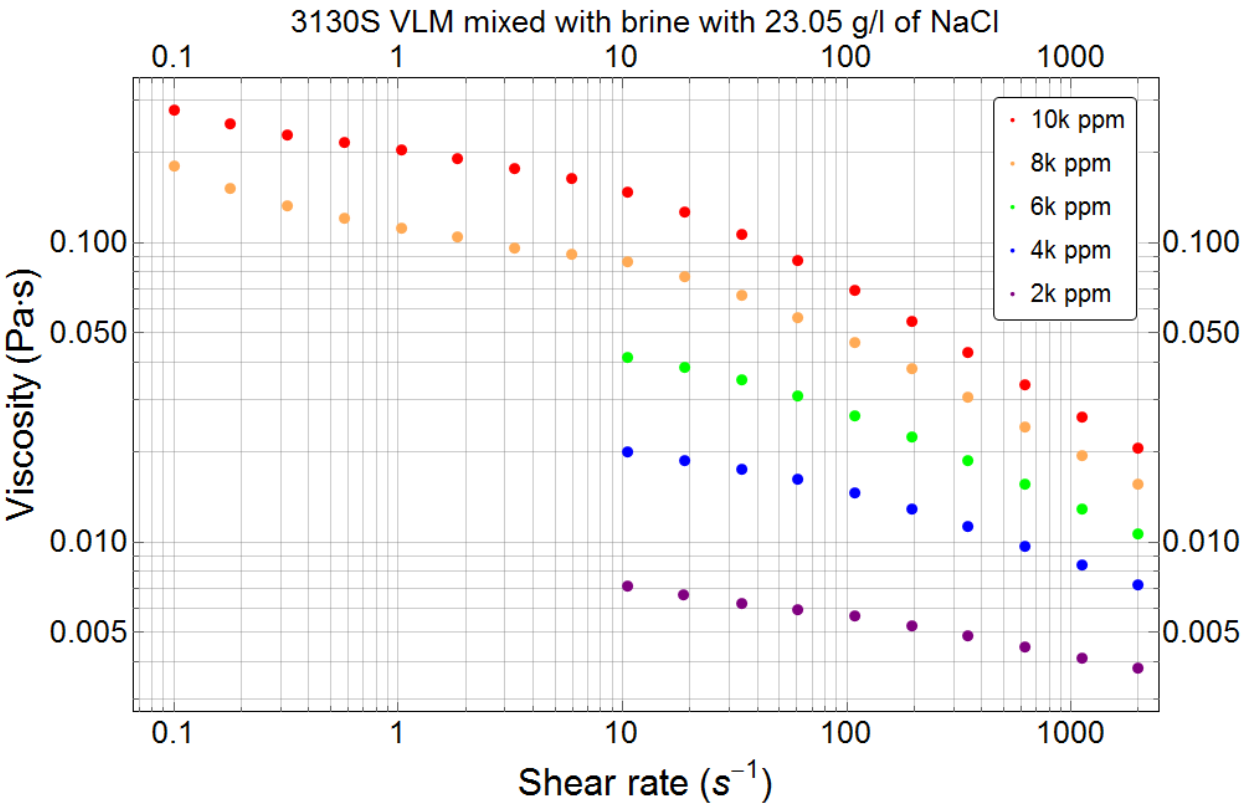

Figure A. 20: Viscosity vs shear rate for 3130S VLM mixed with Brine with 23.05 g/l of NaCl.

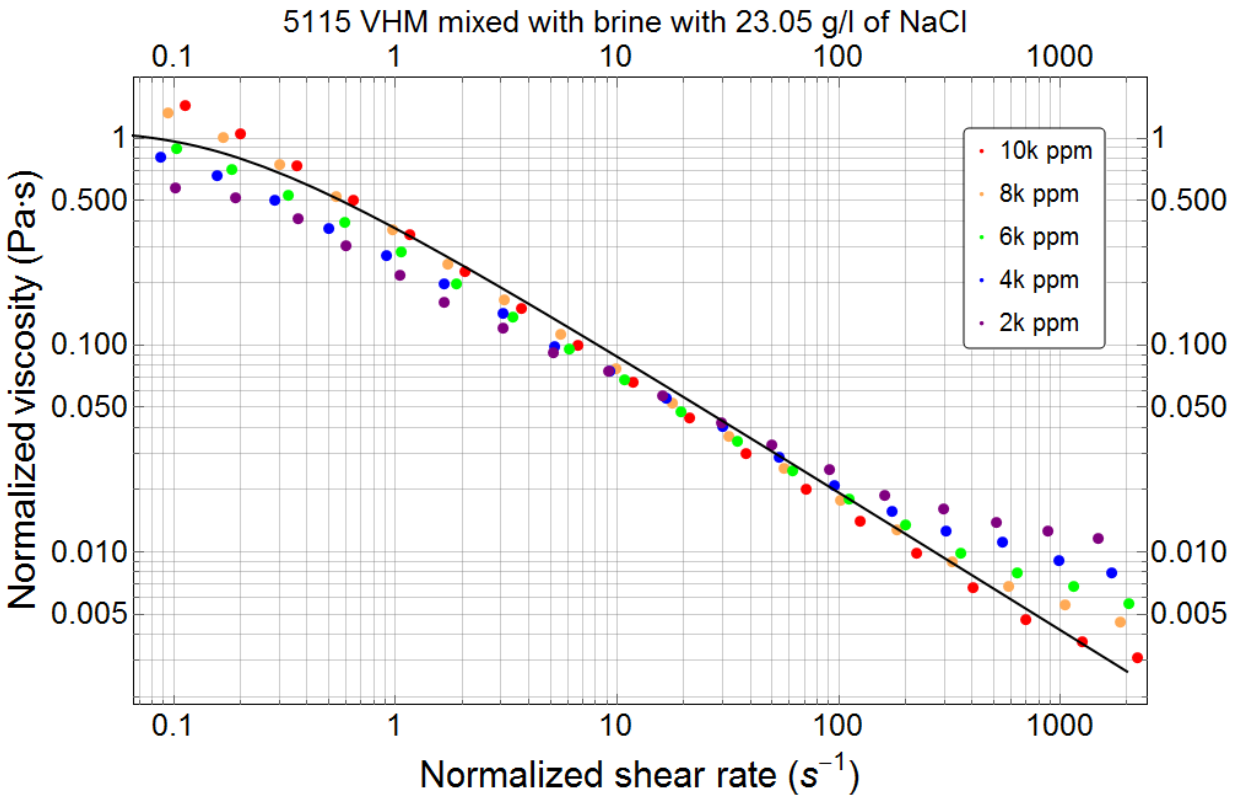

Figure A. 21: Normalized viscosity vs normalized shear rate for 5115 VHM mixed with Brine with 23.05 g/l of NaCl.

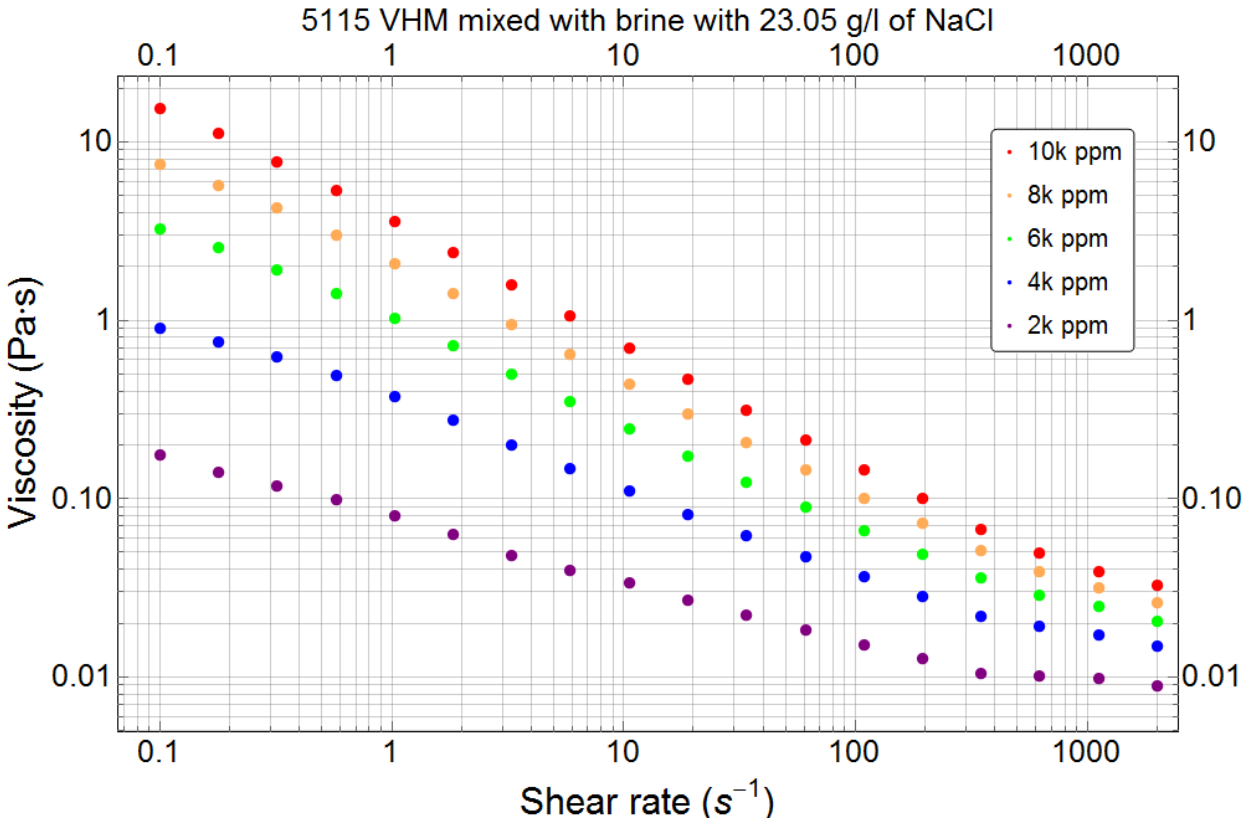

Figure A. 22: Viscosity vs shear rate for 5115 VHM mixed with Brine with 23.05 g/l of NaCl.

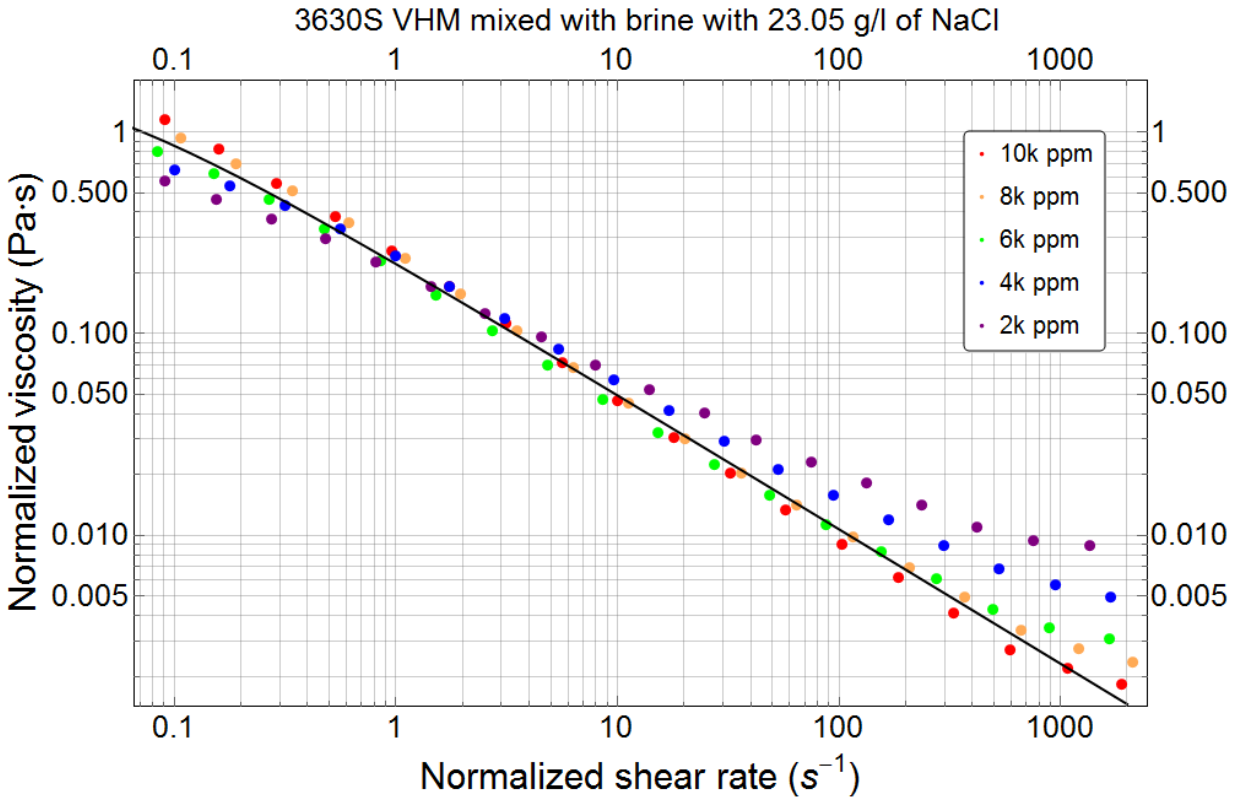

Figure A. 23: Normalized viscosity vs normalized shear rate for 3630S VHM mixed with Brine with 23.05 g/l of NaCl.

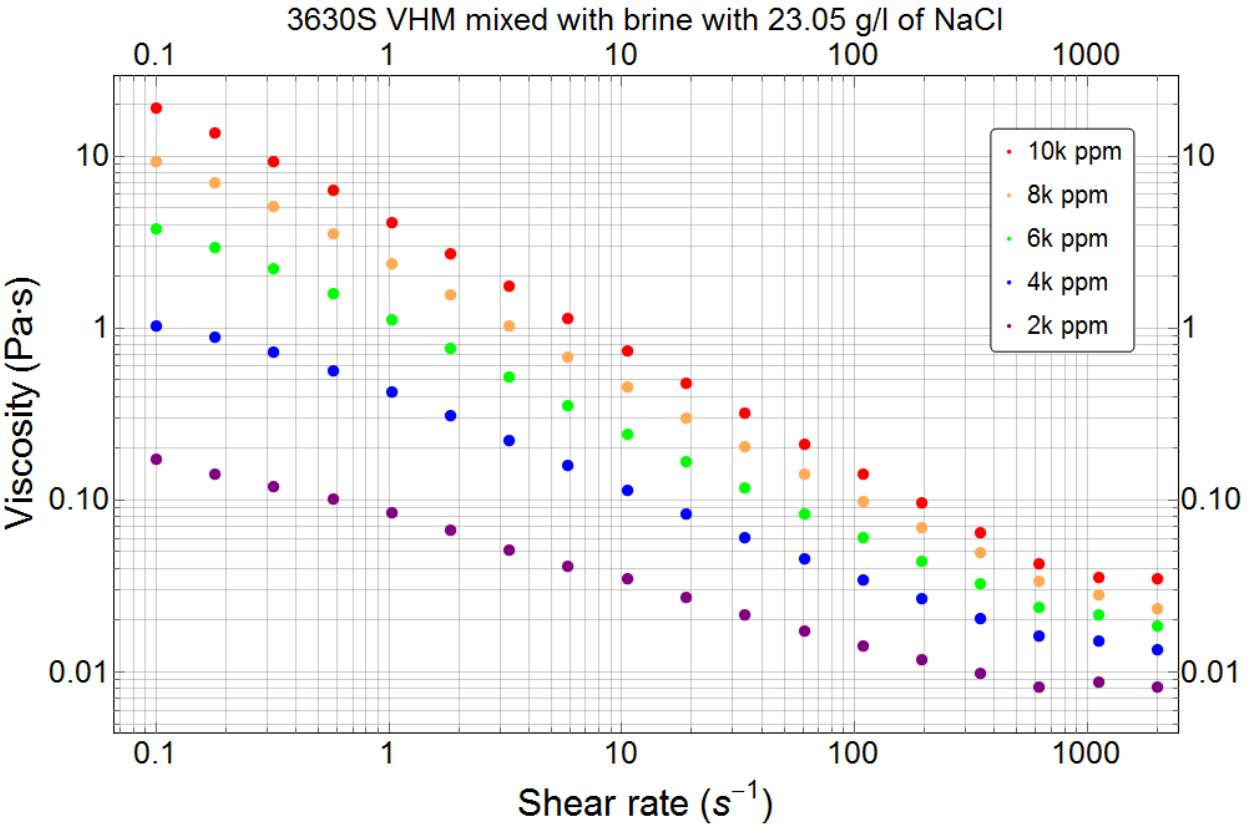

Figure A. 24: Viscosity vs shear rate for 3630S VHM mixed with Brine with 23.05 g/l of NaCl.

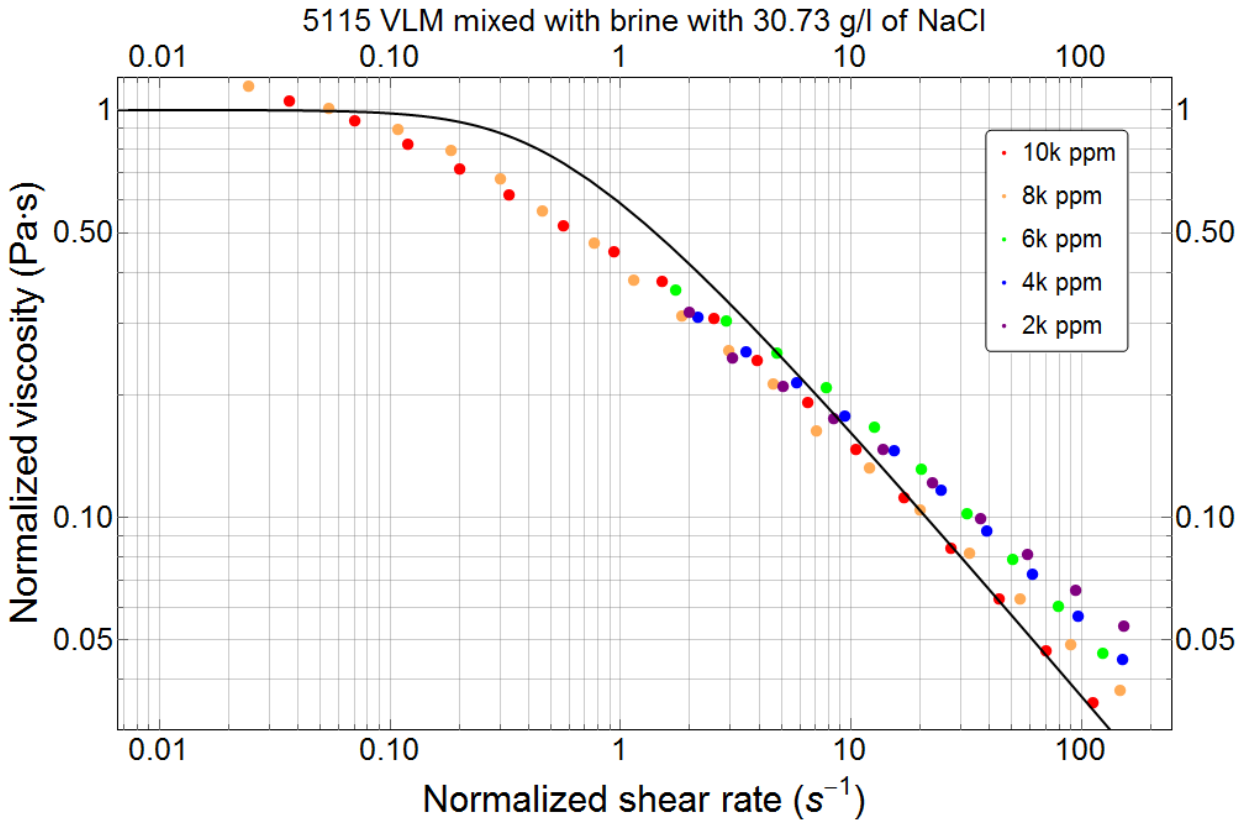

Figure A. 25: Normalized viscosity vs normalized shear rate for 5115 VLM mixed with Brine with 30.73 g/l of NaCl.

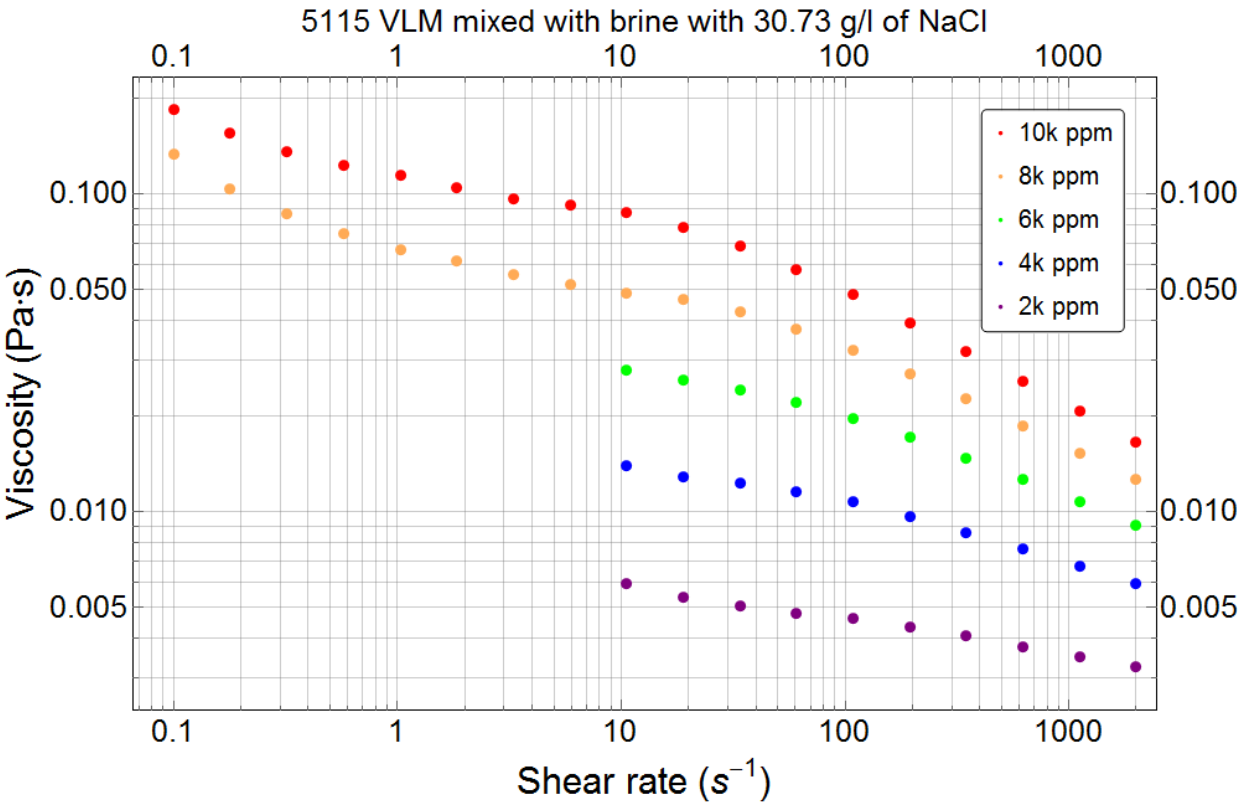

Figure A. 26: Viscosity vs shear rate for 5115 VLM mixed with Brine with 30.73 g/l of NaCl.

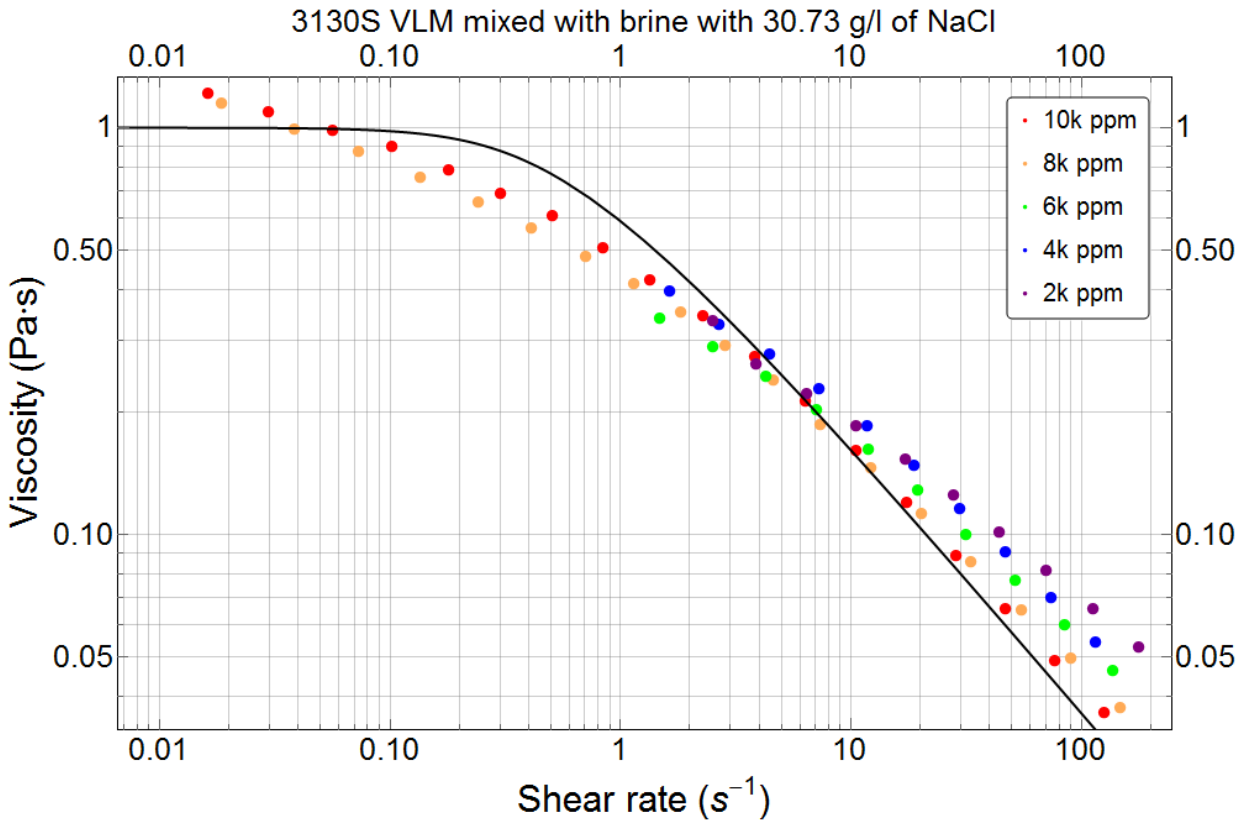

Figure A. 27: Normalized viscosity vs normalized shear rate for 3130S VLM mixed with Brine with 30.73 g/l of NaCl.

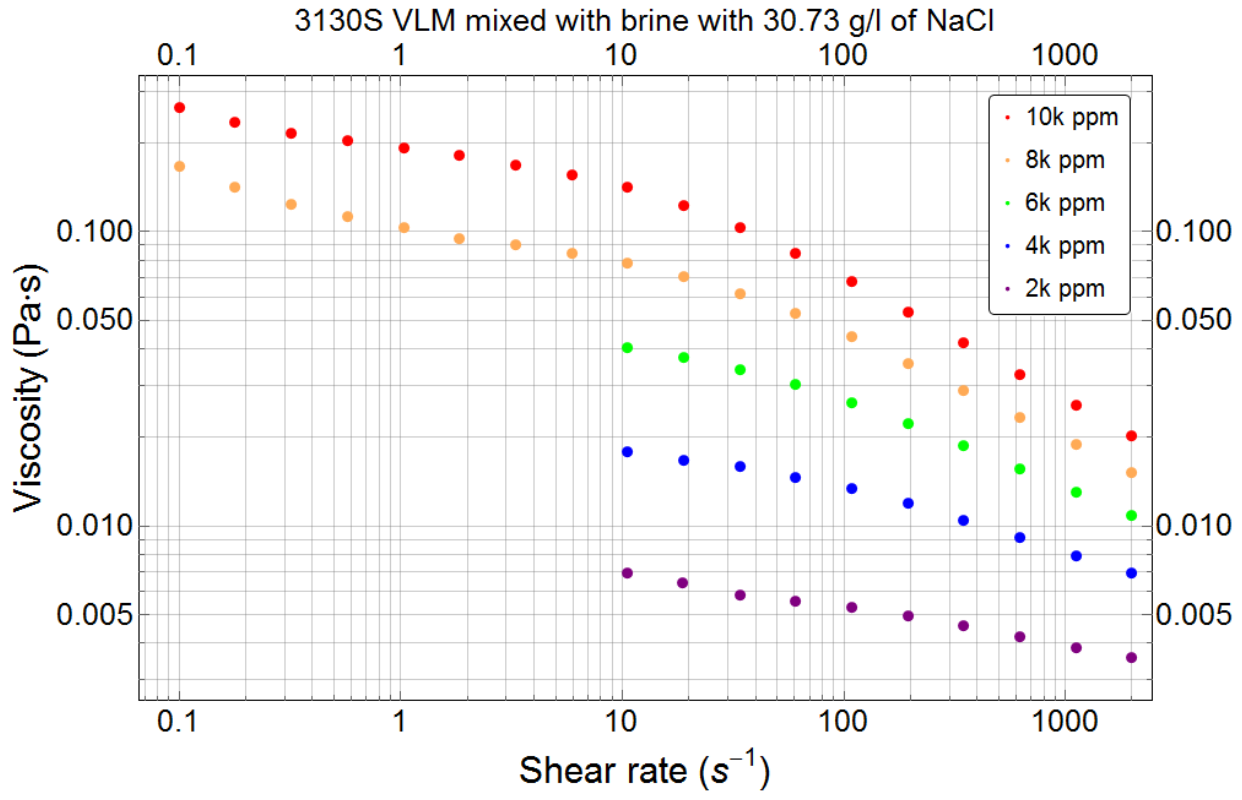

Figure A. 28: Viscosity vs shear rate for 3130S VLM mixed with Brine with 30.73 g/l of NaCl.

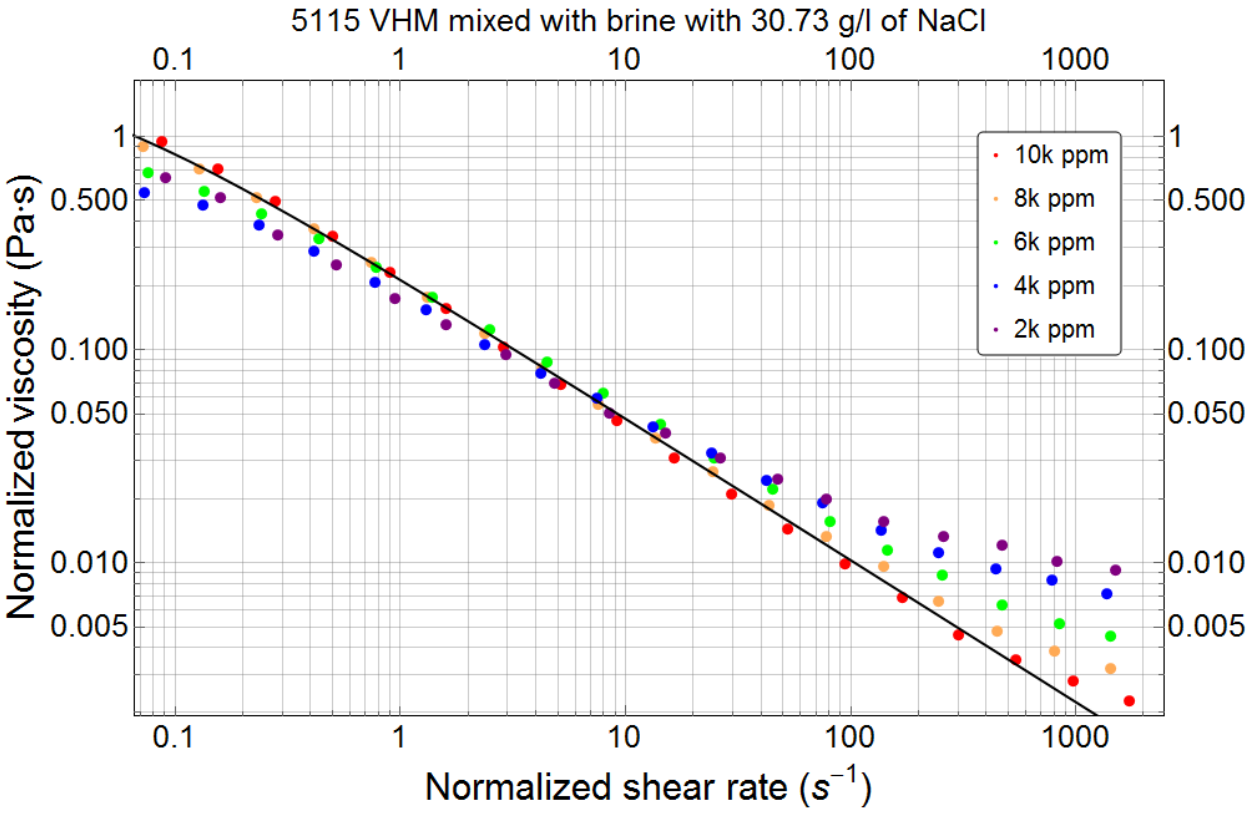

Figure A. 29: Normalized viscosity vs normalized shear rate for 5115 VHM mixed with Brine with 30.73 g/l of NaCl.

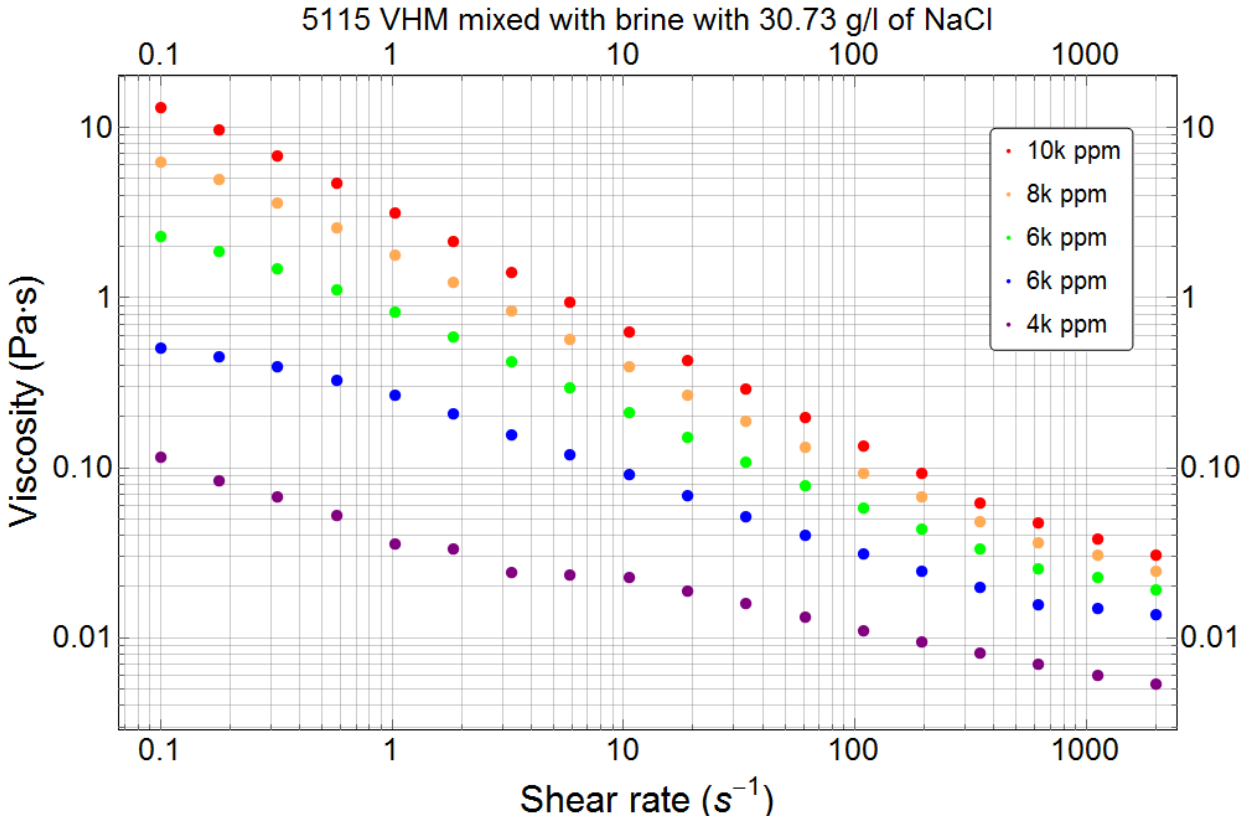

Figure A. 30: Viscosity vs shear rate for 5115 VHM mixed with Brine with 30.73 g/l of NaCl.

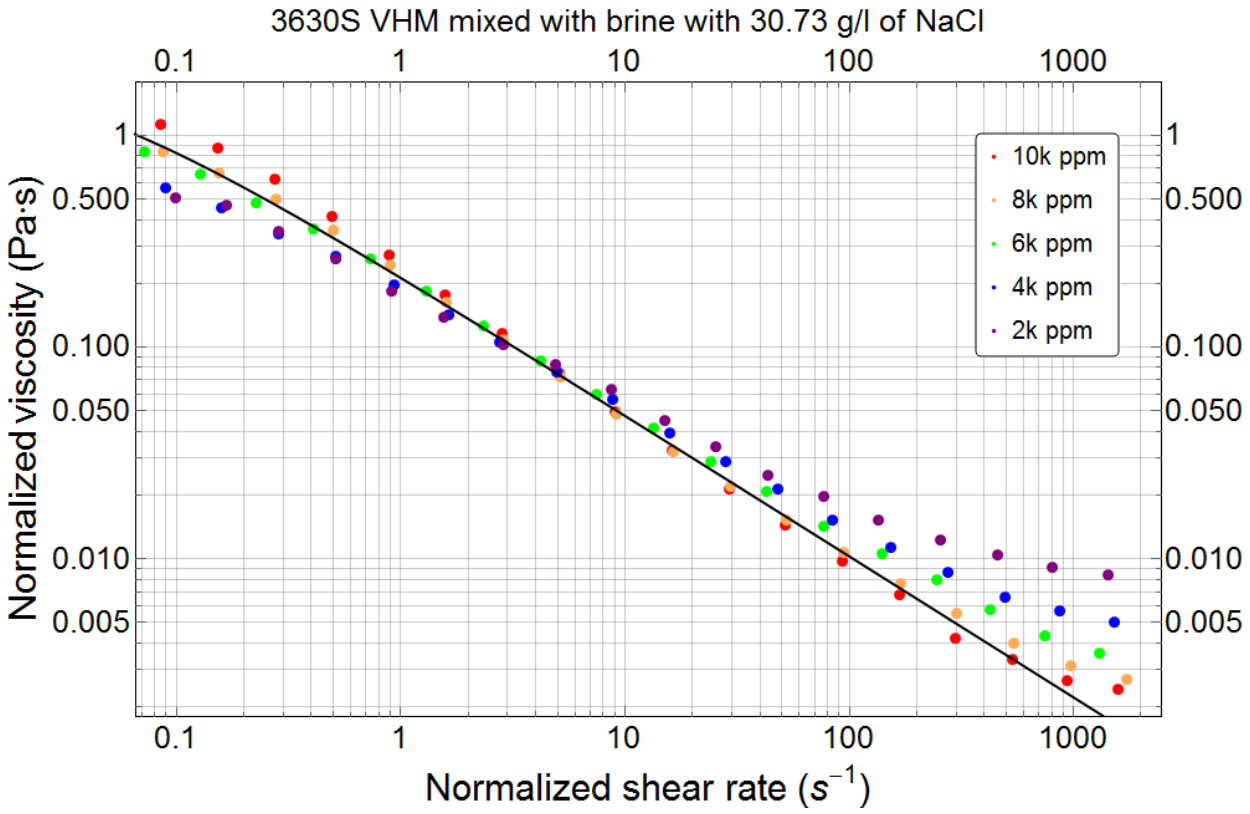

Figure A. 31: Normalized viscosity vs normalized shear rate for 3630S VHM mixed with Brine with 30.73 g/l of NaCl.

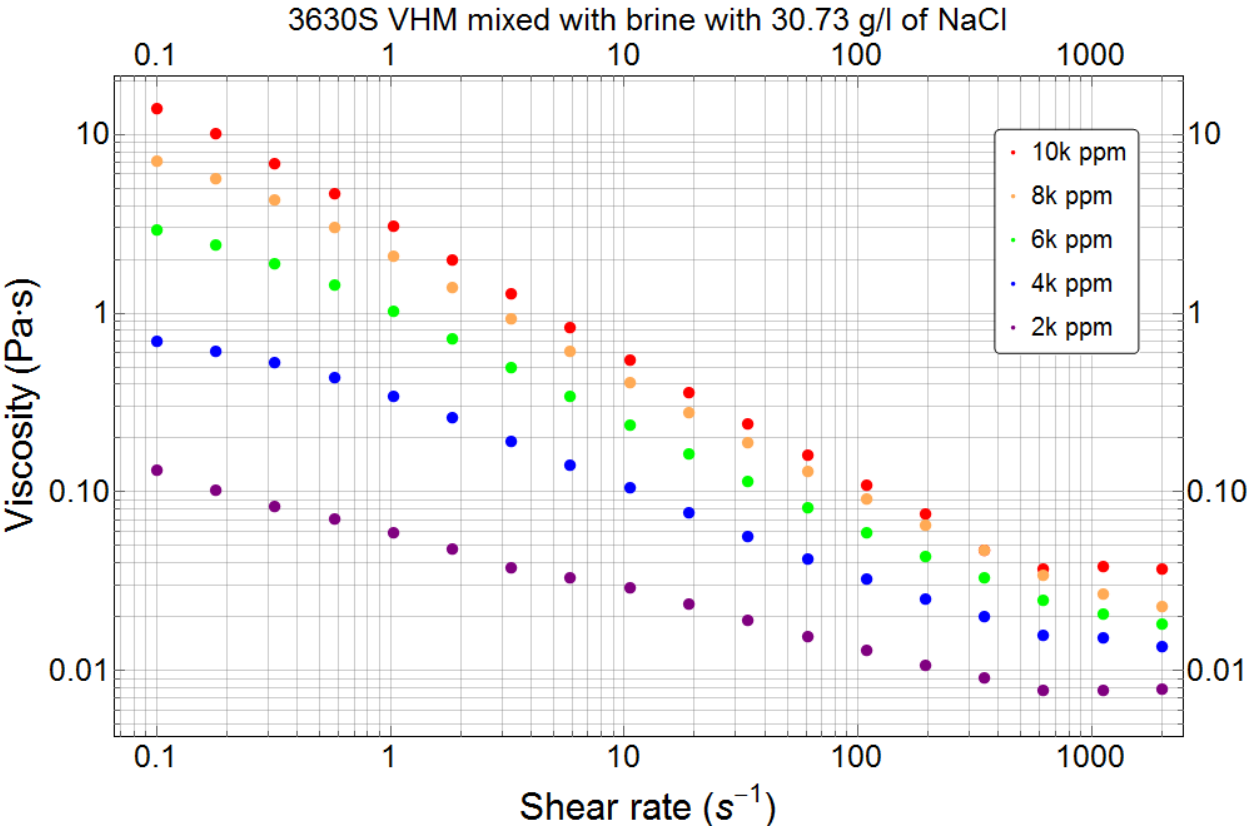

Figure A. 32: Viscosity vs shear rate for 3630S VHM mixed with Brine with 30.73 g/l of NaCl.

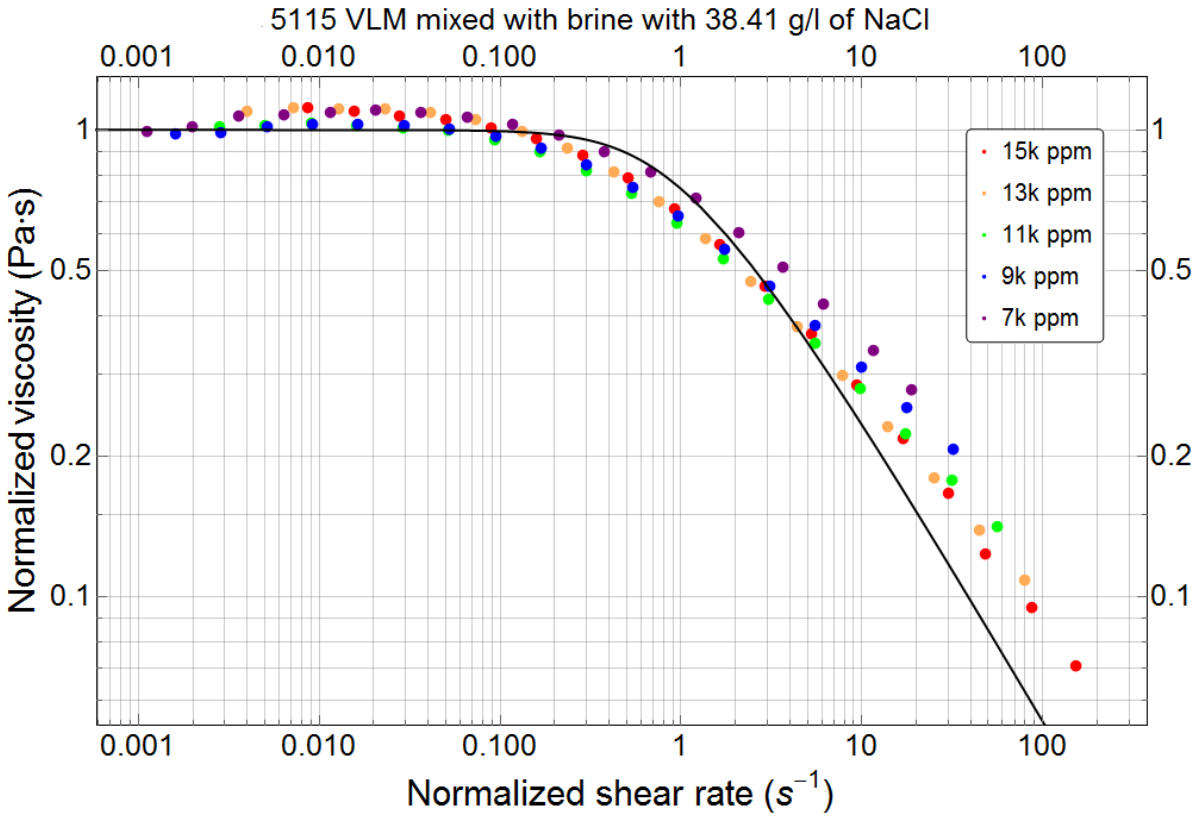

Figure A. 33: Normalized viscosity vs normalized shear rate for 5115 VLM mixed with Brine with 38.41 g/l of NaCl.

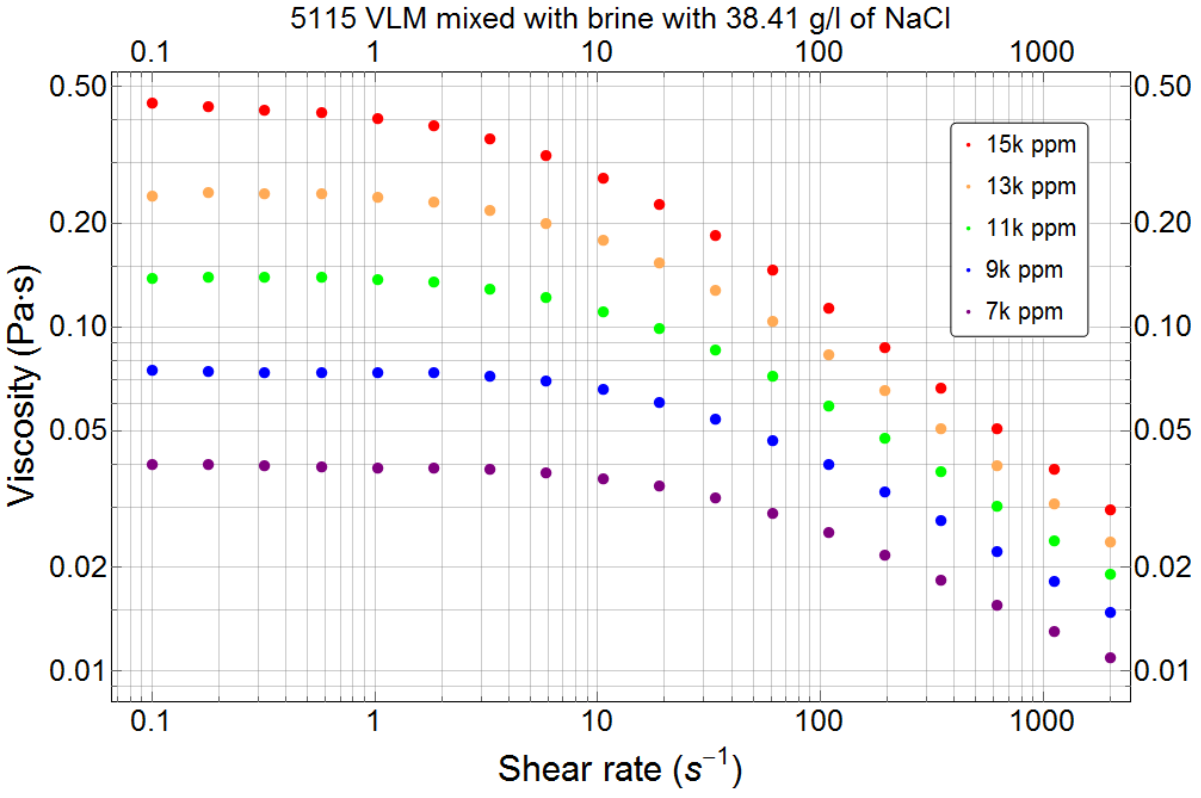

Figure A. 34: Viscosity vs shear rate for 5115 VLM mixed with Brine with 38.41 g/l of NaCl.

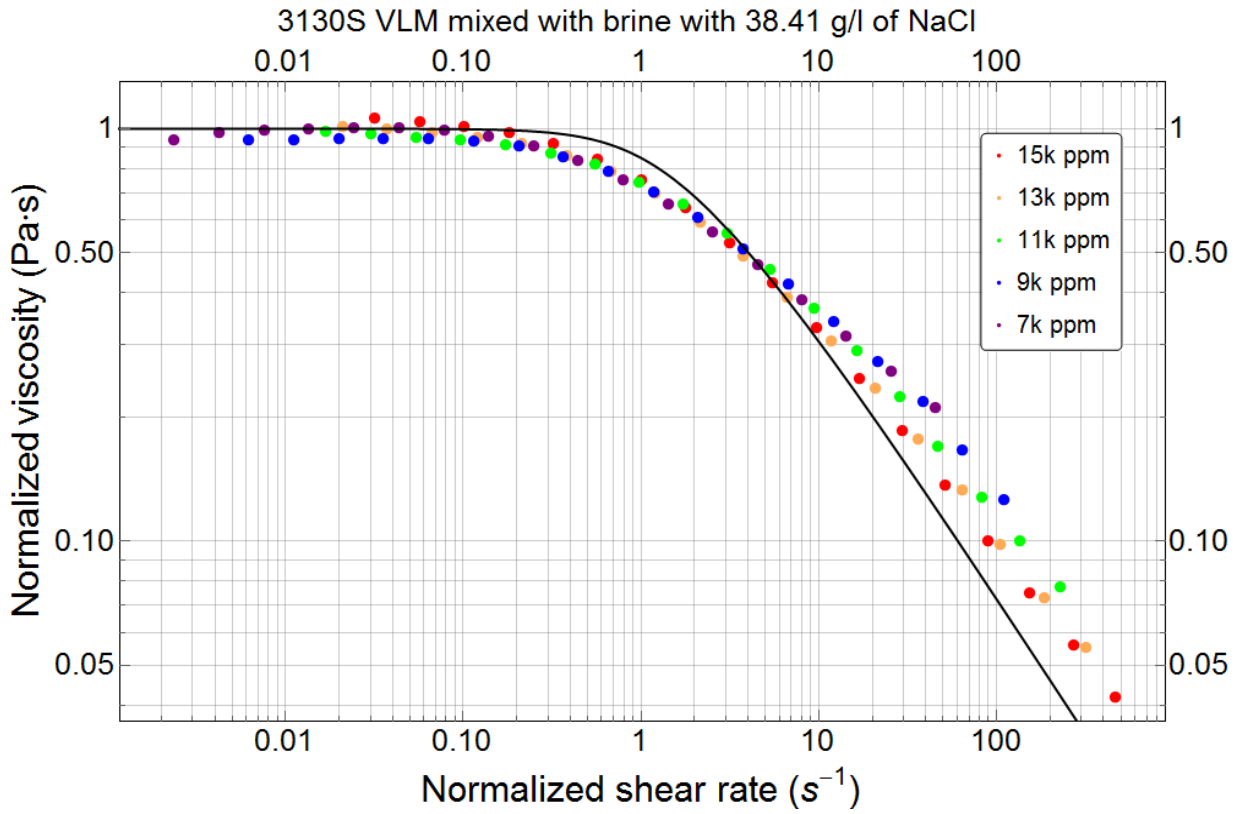

Figure A. 35: Normalized viscosity vs normalized shear rate for 3130S VLM mixed with Brine with 38.41 g/l of NaCl.

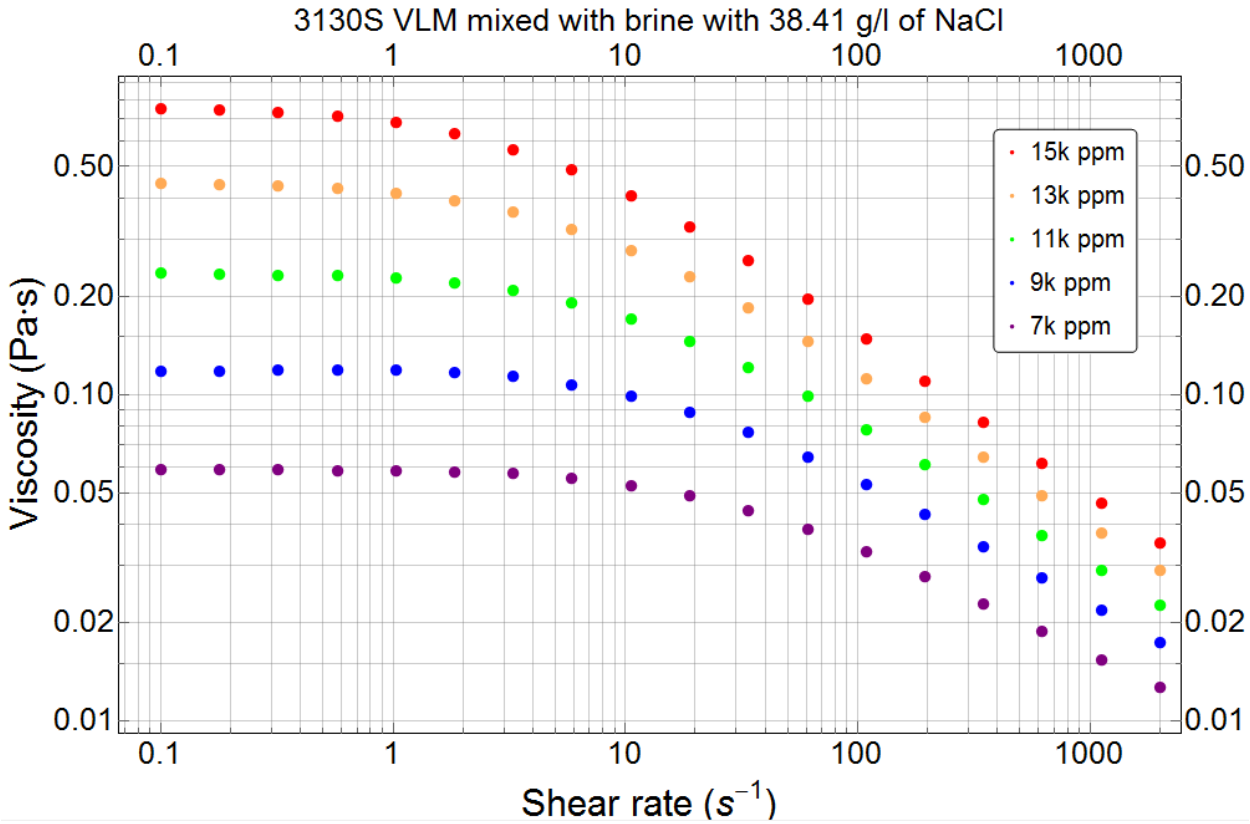

Figure A. 36: Viscosity vs shear rate for 3130S VLM mixed with Brine with 38.41 g/l of NaCl.

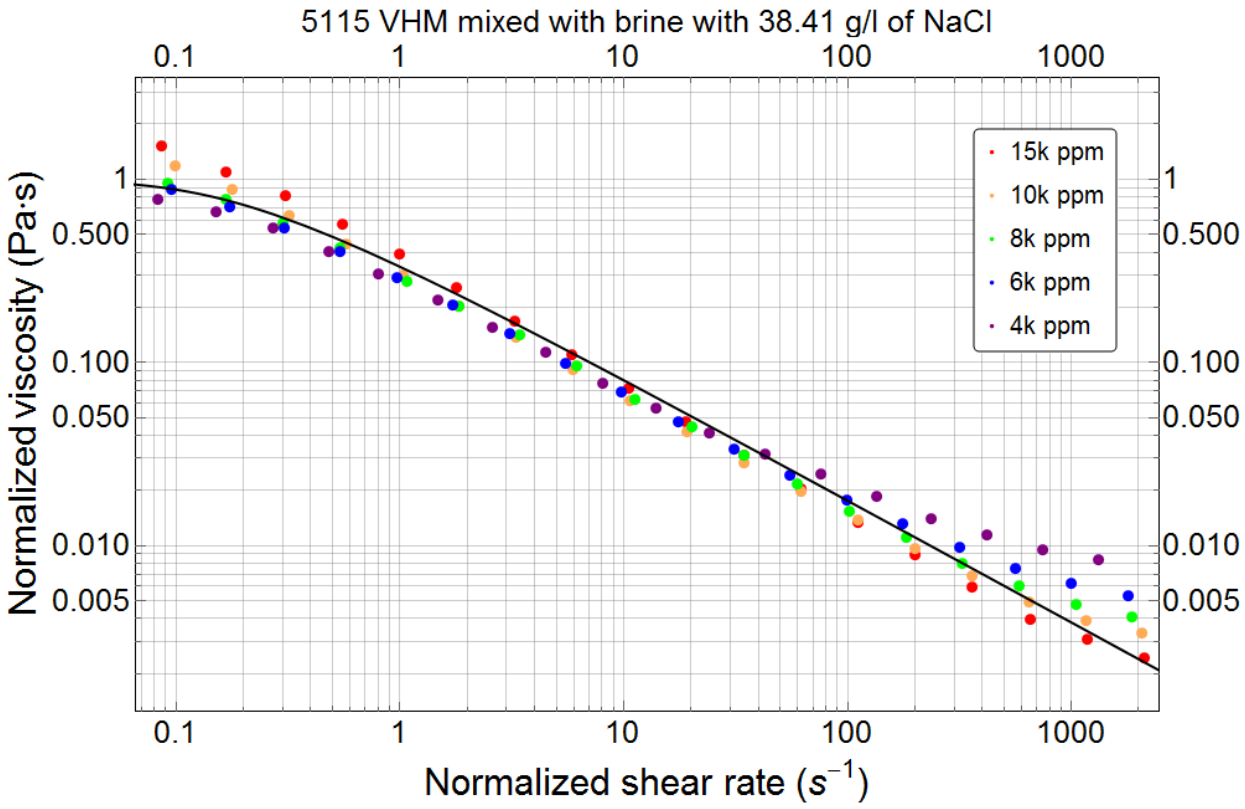

Figure A. 37: Normalized viscosity vs normalized shear rate for 5115 VHM mixed with Brine with 38.41 g/l of NaCl.

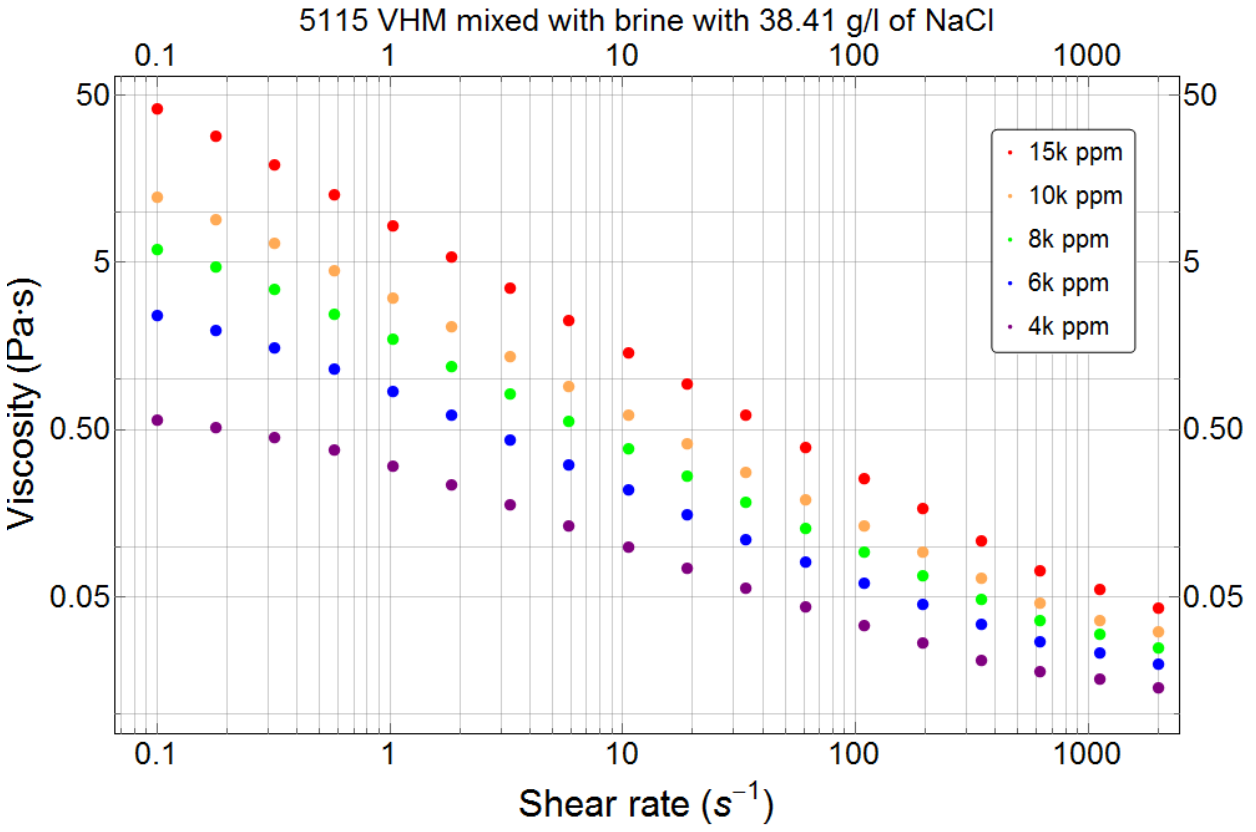

Figure A. 38: Viscosity vs shear rate for 5115 VHM mixed with Brine with 38.41 g/l of NaCl.

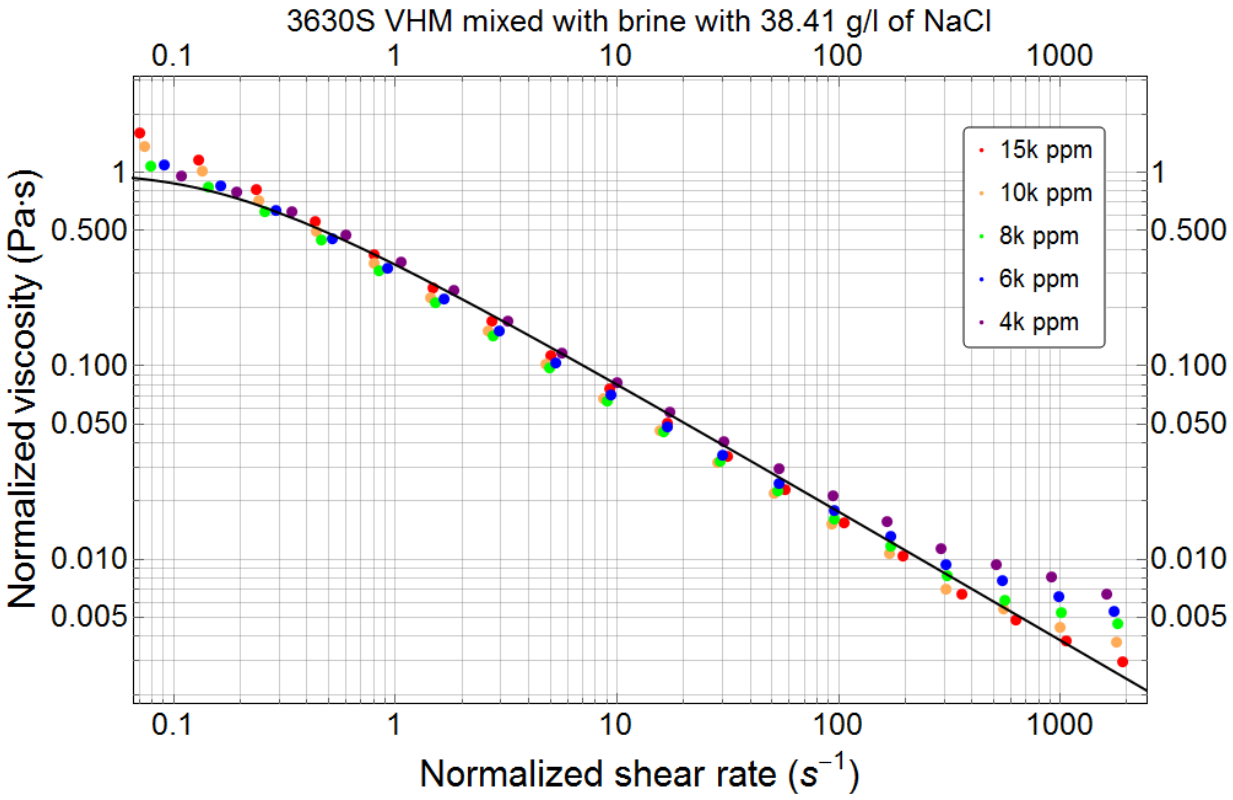

Figure A. 39: Normalized viscosity vs normalized shear rate for 3630S VHM mixed with Brine with 38.41 g/l of NaCl.

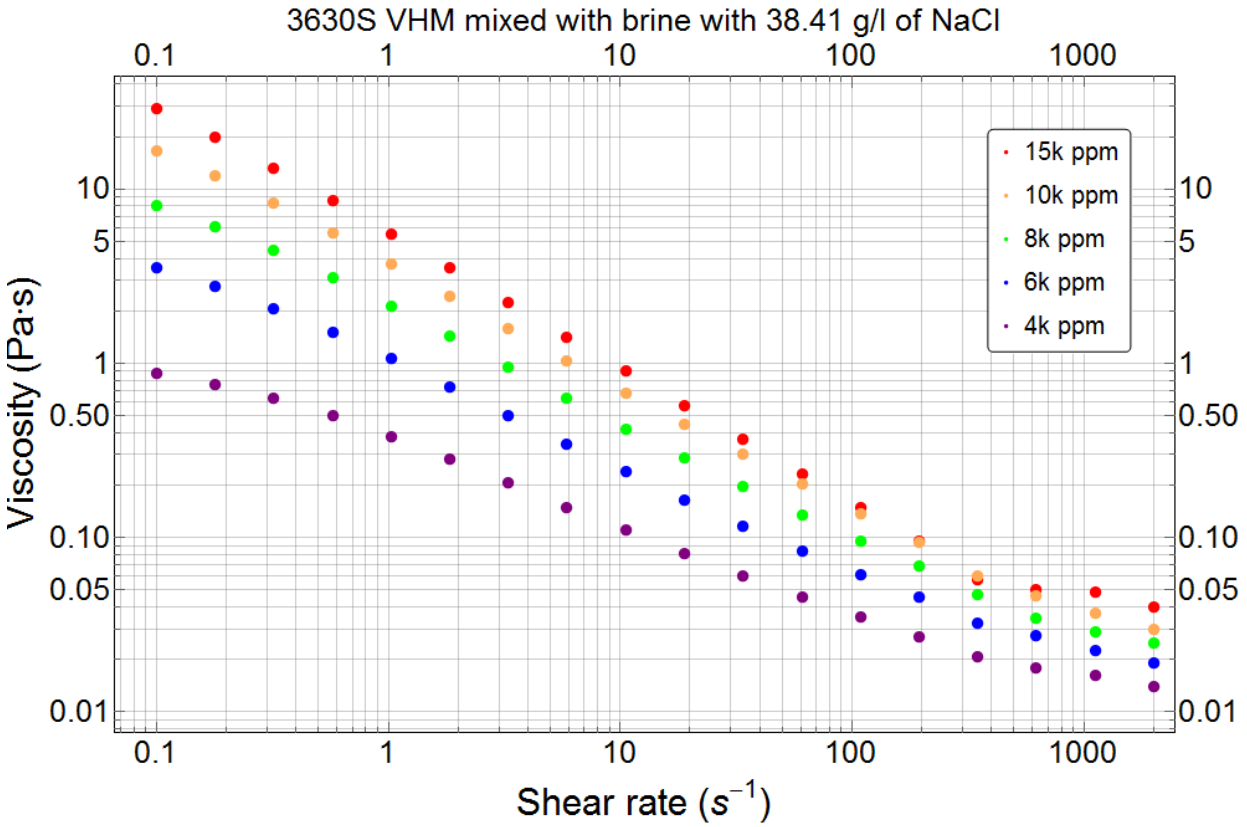

Figure A. 40: Viscosity vs shear rate for 3630S VHM mixed with Brine with 38.41 g/l of NaCl.